Cloning, Expression, Process Analytical Technology (PAT) Enabled Monitoring and Control of Glycoengineered *Pichia pastoris* Cultivation for Human Interferon α2b Production

A Thesis

Submitted for the Partial Fulfillment of the Requirements for the Degree of

DOCTOR OF PHILOSOPHY

by

Katla Srikanth

Department of Biosciences and Bioengineering
Indian Institute of Technology Guwahati
Guwahati 781 039, Assam, India

December 2019

Dedicated to My Parents
and
Family Members

Indian Institute of Technology Guwahati
Guwahati 781 039, Assam, India

DECLARATION

I, hereby declare that the research findings in this thesis titled "**Cloning, Expression, Process Analytical Technology (PAT) Enabled Monitoring and Control of Glycoengineered *Pichia pastoris* Cultivation for Human Interferon α2b Production**" is the result of research work carried out by me under the supervision of Dr. Senthilkumar Sivaprakasam, Department of Biosciences and Bioenginering, Indian Institute of Technology Guwahati, for the award of the degree of Doctor of Philosophy. This work has not been submitted elsewhere for any degree or membership of any institute or university to the best of my knowledge and belief. Also, due acknowledgements have been made, wherever the research findings of other researchers have been cited in this thesis.

Date:

Place:

Katla Srikanth

Roll No- 126106006

Indian Institute of Technology Guwahati
Guwahati 781 039, Assam, India

CERTIFICATE

It is certified that the work described in this thesis entitled "**Cloning, Expression, Process Analytical Technology (PAT) Enabled Monitoring and Control of Glycoengineered *Pichia pastoris* Cultivation for Human Interferon α2b Production**" by Mr. Katla Srikanth for the award of degree of Doctor of Philosophy is an authentic record of the results obtained from the research work carried out under my supervision in the Department of Biosciences and Bioengineering, Indian Institute of Technology Guwahati, India. This work has not been submitted elsewhere for the award of any other degree.

Date:

Dr. Senthilkumar Sivaprakasam

(Thesis Supervisor)

Acknowledgement

The journey of the Ph.D. program has been a roller coaster ride with ups and downs, and the successful completion of the ride was only possible because of several instrumental people. I want to take this opportunity to offer my sincere gratitude to everyone for making this journey worthwhile.

First and foremost, I would like to express my sincere gratitude to my Ph.D. supervisor Dr. Senthilkumar Sivaprakasam, for providing me the golden opportunity and platform to learn and excel in the research career. I wish to further thank my supervisor for continuous support and encouragement throughout my Ph.D. tenure. Under his supervision, I could not only execute my ideas freely but also realize my dreams and thus, amicably do research. His words of faith, invaluable guidance, motivation, moral support, and the never-ending kindness throughout my Ph.D. journey helped me to grow as an independent researcher and as an individual.

I am grateful to Dr. B. Anand, Mechanistic Approach to Biology (MAB) Laboratory, Department of Biosciences and Bioengineering, IIT Guwahati for providing the opportunity to learn and collaborate in performing the molecular biology related experiments. I am thankful to him for the discussions and valuable suggestions that helped me to move forward in my research work. I owe my sincere gratitude for providing the lab space and allowing me to work along with his research group.

I am grateful to Dr. Anil Mukund Limaye and Mr. Uttariya Pal, Molecular Endocrinology Laboratory, Department of Biosciences and Bioengineering, IIT Guwahati and Dr. C.T. Ranjith Kumar and Ms. Smita Hingane, THSTI for providing the opportunity to collaborate in performing the antiproliferative studies and antiviral studies for the purified protein

I owe my sincere gratitude to my doctoral committee members, Prof. Kannan Pakshirajan, Prof. Debasish Das, and Dr. Anil Mukund Limaye for their constructive suggestions, motivation, and support which has helped me to improve the quality of my research work.

I owe my sincere gratitude and grateful to Mr. Naresh Mohan , my colleague in lab for his immense help and support in completing the PAT related objectives. He was instrumental with his immense knowledge in process monitoring and control, with which I could be able to successfully accomplish the PAT oriented objectives.

I would like to especially thank Mr. Yoganand (MAB Lab) for his support, help and untiring discussions in the area of molecular biology which made me get familiar with the subject and helped me in moving forward in my research work.

I am very much thankful to Mr. Subbi Rami Reddy, Mr. Sai Pavan, and Mr. Bappa Karmakar for their unconditional support and encouragement in completing my research objectives. I would also like to thank my lab members, Mr. Ganesh Nehru, Mr. Kiran Gali, Ms. Niveditha, and Ms. Indumathi, for their direct or indirect support during my Ph.D. research work.

I would like to extend my sincere gratitude to Prof. Latha Rangan, Head of the Department, Biosciences and Bioengineering, IIT Guwahati, and Prof. Kannan Pakshirajan, Prof. V. Venkata Dasu, Prof. Arun Goyal, Former Heads of the Department, Biosciences and Bioengineering, IIT Guwahati for providing me the necessary facilities that helped to pursue my research work.

I am grateful to Department of Biosciences and Bioengineering and Central Instrumental Facility (CIF), IIT Guwahati for providing me all the required support for carrying out my thesis work. I am also thankful all the staff members of Department of Biosciences and Bioengineering, IIT Guwahati.

I am thankful to Ministry of Human Resource and Development (MHRD) for providing me the Ph.D. fellowship. I am grateful to Department of Science and Technology (DST), Science and Engineering Research Board (SERB) for providing the grants (SB/FTP/ETA-0448/2012) to carry out the research work and International Travel Support (ITS) for sharing my research work at European Congress on Biotechnology (ECB 2018), Geneva, Switzerland.

I would like to thank senior colleagues Muthusivaramapandian and Basavaraj for their help and friends Durga Sravani, Payel, Arun, Saumya, Himanshu, Siddharth, Mehak, Anuma, Praveen, Rahul, Gaurav, Asif, Mahesh, Sandipan, Manishekar, Rakesh, Sunanda, Dhamodharan, Satish and other well wishers because of whom the stay at IIT Guwahati has become more memorable and wonderful.

Most importantly I would thank my parents who have been very supportive and understanding throughout the journey of Ph.D. Whatever I have achieved today is only because of them. I would like to specially thank my wife Bhargavi Himamsha for the love and support during the Ph.D. tenure. Also, a special mention about my little son Vihaan Srimadhav who has brought the happiness and luck. Finally I am indebted to the almighty God who made everything possible.

Katla Srikanth

Table of Contents

List of Figures vii
List of Tables xiv
Glossary of Acronyms xv
Synopsis xxiii
Chapter 1: Introduction and review of literature 3
1. Interferons 3
1.1. Human interferon alpha 2b 4
1.2. Biological Route for the Production of Recombinant huIFNα2b 5
1.3. *P. pastoris* as expression system for the production of huIFNα2b 11
1.4. Signifiance of post translational modifications 14
1.5. Factors controlling glycosylation 17
1.6. Batch and fed-batch cultivation of *P. pastoris* 20
1.6.1. Batch cultivation of *P. pastoris* 20
1.6.2. Fed-batch cultivation of *P. pastoris* 21
1.7. Bioprocess Monitoring and Control 23
1.7.1. Dielectric Spectroscopy 23
1.7.2. Biocalorimetry 25
Definition of the Problem 28
Objectives 30
Chapter 2: Cloning, expression, purification and characterization of recombinant huIFNα2b in *Pichia pastoris* 33
Abstract 33
2.1. Introduction 34
2.2. Materials and methods 37
2.2.1. Strains, media, and chemicals 37
2.2.2. Identification of key location for the generation of N-glycosylation motif 38
2.2.3. Cloning of human huIFNα2b gene and construction of expression vector 38
2.2.4. Transformation of *P. pastoris* strains and screening for recombinant strain 39
2.2.5. Shake flask studies for the expression of recombinant huIFNα2b 40
2.2.6. High cell density cultivation 41

2.2.7. Purification of recombinant huIFNα2b 41
2.2.8. Glycosylation Analysis 42
2.2.9. N-Glycan Analysis 43
2.2.10. Biological assay of huIFNα2b 44
2.2.10.1. Replicon Assay 44
2.2.10.2. Cell Viability Assay 45
2.2.11. Pharmacokinetic studies 45
2.2.12. Pharmacokinetic data analysis 46
2.3. Results 47
2.3.1. Identification of key location for the generation of N-glycosylation motif 47
2.3.2. Construction and transformation of expression vector 47
2.3.3. Expression and purification of recombinant huIFNα2b 50
2.3.4. Glycosylation analysis of recombinant huIFNα2b 55
2.3.5. N- Glycan analysis 56
2.3.6. Biological activity of huIFNα2b 59
2.3.7. Pharmacokinetic studies in rats 62
2.4. Discussion 63
2.5. Conclusion 69
Chapter 3: Medium optimization studies for high level extracellular production of recombinant huIFNα2b in glycoengineered *Pichia pastoris* 73
Abstract 73
3.1. Introduction 74
3.2. Materials and Methods 77
3.2.1. Strain 77
3.2.2. Media 77
3.2.3. Inoculum preparation 78
3.2.4. Sampling and Analysis 78
3.2.5. Design of experiments (DoE) based optimization 79
3.2.5.1. Plackett-Burman Design 79
3.2.5.2. Optimization by Response Surface Methodology 80
3.2.5.3. Modelling and optimization by Artificial Neural Network linked Genetic Algorithm 81
3.2.5.4. Model validation experiments 83
3.2.6. Bioreactor operation 84

3.2.7. Dielectric spectroscopy for real-time monitoring of biomass 85
3.2.8. Oxygen uptake rate estimation 86
3.2.9. Kinetic Modeling 86
3.2.10. Purification of glycosylated huIFNα2b 87
3.2.11. Deglycosylation analysis 88
3.2.12. Anti-proliferative assay 88
3.3. Results 89
3.3.1. Screening of medium components and process parameters for huIFNα2b production 89
3.3. 2. Optimization of significant variables by RSM-BBD 91
3.3.3. Optimization by ANN linked GA 95
3.3.4. Model validation experiments 97
3.3.5. Monitoring of viable cell density using dielectric Spectroscopy and respirometry 98
3.3.6. Kinetic Modeling 101
3.3.7. Purification and deglycosylation analysis of glycosylated huIFNα2b 103
3.3.8. Anti-proliferative assay 104
3.4. Discussion 106
3.5. Conclusion 110
Chapter 4: Dielectric spectroscopy as PAT tool for real-time monitoring and control of specific growth rate in glycoengineered *Pichia pastoris* fermentation process for the production of recombinant huIFNα2b 113
Abstract 113
4.1. Introduction 115
4.2. Materials and Methods 119
4.2.1. Strain and media 119
4.2.2. Inoculum preparation 119
4.2.3. Bioreactor operation 120
4.2.4. Offline Analysis 121
4.2.5. Specific growth rate estimator (μ_{est}) 121
4.2.6. Investigation on the effect of the feeding strategies on μ_{est} 122
4.2.7. Feed rate control 123
4.2.7.1. Pulsed feed rate 123
4.2.7.2. Exponential feed rate 124

4.2.8. Oxygen uptake rate measurement....126
4.2.9. Purification of recombinant huIFNα2b....127
4.2.10. Biological activityof recombinant huIFNα2b....127
4.3. Results....129
4.3.1. Specific growth rate estimator ($\mu_{est,}$ h^{-1})....129
4.3.2. Growth characteristics of *P. pastoris* during growth and induction phases of huIFNα2b production....130
4.3.3. Design of PID Feedback loop for the exponential methanol feeding strategy at different μ_{sp}....133
4.3.4. Control characteristics of capacitance based μ_{est}....138
4.3.5. Improvement in huIFNα2b productivity....141
4.3.6. Purification and biological activity of recombinant huIFNα2b....142
4.4 Discussion....146
4.4.1. Specific growth estimator....146
4.4.2 Effect of repeated pulsed feed on specific growth rate....146
4.4.3. Control of specific growth rates, μ_{est} at various μ_{sp}....148
4.4.4. Response of μ dependency in the controller function....149
4.4.5. Relationship between μ_{est} and $q_{huIFN\alpha2b}$....150
4.4.6. Purification and biological activity of recombinant huIFNα2b....152
4.5. Conclusion....153
Chapter 5: Biocalorimetric monitoring of glycoengineered P. pastoris cultivation for the production of recombinant huIFN2b: A quantitative study based on mixed feeding strategies....157
Abstract....157
5.1. Introduction....158
5.2. Materials and Methods....161
5.2.1. Strain and Media....161
5.2.2. Inoculum preparation....161
5.2.3. Real-time monitoring of huIFNα2b production by glycoengineered *P. pastoris* growth using heat PAT tools....162
5.2.3.1. Biocalorimeter experimental setup and principle....162
5.2.3.2. Dielectric Spectroscopy....164
5.2.4. Exhaust Gas Analyzer....165
5.2.5. huIFNα2b production....165

5.2.6. SCADA application....166
5.2.7. Feed program....167
5.2.8. Offline Analysis....168
5.3. Results....170
5.3.1. Assessment of mixed feeding strategies and their impact on huIFNα2b productivity....170
5.3.2. Calorespirometry and dielectric spectroscopy based monitoring of *P. pastoris* cultivation....172
5.3.3. Stoichiometric heat yield coefficient measurement....177
5.4. Discussion....179
5.4.1. Influence of constant feed rates exhibiting different proportions of mixed substrates....179
Calorimetric insight of the influence of mixed feed and methanol as sole substrate on huIFNα2b production....182
5.5. Conclusion....185
Chapter 6: Conclusions and Future Perspective....189
Bibliography....193
List of Publications....211
List of Conferences....213

List of Figures

Figure 1.1 Synthesis and biological actions of huIFNα2b through JAK-STAT pathway 5

Figure 1.2 Differences in glycosylation (post-translational modification) between the recombinant protein produced from wild type *P. pastoris* and glycoengineered *P. pastoris* (SuperMan5) strains. 15

Figure 1.3 Schematic representation of pAOX1 regulated batch cultivation of *P. pastoris* 21

Figure 1.4 Schematic representation of pAOX1 regulated fed-batch cultivation of *P. pastoris* 22

Figure 2.1 Schematic representation of N-glycoengineering approach and recombination events in *P. pastoris*.....39

Figure 2.2 Agarose gel displaying the colony PCR products of *E. coli* TOP10F′ cells transformed with ligation mixtures of linearized pPICZαA with native (Lane 1-5) or variant (Lane 6-10) of huIFNα2b encoding gene fragment is presented. Positions corresponding to the the molecular weight of various fragments in DNA marker lane (M) is shown on the right whereas position corresponding to the amplicon is represented on the left. 47

Figure 2.3 Agarose gel displaying the colony PCR products of *P. pastoris* Superman5 (pep4Δ prb1Δ) cells with no plasmid insert (Lane 1, control) or cells transformed with linearized pPICZαA-huIFNα2b-variant plasmid (Lane 2-7). Positions corresponding to the PCR products are indicated on the right whereas DNA marker (M) positions are represented on left.....48

Figure 2.4 Agarose gel displaying the colony PCR products of *P. pastoris* Superman5 (pep4Δ prb1Δ) cells transformed with linearized pPICZαA-huIFNα2b-native plasmid (Lane 1-5). Positions corresponding to the PCR products are indicated on the right whereas DNA marker (M) positions are represented on left. 49

Figure 2.5 Agarose gel displaying the colony PCR products of *P. pastoris* X33 cells transformed with linearized pPICZαA-huIFNα2b-native (Lane 1-3) or pPICZαA-huIFNα2b-variant plasmid (Lane 4-6). Positions corresponding to the PCR products are indicated on the right whereas DNA marker (M) positions are represented on left. 49

Figure 2.6 Dynamic profile of high cell density cultivation of *P. pastoris* SuperMan5 strain for the production of glycosylated huIFNα2b.....50
Figure 2.7 SDS-PAGE of fractions collected during His-tag affinity purification of huIFNα2b from the culture supernatant after HCDC of recombinant SuperMan5 strain.. Lane 1: crude supernatant, Lane 2: flow-through fraction, Lane 3: wash fraction, Lanes 4-11 corresponds to different elution fractions.. The protein molecular weight ladder (L) positions are represented on right whereas positions corresponding to non-glycosylated and glycosylated huIFNα2b are marked on the left. 51
Figure 2.8 SDS-PAGE of fractions collected during His-tag affinity purification of huIFNα2b from the culture supernatant after HCDC of recombinant X33 strain Lane 1: crude supernatant, Lane 2: flow-through fraction, Lane 3: wash fraction, Lanes 4-13 corresponds to elution fractions. The protein molecular weight ladder (L) positions are represented on left whereas positions corresponding to non-glycosylated and hyperglycosylated huIFNα2b are marked on the left.....52
Figure 2.9 SDS-PAGE of fractions collected during Concanavalin A purification of glycosylated huIFNα2b (SuperMan5) from the pooled fraction of His-tag affinity purification elutes Lane: initial sample, Lane 2: flow-through fraction, Lane 3: wash fraction, Lane 4: elution fraction. The protein molecular weight ladder (L) positions are represented on right whereas positions corresponding to non-glycosylated and glycosylated huIFNα2b are marked on the left. 52
Figure 2.10 SDS-PAGE analysis of by concanavalin A (Con A) chromatography purification of glycosylated huIFNα2b (X33) from the pooled fraction of His-tag affinity purification elutes. Lane 1: initial sample, Lane 2: flow-through fraction, Lane 3: wash fraction. Lane Lane 4-10 corresponds to elution fractions. The protein molecular weight ladder (L) positions are represented on left whereas positions corresponding to and hyperglycosylated huIFNα2b is marked on the left. 53
Figure 2.11 Immunodetection of hyperglycosylated huIFNα2b from X33 strain before and after treatment with PNGase F. A shift in the band with the loss of smear pattern can be observed after PNGase F treatment which specifically removed N-glycans. 54
Figure 2.12 SDS-PAGE analysis of size exclusion chromatography purification of non-glycosylated (native) huIFNα2b. A) From SuperMan5 strain, Lane 1: initial sample after his- chromatography, Lane 2-14 corresponds to elution fractions. The protein molecular weight ladder (L) positions are represented on the left. B) From X33 strain, Lane 1-13

corresponds to elution fractions and the protein molecular weight ladder (L) positions are represented on the right. 55
Figure 2.13 SDS-PAGE analysis of deglycosylation experiment for the purified non-glycosylated and glycosylated huIFNα2b from recombinant SuperMan5. Non-glycosylated huIFNα2b (lanes 1-3), glycosylated huIFNα2b (lanes 4-5), Absence (-) or presence (+) of PNGaseF is indicated on top of each lane. The protein molecular weight ladder (L) positions are shown on the left. Treatment of non-glycosylated with PNGase F did not show any difference in migration. Glycosylated huIFNα2b treated with PNGase F showed the difference in migration as compared to untreated. 56
Figure 2.14 MALDI-TOF mass spectrum of enzymatically released N- glycans from glycosylated huIFNα2b obtained from A) *P. pastoris* SuperMan5, the major signal at m/z 1579.67 corresponds to $Man_5GlcNAc_2$ glycan and other minor signals (m/z 2191.92, 2395.99, 2600.08) correspond to Man_8, Man_9 and Man_{10} glycans. B) *P. pastoris* X33, the major signals (m/z 2600.094, 2804.185, 3008.323, 3212.397, 3416.462, 3620.538, 4028.656, 4232.741) correspond to $Man_{10\text{-}18}GlcNAc_2$ N-glycans. 58
Figure 2.15 Antiviral activities of different forms of huIFNα2b against HCV and HEV replication. The dose dependent % inhibition of HCV (A) and HEV (B) subgenomic replicon after 48 h of post treatment in Huh7.5/Huh7.0 cells by different forms of huIFNα2b along with standard are depicted. The data represented are the means (± SEM) of three independent experiments. Statistical significance of the data was tested against the control by ANOVA followed by Dunnett's corrected *t* test (* $P < 0.05$; ** $P < 0.01$; *** $P < 0.001$; **** $P < 0.0001$; n.s- not significant).....60
Figure 2.16 Cytotoxicity analysis of different forms of huIFNα2b. (A) HCV (B) HEV. The % viablility of the cells (Huh7.5/Huh7.0) after the 2 h of treatment and the mean values (± SEM) are depicted.....61
Figure 2.17 Glycosylated huIFNα2b expressed by *P. pastoris* X33 and SuperMan5 strain 64
Figure 3.1 ANN architecture topology with input, hidden and output layers 82
Figure 3.2 Pareto chart for screening of significant variables by PBD. Y-axis represents different variables considered for PBD and the X-axis represents the standardized effect of the variables. The variables having standardized effect value greater than 5.84 are considered as significant at 99 %.....89

Figure 3.3 Contour plots of RSM-BBD optimization representing the interaction of A) Glycerol and ammonium sulphate. B) Methanol and ammonium sulphate. C) Glycerol and methanol 95
Figure 3.4 Scattered diagrams comparing the experimental data with the ANN predicted data at each stage. A) Training, B)Validation, C) Testing and D) Final 96
Figure 3.5 Evolution of best and mean fitness function through iteration by GA and optimum results of the three variables considered (1: glycerol, 2: ammonium sulphate, 3: methanol). A) Fitness graph and B) Variables optimum values graph.....97
Figure 3.6 Parity plot for RSM predicted (R^2=0.973) (A) and ANN predicted (R^2=0.999) (B) huIFNα2b titer with the observed huIFNα2b titer. 98
Figure 3.7 Dynamic plot representing capacitance (black line) and OUR (green line) in comparison with offline DCW (circle), measurements during fermentation process.....99
Figure 3.8 Correlation plot for the online capacitance (ΔC) and DCW with R^2=0.959. 100
Figure 3.9 Dynamic plot for offline DCW (red filled circle with continuous line), glycerol (brown invert triangle with continuous line), methanol (green cross with continuous line) and huIFNα2b (violet filled square with continuous line) during the high cell density cultivation. The data points represented in this plot are average values with standard error. 101
Figure 3.10 Experimental data (points) and simulation (continuous lines) of glycerol phase growth of *P. pastoris* on optimized medium a) Monod model (R^2 (biomass) =0.98 and R^2 (substrate) =0.98), b) Moser model (R^2 (biomass) =0.92 and R^2 (substrate) =0.99) and c) Contois model (R^2 (biomass) =0.97 and R^2 (substrate) =0.91), Capacitance (blue circle), Substrate (red triangle). 102
Figure 3.11 Purification of recombinant huIFNα2b expressed in the basal salt medium in bioreactor study by His-Tag affinity chromatography. Lanes 1-13 shows elution fractions and Lane L shows protein ladder. 103
Figure 3.12 Purification of glycosylated recombinant huIFNα2b by concanavalin A (Con A) chromatography. Lane 1 shows initial sample, Lane 2 shows flow-through fraction, Lane 3 shows wash fraction, Lane 4 shows elution fraction and Lane L shows protein ladder. 104

Figure 3.13 Deglycosylation analysis of the purified glycosylated recombinant huIFNα2b. Lane L shows protein ladder, Lane 1 shows untreated protein sample, and Lane 2 protein sample treated with PNGaseF. 104
Figure 3.14 Anti-proliferative activity of the purified recombinant huIFNα2b on breast cancer cell lines (MCF7). Y-axis represents % relative cell viability whereas X-axis represents the type of huIFNα2b used. The values are statistically significant at P<0.001 (***) as analyzed by ANOVA.....105
Figure 4.1 Schematic representation of the Dielectric Spectroscopy principle.....117
Figure 4.2 Schematic representation of bioreactor experimental setup with the PID control of specific growth rate based on capacitance signal.....121
Figure 4.3 PID control loop representing overall process flow and controller action. ε(S), P(S), F(S), G(S), C(S) are the respective transfer functions.....123
Figure 4.4 Correlation between the developed capacitance signals, ΔC (pF/cm) with the DCW (g/L) obtained at two different control runs. 130
Figure 4.5 Typical dynamic plot of *P. pastoris* huIFNα2b fermentation (μ_{sp}=0.03 h^{-1}) representing various process analyzers viz. Capacitance (pF/cm) (Black continuous), CER (m.mol/L.h) (Green continuous), OUR (m.mol/L.h) (Pink Continuous) and compared with corresponding offline values such as DCW (g/L) (red continuous with filled circle) and huIFNα2b (mg/L) (blue continuous with filled square). 131
Figure 4.6 A) Dynamic methanol uptake profile by *P. pastoris* cultivation during repeated methanol pulse feeding at the induction phase: Duration 62 – 64 h (Open Circles), Duration70 – 72 h (Open Triangles), Duration 77 – 79 h (Open Squares). $q_{s,met}$ was calculated from the ratio of volumetric methanol utilization (g/L.h) to biomass concentration. B) Influence of methanol (Open Triangles) utilization (g/L) on developed capacitance signal (ΔC), pF/cm (Continuous dark grey line) at 70 – 72 h.....133
Figure 4.7 Exponential feedback control of methanol (Dark grey line) during induction phase: Capacitance signal, ΔC (Dark Continuous line); Methanol (Dark grey line); Scatter plots representing methanol concentration values during various μ_{sp} runs: A) Open Open Circles ($\mu_{sp} = 0.015\ h - 1$), B) Open Squares ($\mu_{sp} = 0.03\ h - 1$, C) Open Triangles down ($\mu_{sp} = 0.04\ h - 1$), D) Open Triangles up ($\mu_{sp} = 0.06\ h - 1$) 137

Figure 4.8 PID controller performance based on comparative evaluation of μ_{sp}, μ_{est} and $\mu_{offline}$ values: Dark continuous lines representing μ_{sp}, Dark grey continuous lines representing $\mu_{est,}$ Dark circles with continuous lines representing $\mu_{offline}$.....140
Figure 4.9 Influence of specific growth rate on A) DCW and B) Influence of specific growth rate on huIFNα2b production: Open Circles(μ_{sp}=0.015 h^{-1}), Open Squares (μ_{sp}=0.03 h^{-1}), Filled triangles (μ_{sp}=0.04 h^{-1}), Open Triangles (μ_{sp}=0.06 h^{-1}).....141
Figure 4.10 Influence of different specific growth rate (μ_{sp}) on huIFNα2b titer, specific productivity (q_P) and protein yield coefficient ($Y_{P/X}$).....142
Figure 4.11 Purification of recombinant huIFNα2b by His-Tag affinity chromatography. Lanes 1-9 shows elution fractions and Lane L shows protein ladder. In lane 1-9, 25 µL of sample was loaded and in lane L, 10 µL of protein ladder was loaded. 143
Figure 4.12 Purification of recombinant glycosylated huIFNα2b by Con A chromatography. Lanes 1 shows elution fraction containing purified huIFNα2b and Lane L shows protein ladder. In lane 1, 15 µL of sample was loaded and in lane L, 10 µL of protein ladder was loaded 143
Figure 4.13 Antiproliferative effect of the purified huIFNα2b and standard huIFNα2b against breast cancer cell lines. A) T47D B) MCF7. The assay was performed in five replicates. The values are statistically significant at P<0.001 (***) as analyzed by ANOVA. 145
Figure 5.1 Schematic representation of biocalorimetric setup for glyoengineered *P. pastoris* cultivation using methanol as sole carbon source and mixed substrates for huIFNα2b production. ΔC; change in capacitance, T_j; jacket temperature, T_r; temperature of the reaction broth 164
Figure 5.2 Dynamic plots representing OUR, CER and feed rate profileduring different feeding strategies.A. Methanol, B. Methanol + Glycerol, C. Methanol + Sorbitol were continuously fed at their respective flow rates (Black Continuous) and the residual concentrations of substrates were measured and represented: Methanol (Filled upright triangle), Glycerol (Open circles) and Sorbitol (Open squares). Comparison plot representing OUR (Red Continuous) and CER (Green Continuous) signals in concordance with the feed rates. 1: Glycerol growth phase, 2: Pulsed methanol feed during adaptation/transition phase and 3: continuous methanol feed under fully adapted condition (significant increase in biomass).....172
Figure 5.3 Dynamic plot representing the production of huIFNα2b (Green upright triangles) by glycoengineered *P. pastoris* using methanol as sole carbon source and co-

feeding sorbitol and glycerol with methanol. A). Methanol, B). Methanol + Glycerol, C. Methanol + Sorbitol. Correlation between heat rate signal (Continuous black), capacitance signal, ΔC (Continuous red) and DCW (Filled circles) were represented in the same plot. 176

Figure 5.4 Heat yield coefficients of biomass formation and O_2 utilization during glycerol (A and C) and induction (B and D) phases respectively of different co-substrates and methanol as sole carbon source. Methanol (Open circles), Methanol + Glycerol (Open squares) and Methanol + Sorbitol (Open upright triangles). 178

List of Tables

Table 1.1 Expression of recombinant huIFNα2b in different expression systems 8

Table 1.2 Advantages and disadvantages of different recombinant expression systems in huIFNα2b production.....9

Table 1.3 List of approved Interferon alpha 2b drugs in the market.....10

Table 1.4 Examples of N-glycoengineering in human proteins of therapeutic importance 16

Table 1.5 Feedback control strategies with different PAT tools implemented for production of different recombinant proteins of therapeutic importance in *P. pastoris*...27

Table 2.1 Mean (±SEM) value of the pharmacokinetic parameter after single dose subcutaneous administration of huIFNα2b sample in female Wistar rats (n=3 per each huIFNα2b).....62

Table 2.2 Production of huIFNα2b in batch and fed batch cultivation processes.....65

Table 3.1 Levels of the medium components and parameters used in Plackett-Burman design 80

Table 3.2 Comparison of statistical parameters of artificial neural network model. 82

Table 3.3 Plackett-Burman experimental design with response 90

Table 3.4 Coded levels and actual values of medium components for RSM-BBD.....91

Table 3.5 BBD experimental design with predicted and observed response 93

Table 3.6 ANOVA table of RSM experiments for huIFNα2b production.....94

Table 3.7 Comparison table for RSM-BBD and ANN-GA validation experiments.....98

Table 3.8 Estimated kinetic parameter values for the selected kinetic models.....102

Table 4.1 Assessment of pulsed feed strategy on μ_{est} during methanol induction phase 132

Table 4.2 Assessment of feedback control strategies employing different μ_{sp} 135

Table 4.3 Assessment of PID controller performance 139

Table 4.5 Production of huIFNα2b in batch and fed batch cultivation processes.....152

Table 5.1 Non-biological heat rates due to different reactor operating parameter and their corresponding governing equations 163

Table 5.2 Growth kinetic, huIFNα2b concentration and heat yield parameters obtained for 3 distinct feeding combinations of methanol 175

Glossary of Acronyms

AARD	Absolute Average Relative Deviation
AIDS	Acquired Immuno Deficiency Syndrome
ANN	Artificial Neural Network
ANOVA	Analysis of Variance
AOX	Alcohol Oxidase
BBD	Box- Behnken Design
BMGY	Buffered Glycerol-Complex Medium
BMMY	Buffered Methanol-Complex Medium
BioPAT	BioProcess Analytical Technology
CER	Carbon-dioxide Evolution Rate
CHO	Chinese Hamster Ovary
ConA	Concanavalin A
CPP	Critical Process Parameter
CQA	Critical Quality Attribute
DAQ	Data Acquisition
DCW	Dry Cell Weight
DNA	Deoxyribonucleic Acid
DO	Dissolved Oxygen
DoE	Design of Experiments
DPBS	Dulbecco's Phosphate Buffered Saline

DR	Data Reconciliation
DS	Dielectric Spectroscopy
DMEM	Dulbecco's Modified Eagle Medium
DMSO	Dimethyl Sulfoxide
DTT	Dithiothreitol
EDTA	Ethylenediaminetetraacetic Acid
ELISA	Enzyme Linked Immuno Sorbent Assay
ER	Endoplasmic Reticulum
FBS	Fetal Bovine Serum
FDA	Food and Drug Administration
FLD	Formaldehyde Dehydrogenase
FTIR	Fourier-Transform Infrared Spectroscopy
GA	Genetic Algorithm
GAP	Glyceraldehyde-3-Phosphate
GlcNAc	N-acetylglucosamine
GM-CSF	Granulocyte-Macrophage Colony-Stimulating Factor
HCDC	High Cell Density Cultivation
HCV	Hepatitis C Virus
HEK	Human Embryonic Kidney
HEV	Hepatitis E Virus
HPLC	High Performance Liquid Chromatography
HSA	Human Serum Albumin

huIFNα2b	Human interferon alpha 2b
IFN	Interferon
IFNAR	Interferon Alpha/Beta Receptor
ISG	Interferon Stimulated Gene
ISGF3	Interferon Stimulated Gene Factor 3
ISRE	Interferon Stimulated Response Element
JAK	Janus Kinase
LB	Luria-Bertani
MALDI-TOF	Matrix-Assisted Laser Desorption/Ionization, Time of Flight
Man	Mannose
MM	Minimal Methanol
MS	Mass Spectrometry
MTT	3-(4,5-dimethylthiazol-2-yl)-2,5-diphenyl tetrazolium bromide
NESP	Novel Erythropoiesis Stimulating Protein
OCH	α1, 6 Mannosyl-transferase
OD	Optical Density
ODE	Ordinary Differential Equation
OST	Oligosaccharyltransferase
OTR	Oxygen Transfer Rate
OUR	Oxygen Uptake Rate
pAOX	Alcohol Oxidase Promoter
PAT	Process Analytical Technology

PBD	Plackett-Burman Design
PBS	Phosphate Buffer Saline
PCR	Polymerase Chain Reaction
PEG	Polyethylene glycol
pGAP	Glyceraldehyde-3-Phosphate Promoter
PHO	Phosphate-Responsive
PID	Proportional Integral Derivative
PMAA	Partially Methylated Alditol Acetates
PNGase F	Peptide -N-Glycosidase F
PTM	*Pichia* Trace Metals
PVDF	Polyvinylidene difluoride
QbD	Quality by Design
RMSE	Root Mean Square Error
RNA	Ribonucleic Acid
RPM	Revolutions Per Minute
RSM	Response Surface Methodology
SCADA	Supervisory Control And Data Acquisition
SEM	Standard Error of the Mean
scFv	Single Chain Variable Fragment
SDS-PAGE	Sodium Dodecyl Sulfate–Polyacrylamide Gel Electrophoresis
STAT	Signal Transducer and Activator of Transcription Proteins
VCV	Viable Cell Volume

YNB	Yeast Nitrogen Base
YPD	Yeast extract Peptone Dextrose
YPG	Yeast Peptone Glycerol
YPDS	Yeast extract Peptone Dextrose Sorbitol

List of Notations

Variables

ΔC	capacitance, $^{pF}/_{cm}$
G	conductivity, $^{mS}/_{cm}$
K_S	saturation constant $^{g}/_{L}$
K_{SC}	contois saturation constant $^{g}/_{L}$
n	moser constant
F_{FB}	methanol flow rate regulated by feed – back controller, L/h
F_0	initialized feed rate, L/h
F_M	methanol feed rate, L/h
$\dot{m}_g$	mass flow rate of gas, L/s
$\dot{m}_w$	mass flow rate of water, L/s
q_J	heat flow from reaction broth to jacket, W/L
q_C	compensation heat rate, W
q_E	environmental heat loss, W/L
q_S	agitation heat rate, W/L
q_A	aeration heat loss, $^{W}/_{L}$
q_B	biological heat rate, W/L
q_p	specific productivity, g/g. h
r_p	volumetric productivity, mg/L. h
r_x	volumetric rate of biomass production, g/L. h
S	residual substrate concentration, g/L
$C_{p,r}$	specific heat of reaction broth, kJ/(kg K)
T_r	reactor temperature, K
$T_{j,in}$	jacket inlet temperature, K
T_{jout}	jacket outlet temperature, K
$y_{O2,in}$	mole fraction of O_2 in air inlet stream

$y_{O2,out}$	mole fraction of O_2 in air outlet stream
$y_{CO2,in}$	mole fraction of CO_2 in air inlet stream
$y_{CO2,out}$	mole fraction of CO_2 in air outlet stream
$y_{inert,in}$	mole fraction of N_2 in air inlet stream
$y_{inert,out}$	mole fraction of N_2 in air outlet stream
r_{O_2}	volumetric rate of O_2 utilization, $^{m.\,mol}/_{L.\,h}$
r_{CO_2}	volumetric rate of CO_2 production, $^{m.\,mol}/_{L.\,h}$
S_{met}	methanol concentration in Feed stream, g/L
k_c	proportional controller gain
$q_{s,met}$	specific utilization rate of methanol per unit biomass, $\frac{g.\,methanol\ utilized}{g.\,biomass.\,h}$
q_S^{max}	maximum substrate uptake
$q_{huIFN\alpha2b}$	specific huIFNα2b productivity, $\frac{mg\ huIFN\alpha2b}{g.\,biomass.\,h}$
V_R	volume of reaction broth, L
V_0	reactor volume, L
X_0	initial biomass concentration, g/L
$Y_{X/_{gly}}$	biomass yield during glycerol phase, $\frac{g.\,of\ biomass\ formed}{g.\,of\ glycerol\ consumed}$
$Y_{X/_{met}}$	biomass yield during methanol phase, $\frac{g.\,of\ biomass\ formed}{g.\,of\ methanol\ consumed}$
$Y_{C/_{gly}}$	biomass yield during glycerol phase, $\frac{capacitance.\,of\ biomass\ formed}{g.\,of\ glycerol\ consumed}$
$Y_{Q/_X}$	biomass heat yield coefficient, kJ/g
$Y_{P/_X}$	product yield coffecient
$Y_{Q/_{O_2}}$	oxygenic heat yield coefficient, kJ/mol. O_2
$Y_{Q/_S}$	biomass heat yield coefficient, $kJ/C-mol$
$Y_{X/_S}$	biomass yield per substrate consumed
$Y_{X/_{IP}}$	biomass yield per substrate consumed during induction phase
$Y_{X/_{O_2}}$	biomass yield due to oxygen uptake

Greek Symbols

ϵ	permittivity, F/m
μ	specific growth rate, h^{-1}
μ_{est}	estimated specific growth rate, h^{-1}
μ_{gly}	specific growth rate during glycerol phase, h^{-1}
μ_{met}	specific growth rate during methanol phase, h^{-1}
μ_{sp}	specific growth rate (set point), h^{-1}
μ_{max}	maximum specific growth rate, h^{-1}
$\mu_{offline}$	offline specific growth rate, h^{-1}
μ_{IP}	induction phase specific growth rate, h^{-1}
τ_I	integral time (Reset rate), min.
τ_D	derivative time, min
τ	torque, N. m

Synopsis

The emergence of the biopharmaceutical industry through the advent of recombinant therapeutic proteins has represented a significant revolution in modern medicine and is currently represents the most important segment in the global pharmaceutical market growing at a faster pace. Interferon alpha 2b (cytokine) is one of the biopharmaceuticals which has gained much importance for its antiviral, antiproliferative and immunomodulatory functions. FDA approved recombinant human IFN-α2b drugs available in the market are predominantly produced from the *E. coli* expression system, which is non-glycosylated and pegylated. Like other low molecular weight protein drugs, IFN-α2b has a relatively short serum half-life following subcutaneous injection. Due to its fast renal clearance from the blood, unmodified IFN-α2b monotherapy requires multiple doses during treatment resulting in the onset of adverse effects. To overcome the short serum half-life of IFN-α2b, pegylated IFN-α2b was developed by chemical conjugation of polyethylene glycol (PEG) molecules. The most common problem allied with refolded and pegylated IFN-α is the formation of neutralizing antibodies. These antibodies were found to be associated with treatment failure in HCV-infected patients. Human IFN-α2b expression in mammalian cell lines results in significant heterogeneity in glycan moieties, inconsistent product quality and high production cost which are significant drawbacks of this expression platform. Potential scope exists for the design and development of a successful expression platform for enhanced humanized IFN-α2b production with the improved pharmacokinetic property. This proposed work addresses the above said drawbacks and challenges by successful enhanced production of homogenous N-glycosylated human IFN-α2b with improved biological properties in

glycoengineered *P. pastoris* through glycoengineering, medium optimization and Process Analytical Technology (PAT) approaches.

Chapter 1 covers the background, brief review of literature and definition of the problem for the present study with detail emphasis on the bottlenecks involved with different huIFNα2b production platforms, approaches that can be taken up and the envisaged objectives to resolve the issues in the current state of the art technology. It specifically reviews the *Pichia pastoris* as a expression host for recombinant proteins and the studies reported for production of huIFNα2b using this system. It also describes the PAT enabled approaches for the bioprocess monitoring and control of the fermentation process with particular emphasis on dielectric spectroscopy and biocalorimetry as PAT tools.

Chapter 2 describes the successful expression of homogenous human-like N-glycosylated huIFNα2b by the application of glycoengineering strategy and the glycoengineered SuperMan5 *P. pastoris* strain. The expressed glycosylated huIFNα2b exhibited a 1.3-fold increase in the plasma half-life compared to non-glycosylated huIFNα2b produced from *E. coli* with no loss of antiviral activity against HCV/HEV system and also the purified glycosylated huIFNα2b was not cytotoxic to the human cell lines. The N-glycosylated huIFNα2b reported in this chapter offers the double advantage of retention of full antiviral activity with improved pharmacokinetic property (plasma half-life), which exemplifies the considerable scope for its commercialization in the near future.

Chapter 3 describes the DoE (PBD, RSM-BBD) and artificial intelligence (ANN-GA) based optimization studies to maximize the production of huIFNα2b in recombinant glycoengineered *P. pastoris.* The optimized medium resulted in 57.18 ± 1.87 mg/L of huIFNα2b at shake flask level with ANN-GA model proved to be the best compared to

RSM-BBD model. A bioreactor study with an optimized medium resulted in biomass yield of 0.856 g/g and huIFNα2b titer of 436 mg/L. It also describes the deployment of dielectric spectroscopy and respirometry as PAT tools to provide real-time insights into the cell physiology during different phases of the fermentation process. The purified glycosylated huIFNα2b was biologically active based on its anti-proliferative activity against human breast cancer cell lines.

Chapter 4 describes the simple and robust PAT (Dielectric spectroscopy) based feed-back control strategy for effective control of specific growth rate (μ, a critical process parameter) during the methanol induction phase for achieving the higher huIFNα2b yield. From the feedback control at different μ setpoint (0.015, 0.03, 0.04, 0.06 h^{-1}), μ_{met} = 0.04 h^{-1} resulted in an enhanced huIFNα2b (1483 mg/L) titer and specific productivity (q_P=0.457 mg huIFNα2b /g.biomass.h) reported till date. The purified huIFNα2b was biologically active exhibiting antiproliferative activity in human breast cancer cell lines (T47D and MCF7).

Chapter 5 describes the calorimetric investigation of glycoengineered *P. pastoris* cultivation for huIFNα2b production with complimentary PAT tools for obtaining the real-time metabolic insight on the assimilation of substrate and co-substrates under mixed feed conditions. From the experiments with different mixed feeding approaches, methanol and sorbitol mixed feeding at 0.8 C-mole/0.2 C-mole was found to be more efficient with 57 % reduction in heat yield and 2 fold enhancement in volumetric productivity of huIFNα2b as compared to sole methanol feeding.

Chapter 6 describes the summary of the key research findings obtained from the present thesis work and provides a glimpse on the future perspective of this research work.

Chapter 1

Introduction and Review of Literature

भारतीय प्रौद्योगिकी संस्थान गुवाहाटी
Indian Institute of Technology Guwahati

Chapter 1

Introduction and review of literature

1. Interferons

In 1957, Alick Isaacs, a British bacteriologist, and Jean Lindenmann, a Swiss microbiologist, co-discovered a soluble factor secreted by influenza virus-infected chick cells. This factor interfered with the natural susceptibility of the other cells in the media to homologous and heterologous viral attacks and was aptly named "interferon" [1]. In 1958, Nagano and Kojima reported similar findings that led to the detailed elucidation of the interferon system [2]. Interferons (IFNs) are pluripotent cytokines produced in response to various synthetic as well as biological stimuli. They represent the first line of defense components, arising from a multigene family with the ability to induce potent antiviral, antiproliferative, and immunomodulatory activities against a broad range of mammalian viruses [3]. Interferons are grouped into three classes called Type I, II, and III IFNs, according to their amino acid sequence. Type I IFNs, discovered in 1957 by Isaacs and Lindenmann, comprise a large group of molecules; mammals have multiple distinct Type I IFN-α genes (13 in humans), one to three IFN-β genes (1 in humans) along with other variants, such as IFN-ω, ε, τ, δ, and κ. The IFN α and β genes are induced directly in response to viral infection, whereas IFN-ω, ε, τ, δ, and κ play less well-defined roles, such as regulators of maternal recognition in pregnancy. Type II IFNs has a single member, IFN-γ, and is secreted by mitogenically activated T cells and natural killer cells, rather than by an indirect response to viral infection [4]. Type III IFNs have been discovered more recently and comprise IFN-λ_1, IFN- λ_2, and IFN-λ_3, also referred to as IL-29, IL-28A, and IL-28B, respectively[5, 6]. These cytokines also induced an indirect response to viral infection and appeared to use the same pathway as

like IFN-α/β genes against viral infection [7]. Type I IFN (IFN-α/β) and Type II IFN (IFN-γ) shared no apparent structural homology. However, functional similarities exist due to a broad overlap in the types of genes that they induce [8]. Type I IFNs primarily consists of IFN-α genes of which IFNα2 has potential therapeutic applications. IFNα2 genes are part of a heterologous group of proteins with similar biological activities. The three principal subtypes of IFNα2 are designated α2a, α2b, and α2c [9]. The individual proteins have molecular masses between 19 and 20 kDa and consist of 165–166 amino acids [10].

1.1. Human interferon alpha 2b

Human interferon alpha 2b (huIFNα2b) is an intronless sequence that encodes a protein polypeptide of 165 amino acids [11, 12]. It contains four cysteine residues forming two disulfide bridges [13] and can trigger multiple responses that may be antiviral, antibacterial, antiproliferative, or even immunomodulatory [14]. Therefore, huIFNα2b either on its own or in combination with other interferons is being extensively used in prophylaxsis of type B and C hepatitis, [15, 16] as well as several cancers such as melanoma,[17-19] AIDS-related Kaposi's sarcoma, [20] chronic myeloid lymphoma, [21] and angioblastoma [22]. The structure of huIFNα2b is composed of five α-helices (A–E) linked by one long overhand connection (AB loop) and three short segments (BC, CD, and DE loops), with the topology of the molecule resembling the classical up-up-down-down four-helix bundle motif [23]. The intronless sequence huIFNα2b exerts its biological actions by binding to cell surface receptors (IFNAR1 and IFNAR2) and thereby activating the JAK-STAT signal transduction pathway [24]. This pathway leads to the activation of the receptor-associated tyrosine kinases JAK1 and Tyk2, which phosphorylate STAT1 and STAT2. Phosphorylated STAT1 and STAT2 interact strongly with each other by recognizing SH2 domains, and the stable STAT1–STAT2 hetero-

dimer is translocated into the nucleus, where it interacts with the DNA-binding protein P48 or IRF-9. The IRF-9–STAT1–STAT2 hetero-trimer is called IFN-stimulated gene factor 3 (ISGF3), and it binds to a sequence motif (the IFN-stimulated response element, or ISRE) in target promoters. This binding brings about transcriptional activation of hundreds of interferon-stimulated genes (ISGs) (Figure 1.1) that are involved in antiviral, antiproliferative, and immunomodulatory activities [25-27].

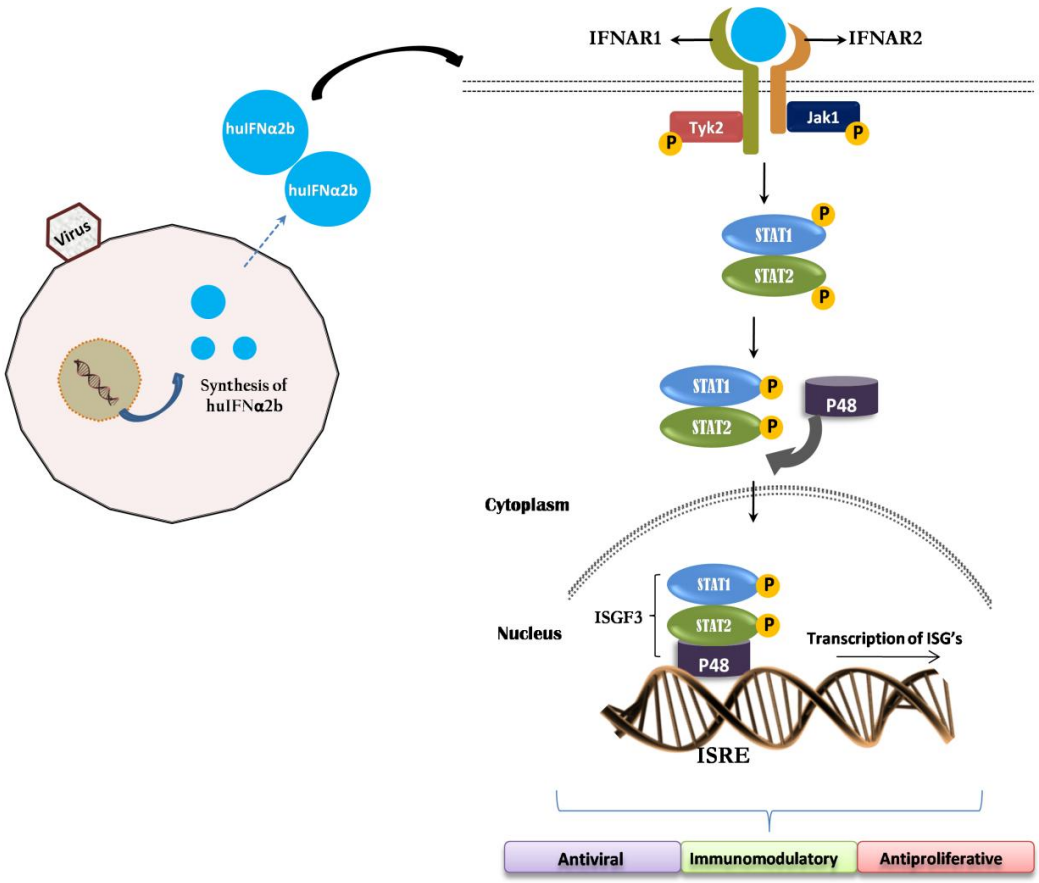

Figure 1.1 Synthesis and biological actions of huIFNα2b through JAK-STAT pathway

1.2. Biological Route for the Production of Recombinant huIFNα2b

Interferons, produced naturally, are scarce and very expensive. With the advent of DNA recombination technologies in the 1980s, recombinant protein production using prokaryotic, eukaryotic, and mammalian expression systems has emerged as a

compelling substitute for the protein extraction from natural sources [28]. Consequently, the production of recombinant huIFNα2b was explored using different expression systems, namely, bacteria, yeasts, insect cell lines, mammalian cell lines, and plants. The Gram-negative bacterium (*Escherichia coli*) is considered as potential host for the production of the recombinant human IFNα [29, 30] owing to its of rapid growth, simple cultivation, and availability of genetic tools. Therefore, the first FDA-approved recombinant huIFNα2b drug (Intron A) was produced using an *E. coli* expression system. Even though the *E. coli* expression system is the preferred host, it has been associated with significant drawbacks for instance, codon bias, the formation of inclusion bodies, and the lack of post-translational modifications. Codon bias is often reported as a significant problem while expressing eukaryotic proteins in *E. coli* because of a difference in codon usage. The low-level expression of human alpha interferons in *E. coli*, especially α2 subtype, is correlated with the presence of clusters of AGA/AGG codons (rare codons in *E. coli*) [31]. Formation of inclusion bodies is another serious problem in which 50 % of the expressed recombinant huIFNα2b was lost during the renaturation process and found to be a major bottleneck for the biopharmaceuticals industry [32, 33]. Besides, the recombinant huIFNα2b produced from *E. coli* lacks the post-translational O-glycosylation to be present on the naturally synthesized protein. This non-glycosylated form of recombinant huIFNα2b has a shorter serum half-life than that of the glycosylated huIFNα2b [34]. Other bacterial expression systems used for the recombinant huIFNα2b production include *Streptomyces lividans* [35] and *Bacillus subtilis* [36]. Mammalian, and other human cell lines are expression systems of choice for the production of secreted recombinant proteins (e.g., antibodies). They allow post-translational modifications, yielding up to milligram to gram quantities of purified product per liter of culture [37-39]. However, the volumetric productivity of human cells

for given proteins such as cytokines (i.e.,huIFNα2b) is often lower by several orders of magnitude. Initially, huIFNα2b for therapeutic use was purified from the human lymphoblastoid Namalwa cell line following induction with Sendai virus. Despite the production of an IFNα with high biological activity, Namalwa cells were abandoned due to limited productivity that was unable to supply an ever-growing demand. The studies have reported the successful production of recombinant huIFNα2b in mammalian cell lines such as CHO and HEK293 [40, 41]. Though mammalian cells produce glycoproteins proximate to humans, the heterogeneity of glycans obtained, batch to batch variation, low yield, challenges of scale-up, associated problems, and high production costs are major drawbacks of this expression platform [42]. Other systems that have been tested for the production of huIFNα2b (Table 1.1) include avian eggs, [43, 44] insect cells [45], mouse myeloma cell line [46], transgenic mice milk [47], and carrot plants [48]. All these expression systems are also associated with the drawbacks related to mammalian and prokaryotic expression systems. The advantages and disadvantages of different recombinant expression systems for recombinant huIFNα2b production are detailed in Table 1.2. FDA approved recombinant huIFNα2b drugs available in the market are predominantly produced from bacterial (*E. coli*) expression systems, which are non-glycosylated and pegylated. A comparative assessment of the biological activity, brand, and origin of huIFNα2b expressed in different hosts are listed in Table 1.3.

Table 1.1 Expression of recombinant huIFNα2b in different expression systems

Host	huIFNα2b Conc. (mg/l)	Glycosylation	Reference
E.coli	75	No	[49]
E.coli	5200	No	[33]
E.coli	3500	No	[32]
E.coli	0.336	No	[50]
S. lividans	0.01	No	[51]
Y. lipolytica	425	-	[52]
P. pastoris	400	-	[53]
P. pastoris	450	-	[54]
P. pastoris	200	-	[55]
P. pastoris	600	-	[56]
P. pastoris	300	-	[57]
Insect Sf9 cells	-	Partial	[58]
HEK 293 cells	333	Yes	[41]
Mouse NS0 cells	120	Yes	[46]
Hen Egg	0.27	Partial	[44]
Transgenic mice milk	0.03	-	[47]
Tobacco BY2 cells	0.02	No	[59]
Carrot	-	-	[48]

Table 1.2 Advantages and disadvantages of different recombinant expression systems in huIFNα2b production

Expression System	Advantages	Disadvantages
E. coli	• Very fast growth rate • High protein yields • Low production cost	• Lack of post-translational modifications • Formation of inclusion bodies and thereby affecting structure and increase in purification cost • Presence of endotoxins
Yeast (Wild Type)	• Fast growth rate • High protein yield • Performs post-translational modifications • Proper protein folding	• Lack of complex post-translational modifications • Hypermannosylation-type glycosylation
Insect Cell Lines	• Good expression yield • Proper protein folding • Perform post-translational modifications	• Slow growth rate • High production cost • Complex non-human type of glycosylation
Mammalian Cell Lines	• Proper protein folding • Perform simple and complex post-translational modifications	• Slow growth rate • Protein with non-human glycoforms including N-glycolylneuraminic acid • High production cost • Very low protein yield • Viral contamination • Batch to batch variation and product heterogeneity

Table 1.3 List of approved Interferon alpha 2b drugs in the market

huIFNα2b brand name	Type of huIFNα2b molecule	Expression host	Specific activity (IU/mg)	Manufacturer
Intron A	Non-glycosylated	*E. coli*	2.6×10^8	Merck Sharp and Dohme
Shanferon	Non-glycosylated	*P. pastoris*	4.4×10^8	Shantha Biotechnics Pvt. Ltd.
Intalfa 2b	Non-glycosylated	*E. coli*	2.6×10^8	Intas Pharmaceuticals Pvt. Ltd.
Viraferon	Non-glycosylated	*E. coli*	2.6×10^8	Fulford (India) Ltd.
Realfa 2b	Non-glycosylated	*E. coli*	2.6×10^8	Kee Pharma Ltd.
Viraferon-peg	Pegylated	Chemical conjugation of PEG molecule to *E. coli* expressed huIFNα2b	0.7×10^8	Fulford (India) Ltd.
PegIntron	Pegylated	Chemical conjugation of PEG molecule to *E. coli* expressed huIFNα2b	0.7×10^8	Schering Corporation

Inorder to overcome the disadvantages of other expression platforms (bacteria, mammalian cell lines, insect cell lines, and plants), yeasts are preferred as the most suitable and attractive hosts for the production of various recombinant proteins/biopharmaceuticals among the different eukaryotic microorganisms. They offer numerous advantages over other expression systems and include superior fermentation characteristics, such as high cell density cultivation, lower nutritional demands, extracellular secretion of produced recombinant proteins, and high protein yields, which make the production process more economical [60]. Besides, the recombinant products produced through yeast platforms are free of endotoxins, oncogenic, and viral DNA. Yeast species used for recombinant huIFNα2b production includes *S. cerevisiae*, *P. pastoris*, and *Y. lipolytica*. Though studies have shown the successful expression of huIFNα2b in *S. cerevisiae* is reported [61], it is associated with various metabolic bottlenecks, such as inefficient secretion of the produced protein, protein misfolding in the endoplasmic reticulum, low protein yields (because of its crab tree–positive nature), hyperglycosylated and the presence of terminal allergic α-1,3 mannose in attached N-glycan. These disadvantages have led to the development of alternate nonconventional yeasts (*P. pastoris* and *Y. lipolytica*) for the expression of huIFNα2b. On the other hand, *Y. lipolytica* offers many advantages over the conventional yeast (*S. cerevisiae*) but the protein titers are far lower as compared to *P. pastoris* and require further investigation enhance huIFNα2b yield.

1.3. *P. pastoris* as expression system for the production of huIFNα2b

P. pastoris, a methylotrophic or ascosporous yeast, was first isolated in 1919, and later in the 1980s it was transformed into a heterologous host system for the production of various recombinant proteins [62]. *P. pastoris* proved to be a successful expression system for the production of different therapeutic proteins.

It offers numerous advantages, which include

- Strongly and tightly regulated inducible AOX1 (alcohol oxidase) promoter which is well suited for controlled expression of foreign genes.
- Ease molecular genetic manipulation similar to technique adapted for *S. cerevisiae.*
- Availability of well developed *P. pastoris* strains and vectors as expression kits to academic research laboratories.
- The strong preference of *P. pastoris* for respiratory growth, a key physiological trait that greatly facilitates its culturing at high-cell densities relative to fermentative yeasts.
- Ease of purification of the extracellular expressed recombinant protein, since *P. pastoris* do not secrete much of its native proteins outside cells.

It has many advantages over conventional yeast (*S. cerevisiae*), including less extensive hypermannosylation, absence of immunogenic α-1,3 mannose, crabtree negative, and high protein yields. The success of *P. pastoris* in the production of recombinant proteins is directly linked to the very strong and tightly regulated promoter of the gene encoding the first enzyme of the methanol utilization pathway, AOX1. *P. pastoris* contains two alcohol oxidase promoters, AOX 1 and AOX 2, of which AOX 1 is more tightly regulated and expressed when compared to AOX 2. Based on the AOX promoter's activity for methanol utilization, Mut^+ (methanol utilization positive), Mut^- (methanol utilization negative), and Mut^s (methanol utilization slow) are the three available *Pichia* phenotypes. Expression level of AOX 1 is about 30 % of total soluble protein [63]. Apart from AOX 1 and AOX 2 promoters, alternative promoters are also present for the expression of recombinant proteins, which include GAP, FLD1, PEX8, and YPT1; however, AOX 1 remains the best option. There are different secretion signals, such as

PHO1 and α-pre pro sequence (*S. cerevisiae*), available for *P. pastoris* to facilitate the release of recombinant proteins either in the intracellular or the extracellular environment. Of all the secretion signals available for *Pichia* vectors, α-pre pro sequence has been reported as the best for the extracellular secretion of recombinant protein. The first report on the expression of recombinant huIFNα2b showed an expression level of 400mg/L with a biological activity of $1x10^7$ IU/mg, [53] which is lower than natural human interferon ($2x10^8$ IU/mg) [64]. In another study, authors showed an expression level of 298 mg/L with activity levels of $1.9x10^9$ IU/mg using *P. pastoris* Mut^+ and pPICZα vector. Also, a decrease in temperature from 30°C to 20°C during the methanol feed phase increased the yield of protein dramatically [65]. The use of three different secretion signals *viz*., native secretion signal, α-pre pro sequence, and mutated α-pre pro sequence addressed the for efficient expression of recombinant huIFNα2b [55]. Plasmid with a huIFNα2b gene along with a mutated α-pre pro sequence showed a single band of 19.2 kDa by MALDI-TOF. Conversely, plasmids with a huIFNα2b gene along with a α-pre pro sequence showed two distinct bands at 19.8 and 20.2 kDa, of which the latter was a co-contaminant [55]. Shardul Salunkhe *et al*., (2010) depicted the strategies to maximize the expression of recombinant huIFNα2b in *P. pastoris* [57]. Dimethyl sulphoxide as added as a media component in order to reduce the expression of the isoform contaminant of 20 kDa and 93 % recovery of the protein was achieved using single-step anion exchange chromatography. Atef Ayed *et al*., (2008) demonstrated that huIFNα2b is highly sensitive to the protease activity during high cell density culture of *P. pastoris* [56] and employed a strategy of adding casamino acids at 0.1 % (w/w) and 10 mM EDTA, which significantly improved the huIFNα2b expression and prevented proteolysis. In order to improve the expression level, three different methanol feeding strategies were adapted and achieved a yield of 600 mg/L using a smooth increase in

methanol feeding. All the above reported literature for huIFNα2b production using different *P. pastoris* strains have focused on different strategies viz., molecular startegies, medium formulation and bioprocess strategies for proper and enhanced expression. None of these literature have studied the importance of glycosylation for enhancing the serum/plasma half-life of the huIFNα2b. The present thesis work addresses this gap and focuses on the production of human-like glycosylated huIFNα2b using glycoengineered *P. pastoris*. The thesis also focuses on the development of an effective process control strategy using PAT tools for enhanced production of huIFNα2b while maintaining the product quality.

1.4. Signifiance of post translational modifications

Post-translational modifications are the processes that are involved in modification of protein composition. Yeast can perform complex post-translational modifications similar to those performed in higher eukaryotes, including correct folding, disulphide bond formation, proteolytic processing of signal sequences, and N- and O-linked glycosylation. In a few cases, protein folding and disulphide bond formation have been identified as the rate-limiting steps in the production of recombinant proteins[66]. Hence the ability of the organism to process, fold, and secrete the recombinant products determines the productivity of the expression system. Of all the post-translational modifications, glycosylation is the most abundant process across most extant life-forms, influencing in vivo activity, folding, thermal stability, receptor binding, and solubility. Yeast has the ability to perform both N- and O-glycosylation, and it varies from species to species and is different from mammalian cell processes [67]. The N-linked glycosylation pathway in the endoplasmic reticulum (ER) is conserved between yeast and higher eukaryotes. N-glycan processing pathways are greatly diverse among species after transportation of $Man_8GlcNAc_2$ containing glycoproteins to the Golgi apparatus

[67]. *S. cerevisiae* has the most extensive hyperglycosylation, typically adding 50–150 mannose residues, while *Y. lipolytica* was reported to add 8–10 residues [68] and *P. pastoris* can add up to a total of 20 residues. Terminal mannose residues in N-linked glycans are added in *S. cerevisiae* by an α-1,3 bond, which is considered to be allergenic; whereas in *P. pastoris*, a nonallergenic α-1,2 bond is present [69]. Since, the glycoproteins produced from wild-type *P. pastoris* are of non-human type, glycoengineered *P. pastoris* was developed to exhibit humanlike N-glycosylation [70]. One such strain is GlycoSwitch *P. pastoris* (SuperMan5) in which the gene α-1,6 mannosyltransferase (OCH1- responsible for extension of the mannose chain) was deleted and α-1, 2-mannosidase was introduced to produce Man5 glycan by trimming Man8 glycan. This strain produces homogenous glycoproteins with human-type N-glycosylation [71]. Differences in the glycosylation pattern of wild-type *P. pastoris* and glycoengineered *P. pastoris* is depicted in Figure 1.2.

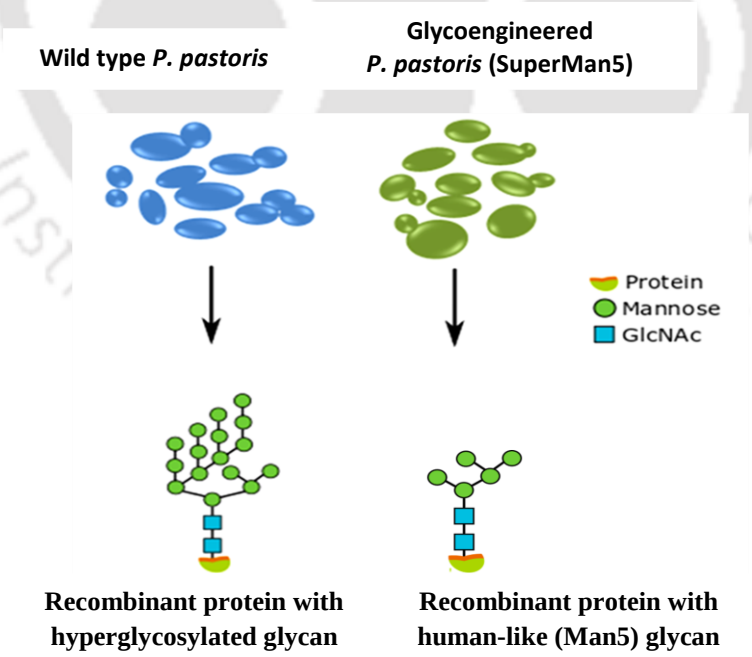

Figure 1.2 Differences in glycosylation (post-translational modification) between the recombinant protein produced from wild type *P. pastoris* and glycoengineered *P. pastoris* (SuperMan5) strains.

FDA-approved recombinant huIFNα2b drugs available in the market are predominantly produced from bacterial (*E. coli*) expression systems, which are non-glycosylated and pegylated and the unmodified huIFNα2b possesing a relatively short serum half-life [72]. Because of its short half-life, unmodified huIFNα2b monotherapy requires multiple doses in a week during the course of treatment, thereby promoting the adverse side effects and affecting the patient quality life [73]. The unfavourable pharmacokinetics of huIFNα2b necessitated the development of new pharmaceutical formulations of the interferon, which can reduce the daily frequency of administration to once in a week. N-glycosylation is one of the critical post-translational modifications that influence the clearance rate and biological activity of therapeutic proteins by increasing the hydrodynamic volume of the protein and thereby modulating the pharmacokinetic properties. N-glycosylation through N-glycoengineering approach was proved to enhance the pharmacokinetic properties/biological activity of different therapeutic proteins as depicted in Table 1.4.

Table 1.4 Examples of N-glycoengineering in human proteins of therapeutic importance

Name of the Protein	Effect of N-glycoengineering	Reference
Adalimumab Fab	Prevention of protein aggregation	[74]
Alpha-1 antitrypsin	Enhanced circulatory half-life	[75]
Erythropoietin	Improved *in vivo* activity and slow clearance	[76]
Follicle Stimulating Hormone	Increased serum half-life and increased in vivo potency	[77]
MpI-Ligand	Increased *in vivo* biological activity with longer duration of action	[76]
Novel erythropoiesis stimulating protein (NESP)	Improved serum half-life and greater in vivo potency	[78]
Leptin	Improved *in vivo* activity and duration of action	[76]

Studies have been reported for the enhancement of serum half-life (pharmacokinetic property) of huIFNα2b through the process of pegylation [79] and through mammalian cell expression [41, 80] for human-like glycosylation. These strategies are associated with serious drawbacks

- Lysosomal storage disease and severe loss of biological activity (pegylation).
- Heterogeneity of the glycans, batch to batch variation and high production costs (Mammalian cell based expression).

Keeping in view of these drawbacks, the present thesis work is focussed to produce novel human-like glycosylated huIFNα2b with greater homogeneity, improved pharmacokinetic property with no loss in biological activity, enhanced huIFNα2b titer using N-glycoengineering, medium optimization and PAT enabled real-time monitoring and control studies.

1.5. Factors controlling glycosylation

Glycosylation is regarded as one of the most essential properties of the therapeutic protein, influencing the biological activity, serum half-life and immunogenicity. The control and maintenance of a consistent glycoform profile during glycoprotein manufacturing is still a considerable challenge (Walsh & Jefferis, 2006), due to the high variability inherent to the process of glycosylation. Regulatory agencies around the world require biopharmaceutical companies to both characterize and maintain product quality attributes (including glycosylation) within defined acceptable limits. The different factors influencing the protein glycosylation are as follow.

Cell type: The choice of an expression system has a profound impact on the maximum product yield that is possible to obtain as well as product quality [81]. Diversity of expression systems have been considered for the production of therapeutic proteins, including bacteria [82], yeast [83], insect [84, 85], plant [86] and mammalian [87] cells,

each varying widely in the ability to perform human-like glycosylation [88]. Consequently, the choice of the adequate host will depend on the product and of the intended application. For a human therapeutic protein, selection of expression system with human type glycosylation and with enhanced production would be the best choice.

Cell glycoengineering: Host cell engineering has been the most intensely pursued glycoengineering approach in recent years, through modifications of the glycosylation pathway to obtain a final product with advantageous properties [89, 90]. This approach has been used to improve the characteristics of glycoproteins produced by mammalian cells, and to modify the glycosylation mechanisms of non-mammalian cells to enable their use in therapeutic glycoprotein production. For example, N-glycoengineering of the yeast *P. pastoris* has proven to be successful in the production of the therapeutic proteins with homogenous human-type N-glycosylation [91]

Protein engineering strategies: Inserting additional N-linked sites has been proven to be clinically beneficial for recombinant glycoproteins. Two new N-linked glycosylation sites were incorporated into recombinant human erythropoietin (rhEPO) via site-directed mutagenesis into the polypeptide chain, creating darbopoetin alfa, which substantially increased in vivo activity and PK [78, 92]. In another study [77], protein engineering was applied to FSH by introducing additional N-linked glycosylation sites into the molecule through structure-aided, site-directed mutagenesis within the FSH molecule and by the addition of N-terminal extensions. The resulting molecule (FSH1208) was found to have a 3- to 4-fold increased serum half-life, compared with wild-type recombinant FSH. This strategy of incorporating new N-linked sequons to improve activity and PK has also been successful with antibody fragments [93]. Although the design of proteins with increased glycosylation is possible, understanding how effective the cell machinery is in producing

these recombinant proteins is critical in bridging the gap between characterization and production.

Manufacturing mode: Mode of cell culture production has a pronounced influence on the resulting protein glycosylation [94]. From the three most common production modes viz., batch, fed-batch and perfusion, the perfusion mode is found to be advantageous for the protein glycosylation (overall sialyation) as compared to the fed-batch mode [95]. Also, the type of reactor appears to affect protein glycosylation, with differences found on the levels of sialylation [96] and galactosylation [97].

Culture medium and culture conditions: Cell growth environment is determined by the culture medium, which has a pivotal influence on product quality [98, 99]. The mammalian cell culture media is typically a mixture of different chemically defined and undefined (e.g., peptones, plant hydrolysates, and serum) components [100]. Literature reports have shown the effects of some of these undefined components on protein glycosylation [101]. A monoclonal IgG1 produced by mouse hybridoma in serum-free media had higher levels of terminal NANA and Gal compared to cultures with serum [102]. Serum and animal-derived components are currently avoided in the biopharmaceutical industry due to regulatory and safety issues [103]. Supplement of the medium with lipids and carriers (dolichol) have been shown to enhance the N-glycan site occupancy of IFN-γ [104] in addition to sugar nucleotides [105].

Culture conditions optimization of the cultivation process viz., dissolved oxygen (DO), carbon dioxide, pH, and temperature found to influence the product yield and also shown to affect the protein glycosylation [100]. Monitoring and control of DO during the bioprocess plays a pivotal role in cell viability and metabolism which influence glycosylation. Culture pH and carbon dioxide are related to each other and affect the

glycosylation of protein, specifically sialylation [106], glycan occupancy [107] and galactosylation [106, 108].

1.6. Batch and fed-batch cultivation of *P. pastoris*

1.6.1. Batch cultivation of *P. pastoris*

P. pastoris batch cultivation generally involves a growth phase on a carbon source (glycerol/glucose) for biomass production, transition phase and an induction (protein production) phase to induce the required recombinant protein expression, using an inducer (methanol/glucose/glycerol). The AOX1 regulated batch cultivation of *P. pastoris* generally consists of glycerol batch phase, transition phase and the methanol induction phase. The main purpose of the glycerol batch phase (growth phase) is to achieve the required biomass before the methanol induction phase. During the glycerol phase, *P. pastoris* utilizes glycerol as a growth substrate and generally grows at a higher specific growth rate of approximately 0.2 h^{-1}. The glycerol growth phase is typically initiated with a glycerol concentration of 40 g/L, as higher levels are inhibitory to growth [109] . The completion of the glycerol growth phase is indicated by a sudden spike in the dissolved oxygen (DO). Biomass production is followed by a transition phase during which limited methanol is added. This transition phase helps in depletion of residual glycerol (which acts a repressor of pAOX1), aiding cellular adaptation to methanol [110] and leading to higher productivities [111]. The transition phase is followed by methanol induction (protein production) phase, where methanol acts as both carbon source and pAOX1 inducer. During the induction (protein production) phase methanol is added either by pulse feeding or continuous feeding. As compared to the growth phase, the specific growth rates are far lesser during the induction phase and a linear increase in biomass as a contrast to an exponential increase in biomass during the growth phase. The yield of the recombinant protein varies with the specific growth rates and induction time.

In 2008, authors reported the use of *P. pastoris* GS115 yielded 200 mg/L of huIFNα2b in a batch process using glycerol and methanol as carbon sources for the growth and induction phases, respectively [55]. Different phases of the batch cultivation of *P. pastoris* are depicted as Figure 1.3.

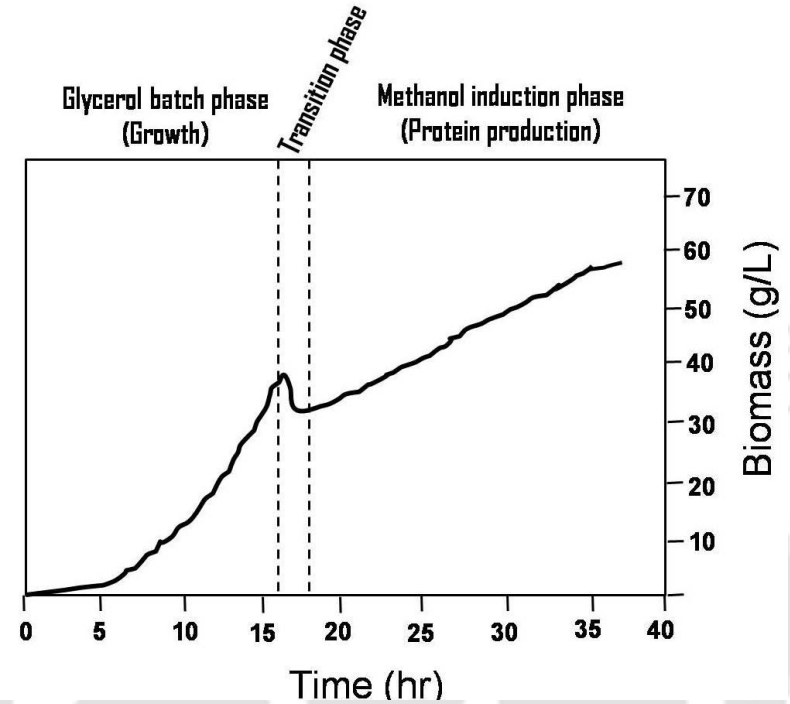

Figure 1.3 Schematic representation of pAOX1 regulated batch cultivation of *P. pastoris*

1.6.2. Fed-batch cultivation of *P. pastoris*

Fed-batch fermentation of *P. pastoris* involves four phases: (1) batch growth on glycerol, (2) fed-batch growth on glycerol for high cell density, (3) transition phase and (4) protein production (induction phase) with pulsed or continuous addition of methanol as an inducer. The first two phases are collectively for the biomass production at a high cell density using glycerol as a carbon source. The completion of glycerol growth (batch) phase is indicated by a sudden spike in the DO followed by the exponential/linear feeding of glycerol (fed-batch) for attaining high cell density before methanol induction

phase. The length of the fed-batch depends on the amount of required biomass before the induction. This is followed by a transition and induction (protein production) phases, which are same as described in the previous section (Figure 1.4).

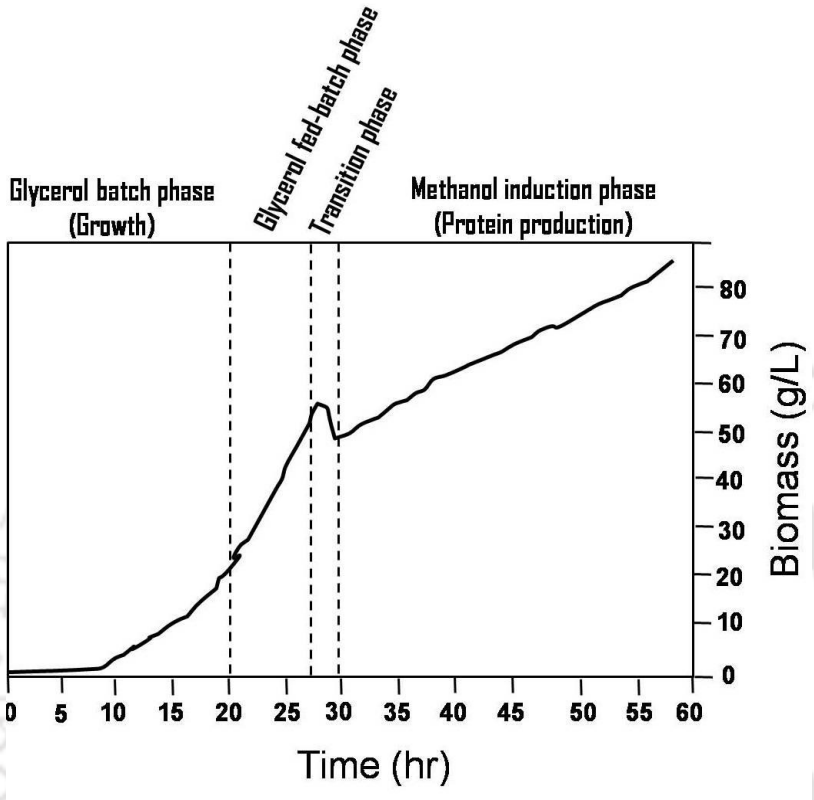

Figure 1.4 Schematic representation of pAOX1 regulated fed-batch cultivation of *P. pastoris*

Only few reports are available related to the fed-batch production of huIFNα2b using different *P. pastoris* strains with pAOX1 promoter and a maximum yield of 600 mg/L was achieved [56, 57, 65].

Fed-batch cultivation of *P. pastoris* with the constitutive promoter (pGAP) is typically divided into two phases viz., a batch phase for the initiation of biomass and an exponential/constant fed-batch phase for further increase in biomass to achieve high protein titers.

1.7. Bioprocess Monitoring and Control

Bioprocess monitoring and control of the fermentation process is becoming a mandate for the industries involved in the manufacturing of biopharmaceuticals to ensure product quality and consistency. Real-time monitoring and control of bioprocess for the development of effective process strategy for recombinant protein production is possible by employing Process Analytical Technology (PAT). United States Food and Drug Administration (USFDA) in 2004 has introduced the PAT initiative aiming to measure, analyze, monitor and ultimately control the bioprocesses through the measurement of Critical Process Parameters (CPP) which affect Critical Quality Attributes (CQA) [112-114]. Efficient and accurate monitoring of key process variables is essential for effective process control and maintenance of the conditions optimal for recombinant protein production. For instance in *P. pastoris* cultivation the CPPs include specific growth rate and residual methanol concentrations. Recent progress in on-line monitoring techniques enable real-time quantification of these CPPs. Off line measurements and estimation of CPPs had been in practice for several decades, which is time consuming, laborious and doesn't provide real-time insight of the ongoing process. In order to circumvent the bottlenecks associated with offline measurements, application of PAT tools for reliable and the real-time monitoring of CPPs offers advantages for efficient process control and achieving desired product quality. Application of PAT tools *viz*., Dielectric Spectroscopy, Biocalorimetry, Fourier Transformed mid Infrared Spectroscopy (FTIR), Near Infrared Spectroscopy (NIR) could provide process related information of multivariate nature, through non-destructive, non-invasive and real-time measurements.

1.7.1. Dielectric Spectroscopy

Dielectric spectroscopy (DS) exploits the complex electrical properties of viable cells and has an advantage of rapid non-contact measurements. Any such complex, passive,

electrical system can be defined by two characteristics: capacitance measured in Farads (F) and conductance measured in Siemens (S). DS is emerging as a promising PAT tool [115, 116] and can provide realtime information about the the total and viable cell volume (VCV), because cells with intact membranes only can act like capacitors under the influence of an electrical field. Obtaining information about the viable cell volume is crucial in a fermentation process, for instance to determine the appropriate time for induction of recombinant protein production. In addition, few value-added products are growth associated and could be indirectly monitored using DS. The measurement of VCV could be useful parameter to estimate the specific product formation rate on real-time. In order to design control strategies to maintain a desired specific growth rate or the product formation rate, it is crucial to acquire real-time information about biomass growth. The application of DS for real-time monitoring of biomass for bacterial [117], yeast [118], filamentous fungi [119], mammalian [120] and hybridoma [121] cell populations are well reported. DS is also been used to detect changes in the cell physiological state and morphology, and furthermore to quantify these changes through membrane capacitance evolution in heterologous phytase production by *P. pastoris* in fed batch and continuous culture [122]. The effect of cultivation parameters such as glucose starvation, pH, perfusion rate, temperature or batch length on glycosylation have been investigated in detail for mammalian cells [123-125]. Studies focussed on protein activity and its aggregation are reported for *P. pastoris* fermentation. For instance, it has been reported that the product quality can be improved by maintaining a high residual methanol concentration [126], growing cells at low rates [127], lowering the cultivation temperature [128], or reducing stirring rate and aeration [129] were addressed in literature. Based on the published literature reports, the specific growth rate and residual methanol concentration are found to have profound effect on protein production and its

glycosylation pattern. Studies addressed the effect of changes in the specific growth rate (μ) on the glycosylation pattern [130] or on the secretory expression [131] of recombinant proteins and described the importance of maintaining threshold values of μ in order to avoid overflow metabolite production [132]. The afore-mentioned factors provides a huge scope for DS towards real-time monitoring and control of specific growth rate facilitating enhanced process understanding and delivering constant product quality.

1.7.2. Biocalorimetry

Biocalorimetry facilitates a quantitative interpretation of metabolic heat generated from living systems as a useful 'process signal' for monitoring purposes and 'Biocalorimetry' had become popular among scientists and academics for monitor and control of biochemical reactions [133, 134]. Recently, biocalorimetry is gaining interest for its application in real-time bioprocess monitoring due to its non-invasive and instantaneous mode of operation [135]. Indeed, measured metabolic heat signals during a bioprocess provide a global insight into metabolic activity of living cells [136, 137]. Further studies illustrated that heat-flow biocalorimeters are high performing (bio) reactors suitable for all kind of bioprocess applications viz., cultivation of different cell lines, quantitative studies including process monitoring and control [138] and biothermodynamic studies [139]. For instance, authors first reported the existence of endothermic microbial growth by cultivation of acetotrophic methanogen, *Methanosarcina barkeri* in the BioRC1 Biocalorimeter [140]. In the case of a pure aerobic respiratory metabolism where the substrate is entirely converted into biomass, water, carbon dioxide and heat, the signal measured by a biocalorimeter (BioRC1) can be related to the actual biomass concentration as well as to specific growth rate. Product quality, as well as the productivity of a process is influenced by the specific growth rate and its fluctuation.

Controlling this CPP is an important step towards quality by design as encouraged by the FDA initiative (FDA 2004) [112]. The development of a robust biomass and specific growth rate estimator based on heat-measurements has its importance in the framework of the FDA's PAT initiative, since it gives a real-time insight into the on-going industrial processes [134]. Authors showed biocalorimetry as robust in-line monitoring and control of aerobic fed-batch cultures of crabtree-negative yeast cells with the help of reliable biomass and specific growth rate estimator based on heat flow measurements [134]. Also, the potential of the biocalorimetry to control the specific growth rate on real-time with the use of proportional integral (PI) feedback control was illustrated. DS and Biocalorimetry have proved to be potential and robust PAT tools to monitor biomass on real-time and also control of specific growth rate (CPP) for high yield recombinant protein production. Integration of a heat flow biocalorimetery and DS into a PAT platform would provide the end-user an insight into metabolic changes encountered in an on-going bioprocess and ensure a robust process control leading to enhanced product yield and quality. Studies addressing the feed-back control of CPP's viz., specific growth rate using different PAT tools during the production process of various recombinant proteins of therapeutic importance in *P. pastoris* are highlighted in Table 1.5.

Table 1.5 Feedback control strategies with different PAT tools implemented for production of different recombinant proteins of therapeutic importance in *P. pastoris*

Strain	Substrate	Type of feedback control	Product	Reference
P. pastoris GS115	Methanol	Mid-IR based control	Avidin	[130]
P. pastoris GS115	Methanol	Methanol sensor based control	Botulinum neurotoxin A-galactosidase	[141]
P. pastoris GS115	Methanol	Methanol sensor based control	ScFv A33-monoclonol antibody	[142]
P. pastoris X33	Methanol	Methanol sensor based control	Rhizopusoryzae lipase	[143]
P. pastoris-PPC43AZ	Glycerol	Capacitance based control	-	[144]
P. pastoris X33	Glycerol	DO based control	single chain antibody fragment (scFv)	[145]
Glycoengineered P. pastoris YGLY4140	Glycerol Methanol	NIR based control	monoclonal antibody	[146]
P. pastoris	Glycerol	Calorimetry based control	HSA	[147]

Definition of the Problem

The literature survey substantiates that recombinant huIFNα2b has been expressed on various platforms, which includes bacteria, yeast, insect cell lines, mammalian cell lines and plants. Expression of recombinant huIFNα2b in *E. coli* yielded high huIFNα2b titer but the expressed protein forms inclusion bodies and loses the activity during renaturation process. Also, the expressed protein lacks post-translational modifications and exhibited very less plasma life. The plasma life of huIFNα2b expressed by *E. coli* increased to certain extent through pegylation but could affect the patient's quality life on long-term use. To achieve the post translational modifications of the recombinant huIFNα2b insect cell lines and mammalian cell lines were considered as viable platform. But, the expressed huIFNα2b yield is low and the protein is partially glycosylated. Mammalian cell lines were used to express rightly processed glycosylated huIFNα2b but it is limited by low yield, high cost, challenges of scale-up, and the problems associated with purification. Other systems like milk of transgenic mice, hen egg and carrot plants were also attempted for the expression of recombinant huIFNα2b but suffer from bottlenecks *viz.*, yield, activity and post translational modifications. Few literature reports are available for the expression of recombinant huIFNα2b in *P. pastoris* but failed to report the extent of post translational modifications of the expressed protein and the maximum protein yield reported was 600mg/L. No literature report available on real-time monitoring of the recombinant huIFNα2b production employing PAT tools addressing scope of CPPs and their influence on product (huIFNα2b) quality. The huIFNα2b drugs currently approved by FDA and therapeutically in use are expressed *by E. coli* system.

The present thesis work is aimed to address the gaps pertaining to recombinant huIFNα2b expression on various systems. The primary focus the present thesis is i) Design and development of high yield *P. pastoris* expression platform recombinant huIFNα2b, ii) development of effective process strategy by integrating PAT tools for real-time monitoring and control of *P. pastoris* cultivation for huIFNα2b production. Glycoengineered *P. pastoris* strain is employed in this thesis work for successful expression of glycosylated huIFNα2b. Medium optimization studies employing the Design of experiments (DoE) and statistical optimization methods are performed to enhance the yield of recombinant huIFNα2b production in glycoengineered *P. pastoris*. The reported suggests that DS and Biocalorimetry as potential PAT tools for successful monitoring of the biomass concentration and specific growth rate in different bioprocess systems. The CPPs associated with the glycoengineered *P. pastoris* fermentation for the production of glycosylated huIFNα2b could be monitored on real-time by DS, calorimetric and respirometric measurements. An effective process strategy ensuring high huIFNα2b production and its quality (desired glycosylation profile) could be developed by elucidation and control of CPPs by the application of PAT tools.

Objectives

- Cloning and expression of recombinant huIFNα2b in glycoengineered *P. pastoris.*
- Media and process conditions optimization studies for high level expression of recombinant huIFNα2b by statistical optimization methods.
- Batch and Fed-batch studies for expression of recombinant huIFNα2b in glycoengineered *P. pastoris.*
- Real time monitoring of glycoengineered *P. pastoris* cultivation for recombinant huIFNα2b production by PAT tools Dielectric spectroscopy, Biocalorimetry and Respirometry
- Development and implementation of effective process control strategy for the enhanced production of glycosylated huIFNα2b.
- Purification and biological characterization of the expressed glycosylated huIFNα2b.

Chapter 2

Cloning, expression, purification and characterization of recombinant huIFNα2b in glycoengineered *Pichia pastoris*

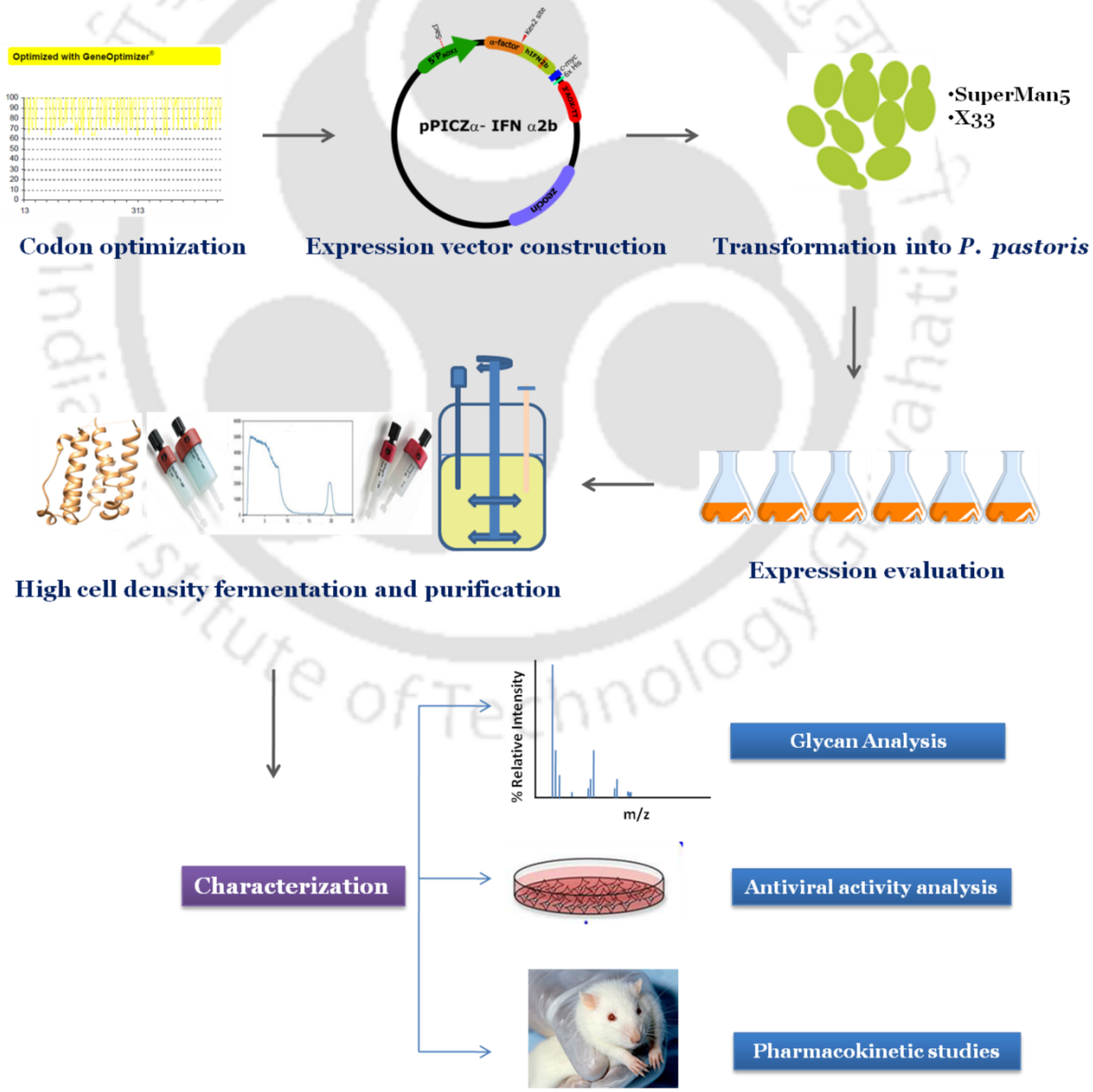

भारतीय प्रौद्योगिकी संस्थान गुवाहाटी
Indian Institute of Technology Guwahati

Chapter 2

Cloning, expression, purification and characterization of recombinant huIFNα2b in *Pichia pastoris*

Abstract

Human interferon alpha 2b (huIFNα2b) is a type I interferon exhibiting antiviral, anti-proliferative and immunomodulatory activities. The clinical outcome of the approved recombinant huIFNα2b drugs in the market suffers from short plasma half-life, rapid clearance and other side effects. The huIFNα2b expression in mammalian cell lines results in significant heterogeneity in glycan moieties, inconsistent product quality and high production cost. Potential scope exists for the design and development of a successful expression platform for enhanced huIFNα2b production with improved pharmacokinetic property. Glycoengineering strategy was employed to construct huIFNα2b with potential N-glycosylation site to evade the drawbacks of approved recombinant huIFNα2b drugs. Heterogeneity of glycosylation and hypermannosylation in the wild-type strains of *Pichia pastoris* was circumvented by employing glycoengineered strain (SuperMan5) to produce glycosylated huIFNα2b with human type N-glycans. Recombinant SuperMan5 strain expressed human type N-glycosylated huIFNα2b with greater homogeneity elucidated by glycan analysis (MALDI-TOF/MS). The purified glycosylated huIFNα2b was biologically active, inhibiting the viral replication of HCV and HEV at 85 % and 66 %, respectively. Pharmacokinetic studies in Wistar rats revealed 1.3 fold increase in plasma half-life for glycosylated huIFNα2b compared to standard huIFNα2b produced by *E. coli*.

2.1. Introduction

The interferons (IFNs) are a group of signaling proteins (cytokines) with multiple biological functions *viz.*,antiviral, antiproliferative and immunomodulatory activities against a broad range of mammalian viruses [3]. Interferons are classified as Type I, Type II and Type III, respectively based on their receptor types on cell membrane surface. Type I IFN majorly consists of IFN-α genes and IFN α2 has potential therapeutic applications. huIFNα2b is a protein polypeptide of 165 amino acids with wide clinical applications [9]. huIFNα2b alone or in combination is being used as standard therapeutic drug for chronic hepatitis B [15], hepatitis C [16], few types of cancer such as melanoma [19] and AIDS-related Kaposi's sarcoma [20]. Several bacterial systems were used for the expression of recombinant huIFNα2b *viz.*, *Escherichia coli* [148], *Streptomyces lividans* [35] and *Bacillus subtilis* [36]. FDA approved recombinant huIFNα2b drugs available in the market are predominantly produced from bacterial (*E. coli*) expression systems, which are non-glycosylated and pegylated. Like other low molecular weight protein drugs, huIFNα2b has a relatively short serum half-life following subcutaneous injection [72]. Due to its fast renal clearance from the blood, unmodified huIFNα2b monotherapy requires multiple doses during the course of treatment resulting to onset of adverse effects [73]. To overcome the short serum half-life of huIFNα2b, pegylated huIFNα2b was developed by chemical conjugation of polyethylene glycol (PEG) molecules. Subsequent improvement in the pharmacodynamics and pharmacokinetics was validated with reduced plasma clearance and immunogenicity [149]. The most common problem allied with refolded and pegylated IFN-α is the formation of neutralizing antibodies. These antibodies were found to be associated with treatment failure in HCV-infected patients [150, 151]. An alternative approach for improving the pharmacokinetic properties of huIFNα2b is the

use of a glycoengineering strategy to obtain analogs with newly introduced potential N-glycosylation sites [152]. The huIFNα2b therefore stands as the perfect candidate for glycoengineering, as the major routes of IFNα elimination from the circulatory system is through receptor-mediated endocytosis, proteolysis and kidney filtration [80, 153, 154]. N-glycosylation is a critical post-translational modification which affects the efficacy of therapeutic proteins by influencing their biological activity and clearance rate, especially through the modulation of the pharmacokinetic properties. The protein half-life in circulation is the crucial pharmacokinetic property, and it was proved to be enhanced by glycosylation in different therapeutics for example interferon and erythropoietin [98, 155-157]. Using the N-glycoengineering approach, glycosylated huIFNα2b was successfully expressed in CHO.K1 cell lines with improved pharmacokinetic properties and efficacy [80]. Also reports are available for the expression of glycosylated huIFNα2b in few other mammalian (HEK293, NSo) cell lines [41, 46]. Though mammalian cells produce N- linked glycoproteins proximate to humans; the heterogeneity of glycans obtained, batch to batch variation, and high production costs are major drawbacks of this expression platform. For instance, it has been reported that up to 80 % of erythropoietin produced in CHO cell is deserted due to incorrect glycosylation [71]. Glycosylated huIFNα2b expressed in insect cells suffers from potentially immunogenic high-mannose type glycosylation [45]. Yeasts are proven to be suitable hosts for the expression of heterologous proteins owing to their advantages over bacteria, plants, mammalian and insect cell lines. For instance, yeasts combine the ease of genetic manipulation with high cell density cultivation on inexpensive medium at a higher growth rate and possess the capability of complex post-translational modifications [158]. In addition, the recombinant proteins expressed through yeast platform are free of endotoxins, oncogenic, and viral DNA [159]. *P. pastoris* proved to be a successful expression system

for the production of different therapeutic proteins. It offers numerous advantages which include ease of genetic manipulation, strong inducible AOX1 promoter, high cell density cultivation in defined medium and post-translational modifications. Wild-type *P. pastoris* glycosylation generally yields protein-bound oligosaccharides of much shorter chain length compared to *S. Cerevisiae* [160]. Since the glycoproteins produced from wild-type *P. pastoris* are of non-human type, glycoengineered *P. pastoris* was developed to exhibit human-like N-glycosylation [70]. One such strain is GlycoSwitch® *P. pastoris* (BioGrammatics, Inc.) which can produce homogenous glycoproteins with human type N-glycosylation [71, 161]. Glycoengineered *P. pastoris* was genetically engineered for successful production of chymase [162] and GM-CSF [91]. Only few literature reports are available for the production of huIFNα2b in *P. pastoris* [55, 56, 65] but none of them address the significance of glycosylation. This present chapter highlights the successful expression of homogenous N-glycosylated huIFNα2b in a glycoengineered *P. pastoris* and enumerate the influence of glycosylation on huIFNα2b therapeutic properties.

The main objective of this chapter is to describe the glycoengineering strategy for the production of novel homogenous N-glycosylated huIFNα2b in glycoengineered *P. pastoris* exhibiting improved plasma half-life. This study also addresses the possible effect of N-glycosylation on the biological activity of the purified glycosylated huIFNα2b compared to the commercially available huIFNα2b therapeutics.

2.2. Materials and methods

2.2.1. Strains, media, and chemicals

E. coli TOP10F′ cells, Easyselect™ *P. pastoris* expression kit from Invitrogen, USA, and a humanized glycoengineered yeast (Glycoswitch® SuperMan5, pep4Δ prb1Δ) from Biogrammatics Inc., USA, were used for cloning and expression studies. All the restriction enzymes and T4 DNA ligase were purchased from New England Biolabs, UK. The huIFNα2b gene with a single N-glycosylation site was codon optimized for *P. pastoris* and was synthesized from GeneArt, USA. Gel extraction kit, PCR purification kit, and plasmid isolation kit were procured from Qiagen, Netherlands. All other chemicals were procured from Sigma, USA, and Himedia, Bangalore. The standards, huIFNα2b of *E. coli* origin was procured from Genscript, China and the pegylated huIFNα2b drug was from Schering-Plough, United States.

Low salt Luria-Bertani (LB) medium, g/L (10 tryptone, 5 yeast extract, and 5 NaCl) was used for cultivation of *E. coli* TOP10F′. Whereas, Yeast extract Peptone Dextrose (YPD), g/L (10 yeast extract, 20 peptone, and 20 dextrose), Yeast extract Peptone Dextrose Sorbitol (YPDS), g/L (10 yeast extract, 20 peptone, and 20 dextrose and 1 M sorbitol), MD, g/L (13.4 YNB , 0.0004 biotin, 20 dextrose) MM, g/L (13.4 YNB, 0.0004 biotin, 5 methanol), Buffered Glycerol-complex medium (BMGY), g/L (10 yeast extract, 20 peptone,13.4 Yeast Nitrogen Base (YNB), 0.0004 biotin, 10 glycerol and 100 mL of 1M potassium phosphate buffer, pH 6.0) and Buffered Methanol-complex medium (BMMY), g/L (10 yeast extract, 20 peptone,13.4 YNB, 0.0004 biotin, 5 methanol and 100 mL of 1M potassium phosphate buffer, pH 6.0) were used for growth and expression studies of huIFNα2b in *P. pastoris* at shake flask level.

High cell density cultivation was performed in basal salt medium, g/L glycerol (40), K_2SO_4 (18.2), $MgSO_4$ (7.28), KOH (4.13), $CaSO_4.2H_2O$ (0.93) and 85 %

orthophosphoric acid (26.7 mL/L) dissolved in deionised water and sterilized in the bioreactor. 5 mL/L PTM4 salts and 2 mL/L of 500X biotin were added to the medium after sterilization,

pH of the culture medium was adjusted to 5.2 by addition of 25 % ammonia (w/v). The PTM1 solution contained, g/L: $CuSO_4.5H_2O$ (6), NaI (0.08), $MnSO_4.H_2O$ (3), $Na_2MoO_4.2H_2O$ (0.2), H_3BO_3 (0.02), $CoCl_2$ (0.5), $ZnCl_2$ (20), $FeSO_4.7H_2O$ (65), biotin (0.2) and H_2SO_4 98 % (5 mL/L).

2.2.2. Identification of key location for the generation of N-glycosylation motif

The key location for generating N-glycosylation motif (NXT, X; can be any amino acid except proline) was identified considering the available three-dimensional structure of huIFNα2b [23, 163]. The glycosylation potential of the selected N-glycosylation motif was assessed by NetNGlyc 1.0 server.

2.2.3. Cloning of human huIFNα2b gene and construction of expression vector

P. pastoris codon optimized huIFNα2b variant gene (huIFNα2b gene with single N-glycosylation site) was ligated into XhoI and NotI digested plasmid pPICZαA to generate pPICZαA-huIFNα2b variant. A native huIFNα2b encoding gene fragment was generated by site-directed mutagenesis PCR and was ligated into XhoI and NotI digested plasmid pPICZαA to generate pPICZαA-huIFNα2b native. T4 DNA ligase was used for ligation reactions and $CaCl_2$ competent cells of *E. coli* TOP10F' strain was used for transforming ligation mixtures. Positive clones were verified by restriction digestion and Sanger sequencing. huIFNα2b native and its variant gene in pPICZαA encompass a N-terminal α-factor signal peptide for extracellular export in *P. pastoris* and a C-terminal 6X Histidine tag for facilitating affinity purification. During the extracellular export, Kex2 protease trims away the α-factor signal peptide in *P. pastoris*.

2.2.4. Transformation of *P. pastoris* strains and screening for recombinant strain

The schematic representation of recombinant events in *P. pastoris* is depicted in Figure 2.1. Transformation of *P. pastoris* was performed as per the standard protocol of electroporation as described in Easyselect™ *P. pastoris* manual.

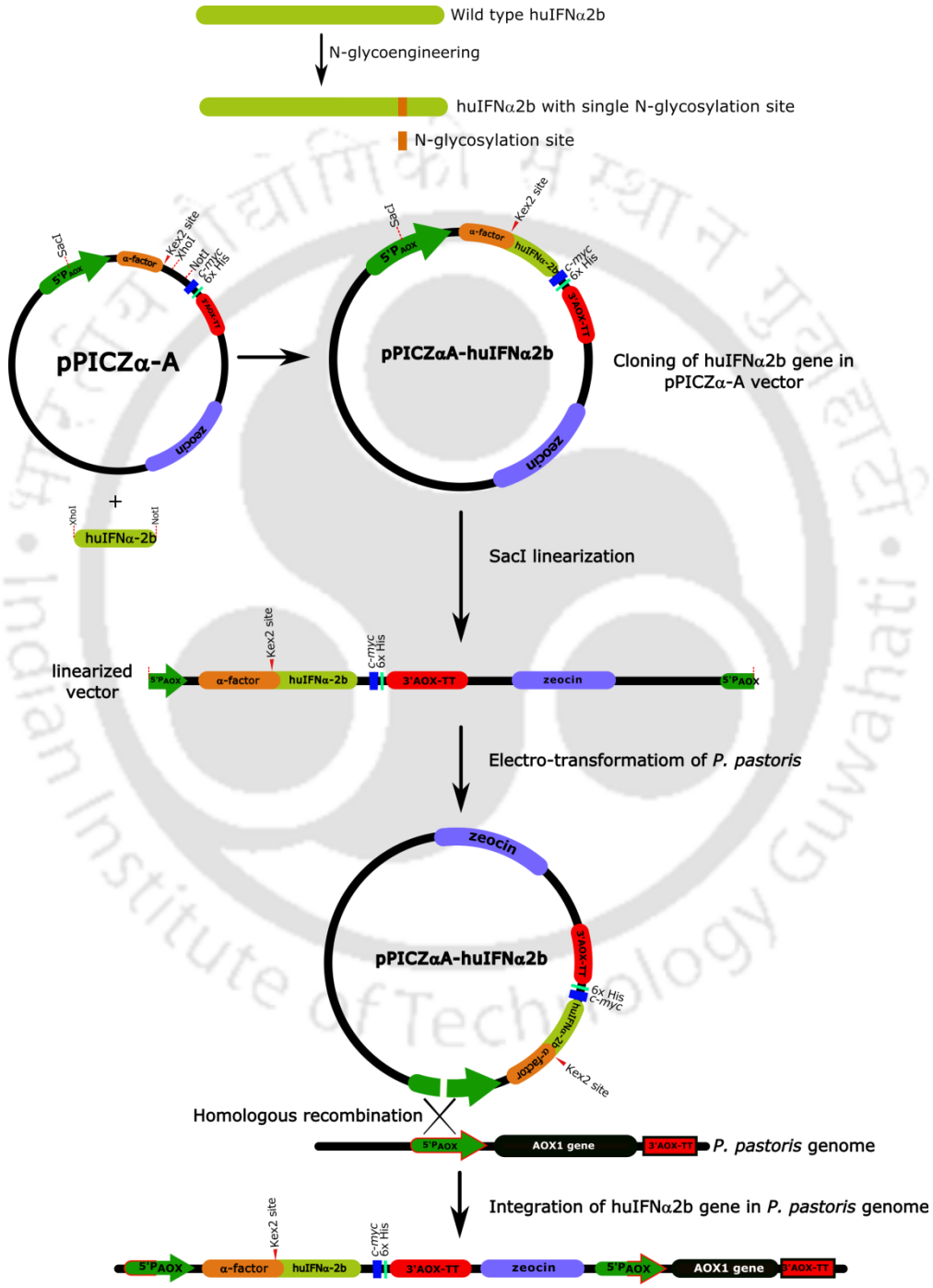

Figure 2.1 Schematic representation of N-glycoengineering approach and recombination events in *P. pastoris*

Wherein competent *P. pastoris* X33 and SuperMan5 (*pep4Δ prb1Δ*) cells (80 µL) were mixed separately with 5µg of *SacI*-linearized pPICZαA-huIFNα2b-variant and pPICZαA- huIFNα2b-native and were transferred into an ice-cold 0.2-cm electroporation cuvette and incubated in an ice bath for 5 min. Immediately after electroporation (at 2 kV, 25 µF, 200 Ω), 1 mL of ice-cold 1 M sorbitol was added to the cuvette and incubated for 1 h at 30˚C without shaking. After incubation the contents were centrifuged and dissolved in fresh YPD medium (350 µL) and plated onto YPDS plates supplemented with 100 µg/mL Zeocin and incubated at 30˚C for 2 days. The transformants bearing the genomic integrants of the pPICZαA-huIFNα2b were confirmed by colony PCR using the primers 5′-AOX1: 5′-GACTGGTTCCAATTGACAAGC-3′, and 3′-AOX1: 5′-GCAAATGGCATTCTGACATCC-3′. The huIFNα2b gene from the positive clone was gel extracted and sequence verified.

2.2.5. Shake flask studies for the expression of recombinant huIFNα2b

The selected positive colonies of recombinant X33 and SuperMan5 with genomic integration of native and variant huIFNα2b gene were used to inoculate 50 mL of BMGY in a 250 mL Erlenmeyer baffled flask and incubated at 30°C and 250 RPM for 24 h. The cells were pelleted by centrifugation at 3000 x g for 10 min, re-suspended in 20 mL BMMY medium containing 0.5 % (v/v) methanol followed by incubation at 30°C and 250 RPM. During induction, methanol was added every 24 h to a final concentration of 0.5 % (v/v). After 4 days (96 h) of induction, the cells were harvested by centrifugation at 10,000 x g for 20 min at 4°C; the supernatant was collected and stored at -20°C for protein quantification. The extracellular expression of recombinant huIFNα2b protein in the selected clones was quantified by huIFNα2b ELISA assay kit (Mabtech AB, Sweden). Positive clones with better expression level of huIFNα2b were selected for the high cell density cultivation.

2.2.6. High cell density cultivation

High cell density cultivation refers to maximize the biomass production by fed-batch feeding of carbon source (Glycerol/methanol) in order to attain higher protein productivity [164]. High cell density cultivation of *P. pastoris* X33/SuperMan5 clones bearing wild-type and variant huIFNα2b gene was carried out in a 7 L bioreactor (Eppendorf, Germany). The seed inoculum was prepared from a glycerol stock of respective recombinant *P. pastoris* cultured in BMGY medium, in Erlenmeyer baffled flask and incubated at 30˚C at 250 RPM until the OD_{600} reached 50. Initial batch fermentation was started with 2.5 L of the basal salt medium in the bioreactor and 10 % (v/v) of inoculum was used. Reactor temperature was maintained at 30˚C throughout the fermentation. pH of 5.2 was maintained during the fermentation with automatic dosing of 30 % (v/v) orthophosphoric acid and 25 % (w/v) ammonia solution. Dissolved oxygen (DO) was maintained above 20 % saturation by controlling the stirrer speed and enriching the air inlet stream with pure oxygen. At the end of glycerol growth phase indicated by DO spike, methanol feed (100 % v/v methanol and 12 mL/L PTM4 salts) was started for induction and continued for 72 hours. Samples were collected at specific time intervals during the induction phase to check the expression levels of recombinant huIFNα2b.

2.2.7. Purification of recombinant huIFNα2b

During the end of high cell density cultivation, the pH of the culture broth was adjusted to 7 and the culture supernatant was collected by centrifugation at 4,500 x g for 10 min. The supernatant was then treated with 1 % (v/v) Triton-X100 for the removal of non-covalent aggregates [56] and was filtered through a 0.22 µm PVDF filter prior to further steps of purification. The glycosylated huIFNα2b was purified by His-tag affinity chromatography followed by Concanavalin A (ConA) lectin chromatography. Whereas

non-glycosylated (native) huIFNα2b was purified by His-tag affinity chromatography followed by size exclusion chromatography.

His-tag affinity chromatography was performed for the clarified supernatant, where it was diluted at 1:1 ratio with the binding buffer (20 mM Tris, 500mM NaCl, 20 mM Imidazole, pH 8) and allowed for binding of recombinant huIFNα2b onto His-Trap 5 mL column (GE Healthcare), at a flow rate of 2 mL/min. The binding step was followed by washing with wash buffer (20 mM Tris, 500mM NaCl, 50 mM imidazole, pH 8). Elution of the bound huIFNα2b was carried out using elution buffer (20 mM Tris, 500mM NaCl, 500 mM imidazole, pH 8) with a linear gradient of 50 mM - 500 mM imidazole at a flow rate of 1 mL/min for 60 min. The glycosylated huIFNα2b was further purified by Con A chromatography. The pooled fraction from His-tag chromatography was diluted with Con A binding buffer (20 mM Tris-HCl, 0.5 M NaCl, 1 mM $MnCl_2$, 1 mM $CaCl_2$, pH 7.4) in 1:1 ratio and applied on a pre-equilibrated Con A column (GE Healthcare). The column was then washed with a 10 column volume of Con A binding buffer. Finally, glycosylated huIFNα2b was eluted from the column with an elution buffer by methyl-α-D-glucopyranoside competition (20 mM Tris-HCl, 0.5 M NaCl, 0.5 M methyl-α-D-glucopyranoside, pH 7.4). The non-glycosylated (native) huIFNα2b was further purified by size exclusion chromatography. The pooled fraction from His-tag chromatography was concentrated using 10 kDa cut-off filter and applied onto pre-equilibrated Hiload 16/60 Superdex 200pg size exclusion column (GE Healthcare) with PBS as elution buffer.

2.2.8. Glycosylation Analysis

N- linked glycosylation of the purified recombinant huIFNα2b was analyzed by enzyme deglycosylation. The protein was treated with PNGase F (New England Biolabs, USA) according to the manufacturer's protocol. Briefly, the purified protein (5 µg) was

denatured with glycoprotein denaturing buffer (0.5 % SDS, 0.04 M DTT) at 100°C for 10 min and then incubated with 2 µL of PNGase F in reaction buffer (0.05 M sodium phosphate, pH 7.5, 1 % NP-40) at 37°C for 16 h. Post to the incubation, protein glycosylation was analyzed by observing the differences in migration pattern of PNGase F treated and untreated samples on silver stained 15 % SDS-polyacrylamide gels.

2.2.9. N-Glycan Analysis

Purified glycosylated huIFNα2b was subjected to N-glycan profiling by MALDI-TOF MS analysis [165]. Briefly, the protocol involved reduction, carboxymethylation, and tryptic digestion of the protein sample. Subsequently, PNGase F digestion was used to release N-glycans, followed by permethylation of the released N-glycans and finally separation of the permethylated N-glycans by reverse phase C18 cartridge. The different acetonitrile elution fractions (15 %, 35 %, 50 % and 75 %) were collected and mixed with 15 mg/mL of 2, 5-dihydroxybenzoic acid (DHB) matrix in 70:30 methanol/water, and then spotted onto a target plate and dried under vacuum. MALDI-MS (MALDI TOF/TOF 5800, AB SCIEX) was employed to obtain the molecular ion signals from the permethylated glycans corresponding to $[M + Na]^+$ adducts. The predominant peak from the MALDI-MS analysis was subjected to MS/MS analysis to obtain important structural information such as branching patterns, antennae structures and linkage positions. MS/MS spectra of the fragment ions were analyzed using the GlycoWorkbench suite, which helps in the annotation of the glycan fragment spectra. To further confirm the linkage of monosaccharides in the glycan, the prepared Partially Methylated Alditol Acetates (PMAAs) from the glycosylated huIFNα2b sample was subjected to linkage analysis by GC-MS.

2.2.10. Biological assay of huIFNα2b

2.2.10.1. Replicon Assay

HCV genotype 3a bicistronic replicon S52/SG-Feo (AII) was a kind gift from Dr. C.M. Rice (The Rockefeller University, New York). The plasmid was linearized with XbaI and transcribed *in vitro* using AmpliScribe T7-Flash transcription kit (Epicentre Biotechnologies Inc., USA). Template DNA was removed with RNase-free DNase followed by phenol/chloroform extraction and precipitation of RNA. RNA quality was assessed by agarose gel electrophoresis. HCV replicon RNA was electroporated into Huh7.5 cells in a 4 mm cuvette (200 volts, 950 µF capacitance, ∞ resistance) using BioRad GenePulser Xcell. Transfected cells were suspended in culture medium and transferred to 10 cm diameter dishes. The replicon-expressing cells were selected by the addition of G418 (0.5 mg/mL) 48 h post transfection. Two weeks later, G418 resistant cells were used for antiviral assays.

HEV genotype 3 replicon (p6/luc) plasmid was a kind gift from Dr. S. Emerson (National Institute of Allergy and Infectious Diseases, National Institutes of Health, Bethesda, Maryland, USA). The plasmid was linearized with MluI and capped transcripts were generated using mMESSAGE mMACHINE Kit (Life Technologies, USA). Template DNA was removed with RNase-free DNase followed by phenol/chloroform extraction and precipitation of RNA. RNA quality was assessed by agarose gel electrophoresis. P6/luc replicon RNA was electroporated into Huh7 cells in a 4 mm cuvette (200 volts, 950 µF capacitance, ∞ resistance) using BioRad GenePulser Xcell. Transfected cells were suspended in culture medium and maintained in a T75 flask with the media being replaced every three days. Replication of HEV was monitored by measuring the luciferase activity of the gaussia luciferase secreted into the medium.

For inhibitor analyses, the different forms of huIFNα2b with standards at different concentrations were added to the wells harboring Huh7.5 cells expressing HCV replicon, and Huh7 cells expressing HEV replicon. The replication activity was determined by measuring the luciferase activity after 48 h of the addition of huIFNα2b protein samples. PBS was used as a vehicle control. The statistical analysis of the data was performed using Analysis of Varaince (ANOVA) followed by Dunnett's corrected unaired *t* test.

2.2.10.2. Cell Viability Assay

Cytotoxicity analysis was performed using water-soluble tetrazolium (WST-1) reagent (Roche, USA) according to the manufacturer's protocol. The viability of the cells was checked using 1:10 dilution of WST-1 reagent to the complete media. Cells were incubated and analyzed for 1 h and 2 h duration. The absorbance was measured at 450 nm and 630 nm, respectively. Difference between the two absorbance readings was plotted as percentage values with PBS treated samples considered as 100 %.

2.2.11. Pharmacokinetic studies

Comparative evaluation of the pharmacokinetic properties of the purified glycosylated huIFNα2b (SuperMan5) was dealt along with recombinant huIFNα2b produced in *E. coli* and the pegylated huIFNα2b by post subcutaneous administration. For the experiments, Wistar rats (female) with an average body weight of 250 g were divided into three groups of three animals each. Animals were maintained in a controlled environment of the experimental animal room maintained at temperature range of 19.8 - 22.8°C, relative humidity of 45 to 68 %, a light/dark cycle of ~12 hours, 20 fresh air changes per hour and free access to food and water. Animals of the three groups were injected subcutaneously with 1.93 µg/Kg, at a dose volume of 2 mL/ kg body weight of *E. coli* derived recombinant huIFNα2b, pegylated huIFNα2b and the glycosylated huIFNα2b

from the present study. Blood was collected during the experimental period under isoflurane anesthesia at different post-injection times. Blood collected was centrifuged and the separated plasma was stored at –80°C for further analysis. Blood samples collected at different time points were assessed for the concentration of glycosylated huIFNα2b and standards in the plasma by ELISA analysis. The protocol and procedures employed for the pharmacokinetic studies were ethically reviewed and approved by Committee for the Purpose of Control and Supervision of Experiments on Animals (CPCSEA).

2.2.12. Pharmacokinetic data analysis

Plasma pharmacokinetic parameters were calculated using the non-compartmental analysis tool of Phoenix software (Version 7.0) and were determined from individual animals in each group. The peak plasma concentration (C_{max}), time to achieve peak plasma concentration (T_{max}), and terminal half-life ($t_{1/2}$) were calculated. All the results were expressed as mean ± SD. The statistical significance of the data obtained were analyzed by paired *t*-test (Microsoft Excel, 2007), comparing the pharmacokinetic data of the glycosylated huIFNα2b with the huIFNα2b of *E. coli* origin [166].

2.3. Results

2.3.1. Identification of key location for the generation of N-glycosylation motif

Suitable single N-glycosylation motif ($N^{104}V^{105}T^{106}$) was generated by mutating G104N to facilitate N-glycosylation at N104 amino acid residue. Based on the assessment by NetNGlyc 1.0 server (potential value: 0.707, and within jury agreement: 9/9), this motif appeared to be highly favourable for N-glycosylation. Hence, we predict N-glycosylation at N^{104} to attribute positive influence on plasma half life and undeterred biological activity.

2.3.2. Construction and transformation of expression vector

Expression vector pPICZαA-huIFNα2b-variant and pPICZαA-huIFNα2b-native were constructed and transformed into *E. coli*, and the transformants were screened through colony polymerase chain reaction (PCR) using 5′AOX and 3′AOX primers (Figure 2.2) and was sequence verified.

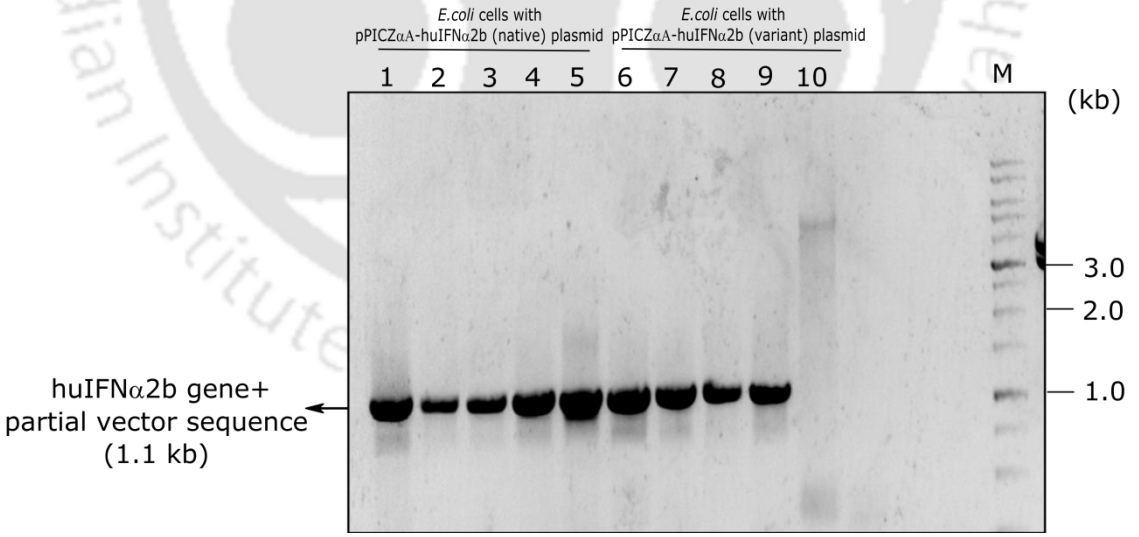

Figure 2.2 Agarose gel displaying the colony PCR products of *E. coli* TOP10F′ cells transformed with ligation mixtures of linearized pPICZαA with native (Lane 1-5) or variant (Lane 6-10) of huIFNα2b encoding gene fragment is presented. Positions corresponding to the the molecular weight of various fragments in DNA marker lane (M) is shown on the right whereas position corresponding to the amplicon is represented on the left.

The result of colony PCR displayed a band of ~1.1 kb size which confirmed the insertion of our gene of interest (huIFNα2b) into expression vector pPICZαA. The resultant PCR product (~1.1 kb) includes, in addition to 520 bp huIFNα2b gene, a 588 bp of the vector sequence as well. SacI linearized expression vectors were transformed into genome of *P. pastoris* strains (X33 and Superman5) at the 5′ AOX1 locus *via* the homologous recombination. The colony PCR analysis of positive transformants of X33 and Superman5 with integrated native and variant huIFNα2b gene resulted in two products of 2.2 kb and ~1.1 kb corresponding to AOX1 gene and huIFNα2b gene along with PCR product of the expression vector, respectively (Figure 2.3, 2.4 and 2.5).

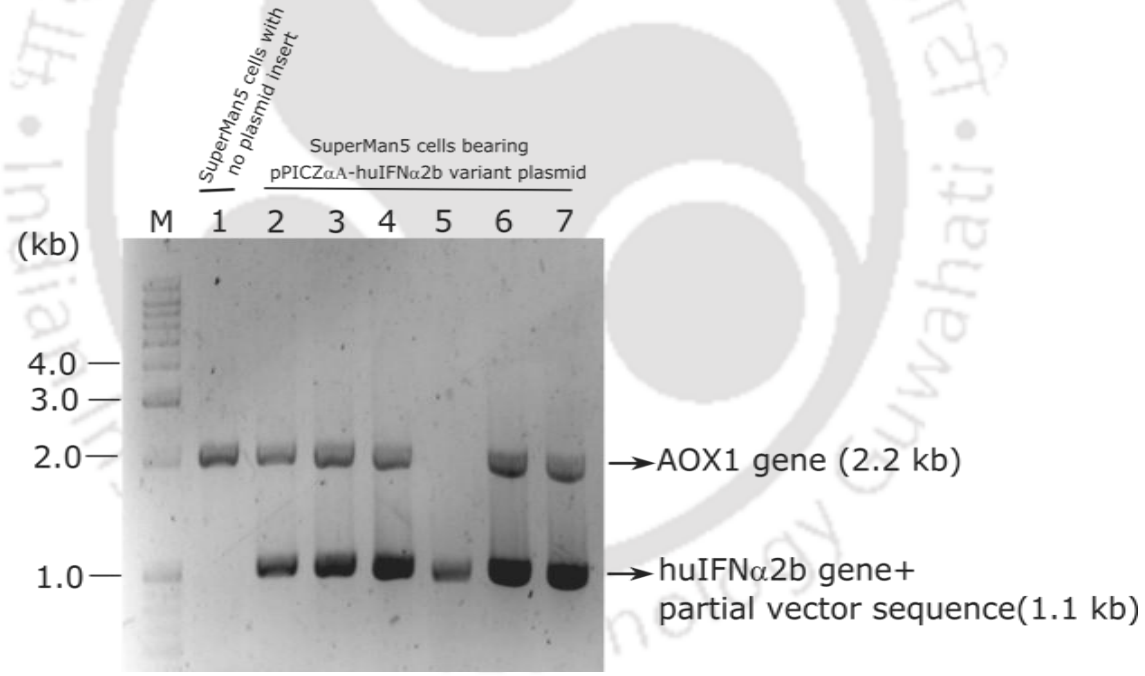

Figure 2.3 Agarose gel displaying the colony PCR products of *P. pastoris* Superman5 (pep4Δ prb1Δ) cells with no plasmid insert (Lane 1, control) or cells transformed with linearized pPICZαA-huIFNα2b-variant plasmid (Lane 2-7). Positions corresponding to the PCR products are indicated on the right whereas DNA marker (M) positions are represented on left.

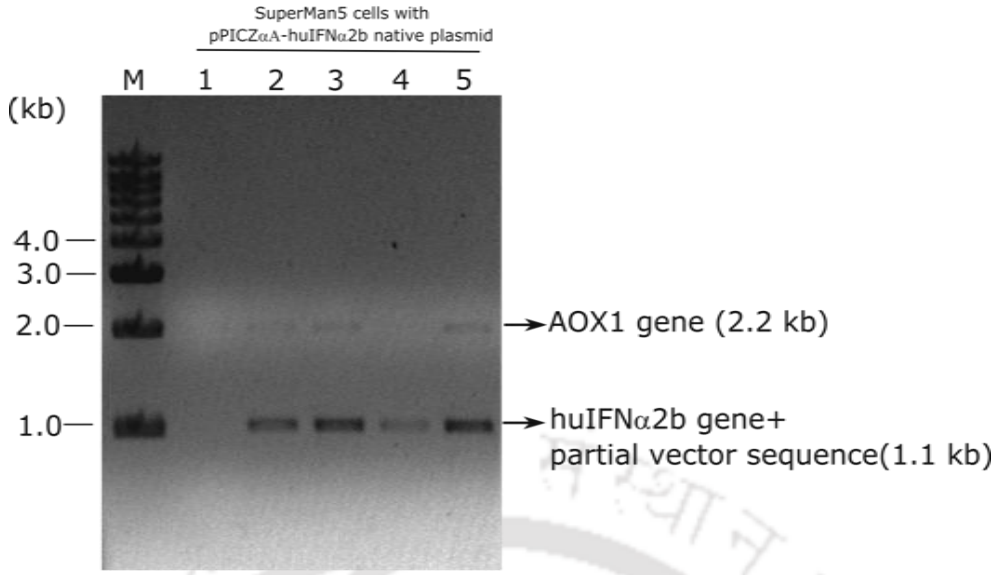

Figure 2.4 Agarose gel displaying the colony PCR products of *P. pastoris* Superman5 (pep4Δ prb1Δ) cells transformed with linearized pPICZαA-huIFNα2b-native plasmid (Lane 1-5). Positions corresponding to the PCR products are indicated on the right whereas DNA marker (M) positions are represented on left.

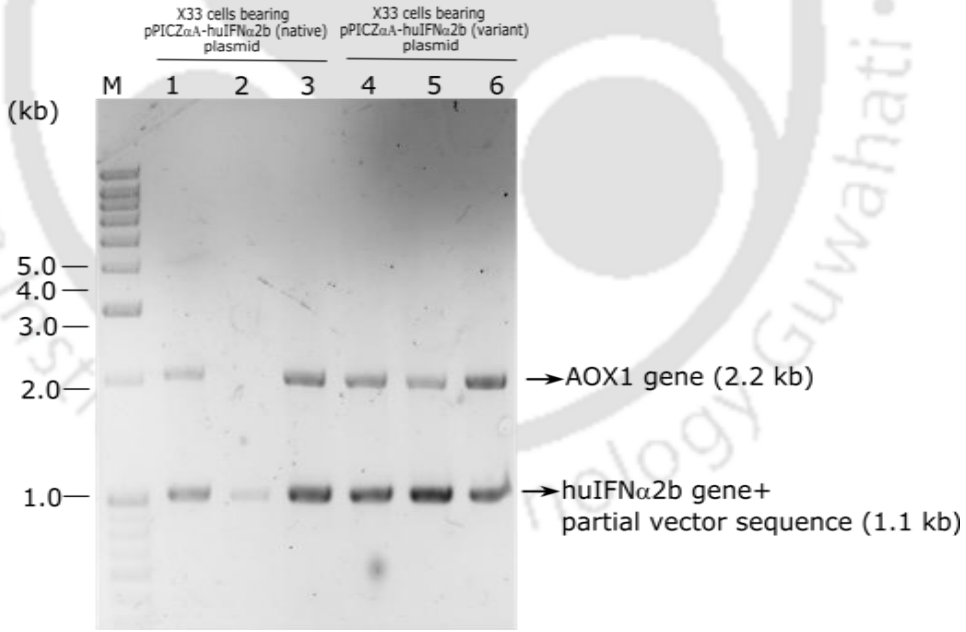

Figure 2.5 Agarose gel displaying the colony PCR products of *P. pastoris* X33 cells transformed with linearized pPICZαA-huIFNα2b-native (Lane 1-3) or pPICZαA-huIFNα2b-variant plasmid (Lane 4-6). Positions corresponding to the PCR products are indicated on the right whereas DNA marker (M) positions are represented on left.

2.3.3. Expression and purification of recombinant huIFNα2b

From the shake flask experiments, the huIFNα2b yield for the *P. pastoris* X33/SuperMan5 clones were quantified by enzyme-linked immunosorbent assay (ELISA) analysis. Clones exhibiting high huIFNα2b yield in BMGY/BMMY medium (12 mg/L) were selected for bioreactor experimental studies. The specific growth rate (μ) was found to be in the range of 0.21-0.23 h^{-1} during the glycerol growth phase and 0.024-0.03 h^{-1} during the methanol induction phase of *P. pastoris* X33/SuperMan5 cultivation in the bioreactor.

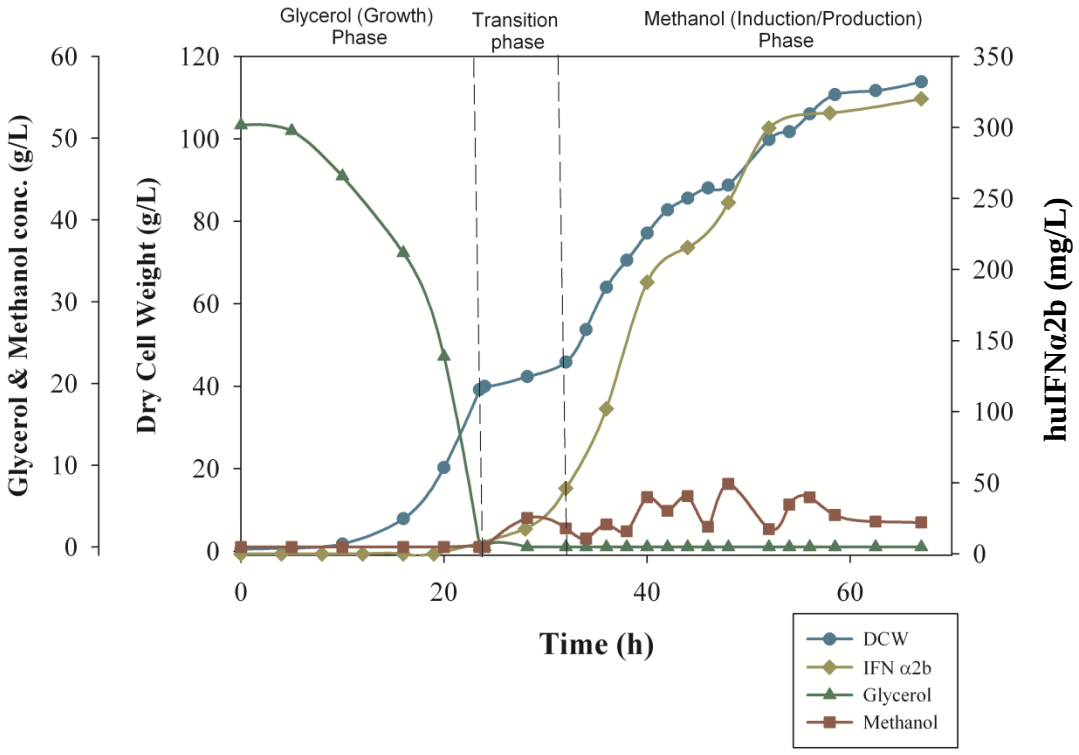

Figure 2.6 Dynamic profile of high cell density cultivation of *P. pastoris* SuperMan5 strain for the production of glycosylated huIFNα2b.

The yields of recombinant huIFNα2b in the culture supernatant of *P. pastoris* X33/SuperMan5 were found to be 350 mg/L and 320 mg/L at a volumetric productivity of 4.86 mg/L.h and 4.77 mg/L.h, respectively in BSM medium. A dynamic profile of the

batch cultivation with different phases for the production of glycosylated huIFNα2b from SuperMan5 strain is presented in Figure 2.6.

Clarified supernatant after the high cell density fermentation of *P. pastoris* X33/SuperMan5 clones expressing glycosylated huIFNα2b was subjected to purification by His-tag affinity chromatography (Figure 2.7), followed by Concanavalin A (ConA) lectin chromatography (Figure 2.8). In His-tag affinity chromatography, huIFNα2b was eluted at imidazole concentration range of 200 mM to 350 mM. The emergence of the proteins in the fractions was monitored by absorbance at 280 nm, and the fractions containing protein were analyzed by sodium dodecyl sulfate polyacrylamide gel electrophoresis (SDS-PAGE).

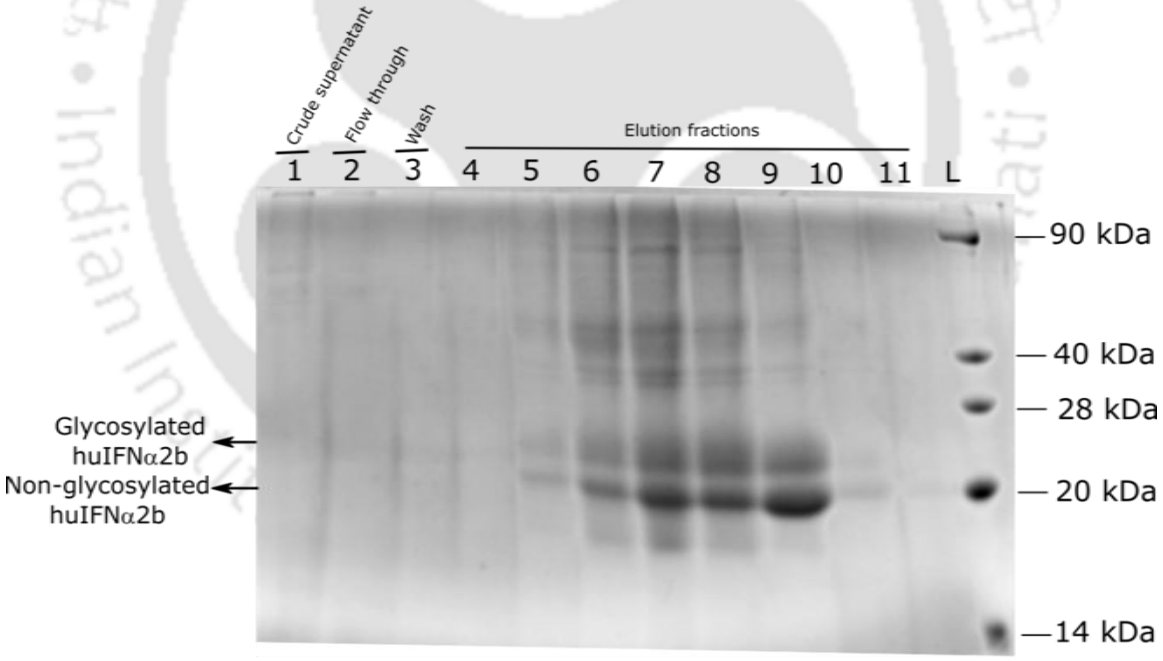

Figure 2.7 SDS-PAGE of fractions collected during His-tag affinity purification of huIFNα2b from the culture supernatant after HCDC of recombinant SuperMan5 strain.. Lane 1: crude supernatant, Lane 2: flow-through fraction, Lane 3: wash fraction, Lanes 4-11 corresponds to different elution fractions.. The protein molecular weight ladder (L) positions are represented on right whereas positions corresponding to non-glycosylated and glycosylated huIFNα2b are marked on the left.

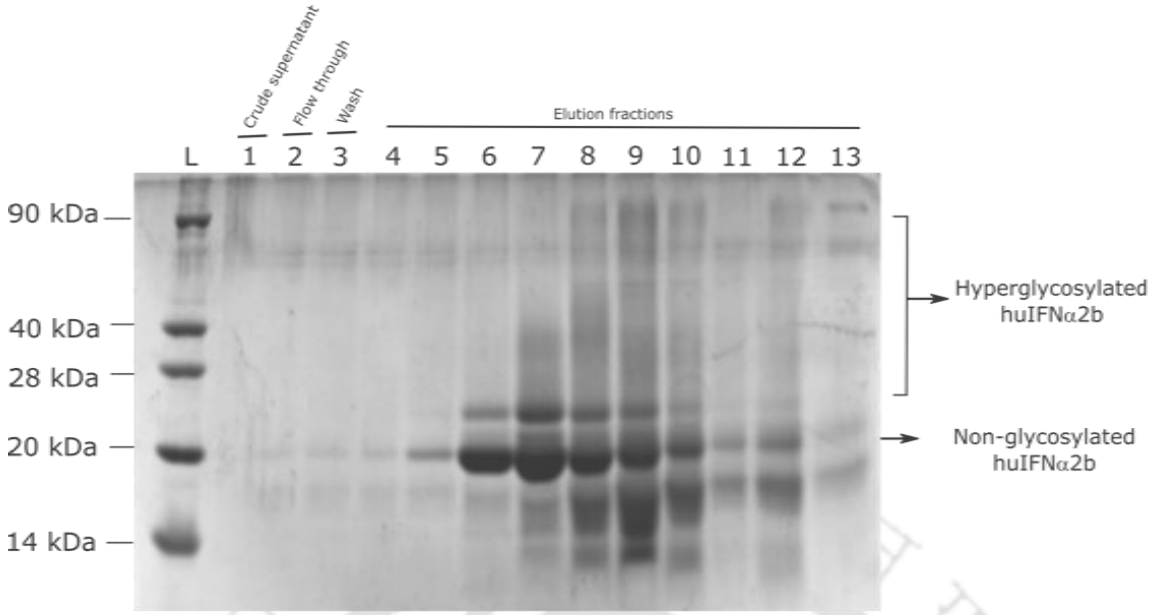

Figure 2.8 SDS-PAGE of fractions collected during His-tag affinity purification of huIFNα2b from the culture supernatant after HCDC of recombinant X33 strain Lane 1: crude supernatant, Lane 2: flow-through fraction, Lane 3: wash fraction, Lanes 4-13 corresponds to elution fractions. The protein molecular weight ladder (L) positions are represented on left whereas positions corresponding to non-glycosylated and hyperglycosylated huIFNα2b are marked on the left.

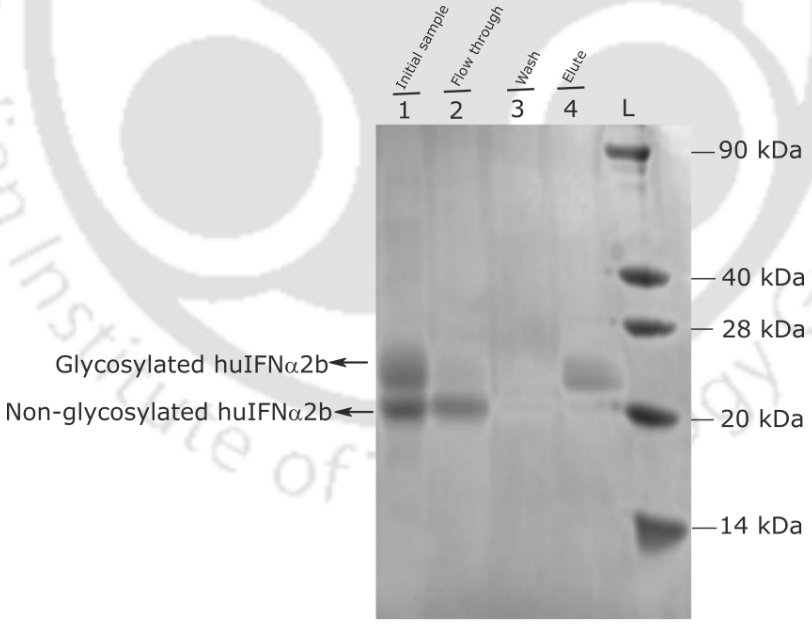

Figure 2.9 SDS-PAGE of fractions collected during Concanavalin A purification of glycosylated huIFNα2b (SuperMan5) from the pooled fraction of His-tag affinity purification elutes Lane: initial sample, Lane 2: flow-through fraction, Lane 3: wash fraction, Lane 4: elution fraction. The protein molecular weight ladder (L) positions are represented on right whereas positions corresponding to non-glycosylated and glycosylated huIFNα2b are marked on the left.

Fractions with huIFNα2b were pooled and subjected to Con A chromatography as earlier described. All the elute fractions collected during the process were subjected to SDS-PAGE analysis (Figure 2.9 and 2.10). The fractions containing purified glycosylated huIFNα2b were pooled, diafiltered and concentrated in 10 kDa cut-off filter against PBS pH 7.4.

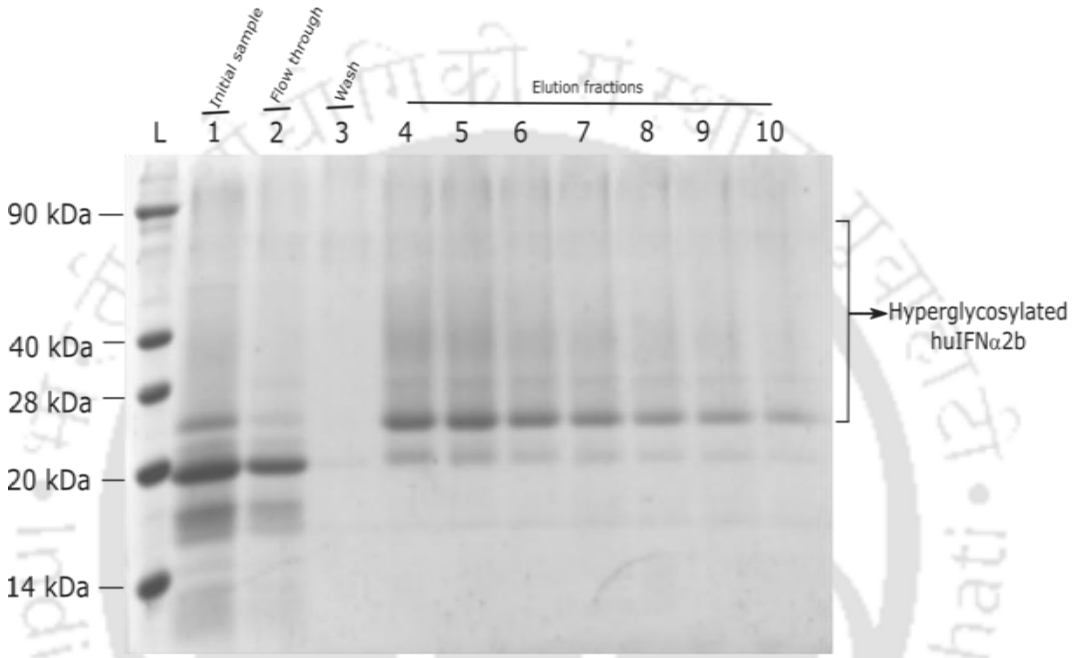

Figure 2.10 SDS-PAGE analysis of by concanavalin A (Con A) chromatography purification of glycosylated huIFNα2b (X33) from the pooled fraction of His-tag affinity purification elutes. Lane 1: initial sample, Lane 2: flow-through fraction, Lane 3: wash fraction. Lane Lane 4-10 corresponds to elution fractions. The protein molecular weight ladder (L) positions are represented on left whereas positions corresponding to and hyperglycosylated huIFNα2b is marked on the left.

The appearance of smear for hyperglycosylated huIFNα2b expressed by X33 strain (Figure 2.11) was confirmed using immunodetection assay, using primary anti-huIFNα2b monoclonal antibody and secondary mouse-IgG1 antibody. The disappearance of smear was observed after deglycosylation of protein with PNGase F enzyme (Figure 2.11).

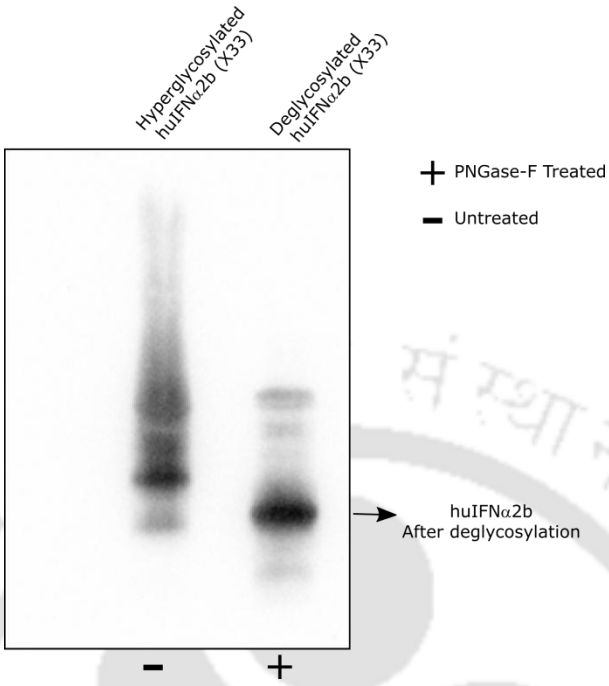

Figure 2.11 Immunodetection of hyperglycosylated huIFNα2b from X33 strain before and after treatment with PNGase F. A shift in the band with the loss of smear pattern can be observed after PNGase F treatment which specifically removed N-glycans.

Similarly, non-glycosylated native huIFNα2b from the clarified supernatant was purified by His-tag affinity chromatography followed by size exclusion chromatography. The fractions containing purified non-glycosylated huIFNα2b were pooled, diafiltered and concentrated in 10 kDa cut-off filter (Figure 2.12 A and 2.12 B). The % purity of the different huIFNα2b expressed in X33 and SuperMan5 strains were found to be greater than 95 % based on ELISA assay.

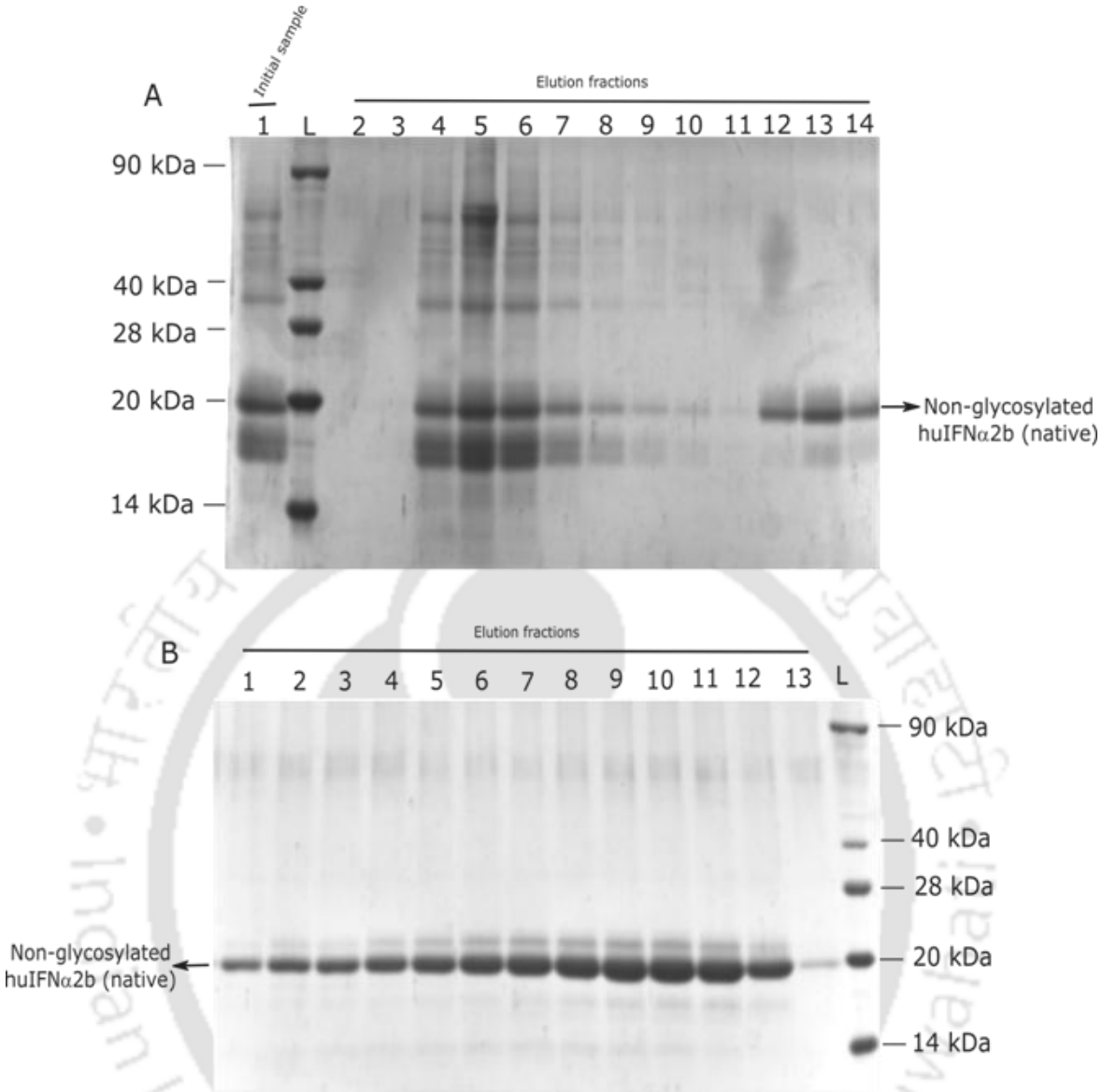

Figure 2.12 SDS-PAGE analysis of size exclusion chromatography purification of non-glycosylated (native) huIFNα2b. A) From SuperMan5 strain, Lane 1: initial sample after his- chromatography, Lane 2-14 corresponds to elution fractions. The protein molecular weight ladder (L) positions are represented on the left. B) From X33 strain, Lane 1-13 corresponds to elution fractions and the protein molecular weight ladder (L) positions are represented on the right.

2.3.4. Glycosylation analysis of recombinant huIFNα2b

Enzymatic deglycosylation analysis was performed for the purified recombinant glycosylated and non- glycosylated huIFNα2b to identify the type of glycosylation. From the analysis, it was observed that the glycosylated recombinant huIFNα2b was N-glycosylated with the removal of N-glycan attached to the protein as evident from the

shift in protein band. A significant reduction of the glycosylated protein and concomitant increase in non-glycosylated form could be observed from the SDS-PAGE gel. Also, there was no observed shift in protein band for the recombinant non-glycosylated huIFNα2b before and after treatment with PNGase F (Figure 2.13). This result also substantiates that the introduced N-glycosylation site in the huIFNα2b was indeed N- glycosylated.

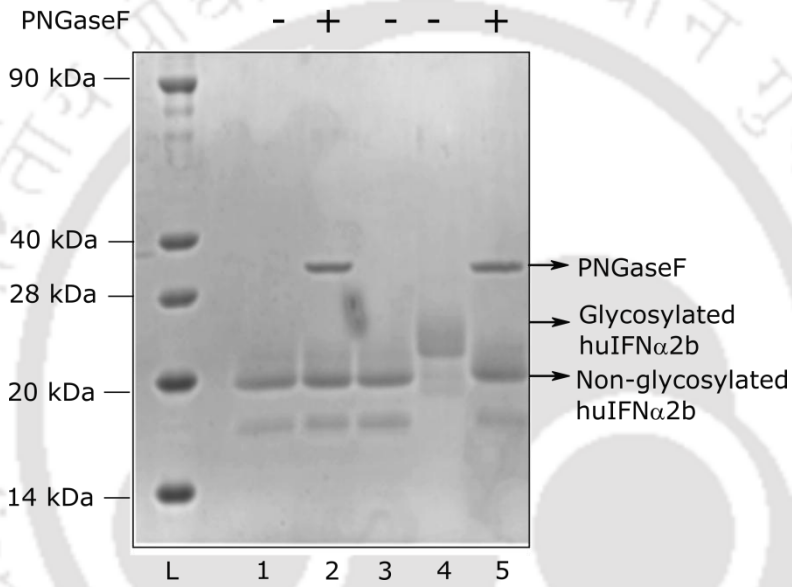

Figure 2.13 SDS-PAGE analysis of deglycosylation experiment for the purified non-glycosylated and glycosylated huIFNα2b from recombinant SuperMan5. Non-glycosylated huIFNα2b (lanes 1-3), glycosylated huIFNα2b (lanes 4-5), Absence (-) or presence (+) of PNGaseF is indicated on top of each lane. The protein molecular weight ladder (L) positions are shown on the left. Treatment of non-glycosylated with PNGase F did not show any difference in migration. Glycosylated huIFNα2b treated with PNGase F showed the difference in migration as compared to untreated.

2.3.5. N- Glycan analysis

N-glycan analysis for the glycosylated huIFNα2b (SuperMan5) by MALDI-TOF/MS analysis revealed that the most prominent peak corresponded to $Man_5GlcNAc_2$ 1579.67 (m/z) and a minor fraction was composed of high mannose glycans which corresponds to $Man_{8\text{-}10}$ $GlcNAc_2$ (m/z 2191.92, 2395.99, 2600.08) (Figure 2.14A). Whereas glycosylated huIFNα2b (X33) yielded predominantly $Man_{10\text{-}18}GlcNAc_2$ (m/z 2600.094,

2804.185, 3008.323, 3212.397, 3416.462, 3620.538, 4028.656, 4232.741) (Figure 2.14B). The predominant peak from the MALDI-TOF MS analysis was subjected to MS/MS analysis to elucidate the structural information. MS/MS spectra of the fragment ions were analyzed using the GlycoWorkbench suite, which helps in the annotation of the glycan fragment spectra. The annotated glycan structure that emerged from the MS/MS analysis of the major glycan peak (m/z 1579.67) of glycosylated huIFNα2b (SuperMan5) was $Man_5GlcNAc_2$ with β1, 4 linked GlcNAc and α1, 2/α1, 6 mannoses. To revalidate the linkage of monosaccharide in the glycan, the prepared Partially Methylated Alditol Acetates (PMAAs) from the glycosylated huIFNα2b sample was subjected to linkage analysis by Gas chromatography–mass spectrometry (GC-MS). From the GC-MS analysis based on the retention time and parallel MS analysis, it is verified that the mannoses present in the glycan sample are α1, 2, α1, 6 linked and the N-acetylglucosamine monosaccharides are β1, 4 linked. The influence of batch-to-batch variability on the glycan profile for glycosylated huIFNα2b expressed by SuperMan5 strain was observed to be negligible. The MALDI-TOF/MS analysis proved that $Man_5GlcNAc_2$ was predominantly found.

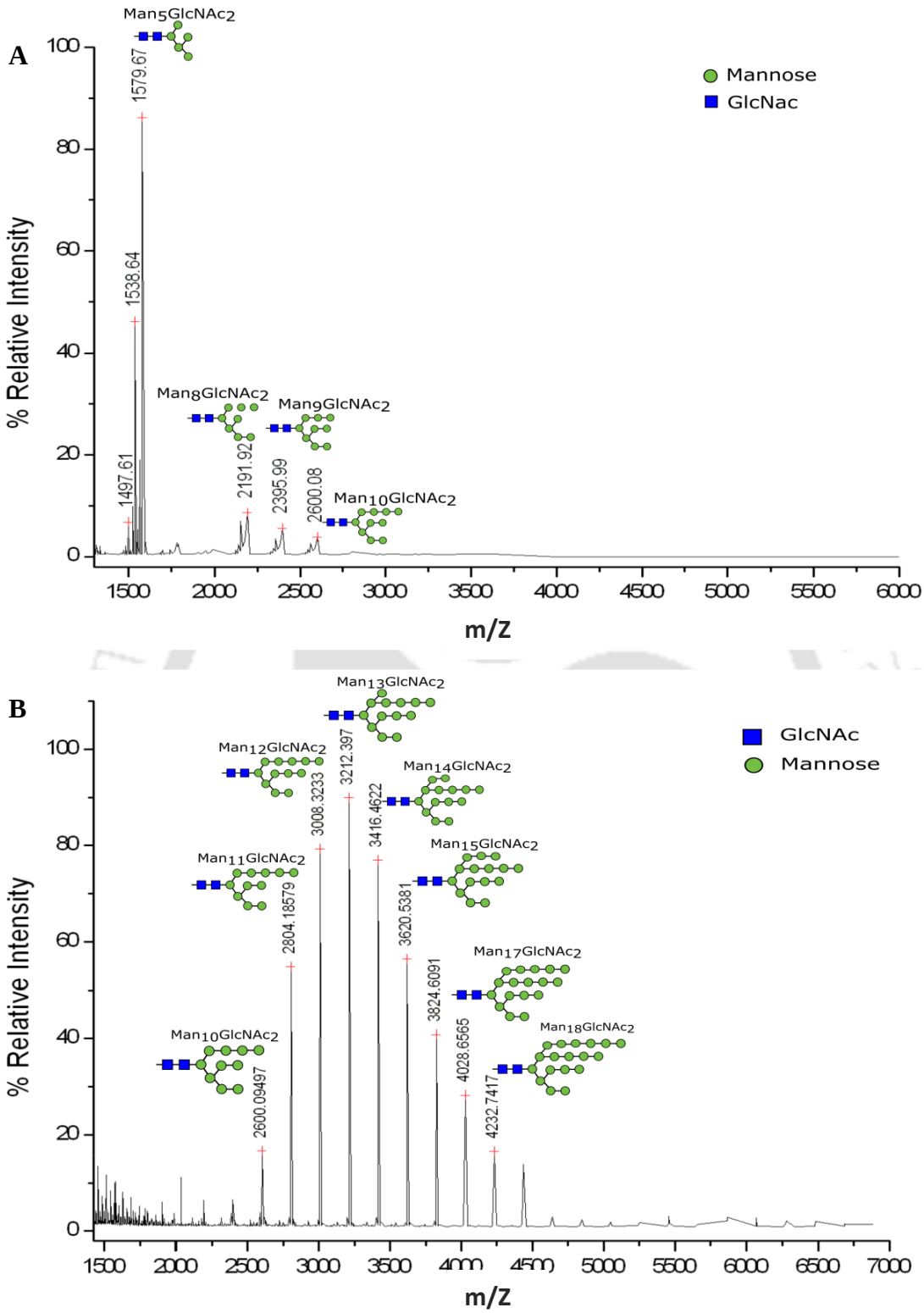

Figure 2.14 MALDI-TOF mass spectrum of enzymatically released N- glycans from glycosylated huIFNα2b obtained from A) *P. pastoris* SuperMan5, the major signal at m/z 1579.67 corresponds to $Man_5GlcNAc_2$ glycan and other minor signals (m/z 2191.92, 2395.99, 2600.08) correspond to Man_8, Man_9 and Man_{10} glycans. B) *P. pastoris* X33, the major signals (m/z 2600.094, 2804.185, 3008.323, 3212.397, 3416.462, 3620.538, 4028.656, 4232.741) correspond to $Man_{10\text{-}18}GlcNAc_2$ N-glycans.

2.3.6. Biological activity of huIFNα2b

The biological (antiviral) activity of the different variants of huIFNα2b was assessed by the antiviral response using the HCV and HEV subgenomic replicon assay systems. All the forms of huIFNα2b displayed significant inhibition of HCV and HEV replication by at least 30 % and the inhibition was concentration-dependent (Figure 2.15A and 2.15B). The greater reduction in the viral (HCV and HEV) subgenomic replication was observed at highest concentration used (10 ng). Retention of antiviral activity by glycosylated huIFNα2b with Man5 glycan (SuperMan5) was validated. From the cell viability/ cytotoxic analysis, it was observed that the glycosylated huIFNα2b and the standards did not exhibit any cytotoxic effect on the cells (Figure 2.16A and 2.16B).

.

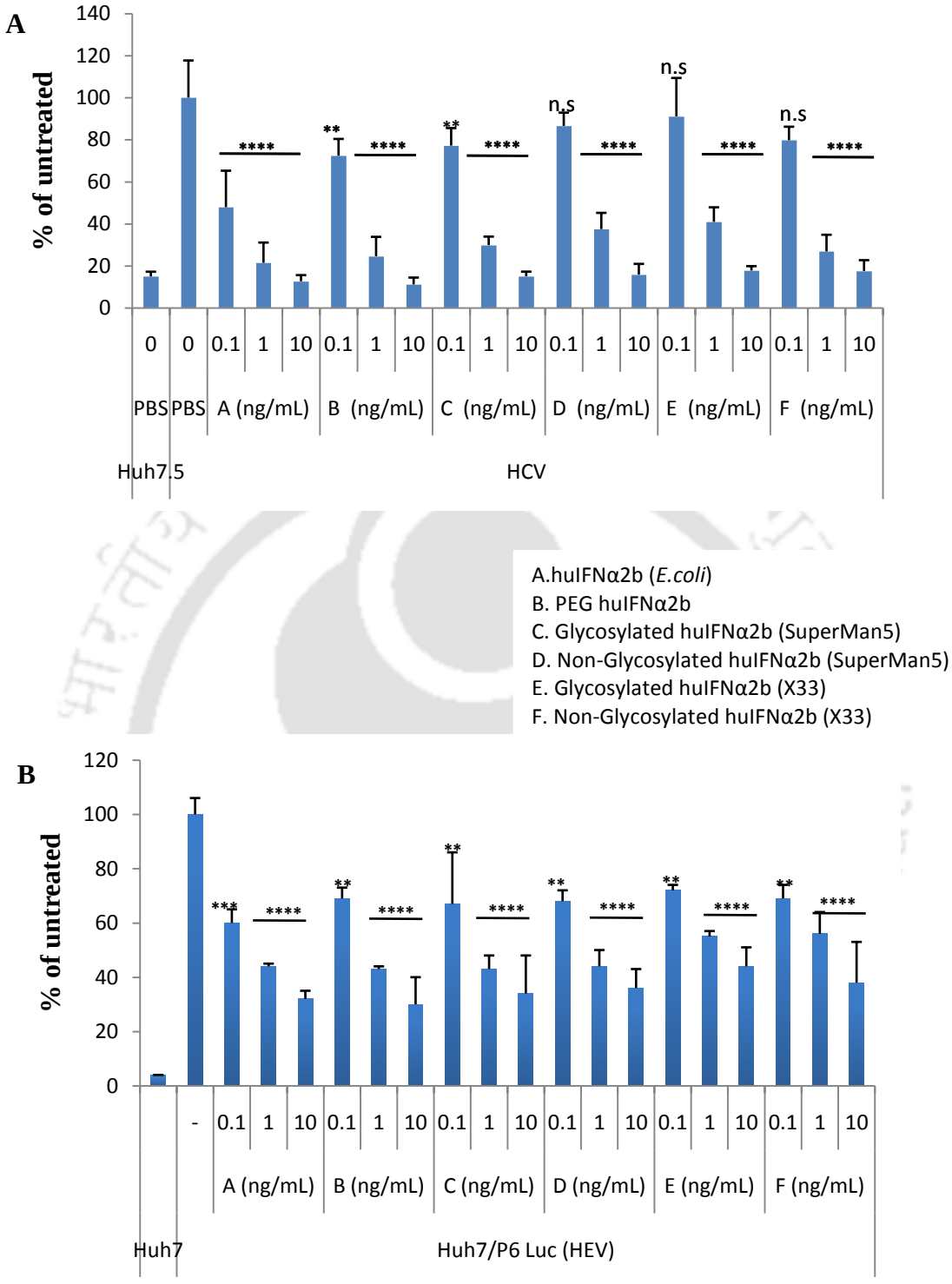

Figure 2.15 Antiviral activities of different forms of huIFNα2b against HCV and HEV replication. The dose dependent % inhibition of HCV (A) and HEV (B) subgenomic replicon after 48 h of post treatment in Huh7.5/Huh7.0 cells by different forms of huIFNα2b along with standard are depicted. The data represented are the means (± SEM) of three independent experiments. Statistical significance of the data was tested against the control by ANOVA followed by Dunnett's corrected *t* test (* $P < 0.05$; ** $P < 0.01$; *** $P < 0.001$; **** $P < 0.0001$; n.s- not significant)

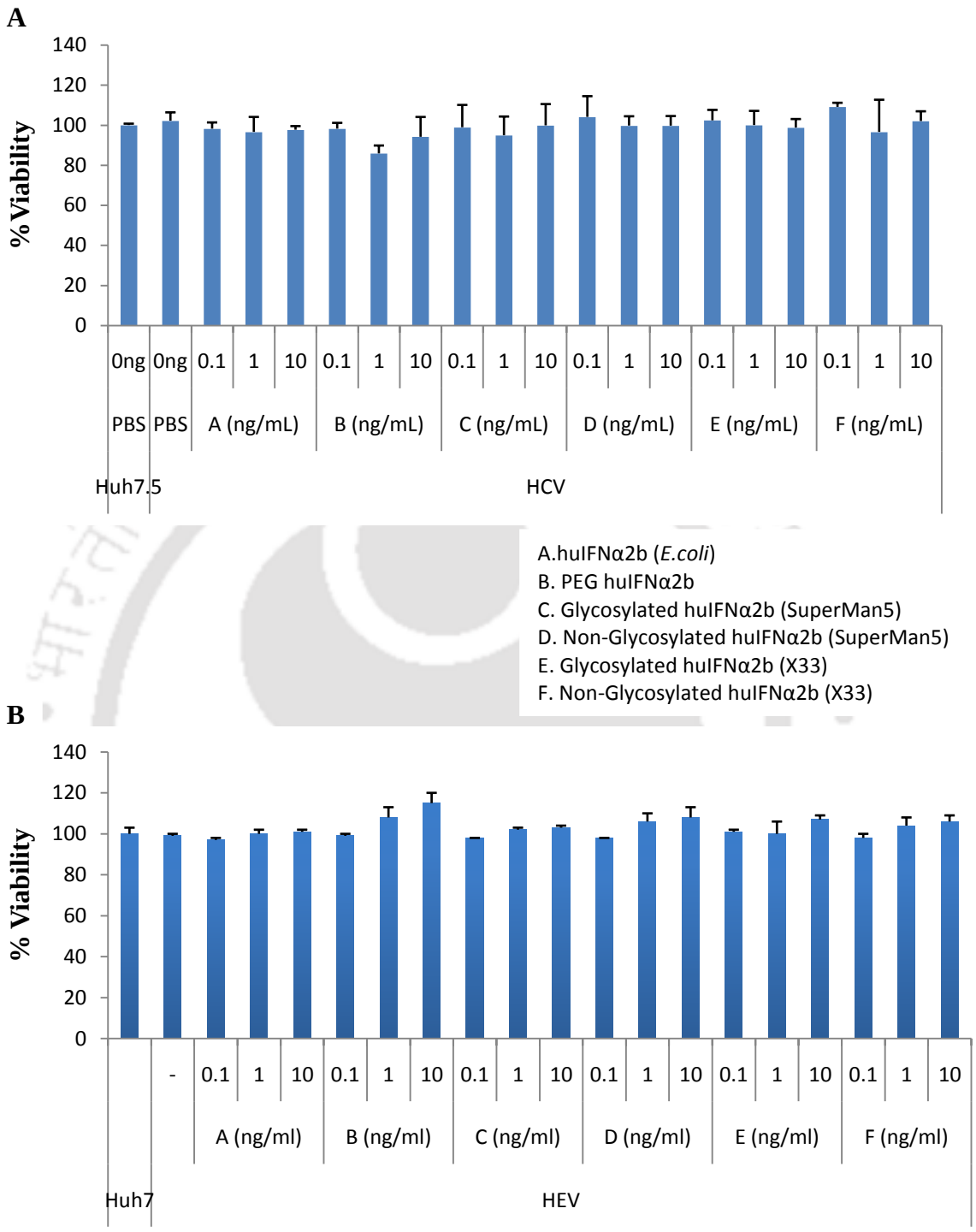

Figure 2.16 Cytotoxicity analysis of different forms of huIFNα2b. (A) HCV (B) HEV. The % viablility of the cells (Huh7.5/Huh7.0) after the 2 h of treatment and the mean values (± SEM) are depicted.

2.3.7. Pharmacokinetic studies in rats

Pharmacokinetics studies in female Wistar rats inferred that, the plasma concentration of the glycosylated huIFNα2b (SuperMan5) reached maximum (C_{max}= 174.51 ± 40.98 pg/mL) at 3.00 ± 1.76 h post injection. Whereas for the glycosylated huIFNα2b (X33) the plasma concentration of the glycosylated huIFNα2b (SuperMan5) reached maximum (C_{max}= 116.56 ± 10.36 pg/mL) at 0.67 ± 0.29 h post injection. For the huIFNα2b -*E. coli* (C_{max}= 432.75 ± 250.41 pg/mL) and pegylated huIFNα2b (C_{max}= 1763.40 ± 11.05 pg/mL), the maximum concentration was reached at 1.17 ± 0.76 h and 5.33 ± 1.15 h, respectively. The plasma half-life of huIFNα2b (*E. coli*) was found to be relatively less ($t_{1/2}$ = 1.36 ± 0.59 h) compared to glycosylated huIFNα2b from SuperMan5 strain ($t_{1/2}$= 1.75 ± 0.36 h) and pegylated huIFNα2b ($t_{1/2}$= 5.87 ± 1.19 h). Whereas the plasma half-life of glycosylated huIFNα2b from X33 strain ($t_{1/2}$ = 1.19± 0.23 h) was lower than the huIFNα2b (*E. coli*), and this could be due to the heterogeneity of the glycans attached on huIFNα2b produced from wild-type (X33) strain. Significantly, the glycosylated huIFNα2b (SuperMan5) of the present study with a single N- glycosylation site showed a 1.3-fold increase in $t_{1/2}$ compared to *E. coli* derived huIFNα2b (Table 2.1).

Table 2.1 Mean (±SEM) value of the pharmacokinetic parameter after single dose subcutaneous administration of huIFNα2b sample in female Wistar rats (n=3 per each huIFNα2b)

Sample	T_{max} (h)	C_{max} (pg/mL)	$t_{1/2}$ (h)
huIFNα2b (*E. coli*)	1.17 ± 0.76	432.75 ± 250.41	1.36 ± 0.59
Pegylated huIFNα2b	5.33 ± 1.15	1763.40 ± 11.05[a]	5.87 ± 1.19[a]
Glycosylated huIFNα2b (SuperMan5)	3.00 ± 1.76[a]	174.51 ± 40.98[b]	1.75 ± 0.36[a]
Glycosylated huIFNα2b (X33)	0.67± 0.29[b]	116.56 ± 10.36[b]	1.19± 0.23

a. statistically significant at α=0.05 by paired *t*-test with huFNα2b (*E. coli*) standard

b. statistically significant at α=0.1by paired *t*-test with huIFN α2b

2.4. Discussion

Low molecular weight therapeutic proteins have lower stability when administered to humans, and require multiple administrations to attain a desired therapeutic efficacy. This leads to compromise in the patient's quality of life with side effects, pain, and inconvenience [73]. Human interferon alpha 2b is one such low molecular weight therapeutic cytokine with short circulating half-life. Till date, pegylation is one such strategy that has been successfully employed to increase the circulating half-life of cytokine (huIFNα2b) by chemical conjugation with the PEG molecule [79]. However, pegylation has its own limitations leading to formation of neutralizing antibodies, resulting in treatment failure [151]. Furthermore, glycoengineering strategy is an alternative approach to enhance the circulating half-life of therapeutic proteins. It enhances pharmacokinetic properties and yields glycosylated analogs with newly inserted sites, that are potential N- glycosylation points [76, 152]. The primary objective of this present study is to develop a glycosylated huIFNα2b with increased plasma half-life without jeopardizing its biological activity.

The selection of site in a protein sequence to generate N-glycosylation motif is very crucial for proteins of therapeutic importance [75]. The rationale behind the selection of this site was being the fact that the N-glycosylation site i) is located in the exposed loop region/outside the alpha-helix structure [163] facilitating high possibility of N-glycan addition and negating the perturbation in the secondary structure ii) is distant to receptor binding site [163], thus negating the feasibility of aborted huIFNα2b binding iii) is at close proximity to the O-glycosylation site (T^{106}) and mimics the native form, which in turn could potentially assist in unaltered cellular interactions. Introduction of potential N-glycosylation site to a native huIFNα2b protein through single-point mutation can be attributed to prolonged plasma half-life. The increase in hydrodynamic radius of

glycosylated huIFNα2b by N-glycosylation resulted in extended plasma half-life of the protein in the circulatory system as reported for therapeutic N-glycosylated alpha-1-antitrypsin [75]. The constructed expression vector bearing the codon optimized the human huIFNα2b gene with a single N-glycosylation site at position 104 in the amino acid sequence where glycine (G) was replaced with asparagine (N). This led to the creation of an N-glycosylation site (N-V-T) in which N was glycosylated, followed by transformation into wild-type *P. pastoris* (X33) and glycoengineered *P. pastoris* (SuperMan5), respectively. The glycosylation of the wild-type *P. pastoris* (X33) is of hypermannosylation type, $Man_8GlcNAc_2$ glycans from the endoplasmic reticulum is further extended by addition of mannoses by α-1,6-mannosyltransferase (OCH1). In contrast to X33 strain, glycoengineered SuperMan5 strain (BioGrammatics, Inc.) could modify $Man_8GlcNAc_2$ glycans to human type $Man_5GlcNAc_2$ glycans (Figure 2.17), and this strategy to control hyperglycosylation acts as an important step in the incorporation of complex glycans in various proteins [71, 161].

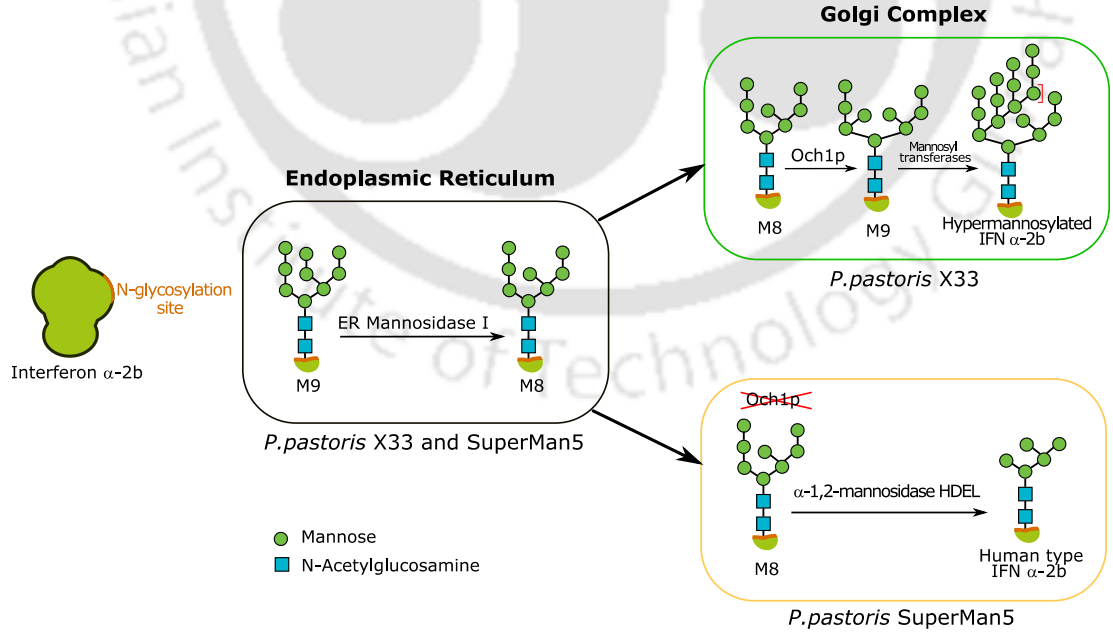

Figure 2.17 Glycosylated huIFNα2b expressed by *P. pastoris* X33 and SuperMan5 strain

High cell density cultivation of recombinant X33 and SuperMan5 successfully expressed glycosylated huIFNα2b and extracellularly secreted into culture supernatant. The huIFNα2b yield (SuperMan5 (350 mg/L) and X33 (320 mg/L)) obtained from high cell density cultivation in the present study is comparable with the yield values previously reported in literature using different yeast expression hosts (Table 2.2). A significant increase in the huIFNα2b yield at bioreactor level compared to shake flask study was due to the controlled bioprocess conditions, especially maintaining the DO concentration at critical level. The DO concentration has direct effect on protein yield in *P. pastoris* fermentation, as alcohol oxidase requires sufficient DO to metabolize available methanol during the methanol fed-batch (induction) phase.

Table 2.2 Production of huIFNα2b in batch and fed batch cultivation processes

Strain used	**Cultivation process**	**huIFNα2b titer (mg/L)**	**Reference**
S. cerevisiae	Batch	15	[61]
P. pastoris GS115	Fed-batch[a]	298	[65]
P. pastoris GS115	Batch[b]	200	[55]
P. pastoris KM71H	Fed-batch[a]	600	[56]
P. pastoris GS115	Fed-batch[a]	300	[57]
Y. lipolytica	Fed-batch	425	[52]
P. pastoris SuperMan5 (glycoengineered strain)	Batch[b]	320	(Present study)
P. pastoris X33	Batch[b]	350	(Present study)

a Includes glycerol batch, glycerol fed-batch and methanol induction phase, b Includes glycerol batch and methanol induction phase

Culture supernatant from high cell density cultivation was subjected to two steps of purification including His-tag chromatography and Concanavalin A (Con A) chromatography. Attachment of 6x His affinity tag to the protein aid in purification, which rarely affects the protein characteristics and the ease of His-tag removal by site-specific protease treatment [167]. His-tag chromatography purification yielded two forms of huIFNα2b; one at 20 kDa which corresponded to non-glycosylated form of huIFNα2b and the other around 22 kDa, which is related to the glycosylated form of huIFNα2b (Figure 2.7 and 2.8). The occurrence of two forms of huIFNα2b could be attributed to parallel co-translational events and presence of potential glycosylation site near the C-terminus [168, 169]. From the polypeptide sequence of huIFNα2b, it was observed that the N-glycosylation site ($N^{104}V^{105}T^{106}$) was nearer to the C-terminus. The presence of both non-glycosylated and glycosylated huIFNα2b could be due to competing co-translational events including translocation and protein folding, where the kinetics of translocation event across the endoplasmic reticulum are rapid compared to translation. Because of these co-translational events, the potential glycosylation site will have brief moment in time to be glycosylated in the presence of oligosaccharyltransferase (OST). Similar findings were reported in relation to expression of different proteins in *P. pastoris* [170, 171]. In order to understand the influence of glycosylation on plasma half-life and the biological activity of huIFNα2b, the glycosylated huIFNα2b was further purified using lectin (Con A) chromatography. Further, the N-glycosylation was verified by treating the purified protein with PNGase F. Treatment with PNGase F resulted in reduction in the molecular mass, confirming the removal of N-linked glycans (Figure 2.11). The MALDI-TOF and MS-MS analysis (Figure 2.14A) indicated that the major fraction N-linked glycan attached to the glycosylated huIFNα2b from SuperMan5 strain was $Man_5GlcNAc_2$, and only a minor

fraction was of the high molecular weight glycans (Man_{8-10}). No significant batch-to-batch variation observed in glycan profile of glycosylated huIFNα2b (SuperMan5) highlights the robustness of the glycoengineered *P. pastoris* strain, and the major glycosylation changes are enforced at genome level [91, 130]. But in case of glycosylated huIFNα2b expressed from X33 strain, the glycans were predominantly of hypermannosylated type ($Man_{10-18}GlcNAc_2$) with heterogeneity (Figure 2.14B) which could led to decrease in plasma half-life in Wistar rats. The minor fraction of high molecular weight glycans of glycosylated huIFNα2b from SuperMan5 strain might be either due to the presence of interfering endogenous mannosyltransferases or the incomplete processing of α-1, 2- mannosidase introduced in SuperMan5 strain, or a combination of both. These results corroborated well with the published reports where > 90 % of the N-glycans attached to the recombinant proteins expressed by SuperMan5 strain are $Man_5GlcNAc_2$ glycans [91, 162]. It has been reported that the carbohydrate addition or amino acid substitutions are known to cause severe loss of huIFNα2b activity because of steric hindrances caused by attachment of carbohydrate moieties which decreases the receptor-binding affinity [80]. Therefore, a comparative evaluation of antiviral activity of the glycosylated huIFNα2b variants against the standard huIFNα2b drugs available in the market was performed in HCV and HEV subgenomic replicon system. HCV and HEV systems were specifically chosen since the huIFNα2b drugs are mainly used for treatment of hepatitis virus infections. HCV and HEV sub-replicon system are considered advantageous owing to their robustness, efficiency and cost-effectiveness compared to conventional antiviral assay where human cell lines were challenged with the virus followed by drug treatment. Interestingly, in our study there was no observed significant difference in the antiviral activity for the glycosylated huIFNα2b (SuperMan5) when compared with the non-glycosylated huIFNα2b of *E. coli*

origin and pegylated huIFNα2b at 10 ng/mL concentration (Figure 2.15A and 2.15B); indicating that N-glycan attachment did not significantly impact antiviral activity. Hence, the antiviral activity results substantiates that the selected N-glycosylation site (in the loop or unstructured region) did not interfere with receptor binding. The antiviral activity of different variants of huIFNα2b against HCV was more pronounced in comparison to that of HEV, where the inhibition was moderate (Figure 2.15A and 2.15B). This moderate to less inhibition of HEV after treatment with huIFNα2b could be attributed to anti-interferon mechanism exerted by HEV in downregulating the interferon-stimulated genes (ISG's) [172]. The *in vivo* studies using Wistar rats effectively addressed the influence of glycosylation on the plasma half-life of the protein and pharmacokinetics. The non-glycosylated huIFNα2b from *E. coli* was observed to be cleared rapidly from plasma ($t_{1/2}$ = 1.36 ± 0.59 h) and is correlated well with extant reports [80]. Conversely, the glycosylated huIFNα2b with a single N- glycosylation site from SuperMan5 *P. pastoris* strain showed improved plasma half-life ($t_{1/2}$ = 1.75 ± 0.36 h). The plasma half-life of glycosylated huIFNα2b was 1.3 fold higher (Table 2.1) than non-glycosylated huIFNα2b. The increase in plasma half-life is significant and is concurrent with the reported literature for different human therapeutics (Alpha-1 antitrypsin, interferon β1) where authors have introduced an additional N-glycosylation site through site directed mutagenesis and obtained a 1.5 to 1.7 fold increase in plasma half-life as compared to their unmodified therapeutics [75, 173]. Although the plasma half-life of pegylated huIFNα2b ($t_{1/2}$= 5.87 ± 1.19 h) was found to be higher owing to the chemical conjugation of 12 kDa polyethylene glycol molecule, it therapeutic use has disadvantages which could affect patient's quality life. The chief disadvantages include the formation of renal tubular vacuolation, lysosomal storage disease because of non-degradable nature of PEG polymer in human body and immunogenicity [174, 175] .

Alternatively, glycoengineering does not involve additional modification of the protein (for e.g. chemical conjugation of PEG molecule) after clone development as the glycosylation is a natural post translation modification (human-like glycosylation) in glycoengineered *P. pastoris*. Though, pegylated huIFNα2b drugs are clinically available, the current research and innovation is focussed on development of biobetter huIFNα2b using inherent ability of the host strain viz., glycosylation to enhance plasma half-life and improve patient's quality life. The present study is first-of-its-kind on this line to develop a human-like glycosylated huIFNα2b using glycoengineered *P. pastoris* with increased plasma half-life possibily envisaging the decrease in the number of dosages and no negative affect on biological activity.

2.5. Conclusion

In summary, N-glycosylated huIFNα2b was successfully expressed with human type $Man_5GlcNAc_2$ glycan with greater homogeneity by the application of glycoengineering strategy and the glycoengineered SuperMan5 *P. pastoris* strain. Glycosylated huIFNα2b of the present study exhibited 1.3-fold increase in the plasma half-life compared to non-glycosylated huIFNα2b produced from *E. coli* .The introduced N-glycosylation site ($N^{104}V^{105}T^{106}$) did not result in loss of antiviral activity against HCV/HEV system and also the purified glycosylated huIFNα2b was not cytotoxic to the human cell lines. The N-glycosylated huIFNα2b reported in this chapter offers the double advantage of retention of full antiviral activity with improved pharmacokinetic property (plasma half-life), which exemplifies the huge scope for its commercialization in near future.

Chapter 3

Medium optimization studies for high level extracellular production of recombinant huIFNα2b in glycoengineered *Pichia pastoris*

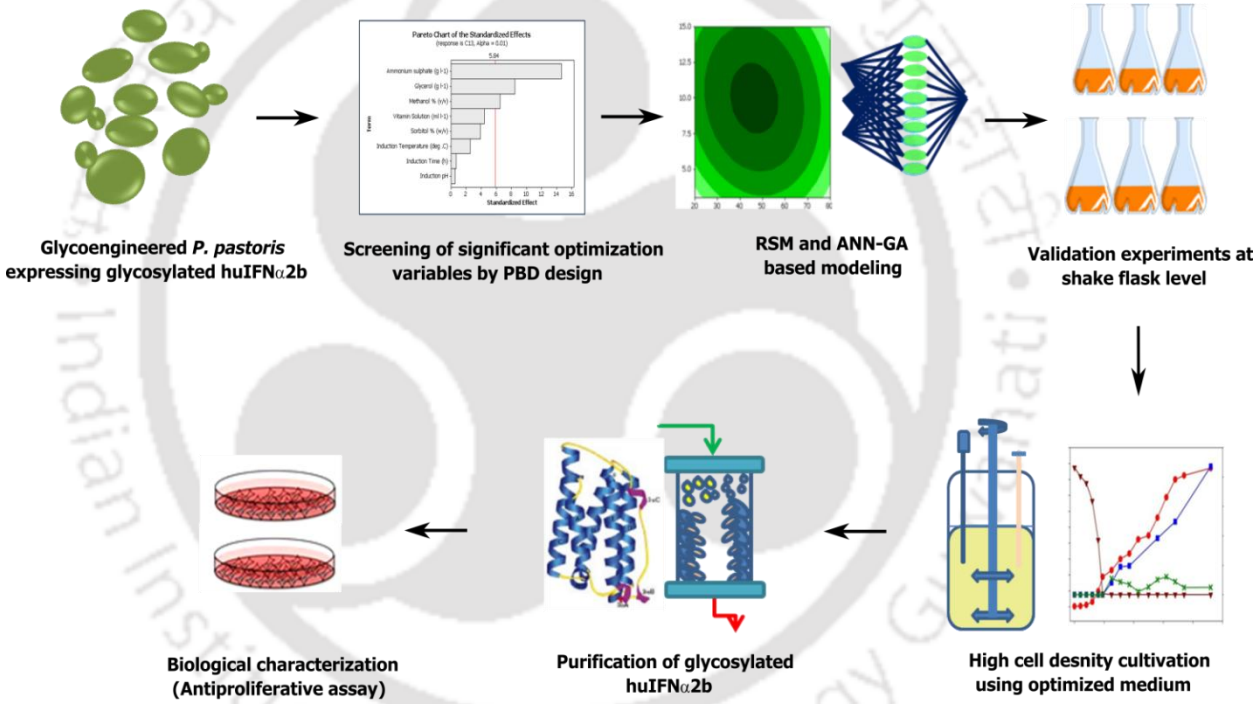

Chapter 3

Medium optimization studies for high level extracellular production of recombinant huIFNα2b in glycoengineered *Pichia pastoris*

Abstract

The present chapter was aimed at design of experiments (DoE) and artificial intelligence based culture medium optimization for high level extracellular production of a novel recombinant human interferon alpha 2b (huIFNα2b) in glycoengineered *Pichia pastoris* and its characterization. Artificial neural network- Genetic algorithm (ANN-GA) model exhibited improved huIFNα2b production and better predictability compared to RSM. The optimized medium exhibited 5-fold increase in huIFNα2b titer compared to the complex medium. A maximum titer of huIFNα2b (436 mg/L) was achieved using the optimized medium in the bioreactor. Real time capacitance data from dielectric spectroscopy was utilized to model the growth kinetics with unstructured models. Biological characterization by antiproliferative assay proved that the purified recombinant huIFNα2b was biologically active, exhibiting growth inhibition on breast cancer cell line. Culture medium optimization resulted in enhanced production of huIFNα2b in glycoengineered *P. pastoris* at both shake flask and bioreactor level. The purified huIFNα2b was found to be N-glycosylated and biologically active.

3.1. Introduction

Recombinant protein production in *P. pastoris* is significantly influenced by some factors like optimum concentration of medium components and different process conditions [169]. Thus, optimization of medium components and process parameters are the key strategies for enhancing the yield of the desired product. Design of Experiments (DoE) such as Plackett-Burman Design (PBD), Response Surface Methodology (RSM) and artificial intelligence methods like Artificial Neural Network (ANN) coupled Genetic Algorithm (GA) are statistical methods which help in identification of significant factors. These factors include building the models, evaluating the effect of factors by studying their interaction, and analyzing the optimum conditions for maximum product formation [176]. Statistical methods (RSM, ANN-GA) help in varying several factors needed to study the interaction among them, with minimum number of experiments compared to classical one-factor-at-a-time approach where each factor is studied independently with a large number of experiments, and these optimization methods for bioprocess are vital for industrial scale up [177-179]. PBD helps in identifying the significant factors influencing protein production and RSM provides the optimum conditions for maximizing the protein production by evaluating the interaction between the identified significant factors. In addition, ANN-GA further optimizes the RSM model to enhance the protein yield, by addressing the complex non-linearity issues of RSM [180]. DoE along with ANN have been successfully employed for the optimization of culture conditions [181, 182].

Real time monitoring of *P. pastoris* growth would provide insight on cell viability in the optimized medium and help in the better understanding of the onset of induction phase in huIFNα2b production. For example, Viable Cell Volume (VCV) is a cardinal bioprocess parameter, which is always under scrutiny, as any physiological change in the cell

population can result to quality downgrade [183]. Typically, biomass is measured by analysis of Dry Cell Weight (DCW), flow cytometry, or measurement of marker molecules using high performance liquid chromatography (HPLC) [184, 185]. Application of these techniques either offline, at-line or by sophisticated on-line interface does not yield viable real time information. Dielectric spectroscopy has emerged as a promising technique for online or real time monitoring of biomass. It offers multiple advantages of non-invasive, *in-situ* operation, selective measurement of viable biomass, simple linear calibration for biomass calculation and short interval measurements [186]. Dielectric spectroscopy works on the principle of polarization of individual cell membranes when an electric field is applied, converting each cell into a capacitor. Dielectric spectroscopy has been employed for online monitoring of biomass for bacteria [117], yeast [118], filamentous fungi [187] and mammalian [120] cell populations. Apart from dielectric spectroscopy, exhaust gas analysis or respirometry has also been used as an PAT tool for biomass monitoring by quantifying oxygen uptake rate (OUR) and carbon dioxide evolution rate (CER) [188].

This present chapter is focused on maximizing the recombinant human huIFNα2b titer, by employing design of experiments, and artificial intelligence based optimization methods. The antiproliferative activity of the purified recombinant huIFNα2b is elucidated using breast cancer cell line. Dielectric spectroscopy (DS) and respirometry are employed as online tools to assess the viability of *P. pastoris* in the optimized medium. Few studies have been reported for the production of huIFNα2b in *P. pastoris* [55-57, 65] and little data has been reported for media optimization studies for enhancing the huIFNα2b titer. To the best of our knowledge, this is the first kind of attempt for enhancing the production of human huIFNα2b in *P. pastoris* SuperMan5 strain by medium optimization studies. Also, in all probability, this present study is a novice

attempt to estimate the kinetic parameters for glycoengineered *P. pastoris* growth, using the measured real-time capacitance data measured by DS.

3.2. Materials and Methods

3.2.1. Strain

A Glycoswitch® *P. pastoris* SuperMan5 (glycoengineered, protease deficient and Mut^+ strain), expressing glycosylated human interferon alpha 2b extracellularly under the control of the AOX1 promoter, was used in this study. The construction of this strain has been described in chapter 2, section 2.2.3 and 2.2.4. The stock culture was maintained at – 80˚C, in YPD media containing 20 % (v/v) glycerol.

3.2.2. Media

Media optimization studies were carried out using basal salt medium. The composition of the medium (in g/L) was 20 glycerol, 18.2 K_2SO_4 , 7.28 $MgSO_4$, 4.13 KOH, 0.93 $CaSO_4.2H_2O$, 5 $(NH_4)_2SO_4$, 26.7 mL/L 85 % (v/v) orthophosphoric acid and 4.4 mL/L PTM4 salts. For the medium preparation, all the medium components except PTM4 salts were sterilized by autoclaving, and PTM4 salts solution was filter sterilized and added to the medium aseptically, after adjusting the pH to 5.5 with 3M NaOH. The PTM4 salt solution contained (in g/L): 2 $CuSO_4.5H_2O$, 0.08 NaI, 3 $MnSO_4.H_2O$, 0.2 $Na_2MoO_4.2H_2O$, 0.02 H_3BO_3, 0.5 $CaSO_4.2H_2O$, 0.5 $CoCl_2$, 7 $ZnCl_2$, 22 $FeSO_4.7H_2O$, 0.2 biotin and 1 mL/L H_2SO_4 98 % (v/v). The vitamin solution (2000X) used for PBD studies was of composition (in g/L) 0.53 thiamine HCl, 1.4 myo-inositol, 0.045 pyridoxine, 0.12 riboflavin, 0.06 nicotinic acid, 0.764 para-aminobenzoic acid, and 0.274 pantothenic acid.

Buffered Glycerol-Complex Medium (BMGY) medium contained (in g/L): 10 yeast extract, 20 peptone, 13.4 YNB, 0.0004 biotin, 10 glycerol (1 % w/v and 99 % purity) and 100 mL of 1 M potassium phosphate buffer, pH 6.0. The composition of Buffered

Methanol-Complex Medium (BMMY) medium remained the same except for the glycerol which was replaced by 5 g/L of 100 % methanol.

3.2.3. Inoculum preparation

YPD medium was used in starter culture preparation with a composition of 1 % (w/v) yeast extract, 2 % (w/v) peptone, and 2 % (w/v) dextrose. The medium with composition of 1 % (w/v) yeast extract, 2 % (w/v) peptone, and 1 % (w/v) glycerol was used for inoculum preparation for the reactor study.

A loop full of recombinant *P. pastoris* culture from glycerol stock vial stored at -80°C was used to inoculate 5 mL of YPD broth for starter culture, and incubated at 30°C and 220 RPM for 48 h. The starter culture was used to prepare the inoculum for reactor studies by inoculating in 170 mL of YPG media and incubated at the afore mentioned conditions for 24 h. 10 % (v/v) inoculum of an optical cell density (OD_{600}) of 4 was used for the reactor study.

3.2.4. Sampling and Analysis

Samples were collected at regular time intervals during the entire fermentation process, and analyzed for biomass, glycerol and methanol concentration, and huIFNα2b titer as described below. Cell concentration of the collected samples was estimated by measuring the optical density at 600 nm, using UV-visible spectrophotometer (GE Healthcare, UK). For dry cell weight (DCW) estimation, 1 mL of the culture broth was centrifuged at 10000 g for 10 min, in a pre-weighed 1.5 mL centrifuge tube, and the supernatant was separated and stored at –20°C for further analysis. The pellet was washed twice with distilled water, re-centrifuged and dried to constant weight at a temperature of 80°C. One OD_{600} corresponds to 0.16 g DCW/L. The concentrations of glycerol and methanol in the samples were analyzed by HPLC (Shimadzu Ltd., Tokyo,

Japan), using a Rezex RHM- monosaccharide H+ Column (Phenomenex Inc, California, USA). 5 mM sulfuric acid was used as the mobile phase with an isocratic flow of 0.6 mL/min at 50°C. Peaks were detected using a refractive index detector and quantified based on the peak height. The concentration of huIFNα2b in the samples was determined by enzyme linked immunosorbent assay (ELISA) analysis using huIFNα2b ELISA kit (Mabtech AB, Sweden).

3.2.5. Design of experiments (DoE) based optimization

3.2.5.1. Plackett-Burman Design

From the preliminary studies, glycerol and $(NH_4)_2SO_4$, were found to be elite carbon and nitrogen sources (data not shown), which supported the growth and production of huIFNα2b. Plackett- Burman Design (PBD) based on the first order model was employed [189] for the screening of media components, which significantly influenced the production of huIFNα2b. PBD evaluated the main effects of the media components being tested independently without any interaction. A total of 12 experimental runs with eight independent factors (media components) *viz.*, glycerol, ammonium sulphate, methanol, induction temperature, induction time, induction pH and vitamins solution, were examined. The PBD experimental design was developed using Minitab 16 statistical software (M/s MINITAB, West Midlands, UK) without the use of dummy variable. All the PBD experiments were performed at shake flask level in 250 mL Erlenmeyer baffled flasks at a temperature of 30°C and speed of 220 RPM. The shake flask study consisted of glycerol and methanol (induction) phases for growth and protein production respectively. Each of the medium components were studied at a high level (+1) and low level (-1) as indicated in Table 3.1.

Table 3.1 Levels of the medium components and parameters used in Plackett-Burman design

Component/Parameter	Symbol	Low level (-1)	High level (+1)
Glycerol (g/L)	X_1	10	30
Ammonium sulphate (g/L)	X_2	2.5	7.5
Methanol (% v/v)	X_3	0.5	1.25
Sorbitol (% w/v)	X_4	0	1
Induction temperature (°C)	X_5	25	30
Induction time (h)	X_6	72	96
Induction pH	X_7	5	6.5
Vitamin solution (mL/L)	X_8	1	3

The medium components which were significant at 99 % confidence level ($P < 0.01$) were considered to have a significant effect, and further optimized by Response Surface Methodology (RSM), using Box- Behnken design (BBD). All the experiments were done in duplicate, and the average of huIFNα2b titer at 96 h post induction of each experiment was taken as the response.

3.2.5.2. Optimization by Response Surface Methodology

RSM along with three factor, three-level BBD was employed to determine the optimum concentration of the significant factors screened by PBD. A total number of 15 experiments having three replicates at the center point were used to predict the influence of the independent experimental factors and their interaction for maximizing the huIFNα2b titer. All the optimization experiments were performed at shake flask level in 250 ml Erlenmeyer baffled flasks at a temperature of 30°C and speed of 220 RPM. The shake flask study consisted of glycerol and methanol (induction) phases for growth and protein production respectively. For this study, Minitab 16 statistical software

(M/s MINITAB, West Midlands, UK) was utilized to generate the experiments and analyse the results. The three factors considered for RSM-BBD are viz., glycerol (X_1, g/L), ammonium sulphate (X_2, g/L) and methanol (X_3, % v/v). The levels of these factors were fixed, based on the results obtained through conventional optimization, by the one-factor-at-a-time approach (data not shown). The response values (Y), *i.e* huIFNα2b titer at 96 h of post induction in each experiment, was the average of the duplicate runs.

A second order polynomial regression model, for generating the optimal response, as the function of the independent factors, is given as equation 3.1

$$Y = \beta_0 + \beta_1 X_1 + \beta_2 X_2 + \beta_3 X_3 + \beta_{11} X_1^2 + \beta_{22} X_2^2 + \beta_{33} X_3^2 + \beta_{12} X_1 X_2 + \beta_{23} X_2 X_3 + \beta_{13} X_1 X_3 \quad (3.1)$$

Where β_0 is a constant, β_1, β_2 and β_3 are the linear terms, β_{11}, β_{22} and β_{33} are the quadratic terms and β_{12}, β_{23} and β_{13} represent the interaction terms. X_1, X_2 and X_3 are the independent factors viz., glycerol (g/L), ammonium sulphate (g/L) and methanol (% v/v).

3.2.5.3. Modelling and optimization by Artificial Neural Network linked Genetic Algorithm

Artificial neural network (ANN) has been proven as a useful tool in media optimization studies, as it mimics different aspects of biological information processing for the data modeling. The control of neurons in the ANN modelling are executed by transfer and summing function. The most commonly used transfer functions are linear (*pureline*), non-linear (log sigmoid (*logsig*) and tan sigmoid (*tansig*) functions [179]. A multi perception feed-forward ANN, with Error-Back-Propagation (EBP), using the Levenberg Marquardt algorithm was employed using neural network fitting (NNF) tool box of MATLAB R2014b. The applied ANN model essentially comprises of three layers of

neurons: an input layer with three input factors, corresponding to the media components (glycerol, ammonium sulphate, and methanol), a hidden layer with an optimized number of neurons (8 neurons), and output layer corresponding to huIFNα2b titer (Figure 3.1). The experimental data from RSM-BBD were divided into into 3 sets of 11, 2 and 2 for training, validation, and testing respectively (Table 3.2), to analyze the performance of developed ANN for predicting the unseen data. Each ANN was trained to minimize the Root Mean Square Error (RMSE) to the lowest value and the correlation coefficient (R^2) close to 1.

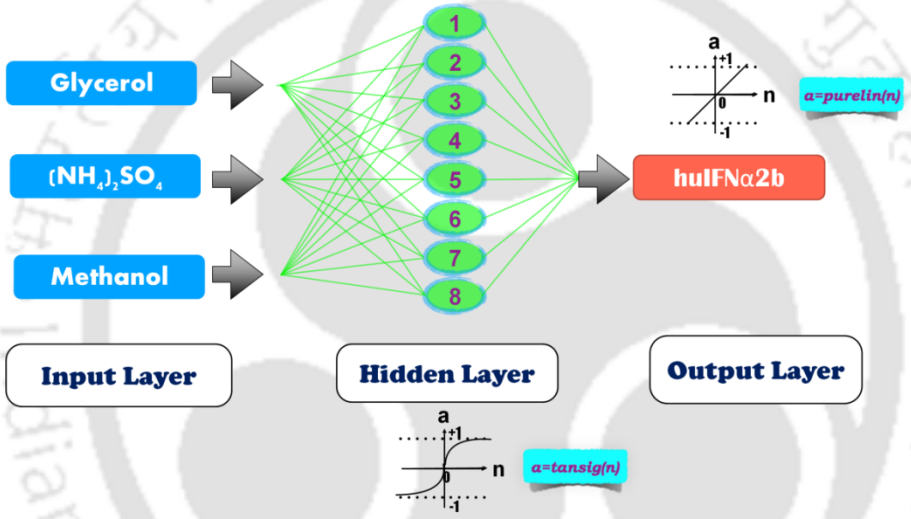

Figure 3.1 ANN architecture topology with input, hidden and output layers

Table 3.2 Comparison of statistical parameters of artificial neural network model.

ANN Sample Randomization (No. of sample data used)	Experimental Run number	R^2	MSE
Training (11)	1, 2, 3, 4, 9, 10, 11, 12, 13, 14, 15	1	1.217e-13
Testing (2)	5, 8	1	3.4689
Validation (2)	6, 7	1	0.1726

Genetic Algorithm (GA) is a stochastic global search tool for optimization, which mimics the process of natural biological evolution. GA was used to optimize the input space of the developed ANN model, in which the fitness of each independent variable (glycerol, ammonium sulphate, and methanol) is evaluated using an objective function (i.e. huIFNα2b titer). The value of this objective function is maximized or minimized to achieve the optimized design, which possesses the optimum concentration of medium components for maximum production of huIFNα2b. The ANN model and GA described in this study were developed using MATLAB 2014b (Mathworks Inc., Natick, USA).

3.2.5.4. Model validation experiments

Validation experiments were performed for the optimum concentration of the medium components obtained through RSM-BBD and ANN-GA models in 250 ml Erlenmeyer baffled flasks at a temperature of 30°C and speed of 220 RPM. The shake flask validation experiments consisted of glycerol and methanol (induction) phases for growth and protein production respectively. The mean average value of the experiments was compared with the predicted value.

The wellness of the RSM and ANN models were evaluated and verified by statistical parameters, RMSE and absolute average relative deviation (AARD), as described elsewhere [190] according to the following equations 3.2 and 3.3.

$$\mathrm{RMSE} = \frac{1}{n}\sum_{i=1}^{n}\left(Y^{i,prd.} - Y^{i,exp.}\right)^2 \qquad (3.2)$$

$$\mathrm{AARD}\ (\%) = \frac{1}{n}\sum_{i=1}^{n}\left(\left|\frac{(Y^{i,prd.} - Y^{i,exp.})}{(Y^{i,exp.})}\right|\right) \times 100\% \qquad (3.3)$$

Where $Y^{i,prd.}$, $Y^{iexp.}$,and n are huIFNα2b titers (Responses obtained from the model) obtained by the predicted model, the experimental data, and the number of experimental data, respectively.

3.2.6. Bioreactor operation

Bioreactor (Biojenik Engineering, Chennai, India) with a working volume of 1.7 L and a bottom driven Rushton turbine, was utilized for the cultivation of glycoengineered SuperMan5 *P. pastoris* strain expressing human huIFNα2b. Inclusion of the bottom driven shaft in this investigation was to overcome O_2 mass transfer limitations during high cell density cultivations, and also to improve biomass yield. An integrated SCADA (supervisory control and data acquisition) was developed in a LabVIEW (National Instruments, Texas, United States) platform to synchronize the process inputs and outputs in line with their set points. It also records the process parameters such as temperature, pH, DO etc at 5 s intervals. 1 vvm of gas (air + O_2) was supplied by manually adjusting the flow rate of O_2 at various instances during reactor operation in order to obtain 25 % DO throughout the process. Agitation rate was maintained at 800 RPM and pH was maintained at 5.4 by adding 25 % (v/v) Ammonia solution and 30 % (v/v) H_3PO_4 as neutralizing agents. Foaming during fermentation was controlled using silicone oil as an antifoaming agent. The entire process of high cell density fermentation (batch fermentation) consisted of three phases: glycerol growth phase, transition phase, and methanol induction phase.

The bioreactor study was performed using the optimized basal salt medium. Glycerol growth phase commenced with 1.7 L of optimized basal salt medium having the composition (in g/L): 48.84 glycerol, 18.2 K_2SO_4 , 7.28 $MgSO_4$, 4.13 KOH, 0.93 $CaSO_4.2H_2O$, and 8.42 $(NH_4)_2SO_4$ 26.7 mL/L 85 % orthophosphoric acid supplemented with 4.4 mL/L PTM4 salt (added after autoclaving) was also used. The temperature was maintained at 30°C during the glycerol growth phase. A sharp rise in the dissolved oxygen (DO) indicated the end of the glycerol phase. Following this phase, a transition phase was started with the addition of 1.5 g/L of methanol which allowed the cells to

adapt and utilize the methanol during the induction phase. Once the cells were completely transitioned and adapted to methanol, the methanol feed (100 % methanol + 12 mL of PTM4 per liter) commenced in order to initiate the methanol induction phase. The temperature during the methanol phase was maintained at 28°C, which was optimized previously. DO spike method based pulse feeding of the methanol feed (1.4 %, v/v) was employed in this study. During the entire batch fermentation process, samples were collected at a regular time interval of 4 h and analyzed for biomass, glycerol and methanol concentration, and huIFNα2b titer as previously described in the sampling and analysis section. Bioreactor experiments were done in duplicate, and the average values with standard error were plotted.

3.2.7. Dielectric spectroscopy for real-time monitoring of biomass

Bioreactor set up was equipped with a capacitance probe (Aber Instruments, Aberystwyth, United Kingdom), for monitoring the VCV of *P. pastoris* [191-193]. The probe tip consists of a ceramic portion with 2 annular rings surrounding it, and produces an electric field at an applied frequency. The Capacitance (0 – 200 pF/cm), C and Conductivity (0 – 40 mS/cm), and G values were logged at every 4s interval, in the Futura tool application (Aber Instruments, Aberystwyth, United Kingdom), at dual frequencies of 0.58 MHz and 15 MHz, respectively, and subtracted to obtain relative values. Thus obtained values of ΔC and ΔG were the mean average at every 100 data points, and plotted against time to obtain a dynamic profile of glycoengineered *P. pastoris* growth. Continuous capacitance data was also utilized to study the *P. pastoris* growth kinetic modeling.

3.2.8. Oxygen uptake rate estimation

The composition of flue gases like O_2 and CO_2, in the exit stream of bioreactor, was estimated using Exhaust gas Analyzer (Ultramat 23, Siemens AG, Berlin and Münich, Germany) according to paramagnetic and IR based techniques, respectively. Appropriate percentages of the flue gases can be computed to Oxygen uptake rate (OUR) and Carbon dioxide emission rate (CER), using the following relationships (Eqn 3.4 and 3.5).

$$\text{OUR, } {}^{mg}/_{L.s} = \frac{\dot{m}_g}{V_R}\left[y_{O2,in} - y_{O2,out}\left(\frac{y_{inert,in}}{y_{inert,out}}\right)\right] \quad (3.4)$$

$$\text{CER, } {}^{mg}/_{L.s} = \frac{\dot{m}_g}{V_R}\left[y_{CO2,out}\left(\frac{y_{inert,in}}{y_{inert,out}}\right) - y_{CO2,in}\right] \quad (3.5)$$

Volumetric rates, r_{O_2} and r_{CO_2}, would provide direct information about the growth rate and their ratio, thus indirectly implying cellular respirative/fermentative metabolism [188] of *P. pastoris*. Therefore OUR and CER measurements were also recorded in the SCADA, and a dynamic plot of OUR was generated against time.

3.2.9. Kinetic Modeling

Discrete data (6 data points sampled from real time continuous capacitance data at specified time interval in concurrence with the offline biomass data) obtained during glycerol phase of the batch fermentation in the reactor was used to model the biomass growth and substrate consumption. Substrate limited unstructured growth models were used to represent the dynamic behaviours of the biomass and substrate in the glycerol phase.

$$\frac{d\Delta C}{dt} = \mu \Delta C \quad (3.6)$$

$$\text{Monod model, } \quad \mu = \frac{\mu_{max} * S}{K_S + S} \quad (3.7)$$

$$\text{Moser model, } \quad \mu = \frac{\mu_{max} * S^n}{K_S + S^n} \quad (3.8)$$

$$\text{Contois model,} \quad \mu = \frac{\mu_{max} * S}{K_{SC} C + S} \tag{3.9}$$

. $$\frac{dS}{dt} = \left(-\frac{1}{Y_{CS}}\right)\frac{d\Delta C}{dt} \tag{3.10}$$

Where ΔC is the capacitance of biomass (pF/cm); μ_{max} is the maximum specific growth rate (h^{-1}); K_S is the Monod's saturation constant (g/L); n is the Moser constant (Dimensionless number); K_{CS} is the Contois saturation constant (g/L), Y_{CS} is the capacitance of biomass yield on substrate (pF/cm.g)

The differential equations (3.6 and 3.10) were solved using MATLAB ODE 45 solver tool based on Runge-Kutta 4th order method. Kinetic parameters were estimated by minimizing the sum of squared error between the experimental and simulated data using 'fmincon' optimization tool.

The objective function used in the minimization is as follows (Equ. 3.11),

$$SSE = \sum_{i=1}^{n}(C_{model} - C_{exp})^2 + \sum_{i=1}^{n}(S_{model} - S_{exp})^2 \tag{3.11}$$

3.2.10. Purification of glycosylated huIFNα2b

The purification of the glycosylated huIFNα2b was described earlier (Chapter 2, Section 2.2.7). Briefly, the protocol involves two steps of purification, his-tagged affinity chromatography followed by Concanavalin A (Con A) chromatography. His-tagged affinity chromatography helps in capturing the recombinant huIFNα2b present in the clarified supernatant after fermentation along with other host proteins. The pooled fractions containing huIFNα2b were subjected to Con A chromatography for the selective purification of glycosylated huIFNα2b.

3.2.11. Deglycosylation analysis

Deglycosylation analysis was performed by treating the purified glycosylated huIFNα2b with PNGaseF as per the manufacturer's protocol (New England Biolabs, UK) and analyzed through SDS-PAGE.

3.2.12. Anti-proliferative assay

Biological activity of the recombinant huIFNα2b was assessed by its ability to inhibit cell growth in an *in vitro* study using breast cancer cell line (MCF7). MCF7 cell line was maintained in Dulbecco's Modified Eagle Medium (DMEM) high glucose medium supplemented with streptomycin and penicillin antibiotic along with 10 % fetal bovine serum (FBS). Cells were grown in humidified incubator at 37°C and 5 % CO_2. After 70 % of confluency, the adhered cells were washed with Dulbecco's Phosphate Buffered Saline (DPBS) and detached using trypsin-ethylenediaminetetraaceticacid (EDTA) (0.25 %). 5000 cells/well were transferred into a 96-well cell culture plate and incubated overnight at 37°C and 5 % CO_2 for further study. The spent medium was replaced by 200 µL of fresh medium containing either commercial huIFNα2b drug (Intas Pharmaceuticals, India) or purified recombinant huIFNα2b at different concentrations viz., 1 nM, 5 nM, 10 nM and 20 nM. Cells in the medium without huIFNα2b were used as a negative control. The anti-proliferative activity of the huIFNα2b was determined after 96 h of treatment. The viable cell densities were detected after washing with DPBS based on the conversion of MTT into formazan by mitochondrial reductase. 100 µL of MTT (0.5 mg/mL) was added to each well and incubated at 37°C for 3 h. The MTT solution was discarded and the insoluble formazan crystals were dissolved in 100 µL DMSO and incubation at 25°C for 5 min. The absorbance was measured at 570 nm with the reference absorbance of 690 nm. The assay was performed in 5 replicates.

3.3. Results

3.3.1. Screening of medium components and process parameters for huIFNα2b production

The significance of the medium components and process parameters for the production of huIFNα2b was investigated by PBD. Levels of each independent variable are given in Table 3.1, and the experimental design, together with both the observed and predicted responses is shown in Table 3.3. From the results analysis, it was identified that glycerol (X_1), ammonium sulphate (X_2) and methanol (X_3) significantly influenced huIFNα2b titer, at a confidence level of above 99 % (Figure 3.2) and were considered for further optimization by RSM-BBD.

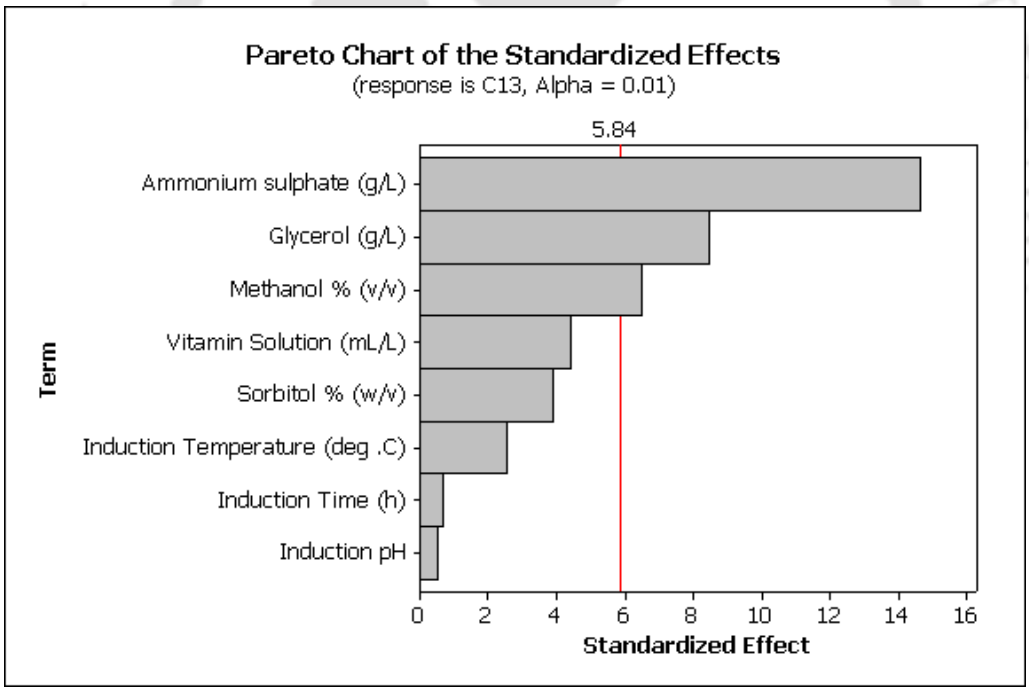

Figure 3.2 Pareto chart for screening of significant variables by PBD. Y-axis represents different variables considered for PBD and the X-axis represents the standardized effect of the variables. The variables having standardized effect value greater than 5.84 are considered as significant at 99 %.

Table 3.3 Plackett-Burman experimental design with response

Run	Independent Variables/Levels								Response huIFNα2b (mg/L)	
	X_1	X_2	X_3	X_4	X_5	X_6	X_7	X_8	Observed	Predicted
1	-1	-1	+1	+1	+1	-1	+1	+1	9.12	7.40
2	+1	-1	-1	-1	+1	+1	+1	-1	1.64	1.48
3	-1	-1	-1	-1	-1	-1	-1	-1	7.53	6.28
4	-1	-1	-1	+1	+1	+1	-1	+1	1.25	2.97
5	+1	+1	+1	-1	+1	+1	-1	+1	21.83	20.58
6	-1	-1	+1	+1	-1	+1	-1	-1	1.09	0.78
7	+1	-1	+1	-1	-1	-1	+1	+1	0.23	1.95
8	+1	+1	-1	+1	-1	-1	-1	+1	4.94	4.78
9	-1	+1	+1	+1	-1	+1	+1	-1	30.43	30.74
10	-1	+1	+1	-1	+1	-1	-1	-1	37.00	38.25
11	-1	+1	-1	-1	-1	+1	+1	+1	21.72	21.41
12	+1	+1	-1	+1	+1	-1	+1	-1	14.21	14.36

X1: Glycerol, X2: Ammonium sulphate, X3: Methanol, X4: Sorbitol, X5: Induction temperature, X6: Induction time, X7: Induction pH, X8: Vitamin solution. All the experiments were done in duplicate and mean average is reported

3.3. 2. Optimization of significant variables by RSM-BBD

The three variables (medium components) *viz.*, glycerol (X_1), ammonium sulphate (X_2) and methanol (X_3) selected by PBD, had a significant effect on huIFNα2b production, and were further optimized by RSM-BBD to determine the optimal levels. The coded levels and real values of the medium components are shown in Table 3.4.

Table 3.4 Coded levels and actual values of medium components for RSM-BBD

Variables	**Coded levels**		
	-1	**0**	**+1**
X1: Glycerol (g/L)	20	50	80
X2: Ammonium sulphate (g/L)	3	9	15
X3: Methanol (% v/v)	0.5	1.25	2.0

The concentrations of the remaining components are same as described in the media section. The experimental design matrix with the predicted and the observed responses (huIFNα2b titer) are shown in Table 3.5. The experimental data from Table 3.5 was used to generate the following 2nd-order polynomial equation (3.12) for huIFNα2b titer by applying multiple regression analysis.

$$Y = -119.445 + 2.938X_1 + 9.649X_2 + 81.764X_3 - 0.027X_1^2 - 0.501X_2^2 - 32.932X_3^2 - 0.029X_1X_2 + 1.367X_2X_3 - 0.104X_1X_3 \quad (3.12)$$

The statistical significance of the regression model was evaluated by analysis of variance (ANOVA), and summarized in Table 3.6 at 95 % significance level. The F value of 103.30 and the p-value of 0 implies that the model was significant, and the non-significant lack of fit value (p= 0.189) indicates the good fit of the model. The determination coefficient (R^2) of 99.24 % for the model implies that 99.24 % variability of response can be explained by the model; in addition, the adjusted R^2 value of 98.50 %

indicates the high significance of the model. All the linear (X_1, X_2, X_3), square (X_1^2, X_1^2, X_1^2), and interaction ($X_1.X_2$, $X_2.X_3$) terms, except the interaction of $X_1.X_3$, were found to be significant with a p-value less than 0.05. The optimal levels of the three medium components were found to be 46.06 g/L glycerol, 10.15 g/L ammonium sulphate, and 1.38 % (v/v) methanol, post RSM-BBD optimization. The response contour plots for RSM-BBD optimization are represented in Figure 3.3.

Table 3.5 BBD experimental design with predicted and observed response

Run Order	Glycerol (g/L)	Ammonium Sulphate (g/L)	Methanol (% v/v)	Response huIFNα2b (mg/L)		
				Observed± SE*	RSM predicted	ANN predicted
1	20	9	2	19.29 ± 1.44	21.68	19.29
2	50	3	2	10.63 ± 0.85	9.18	10.63
3	80	15	1.25	3.56 ± 0.12	4.50	3.56
4	20	9	0.5	7.52 ± 0.41	7.19	7.52
5	50	9	1.25	50.73 ± 4.26	52.22	53.25
6	50	9	1.25	52.68 ± 5.23	52.22	53.25
7	50	15	2	33.24 ± 0.59	31.97	33.36
8	80	3	1.25	3.46 ± 0.44	4.58	4.21
9	50	3	0.5	10.40 ± 1.01	11.66	10.40
10	20	15	1.25	26.58 ± 0.44	25.46	26.58
11	20	3	1.25	5.34 ± 0.59	4.40	5.34
12	50	9	1.25	53.25 ± 5.52	52.22	53.25
13	80	9	0.5	3.86 ± 0.94	1.47	3.86
14	80	9	2	6.29 ± 0.09	6.62	6.29
15	50	15	0.5	8.40 ± 0.85	9.85	8.40

MSE (RSM)= 1.78, AARD(RSM)=8.4 %, MSE (ANN)= 0.48, AARD(ANN)=1.87 %

*All the experiments were done in duplicate and average value with standard error (SE) reported

Table 3.6 ANOVA table of RSM experiments for huIFNα2b production.

Source	DF	SS	Adj MS	F	P
Regression	9	4986.05	554.01	103.30	<0.001[a]
Linear	3	628.72	842.12	157.02	<0.001[a]
X_1	1	215.96	1769.09	329.87	<0.001[a]
X_2	1	220.06	848.23	158.16	<0.001[a]
X_3	1	192.71	856.37	159.68	<0.001[a]
Square	3	4072.53	1357.51	253.12	<0.001[a]
X_1^2	1	1781.35	2208.12	411.73	<0.001[a]
X_2^2	1	1024.17	1200.34	223.25	<0.001[a]
X_3^2	1	1267.01	1267.01	236.25	<0.001[a]
Interaction	3	284.79	94.93	17.70	0.004
$X_1.X_2$	1	111.71	111.70	20.83	0.006
$X_1.X_3$	1	21.81	21.81	4.07	0.100[b]
$X_2.X_3$	1	151.28	151.28	28.21	0.003
Residual Error	5	26..82	5.36		
Lack of Fit	3	23.31	7.77	4.44	0.189[b]

R-Sq = 99.47 % R-Sq(pred) = 92.40 % R-Sq(adj) = 98.50 %, a.Significant at $p < 0.05$ level, b.Not-significant at $p \geq 0.05$ level, DF-degrees of freedom

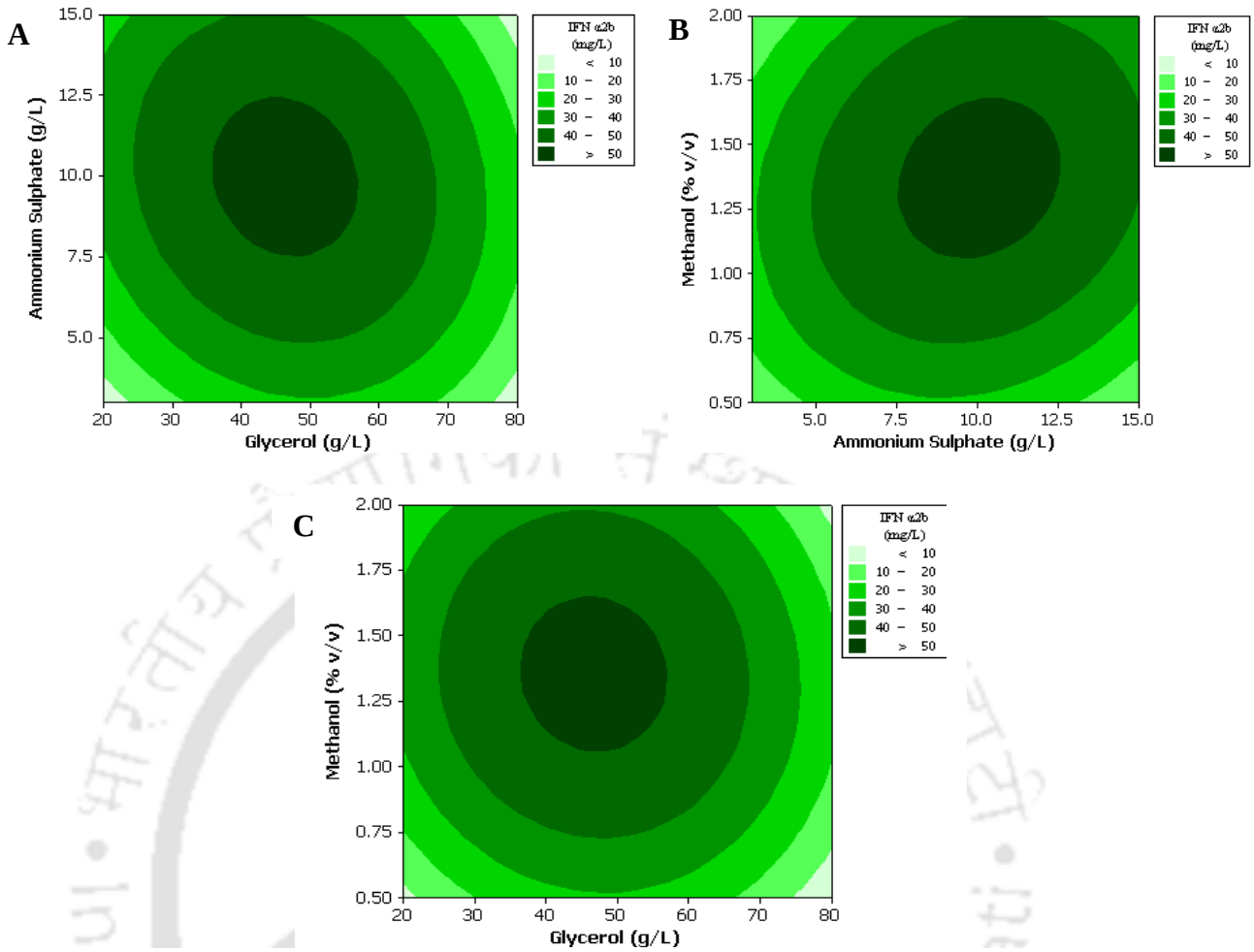

Figure 3.3 Contour plots of RSM-BBD optimization representing the interaction of A) Glycerol and ammonium sulphate. B) Methanol and ammonium sulphate. C) Glycerol and methanol

3.3.3. Optimization by ANN linked GA

The feed-forward ANN with back propagation was used to address the non-linear problems of the RSM. The experimental data from the RSM-BBD was used as input to develop and train the ANN model. Specific experimental runs output (final huIFNα2b titer) and number of experiments used in ANN model for training, testing and validation with corresponding R^2 and MSE values are shown in Table 3.2 described earlier. The computed ANN data during training, testing and validation, were compared with the experimental data in the scattered plot (Figure 3.4). The high determination coefficient (R^2) during training (1), validation (1), testing (1), and all data (0.99954) of the developed ANN model, indicate a high accuracy of the model for predicting huIFNα2b

titer. From the ANN linked GA optimization, the optimal levels of the three medium components was found to be viz., 48.84 g/L glycerol, 8.42 g/L ammonium sulphate and 1.4 % (v/v) methanol (Figure 3.5).

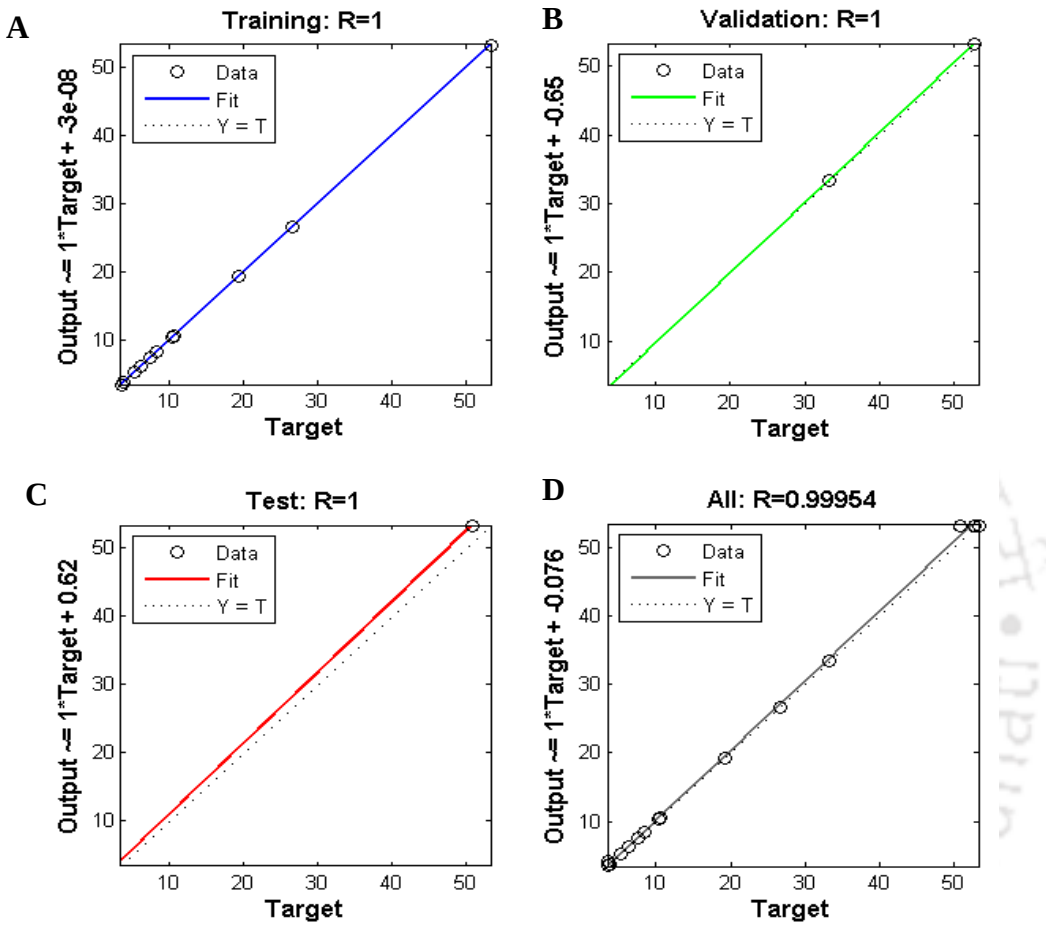

Figure 3.4 Scattered diagrams comparing the experimental data with the ANN predicted data at each stage. A) Training, B)Validation, C) Testing and D) Final

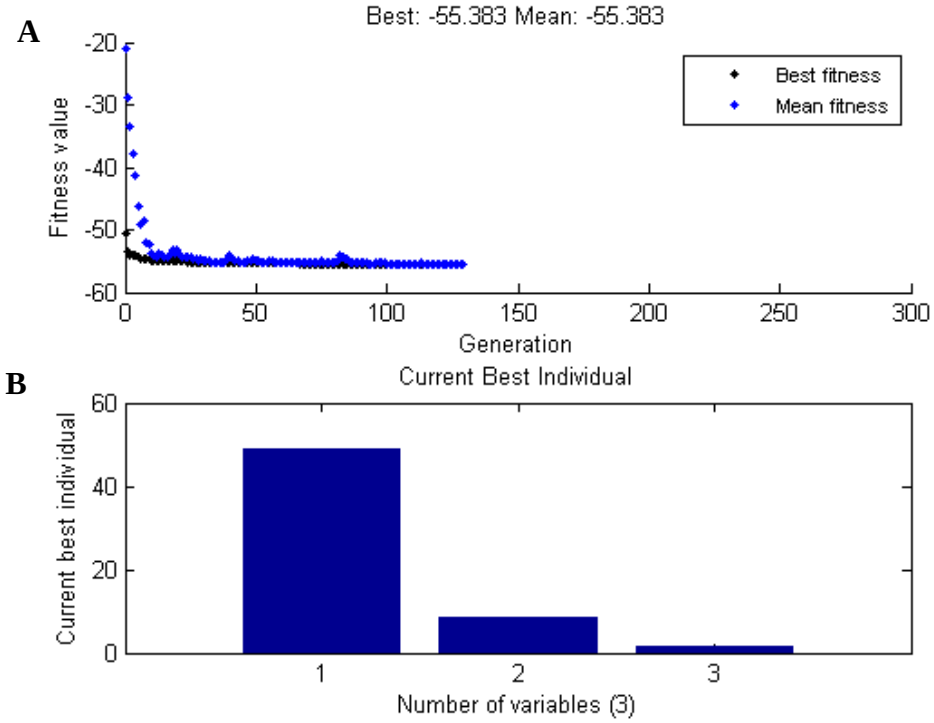

Figure 3.5 Evolution of best and mean fitness function through iteration by GA and optimum results of the three variables considered (1: glycerol, 2: ammonium sulphate, 3: methanol). A) Fitness graph and B) Variables optimum values graph

3.3.4. Model validation experiments

Validation experiments were conducted on the optimization result of RSM-BBD and ANN linked GA and compared with the predicted result in Table 3.7. The experimental huIFNα2b titer (57.18 ± 1.87 mg/L) obtained by ANN was higher compared to huIFNα2b titer (53.06 ± 3.25 mg/L) which was obtained by RSM. The high R^2 value of ANN model, with lower RMSE and AARD values than the RSM-BBD regression model, implies that ANN model was more accurate for the present study (Table 3.7). A 5-fold increase in huIFNα2b titer was obtained for the optimized medium compared to the conventional complex medium (BMGY/BMMY) at shake flask level. The huIFNα2b titer of 10 mg/L was obtained in the complex medium. Figure 3.6 shows the parity plot for the RSM and ANN model predicted huIFNα2b titer with the observed (actual) huIFNα2b titer.

Table 3.7 Comparison table for RSM-BBD and ANN-GA validation experiments

Variable	Optimum concentration			huIFNα2b Conc. (mg/L)		R^2
	Glycerol (g/L)	Ammonium sulphate(g/L)	Methanol (% v/v)	Predicted	Experimental*	
RSM regression model	46.06	10.15	1.38	53.51	53.06 ± 3.25	0.973
ANN-GA model	48.84	8.42	1.4	55.38	57.18 ± 1.87	0.999

*All the experiments were done in triplicate and mean values with standard deviation are reported

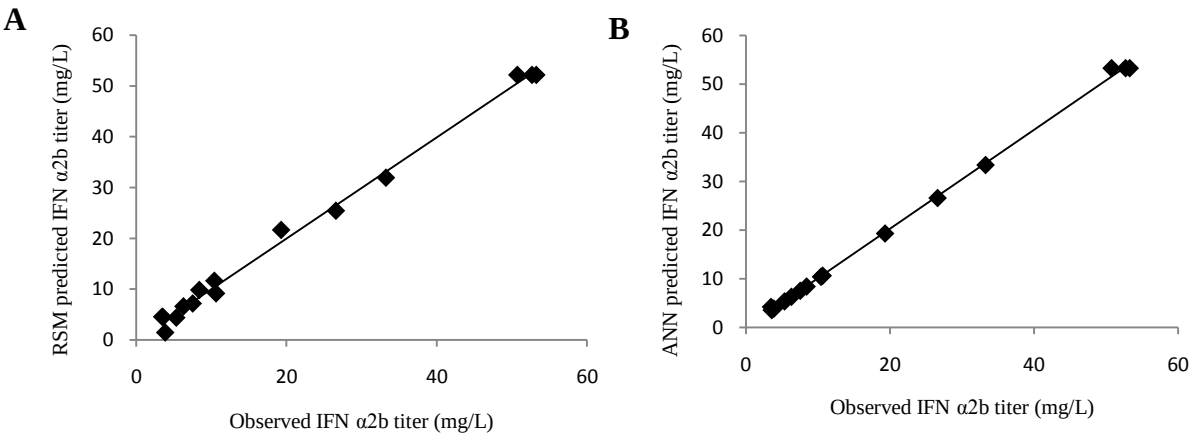

Figure 3.6 Parity plot for RSM predicted (R^2=0.973) (A) and ANN predicted (R^2=0.999) (B) huIFNα2b titer with the observed huIFNα2b titer.

3.3.5. Monitoring of viable cell density using dielectric Spectroscopy and respirometry

The growth of methylotrophic *P. pastoris* was well characterized with distinct phases of growth (glycerol utilization), transition (adaptation) and methanol induction, which were successfully monitored by DS and respirometry. Dynamic plot representing capacitance and OUR signals, were found to exhibit an exponential growth rate during glycerol phase and a linear rate during methanol phase, which also corroborates well with the Dry cell weight (DCW) estimated by offline measurements (Figure 3.7). A linear correlation of

the capacitance and DCW (Figure 3.8) was observed during the entire batch fermentation (DCW= 4.382* ΔC).The glycerol phase culminated by the generation of 37.5 g/L of biomass (capacitance ≈ 14 pF/cm) and at a specific growth rate, μ_{gly} of 0.254 h^{-1} with a high yield coefficient value, $Y_{X/gly} = 0.856$ g. biomass/g. glycerol utilized displayed an enhanced cellular productivity. A slight slump in the capacitance was observed during the transition from glycerol growth phase to methanol induction phase, as corollary to adaptation in the new environment. This change in metabolism was very well characterized/marked by the drop in capacitance and exhaust gas concentration (Figure 3.7).

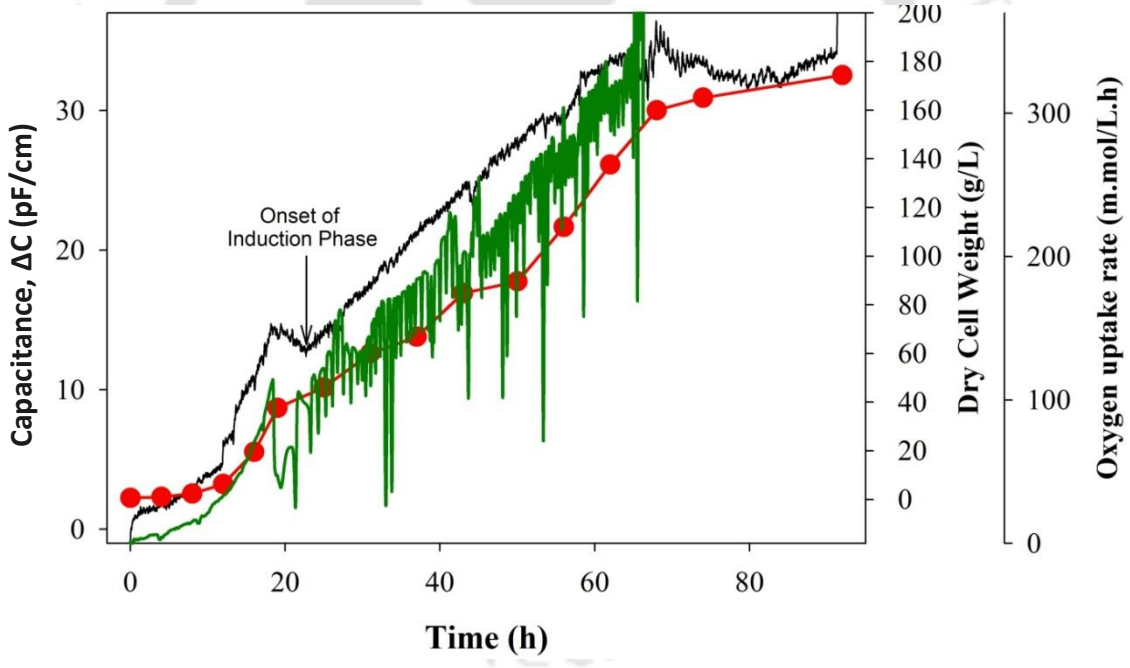

Figure 3.7 Dynamic plot representing capacitance (black line) and OUR (green line) in comparison with offline DCW (circle), measurements during fermentation process.

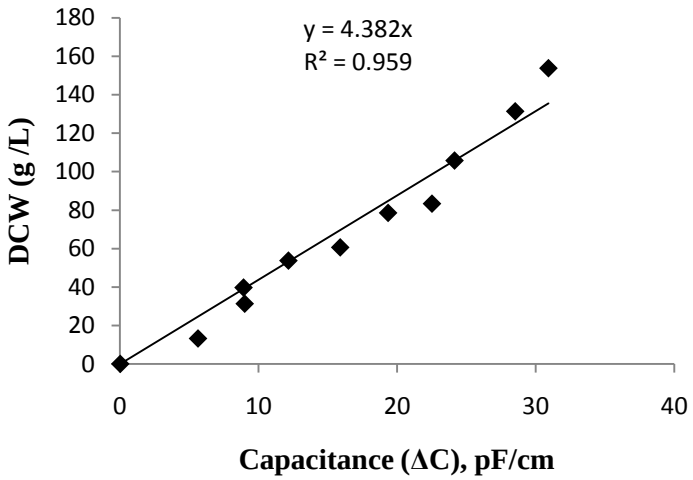

Figure 3.8 Correlation plot for the online capacitance (ΔC) and DCW with R^2=0.959.

During the induction phase, methanol was fed by pulsed addition at a rate of 20 g/h, in order to facilitate a optimal substrate concentration of 1.4 % v/v throughout the experiment. A known quantity of methanol was added as pulse, followed by collection of significant samples, until it was consumed at different time points in the induction phase. This data was employed to compute specific methanol utilization rate$(q_{s,met})$, which was found to be $0.092\ \text{g. methanol/g. biomass. h}$. This phase continued for more than 40 h, and resulted in a cell density of 136.8 g/L, at a relatively slower growth rate, μ_{met} of 0.028 h^{-1}. This was proportionate to the yield of biomass per unit methanol consumed, $Y_{X/_{met}} = 0.13\ \text{g. biomass/g. methanol utilized}$. The huIFNα2b production started after 19 h of fermentation during the methanol induction phase, and reached a maximum huIFNα2b titer of 436 mg/L; and the production of huIFNα2b was found to be growth associated (Figure 3.9).

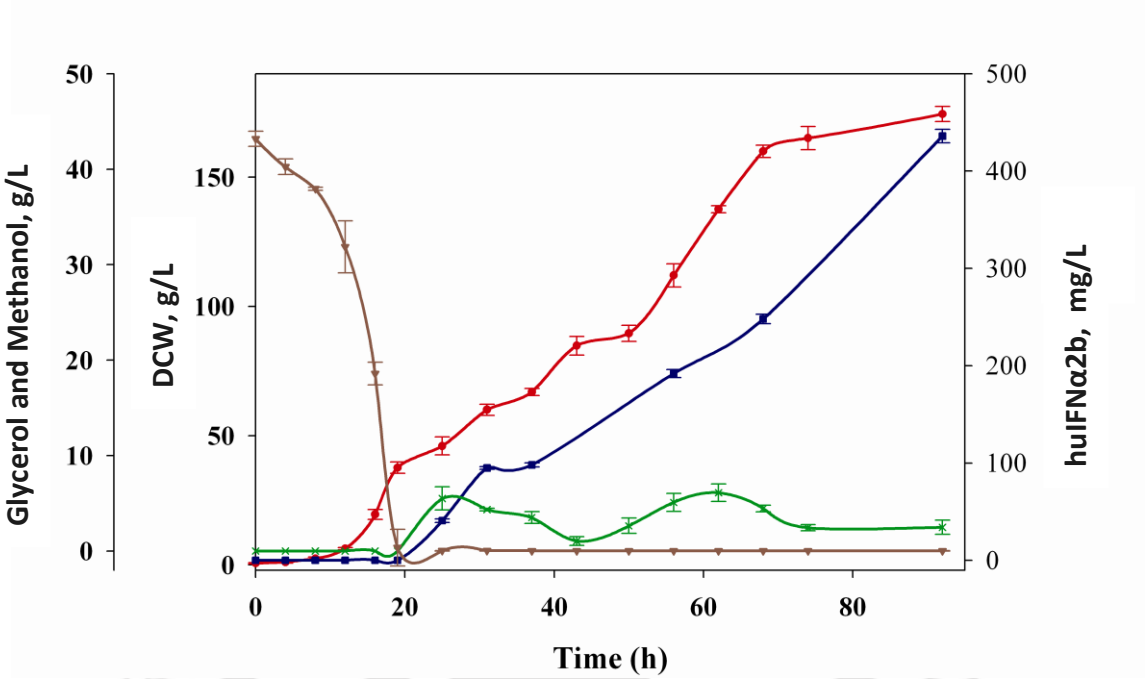

Figure 3.9 Dynamic plot for offline DCW (red filled circle with continuous line), glycerol (brown invert triangle with continuous line), methanol (green cross with continuous line) and huIFNα2b (violet filled square with continuous line) during the high cell density cultivation. The data points represented in this plot are average values with standard error.

3.3.6. Kinetic Modeling

Capacitance data obtained during the glycerol phase of batch fermentation experiment was used in kinetic modelling study, by employing unstructured growth models viz., Monod, Moser, Contois (Figure 3.7). The kinetic parameters of the substrate limited models tested were estimated and presented in Table 3.8. The goodness of fit was estimated using R^2 and RMSE values. Among all the substrate limited models tested, Monod model was observed to exhibit best fit for both the real time capacitance and off-line residual substrate concentration data ($R^2 = 0.98$).

Table 3.8 Estimated kinetic parameter values for the selected kinetic models

Kinetic Model	μ_{max} (h^{-1})	K_S (g/L)	K_{SC} (g/L)	N	Y_{CS} (pF/g.cm)	R^2		RMSE	
						Biomass	Substrate	Biomass	Substrate
Monod	0.327	5.272	-	-	0.395	0.98	0.98	1.64	2.65
Moser	0.265	0.099		0.126	0.340	0.92	0.99	2.16	2.79
Contois	0.428	-	5.763	-	0.395	0.97	0.91	0.91	4.79

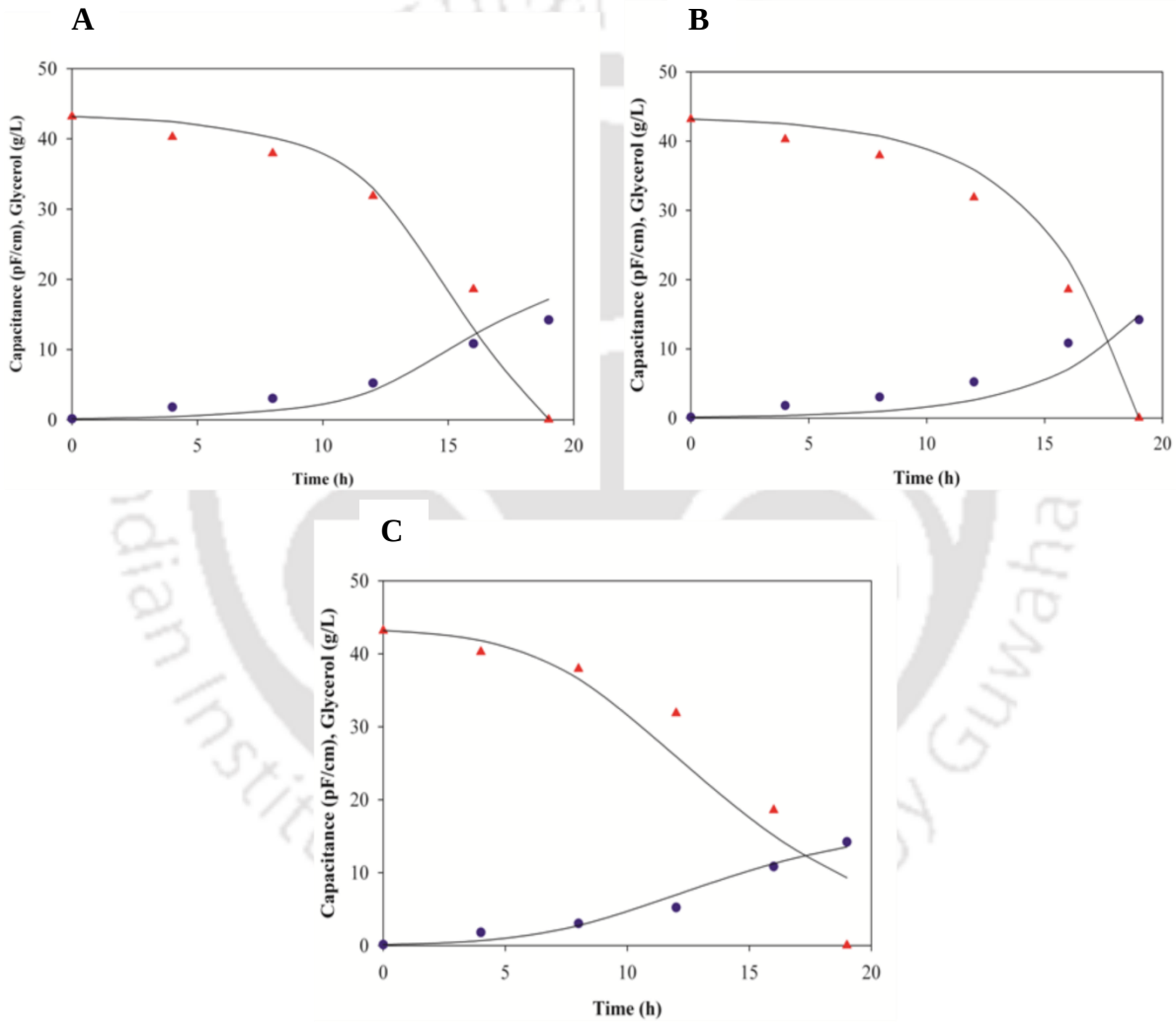

Figure 3.10 Experimental data (points) and simulation (continuous lines) of glycerol phase growth of *P. pastoris* on optimized medium a) Monod model (R^2 (biomass) =0.98 and R^2 (substrate) =0.98), b) Moser model (R^2 (biomass) =0.92 and R^2 (substrate) =0.99) and c) Contois model (R^2 (biomass) =0.97 and R^2 (substrate) =0.91), Capacitance (blue circle), Substrate (red triangle).

3.3.7. Purification and deglycosylation analysis of glycosylated huIFNα2b

The clarified supernatant after fermentation was used for purification of glycosylated huIFNα2b by His-tagged affinity chromatography followed by Con A chromatography. His-tagged affinity chromatography helped in the partial purification of the recombinant huIFNα2b (glycosylated and unglycosylated) with purity of 60 % and recovery of 70 % from the other host cell proteins (Figure 3.11). The pooled sample of his-tagged affinity chromatography was further purified using Con A chromatography (Figure 3.12) for selective recovery of glycosylated huIFNα2b. The purity of the glycosylated huIFNα2b was found to be ~95% with the recovery of 80 % from the pooled elutes fraction of his-tagged affinity chromatography. The deglycosylation analysis proved that the glycosylated huIFNα2b is N-glycosylated. The shift in protein band from ~22 kDa to 20 kDa after incubating with PNGaseF substantiates that N-glycans attached to the glycoprotein were specifically removed (Figure 3.13).

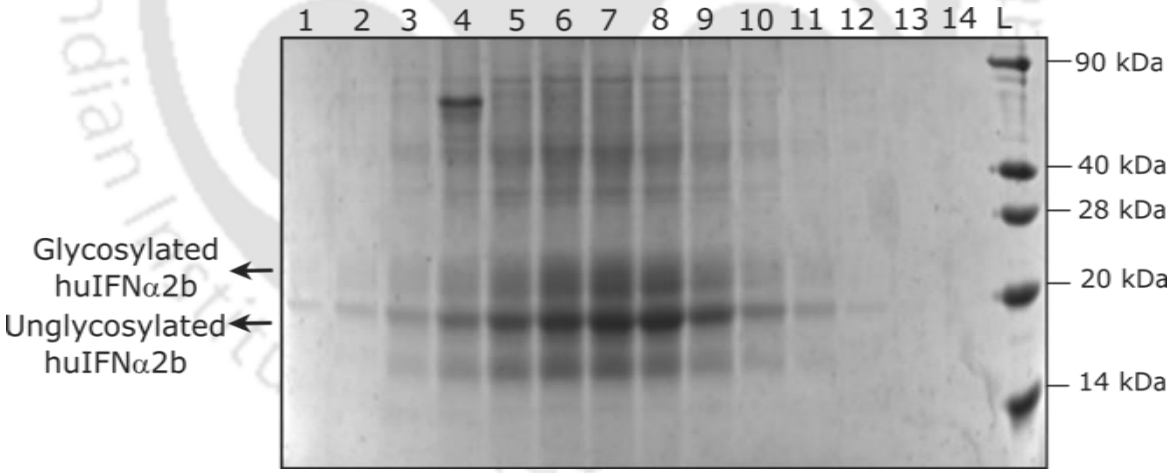

Figure 3.11 Purification of recombinant huIFNα2b expressed in the basal salt medium in bioreactor study by His-Tag affinity chromatography. Lanes 1-13 shows elution fractions and Lane L shows protein ladder.

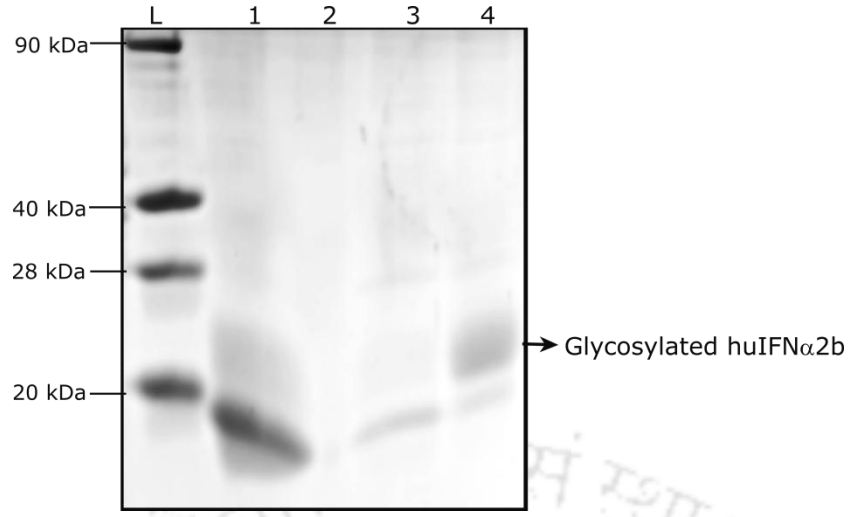

Figure 3.12 Purification of glycosylated recombinant huIFNα2b by concanavalin A (Con A) chromatography. Lane 1 shows initial sample, Lane 2 shows flow-through fraction, Lane 3 shows wash fraction, Lane 4 shows elution fraction and Lane L shows protein ladder.

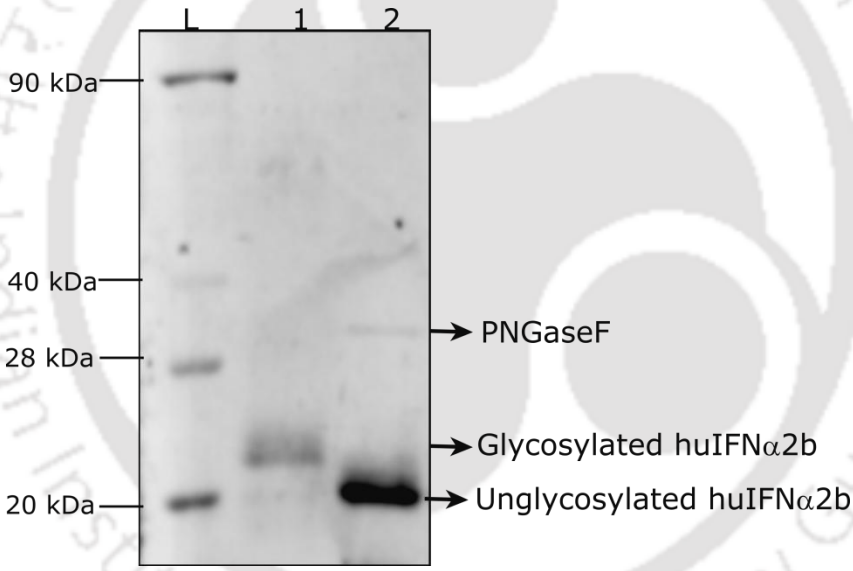

Figure 3.13 Deglycosylation analysis of the purified glycosylated recombinant huIFNα2b. Lane L shows protein ladder, Lane 1 shows untreated protein sample, and Lane 2 protein sample treated with PNGaseF.

3.3.8. Anti-proliferative assay

Anti-proliferative activity is one of the biological attribute exhibited by huIFNα2b and was assessed at varying concentrations of glycosylated huIFNα2b using breast cancer cell line (MCF7). After 96 h of treatment, the growth inhibition of MCF7 cell line was

observed and was dose dependent. Significant reduction (44 %) in cell proliferation was observed at the highest concentration used (20 nmol/L), and the anti-proliferative effect was comparable to that of commercial huIFNα2b drug (Figure 3.14). The assay results were subjected to ANOVA and found to statistically significant at P<0.001.

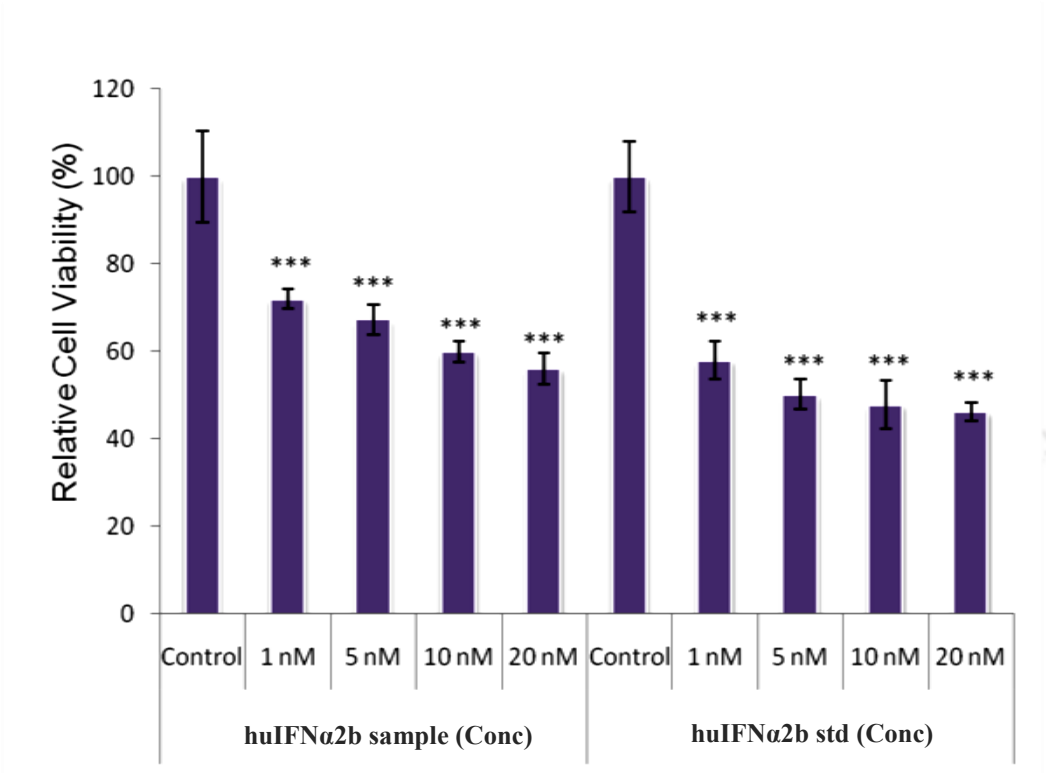

Figure 3.14 Anti-proliferative activity of the purified recombinant huIFNα2b on breast cancer cell lines (MCF7). Y-axis represents % relative cell viability whereas X-axis represents the type of huIFNα2b used. The values are statistically significant at P<0.001 (***) as analyzed by ANOVA.

3.4. Discussion

The regulation of the recombinant protein expression was dependent on the screening parameter chosen and has been discussed in depth [194, 195]. Generally, the influence of different factors on the heterologous protein expression in *P. pastoris* is specific to the expressed protein. This mandates the designing and optimization of individual processes for the production of specific recombinant proteins when employing *P. pastoris.* Also, optimal conditions for expressing the heterologous protein in *P. pastoris* differs according to the type of strain used [196]. In recent years, glycoengineered *P. pastoris* strains have been developed which can produce recombinant proteins, with highly uniform N-glycans compared to the wild-type *P. pastoris* strains [91]. One of such glycoengineered strain, Glycoswitch® SuperMan5 (Biogrammatics Inc., USA), was used in our earlier studies to produce glycosylated huIFNα2b with uniform $(Man)_5(GlcNAc)_2$, (Chapter 2) along with non-glycosylated huIFNα2b

DoE based optimization was employed to enhance the production of recombinant human huIFNα2b production in *P. pastoris* SuperMan5 strain. The application of DoE based optimization is a well established statistical method for optimizing the recombinant protein production in *P. pastoris* [197-199]. PBD identified glycerol, ammonium sulphate and methanol as the significant factors influencing the recombinant huIFNα2b production. Glycerol and methanol plays a major role in central carbon and energy metabolism, and also in protein production in *P. pastoris* [200]. Ammonium sulphate regulates the expression of genes involved in methanol utilization (AOX, PpDHAS, PpDAK) and peroxisomal genes (PpPEX1, 5, 8 and 14) at transcriptional level [201]. BBD is one of the commonly used response surface designs for media optimization. In this study, the experimental data from the BBD design matrix was used to develop RSM and ANN-GA models, for maximizing the huIFNα2b titer. As can be seen from the

response contour plots for RSM-BBD optimization (Figure 3.3), the huIFNα2b titer increased with increase in the concentration of glycerol, ammonium sulphate and methanol. The titer reached maximum at optimal values *viz.*, 46.06 g/L glycerol, 10.15 g/L ammonium sulphate, and 1.38 % (v/v) methanol and decreased further with increase in concentration. This could be due to the inhibitory effect of glycerol on *P. pastoris* growth and protein production, cell toxicity at higher methanol concentration due to oxidative stress, and formaldehyde accumulation [202]. The predicted and observed responses of these models were compared in Table 3.7 and a maximum huIFNα2b titer of 57.18 ± 1.87 mg/L was observed for ANN linked GA model compared to RSM (53.06 ± 3.25 mg/L). Also, the RMSE and AARD values for ANN-GA were found be 0.48 and 1.87 %, respectively. In case of RSM model, the RMSE and AARD values were found to be 1.78 and 8.4 %, respectively. The relatively low RMSE and AARD values for ANN-GA model illustrates its ability to address the non-linearity correlation, but the RSM could address only quadratic non-linear correlation [203]. Figure 3.6 shows the parity plot for the RSM and ANN model predicted huIFNα2b titer with the observed (actual) huIFNα2b titer. The ANN model predictions were observed to be much closer to the line of perfect prediction compared to RSM model.

Batch cultivation studies were conducted with the optimized medium composition. The entire batch fermentation process was monitored continuously by using dielectric spectroscopy and respirometry for biomass monitoring. The fermentation process had two phases viz., glycerol phase and methanol phase. During the glycerol phase, the higher yield of biomass per unit consumption of glycerol was attributed to the greater flux of substrate channeled into the biomass conversion, than by other metabolic activities. This, in turn, resulted in a superior growth rate during glycerol metabolism, which is evident from Figure 3.7 and Figure 3.9. The yield of biomass to glycerol

consumption during the growth phase was found to be 0.856 g. biomass/g. glycerol utilized , which was higher than the reported literature of *P. pastoris* strain expressing huIFNα2b [55]. Both capacitance and OUR signals were found to depict the cell physiology during the course of fermentation. The noisy nature of the OUR signal during the induction phase was due to the metabolic pertubations of *P. pastoris* at the intermittent exhaustion of methanol. During the transition from glycerol growth phase to methanol induction phase, the capacitance signal was well attributed with the change in cell physiology, which was induced by a shift in metabolism to foreign protein production (huIFNα2b). This decrease in capacitance value and cell viability during the transition phase is attributed to the stress caused by protein production (Figure 3.7). Lower protein expression during this phase is due to the presence of trace levels of glycerol, along with the methanol that represses AOX1 activity. During the induction phase, *P. pastoris* utilizes methanol as a carbon source and induces the AOX1 promoter to transcribe and synthesize alcohol oxidase and huIFNα2b. This is evident from an increase in recombinant protein concentration at this phase (Figure 3.9) along with the increase in biomass which could be substantiated by the change in the capacitance profile (Figure 3.7). Relatively lower biomass yield during this phase is corroborated with the maintenance requirements and a major flux diversion towards protein production with methanol being used as a supplement. The concentration of huIFNα2b increases steadily and reaches a maximum product titer of 436 mg/L. During the glycoengineered *P. pastoris* fermentation process, kinetic modeling with real time capacitance data using unstructured growth models was studied (Table 3.8). Even though Monod model has shown best fitting, the model predicted μ_{max}, 0.327 h^{-1} was found to significantly vary from the experimentally determined $\mu_{max,}$ 0.254 h^{-1} from DCW data. Whereas the Moser model predicted μ_{max}, 0.265 h^{-1} is well corroborated with

the experimental value. This value is well in agreement with the reported literature for glycoengineered *P. pastoris* expressing recombinant peroxidase (μ_{max}, 0.28 h^{-1}) [204] and for other recombinant proteins (μ_{max}, 0.24 - 0.29 h^{-1}) expressed by *P. pastoris* [205]. From Table 3.8, the model determined K_s for both Monod and Contois models were estimated as 5.272 and 5.763 g/L, respectively. Whereas, K_s of 0.09 for Moser model was found to be well in agreement with the reported literature [206]. The kinetic model fitting based on real-time capacitance data was observed to be more realistic, taking into account the instantaneous cellular activity, and would be much useful in developing the process strategies at large-scale huIFNα2b production. The recombinant secreted extracellularly in the fermentation broth was present both in glycosylated and unglycosylated form. Glycosylated huIFNα2b was purified from the unglycosylated huIFNα2b using Con A lectin chromatography and Con A selectively binds to the terminal mannose of the glycan moiety attached to the glycosylated huIFNα2b. The purification yield of recombinant huIFNα2b was found to be in concurrent with reported literature [56]. The biological activities of huIFNα2b are driven by binding to the receptor complex (IFNAR1 and IFNAR2) and inducing JAK-STAT signaling pathway, resulting in the activation of interferon-stimulated genes (ISG's) [207]. The anti-proliferative effect of purified huIFNα2b MCF7 cell line is significant (44 % growth inhibition) at a very low dosage (20 nM or 0.4 μg/mL). The huIFNα2b dosage is more than 10-fold lower than the dosages reported for huIFNα2b production by *E. coli* and *P. pastoris* X33 cell lines to achieve comparable drug efficacy [208, 209]. This antiproliferative effect is a result of both apoptosis and cell cycle arrest [210, 211].

3.5. Conclusion

DoE (PBD, RSM-BBD) and artificial intelligence based optimization technique (ANN-GA), were employed for optimization studies to maximize the production of huIFNα2b in recombinant glycoengineered *P. pastoris.* The optimized medium resulted in 57.18 ± 1.87 mg/L of huIFNα2b, and ANN-GA model proved to be the best compared to RSM-BBD model. Bioreactor study with optimized medium resulted in a biomass yield of 0.856 g/g and maximum specific growth rate of 0.254 h^{-1} during the glycerol phase and 0.13 g/g biomass yield and specific growth rate of 0.028 h^{-1} during methanol phase. The huIFNα2b titer of 436 mg/L was the highest reported value in batch fermentation. Deployment of dielectric spectroscopy and respirometry provided real-time insights of the cell physiology during different phases of the fermentation process. The purified glycosylated huIFNα2b was biologically active based on its anti-proliferative activity against human breast cancer cell line.

Chapter 4

Dielectric spectroscopy as PAT tool for real-time monitoring and control of specific growth rate in glycoengineered *Pichia pastoris* fermentation process for the production of recombinant huIFNα2b

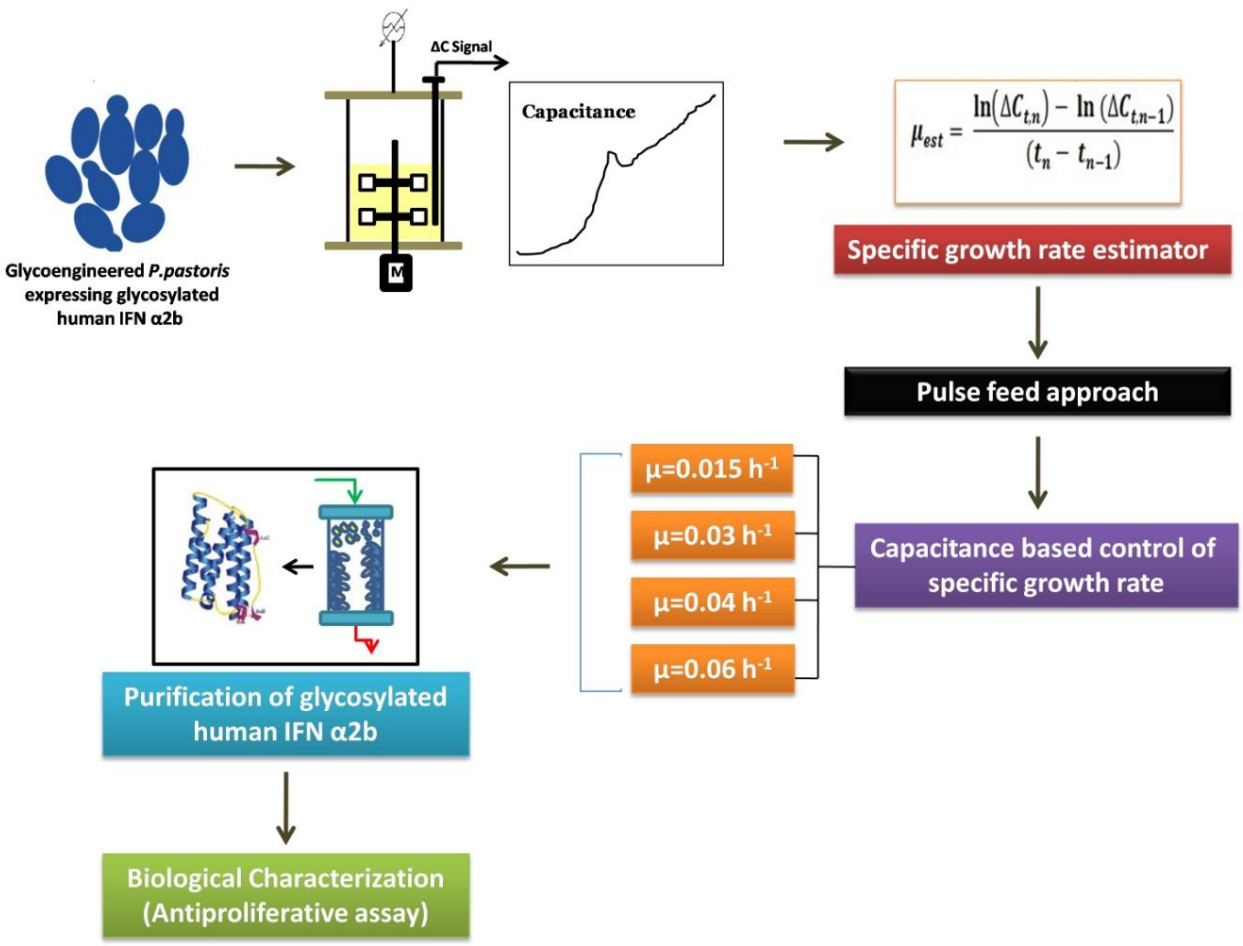

Chapter 4

Dielectric spectroscopy as PAT tool for real-time monitoring and control of specific growth rate in glycoengineered *Pichia pastoris* fermentation process for the production of recombinant huIFNα2b

Abstract

Process variability in bioprocess systems involving genetically engineered strains is a common bottleneck and a real-time insight of the on-going process is crucial to achieve the desired product and its quality. In this study, a process analytical technology (PAT) platform was developed for the monitoring and control of specific growth rate during methanol induction phase (μ_{met}) of glycoengineered *Pichia pastoris* fermentation for human interferon alpha 2b (huIFNα2b) production. The PAT guided approach involves real-time monitoring of capacitance (ΔC) facilitating online estimation of specific growth rate (μ_{est}), which serves as a process input during controller application. Fed-batch experiments using pulsed-feeding of methanol at different dosage (20 g and 30 g) did not significantly influence μ_{met}. Exponential methanol feeding was achieved using a modified proportional, integral and derivative (PID) controller for different predefined specific growth rate set point (μ_{sp}) values, namely 0.015, 0.03, 0.04 and 0.06 h^{-1}. Exponential feeding strategy during the induction phase resulted in two crucial outcomes: (i) controlled methanol feeding rate (regulated by the developed PID controller) balanced the methanol consumption rate ($q_{s,met}$) of the *P. pastoris*; (ii) significant improvement in huIFNα2b titer (1483 mg/L) and specific productivity (> 0.4 mg/g. h) was achieved by the robust control of μ_{met} at optimal (0.04 h^{-1}) value.

The purified huIFNα2b was found to exhibit antiproliferative effect against human breast cancer cell lines. Efficient control of μ_{met} at a very low narrow range was achieved with a long-term controller stability (> 10 h) and the highest titer reported to date for huIFNα2b (at optimal μ_{met}) in the yeast expression platform.

4.1. Introduction

Exploration of various genetic engineering strategies in the yeast expression system had opened up a clear understanding of the secretary pathway of protein processing and regulation of the traffic associated with its transport. This pathway channels the native unprocessed protein towards appropriate folding and post translation modifications, followed by its secretion into the reaction broth. Introduction of stronger inducible promoters at the upstream of the heterologous protein sequence was attempted previously by aiming at higher recombinant product titers. Expression systems like *P. pastoris* had demonstrated their suitability as hosts for managing the excessive transcriptional load towards protein formation. Molecular engineering approaches, however suffer from limitation of higher expression activity, which leads to the retention of improperly folded proteins in their Endoplasmic Reticulum (ER). Yeasts overcome the stress due to higher expression rates by generating unfolded protein responses in their ER lumen [212, 213]. Inappropriately/unfolded protein fractions in the culture supernatants demand extensive purification steps that would be strongly detract from the viable 'Quality by Design' (QbD) perspective. Therefore, optimization of protein titer from *P. pastoris* could be achieved by developing the relationships between the various critical process parameters and product titers.

In eukaryotes especially yeast systems, a good relationship was observed between the specific growth rate (μ) of an organism and their respective protein productivities. Genome level expression studies on *S. cerevisae* reveal that all the 268 genes and 13 transcription factors identified were dependent upon the specific growth rate for their activation [214]. The rates of transcription in such systems were highly dependent upon the μ values maintained. Cultivation of organisms carried out by manipulating μ was determined to have a stronger influence at their metabolic level. *P. pastoris* when

operated at retentostat level i.e. operating the organism at nearly zero specific growth rate ($\mu < 0.001\ h^{-1}$), lead to the transcriptional re-programming followed by the up-regulation of stress related genes and down-regulation of cell cycle machinery. This process strategy allocates less maintenance energy for cell turn over activities through lowest growth trajectories. For all growth associated products, it is well established that the proportionality constant is apparently conserved for a typical μ and q_P (specific productivity) values. This ratio represents the stoichiometric coefficient of the sequence of all pipe-line events in the protein production machinery. Therefore aiming to control μ (critical process parameter) at the process level will lead to the more promising product output.

Gaining real-time insight of the process leading to therapeutic protein production is crucial for enhanced process understanding and robust control of the undesired process perturbations [215]. Process analytical technology (PAT) tools play pivotal roles in maintaining the product quality and achieving maximum productivity through timely monitoring and control [216] of critical process parameters CPP(s). Moreover, bioprocess systems involving therapeutic protein production should embrace the PAT framework which is an initiative by FDA (Food and Drug Administration) for ensuring consistent product quality [112].

Dielectric spectroscopy has evolved as a promising PAT tool, for real-time monitoring and control of bioprocess systems. Non-invasive, *in-situ* operations, selective measurement of viable biomass, simplified linear calibration and short interval measurements are salient features of dielectric spectroscopy [186]. The operational principle involves polarization of individual cell membranes by application of electric field where each cell acts as a tiny capacitor [217]. The measured signal (change in

capacitance, ΔC or permittivity, ε) is a function of volume fraction of cells with intact membrane, thereby negating the quantification of dead cells (Figure 4.1) [218].

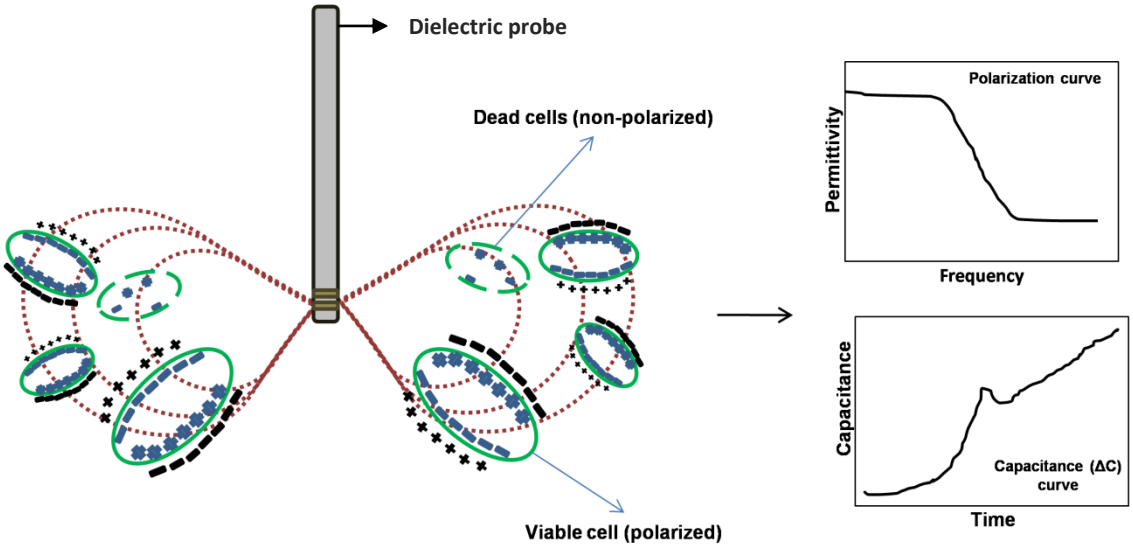

Figure 4.1 Schematic representation of the Dielectric Spectroscopy principle

Dielectric spectroscopy has been successfully employed for real-time monitoring of bacterial [117], yeast [118], filamentous fungi [119] and mammalian [120] cell populations. Studies addressing the feed-back control of specific growth rate using mid-IR, NIR, methanol sensor and calorimetry as a soft sensor [130, 141-147]. Only few studies successfully reported the capacitance based monitoring and control of μ at a desired value for *P. pastoris* and *Penicillium chrysogenum* fermentation processes [144, 187]. Accurate estimation of μ was made possible by this data reconciliation (DR) strategy. However, the reliable performance of DR based μ controller was limited by (i) generation of unforeseen metabolites (ii) quality of measured signal (iii) complex production medium [144]. Right choice of PAT tools for reliable μ estimation followed by an application of simple μ controller for broader range of bioprocess systems remains a quest for bioprocess engineers [216, 219].

In this present chapter, we developed a reliable μ estimator based on real-time capacitance measurements and successfully controlled the methanol feed rate through developed modified PID (Proportional-Integral-Derivative) control strategy for production of huIFNα2b in glycoengineered *P. pastoris*. PID is the most common and widely adopted control algorithm employed in various industries and has been universally accepted for majority engineering applications. Its robust performance at various operating conditions combined with its functional simplicity, allows easy and effective handling by process engineers as compared to advanced control techniques where it requires complicated mathematical approach and more computation to control the process [220]. Control of specific growth rates in the bioprocesses like bacterial, eukaryotic and mammalian cell systems were exclusively carried out for decades using PID control strategy [141, 221, 222]. Optimal PID output is associated with the reduction in noise obtained by varying its basic parametric coefficients of Proportional, Integral and Derivative. This present investigation focusses on elucidating the role of μ on huIFNα2b production on huIFNα2b titer, specific huIFNα2b productivity and methanol accumulation based on insights gained from the real-time capacitance measurements. This first-of-its-kind study delineates the application of a simple robust real-time capacitance based feed-back algorithm to control μ especially at low range ($0.015\ h^{-1} - 0.06\ h^{-1}$) during the induction phase.

4.2. Materials and Methods

4.2.1. Strain and media

Recombinant *P. pastoris* SuperMan5 strain (Mut^+phenotype) expressing huIFNα2b was used in this study. The huIFNα2b expression is under the control of the AOX1 promoter and is secreted in the extracellular media with the help of α-factor signal. The construction of this strain has been described in chapter 2 (section 2.2.3 and 2.2.4). The stock culture was maintained at –80 ˚C, in yeast peptone dextrose (YPD) media containing 20 % (v/v) glycerol. The media compositions used in this study are as follows:

- Starter culture medium (YPD), g/L: yeast extract 10; peptone 20; dextrose 20.
- Pre-culture medium (Yeast extract Peptone Glycerol, YPG), g/L: yeast extract 10; peptone 20; glycerol 20.
- Optimized basal salt medium [223]: glycerol 48.84 g/L; K_2SO_4 18.2 g/L; $MgSO_4$ 7.28 g/L; KOH 4.13 g/L; $CaSO_4.2H_2O$ 0.93 g/L; $(NH_4)_2SO_4$ 8.42 g/L; 85 % H_3PO_4 26.7 mL/L; PTM4 salts 4.4 mL/L. The composition of PTM4 salt solution in g/L: 2 $CuSO_4.5H_2O$, 0.08 NaI, 3 $MnSO_4.H_2O$, 0.2 $Na_2MoO_4.2H_2O$, 0.02 H_3BO_3, 0.5 $CaSO_4.2H_2O$, 0.5 $CoCl_2$, 7 $ZnCl_2$, 22 $FeSO_4.7H_2O$, 0.2 biotin and 1 mL/L H_2SO_4 98 % (v/v).
- Methanol feed solution: methanol 100 % (v/v) + 12 mL PTM4 salts /L methanol.

4.2.2. Inoculum preparation

The starter culture was prepared by inoculating 5 mL of YPD medium with recombinant *P. pastoris* (SuperMan5 expressing huIFNα2b) from the glycerol stock vial stored at -80 ˚C. Pre-culture was prepared by inoculating starter culture in 1 L baffled Erlenmeyer

flask containing 170 mL of sterile YPG medium. The inoculum was incubated at 30°C and 220 RPM for 24 h to a final OD_{600} of 2 to 4.

4.2.3. Bioreactor operation

Recombinant *P. pastoris* cultivation was carried out in a 2.7 L bioreactor (Biojenik Engineering, Chennai), which was equipped with a bottom driven 6 blade Rushton turbine to achieve an efficient Oxygen transfer rate (OTR). Basal salt medium autoclaved at 121°C under1 atm pressure was transferred aseptically into the reactor. Fermentation was initiated by the addition of preculture (10 % v/v) and working volume (V_R) was maintained at 1.7 L. The real-time process signals viz., capacitance (pF/cm), conductivity (mS/cm), dissolved oxygen (%), temperature (°C), pH, methanol feed (g) and methanol feed rate (mL/h) were acquired by NI 6238 Data Acquisition (DAQ) hardware (National Instruments, Texas, USA) with a maximum sampling rate of 250 kS/s per channel. The acquisition of agitation rate was governed by a parallel DAQ device (NI 6002, National Instruments, Texas, USA) operating in tandem with the NI 6238 hardware. A supervisory control and data acquisition (SCADA) interface was developed indigenously using a graphical programming interface (LabVIEW, National Instruments, Texas, USA) platform, which governs data logging (every 5s interval), data preprocessing (e.g. moving average, noise filtering), data display (graphs, archiving) and control algorithms as indicated in Figure 4.2. Reaction (growth) temperature was maintained at 30°C and pH was maintained at 5.4 by the addition of 25 % (v/v) ammonia solution, and 30 % (v/v) H_3PO_4, as neutralizing agents. Batch mode reactor operation was set to continue until complete utilization of glycerol, which was indicated by a sharp rise in dissolved oxygen (DO) signal.

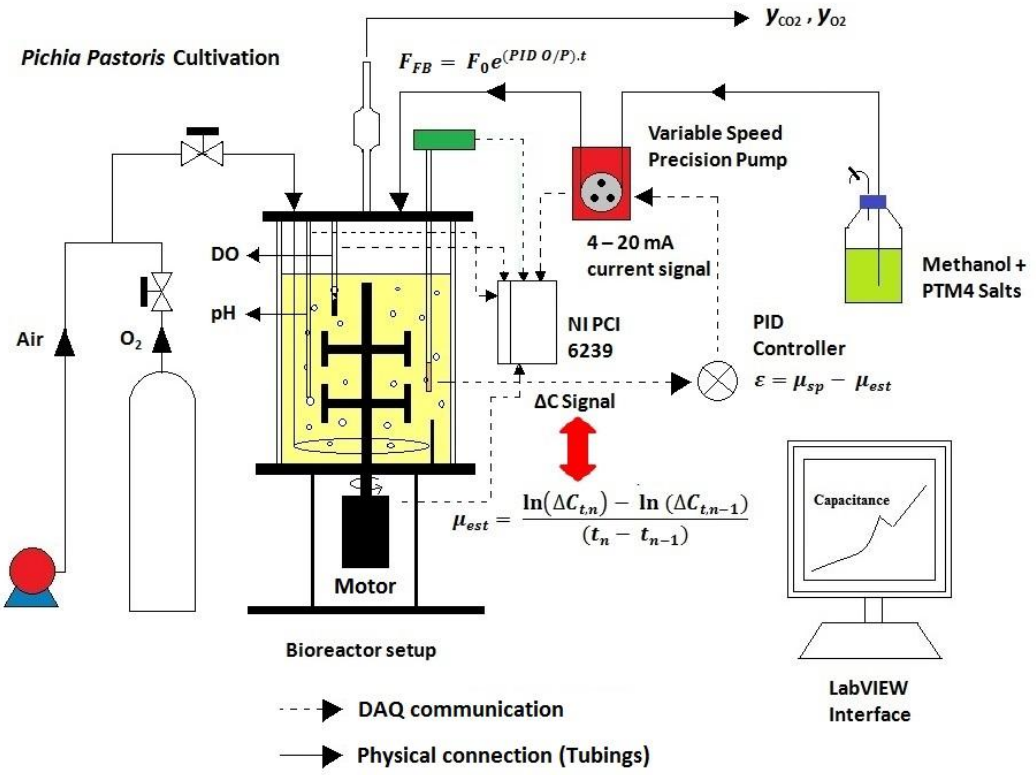

Figure 4.2 Schematic representation of bioreactor experimental setup with the PID control of specific growth rate based on capacitance signal.

4.2.4. Offline Analysis

Optical density (OD) measurements of the collected samples were performed at 600 nm using UV-visible spectrophotometer (GE Healthcare, UK). Biomass concentration (g/L) was estimated by transferring 1 mL of the fermentation broth into pre-weighed 1.5 mL tubes and centrifuging them at 13000 RPM for 10 min at 4°C. The supernatant was separated, and stored at –20 °C for offline analysis of glycerol and methanol through HPLC and huIFNα2b concentration estimation by ELISA analysis using huIFNα2b ELISA kit (Mabtech AB, Sweden).

4.2.5. Specific growth rate estimator (μ_{est})

Dielectric spectroscopic investigation involves capacitance and conductivity measurements of reaction broth containing biomass, product and other analytes [224].

Capacitance probe (Aber Instruments, Aberystwyth, United Kingdom) is segregated into an apex ceramic portion containing 2 annular electrodes and a tapering part extended sufficiently to get immersed into the reaction broth. Head amplifier connected to the probe generates an electric field across the annular electrodes by an applied frequency (0.1 - 20 MHz). Futura tool (Aber Instruments, Aberystwyth, United Kingdom), an in-built application records the capacitance (0 – 200 pF/cm), C and conductivity (0 – 40 mS/cm), G at dual frequencies (580 kHz and 15.560 MHz). ΔC and ΔG values were obtained by subtracting response signal at measurement frequency (580 kHz) from the signal at the reference frequency (15.560 MHz). Sampling rate of the capacitance signal was further amplified (10,000 samples/s) by connecting the probe transmitter to the NI 6238 DAQ device. Mean averaging of ΔC and ΔG at every 100 data points was dealt in order to reduce the noise associated with signal acquisition [225]. Specific growth rate was estimated by using real-time capacitance measurements on a moving window frame of 2 h interval and was computed by the Eqn. 4.1. The interval of 2 h was maintained, considering the slower growth dynamics of *P. pastoris* (SuperMan5) strain during methanol induction phase ($\text{doubling time} \approx 12\ \text{h}$) and ensuring reliable prediction of estimated specific growth rate (μ_{est}). Thus real-time values of μ_{est} serves to process inputs in the proposed PID control and were logged at 5 s intervals.

$$\mu_{est} = \frac{\ln(\Delta C_{t,n}) - \ln(\Delta C_{t,n-1})}{(t_n - t_{n-1})} \quad (4.1)$$

4.2.6. Investigation on the effect of the feeding strategies on μ_{est}

During the fed-batch phase, 2 distinct feeding strategies viz. pulsed feeding and exponential feeding regulated by PID feed-back loop were deployed to study the effect on μ_{est}. The former one deals with addition of defined amount of methanol (first pulse) after complete consumption of glycerol, allowing methanol to be utilized fully and

replenished again (second pulse). This procedure was repeated at regular time intervals to ensure the C-source was available at regular intervals during induced phase growth. The feedback control strategy adopted in this study compares the parsed μ_{est} values to its set point, μ_{sp}. Proportional, Integral and Derivative (PID) controller manipulates the output and adjusts the feed rate in order to minimize error between process input and set value (Figure 4.3). Reliability of μ_{est} model was validated by offline OD_{600} measurements.

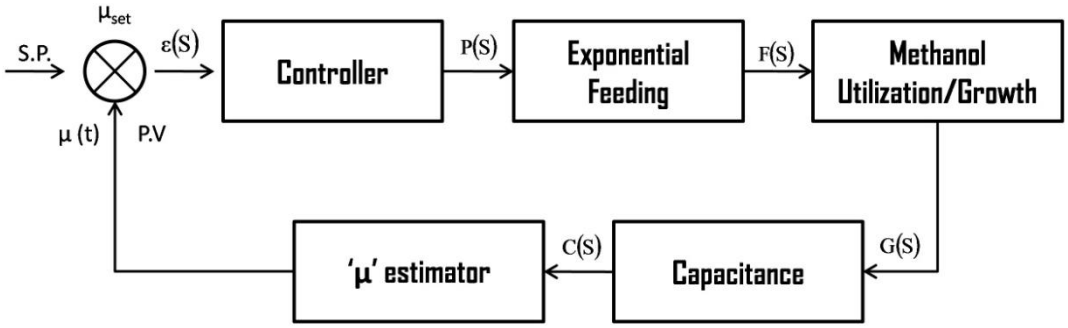

Figure 4.3 PID control loop representing overall process flow and controller action. ε(S), P(S), F(S), G(S), C(S) are the respective transfer functions.

4.2.7. Feed rate control

4.2.7.1. Pulsed feed rate

The complete consumption of residual glycerol in the batch culture was indicated by a rapid rise in DO signal accompanied by a sudden drop in both CER and OUR signals. First methanol pulse (20 g) was initialized to achieve a final concentration of 1.48 % v/v (11.8 g/L) of pure methanol (supplemented with 12 mL of PTM4/L of methanol), in the reaction broth. Preliminary experiments suggested that 1.48 % (v/v) as optimum methanol concentration for increased huIFNα2b production and hence, repeated methanol pulses with a final concentration of 1.48 % (v/v) was continued to assess the effect of optimal methanol pulse on cell metabolism (growth and protein production). The influence of excess methanol on cell metabolism was also investigated by addition

of first methanol pulse (30 g) to attain the final concentration of 2.2 % (v/v) with pure methanol (supplemented with 12 mL of PTM4 per 1 L of methanol) followed by repeated pulsed methanol addition (final concentration of 2.2 % v/v). Complete utilization of methanol was indicated by a rapid rise in DO signal and a drop in OUR/CER signals. Samples were collected at regular time intervals for the assessment of DCW, huIFNα2b titer and residual methanol concentrations and the resultant average values plotted against time.

4.2.7.2. Exponential feed rate

The control of μ at its desired set point value is achieved by feeding the limiting substrate in proportion to the exponential rate of increase in cell concentration. The rate of exponential feeding typically establishes quasi-steady between substrate affinity (k_S) and residual substrate concentration (S) in the reaction broth, which significantly influences the μ value. This feeding strategy is advantageous for any Monod's type of microbial growth and attempts to maintain the methanol concentration (limiting substrate) well above its k_S value.The feed rate equation as shown below (Eqn. 4.2) contains feed-forward and feedback controller components. The former initializes a consistent feeding of limiting substrate (methanol) with respect to the initial biomass concentration, which was developed till batch growth phase i.e. glycerol phase and the latter component determined the positive/negative exponent of the feed rate control [147]. The feed rate is governed by,

$$F_{FB} = F_0 e^{(\text{PID O/P}).t} \quad (4.2)$$

Where F_{FB} is methanol feed rate regulated by feed-back controller, mL/h and $F_0$is Feed forward component, mL/h.

The performance of classical controllers in bioprocess systems is challenged by several factors, which includes dynamic process conditions, cell metabolic perturbations and

instability due to exponential increase in process disturbances [226-228]. A slight modification is adopted in the controller algorithm by including the proportional, integral and derivative terms directly into the exponent term of the growth equation (Eqn.4.4), which could enhance the controller robustness [144]. PID controller computes error based on Eqn. 4.3 and actuates the positive/negative exponent function in response to real-time μ values. PID control loop was designed (Figure 4.2) such that exponential feeding rate during methanol phase was regulated by PID output (PID O/P) and represented by Eqn. 4.4. The main motivation of this approach is that the inherent simplicity of the formulation should contribute to greater controller robustness.

$$\varepsilon(t) = \mu_{sp}(t) - \mu_{est}(t) \tag{4.3}$$

$$\text{PID O/P} = k_c.\varepsilon(t) + \frac{1}{\tau_I}.\int_0^t \varepsilon(t).dt + \tau_D.\frac{d}{dt}.\varepsilon(t) \tag{4.4}$$

The selection of controller parameters viz., proportional controller gain (k_c), integral time (τ_I, min) and derivative time (τ_D, min) plays a pivotal role in the PID controller performance due to the exponential increasing trend of μ related disturbances. Manual tuning method was employed systematically in this study for appropriate selection of the controller parameters [229]. Feed-forward component, F_0 was determined by estimating initial biomass concentration during glycerol phase (X_0) and substituted in the following relationship [193] (Eqn. 4.5)

$$F_0 = \frac{X_0 V_0 \mu_{sp}}{S_{met} Y_{X/_{met}}} \tag{4.5}$$

Where V_0 reactor volume is at the end of glycerol phase, S_{met} is methanol concentration in feed stream (793g/L), and $Y_{X/_{met}}$ is biomass yield during methanol phase.

Methanol feed during induction phase was carried out by a high precision variable speed pump (Watson Marlow 120U, Falmouth, Cornwall, U.K.) and was connected to the PID loop. Feed rates were already pre-calibrated with 4-20 mA current, which operates the

precision pump. PID O/P connected to the precision pump via 4-20 mA signal responses tightly control the dynamic feeding rate. The controller performance was evaluated by calculating the average absolute tracking error for each μ_{sp}. All the experiments were performed in duplicates and the average values are represented in the tables and figures.

4.2.8. Oxygen uptake rate measurement

A laboratory scale exhaust gas analyzer (Ultramat 23, Siemens AG, Berlin and Münich, Germany) was used as a complimentary PAT tool to measure O_2 and CO_2 concentration in the off-gas (exit stream of bioreactor). O_2 and CO_2 concentrations were measured by paramagnetic detection and IR based absorption technique respectively. Gaseous phase mole fractions of O_2 and CO_2 obtained from exhaust gas analyzer measurements was used to estimate oxygen uptake rate, r_{O_2} (OUR) and carbon dioxide emission rate, r_{CO_2} (CER) based on Eqn. 4.6 and Eqn. 4.7 respectively.

$$\text{OUR}, {}^{mg}/_{L.\,s} = \frac{\dot{m}_g}{V_R}\left[y_{O2,in} - y_{O2,out}\left(\frac{y_{inert,in}}{y_{inert,out}}\right)\right] \tag{4.6}$$

$$\text{CER}, {}^{mg}/_{L.\,s} = \frac{\dot{m}_g}{V_R}\left[y_{CO2,out}\left(\frac{y_{inert,in}}{y_{inert,out}}\right) - y_{CO2,in}\right] \tag{4.7}$$

Where $\dot{m}_g$mass flow rate of gas in L/s, V_R is the volume of the reaction broth in L, $y_{O2,in}$ is mole fraction of O_2 in air inlet stream, $y_{O2,out}$ is mole fraction of O_2 in air outlet stream, $y_{CO2,in}$ is mole fraction of CO_2 in air inlet stream, $y_{CO2,out}$ is mole fraction of CO_2 in air outlet stream, $y_{inert,in}$ is mole fraction of N_2 in air inlet stream and $y_{inert,out}$ is mole fraction of N_2 in air outlet stream.

Volumetric rates, $r_{O_2}$and r_{CO_2}could provide direct insight on the cell physiology and their ratio indicates the respiratory quotient [188] of *P. pastoris*. OUR and CER values were estimated by SCADA and logged at every 10 s interval. The O_2 and CO_2 % (mole basis) of inlet air (ambient air) was regularly monitored by the exhaust gas

analyzer in all the reactor runs and their average values maintained a high level of consistency within the range of 20.85-20.9 % and 0.02-0.04 % respectively.

4.2.9. Purification of recombinant huIFNα2b

Glycosylated huIFNα2b from the culture supernatant taken from the optimal control run ($\mu_{sp} = 0.04\ h^{-1}$) was purified as per the protocol described vide in chapter 2, section 2.2.7. In brief the purification protocol included his-tagged affinity chromatography and Concanavalin A (Con A) chromatography steps sequentially. The pooled fractions containing major amounts of the recombinant huIFNα2b after His-tag affinity chromatography were subjected to Con A chromatography for the selective purification of glycosylated huIFNα2b.

4.2.10. Biological activityof recombinant huIFNα2b

Biological activity of the recombinant huIFNα2b was assessed by its ability to inhibit cell growth in the *in vitro* study using breast cancer cell line (T47D and MCF7). T47D cell line and MCF7 cell line were maintained in RPMI medium and DMEM high glucose medium respectively; both media were supplemented with streptomycin and penicillin antibiotic along with 10 % fetal bovine serum (FBS). Cells were grown to 70 % of confluence in humidified incubator at 37°C and 5 % CO_2. Thereafter, the adhered cells were washed with Dulbecco's Phosphate Buffered Saline (DPBS) and detached using 0.25 % trypsin-ethylenediaminetetraaceticacid (EDTA). About $1x10^4$ cells/well were transferred into a 96-well cell culture plate and incubated overnight at 37°C and 5 % CO_2 for further study. The spent medium was replaced by 200 µL of fresh medium containing either commercial huIFNα2b drug or purified recombinant huIFNα2b at different concentrations *viz*., 0.5 nM, 7.5 nM, 20 nM. Cells in the medium without huIFNα2b were used as a negative control. The antiproliferative activity of the huIFNα2b was

determined after 96 h of treatment. The viable cell densities were detected after washing with DPBS based on the conversion of MTT into formazan by mitochondrial reductase. 100 µL of MTT (0.5 mg/mL) was added to each well and incubated at 37°C for 3 h. The MTT solution was discarded and the insoluble formazan crystals were dissolved in 100 µL DMSO and incubated at 25°C for 5 min. The absorbance was measured at 570 nm with the reference absorbance of 690 nm. The assay was performed in 5 replicates.

4.3. Results

4.3.1. Specific growth rate estimator (μ_{est}, h^{-1})

P. pastoris huIFNα2b fermentation runs exhibited a linear correlation ($R^2 > 0.9$) between capacitance and biomass concentration (DCW) data (Figure 4.4). Segregation of various phases such as growth, transition and induction phases could be observed from ΔC signal profile (Figure 4.5). The proportional rise in ΔC signal with respect to an increase in biomass concentrations signal were found to be consistent (R^2 = 0.988 and R^2 = 0.911 for 2 different batch experiments) during all the stages of cultivation viz., exponential, methanol induction, methanol-limited and starvation phases of growth. During the lag phase, the inoculum adapts to the cultivation medium conditions and requires time for the generation of sufficient biomass and thereby the real-time capacitance signal. Hence, the capacitance values during this phase do not corroborate well with the offline biomass. The rate of change in the capacitance value with respect to time was modeled to provide real-time estimation of specific growth rate (μ_{est}).

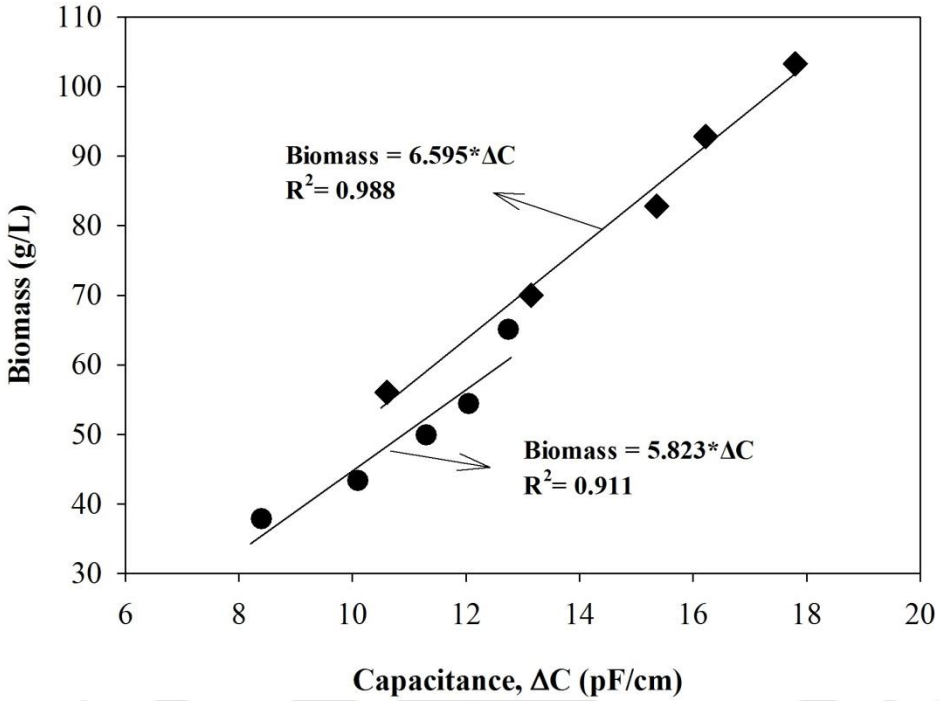

Figure 4.4 Correlation between the developed capacitance signals, ΔC (pF/cm) with the DCW (g/L) obtained at two different control runs.

Reliability of the estimated values (μ_{est}) was validated by comparison with $\mu_{offline}$ data estimated using DCW measurements in accordance with the published reports [144].

4.3.2. Growth characteristics of *P. pastoris* during growth and induction phases of huIFNα2b production

Growth phase is characterized by the utilization of glycerol, which shows repressing effect on the AOX transcription elements. As a result it leads to the channeling of major carbon flux towards biomass formation with relatively lesser maintenance requirement [230]. This can be observed from the higher biomass yields ($Y_{X/gly}$) achieved at the end of glycerol batch phase as shown in Table 4.1. During the batch growth phases of pulsed feed strategy (glycerol as sole carbon source), significant biomass production was achieved (Table 4.1). Sudden drop in the respirometric activity (decrease in CER and OUR signal) and a drastic rise in DO signal indicated the exhaustion of glycerol in the reaction broth. Their levels therefore acted as alarms that signaled the completion of

batch glycerol growth phase (Figure 4.5). After the complete utilization of glycerol in batch growth phase, methanol (100 % v/v methanol supplemented with PTM4 salts) adaptation pulse was added as a supplement, which marked the initiation of transition phase. The latter was characterized by the decrease in viable cell volume post methanol addition, subsequently manifested by the drop of ΔC signal (Figure 4.5).

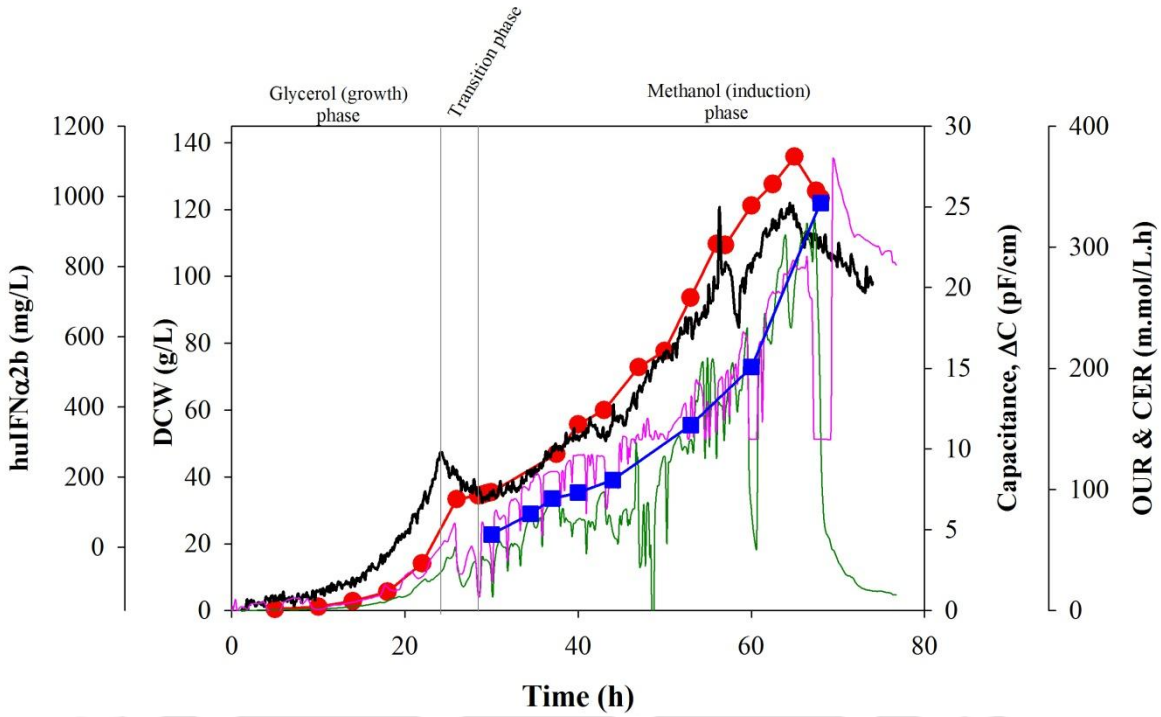

Figure 4.5 Typical dynamic plot of *P. pastoris* huIFNα2b fermentation (μ_{sp}=0.03 h^{-1}) representing various process analyzers viz. Capacitance (pF/cm) (Black continuous), CER (m.mol/L.h) (Green continuous), OUR (m.mol/L.h) (Pink Continuous) and compared with corresponding offline values such as DCW (g/L) (red continuous with filled circle) and huIFNα2b (mg/L) (blue continuous with filled square).

Methanol pulses (4 shorter pulses of 5 g of methanol) were continued until the response from ΔC signal showed a positive upfront. This phase is also regarded as the adaptation phase, in which AOX transcription machinery gets gradually activated and carbon assimilation is shifted from glycerol to methanol after about duration of 3 – 4 h. Induction phase starts at the pulsed feeding of methanol by the methodology as described in the 'Pulse Feed rate' section previously, after the transition phase. Different dosage

rates of methanol used i.e. optimal (20 g) and excess (30 g), its influence in biomass yield and huIFNα2b titer are reported in Table 4.1. Pulsed feeding rate at different levels was found to have negligible effect on their respective μ_{est} values as observed in Table 4.1.

Table 4.1 Assessment of pulsed feed strategy on μ_{est} during methanol induction phase

Pulsed Feed rate	DCW (g/L)	μ_{gly} (h^{-1})	μ_{met} (h^{-1})	$Y_{X/gly}$ (g/g)	huIFNα2b (mg/L)	Volumetric Productivity[a] r_p (mg/L.h)	$Y_{X/met}$ (g/g)
Batch run with pulse feeding (20 g Methanol)	158.4	0.213	0.02718	0.772	436	6.22	0.129
Batch run with pulse feeding (30 g Methanol)	133.12	0.204	0.0262	0.822	627	10.11	0.109

a r_p was computed during induction phases only

Specific rate of methanol utilization ($q_{s,met}$) was determined for 2 different methanol pulsed feeds (20 g and 30 g) and the residual methanol concentration plot (Figure 4.6A) showed that the methanol was fully utilized in both the feed conditions. $q_{s,met}$ estimated for the different pulsed feed (20 g and 30 g) rates were found to be consistent at an average of 0.092 ± 0.013 g/g. h throughout the induction phase (Figure 4.6A) while the ΔC signal was positively influenced by the concomitant methanol utilization by the *P. pastoris* (Figure 4.6B).

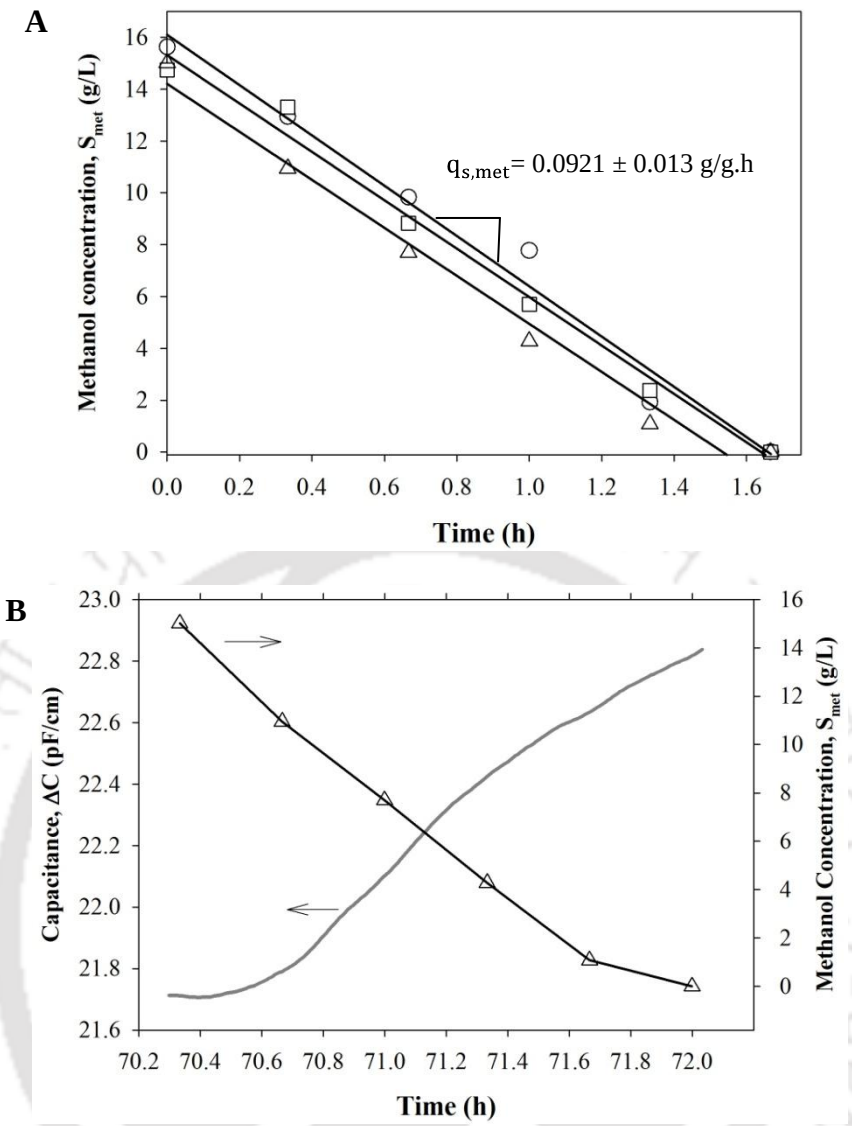

Figure 4.6 A) Dynamic methanol uptake profile by *P. pastoris* cultivation during repeated methanol pulse feeding at the induction phase: Duration 62 – 64 h (Open Circles), Duration70 – 72 h (Open Triangles), Duration 77 – 79 h (Open Squares). $q_{s,met}$ was calculated from the ratio of volumetric methanol utilization (g/L.h) to biomass concentration. B) Influence of methanol (Open Triangles) utilization (g/L) on developed capacitance signal (ΔC), pF/cm (Continuous dark grey line) at 70 – 72 h.

4.3.3. Design of PID Feedback loop for the exponential methanol feeding strategy at different μ_{sp}

In all μ_{met} control runs, the batch growth phase lasted upto 26 – 28 h duration leading to complete glycerol consumption and generated 35 – 40 g/L of biomass. Larger proportion of glycerol consumption, i.e. more than 80 % of substrate ($Y_{X/gly}$ > 0.8 in Table 4.2) was

directed towards the synthesis of biomass, thus generating the required potential cell machinery (high cell density) for the subsequent huIFNα2b production. Adaptation phase encompassed 4 – 5 shorter methanol pulses required to activate de-repressed methanol induced AOX transcription genes. In induction phase, exponential feeding strategy was designed such that methanol accumulation was maintained less than its critical level (> 15 g/L) based on the published resources [110]. Continuously regulated feed was initiated following the adaptation phase in all control runs intended to maintain a different specific growth rate at the desired set point values ($\mu_{sp} = 0.015, 0.03, 0.04 \; and \; 0.06\ h^{-1}$) .The feed-forward and feed-back controller parameter (obtained from Eqn. 4.2) were given as input in the SCADA before proceeding with the μ_{met} control. The lowest (7.65 mL/h) and highest initial feeding rate (28.15 mL/h) of methanol were decided based on desired μ_{sp} values of 0.015 h^{-1} and 0.06 h^{-1} respectively in the feed-forward component of Eqn. 4.5. The performance of the implemented feedback PID control strategy manipulating methanol feed rate to control μ_{met} in response to various μ_{sp} values were tabulated in Table 4.2. In all μ_{met} control runs except $\mu_{sp} = 0.06\ h^{-1}$, exponential feeding rates were observed to be effective (Figure 4.7A, 4.7B and 4.7C) in meeting the biomass growth and protein production requirements owing to the complete utilization of methanol (residual methanol concentration was observed closer to zero for more than 20 h).

Table 4.2 Assessment of feedback control strategies employing different μ_{sp}

μ_{sp} (h^{-1})	DCW (g/L)	r_x (g/L.h)	μ_{gly} (h^{-1}) (Offline)[a]	μ_{met} (h^{-1}) (Offline)	$Y_{X/gly}$ (g/g)	huIFNα2b (mg/L)	r_p (mg/L.h)[b]	$Y_{X/met}$ (g/g)
0.015	119.8	1.61	0.233	0.0181	0.853	550.3	13.75	0.154
0.03	135.7	2.088	0.229	0.0378	0.817	980.4	25.8	0.157
0.04	185.5	2.829	0.252	0.0464	0.88	1483.7	39.04	0.262
0.06	124	2.005	0.245	0.063	0.858	536.2	15.77	0.176

a Maximum Specific growth rate estimated during growth phase

b r_p was computed during induction phases only

Rapid consumption of methanol in all control runs substantiates that dynamic mass balance was established by the PID controller between methanol availability (feed stream) and its immediate consumption by *P. pastoris*. ΔC signal was observed to be a good indicator of methanol assimilation, as it rises sharply during the early induction phase represents effective methanol utilization. In a similar manner, methanol accumulation (Figure 4.7A, 4.7B and 4.7C) in the later induction phase results in the stabilization of ΔC signal after 60 hours. OUR/CER signals corroborated well with ΔC signal in distinct phases of *P. pastoris* huIFNα2b production, but associated with perturbations and noises due to the regulation of airflow rate in order to maintain the desired DO concentration (Figure 4.5). At higher μ_{sp}say (0.06 h^{-1}), the exponential feed rate was repeated at regular time intervals rather than proceeding at a continuous feeding to avoid methanol accumulation to its critical level.

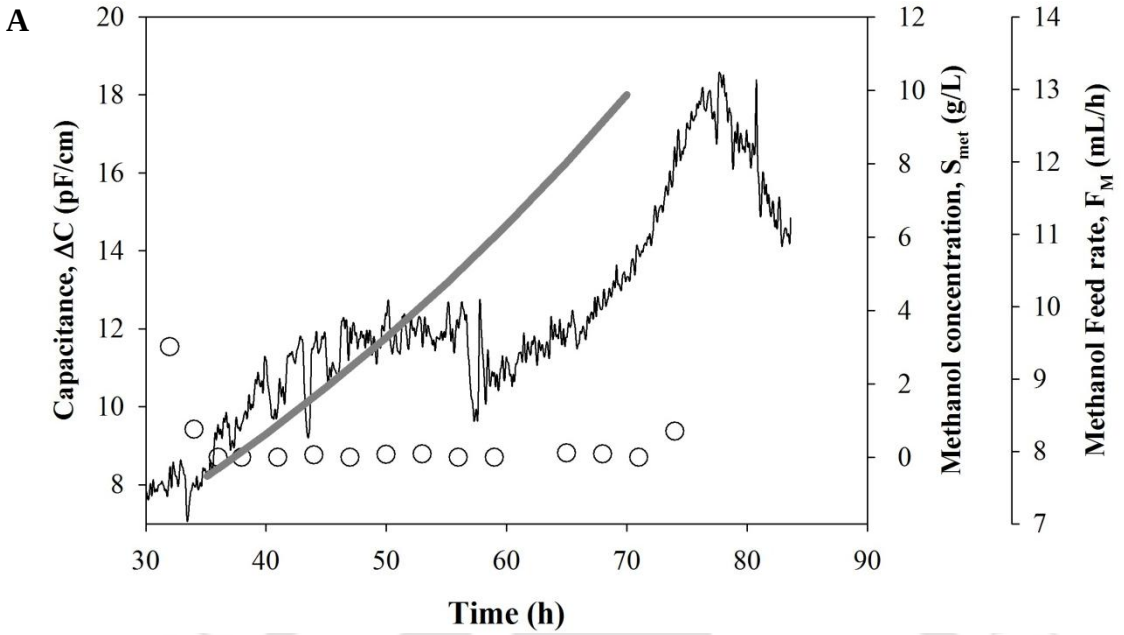

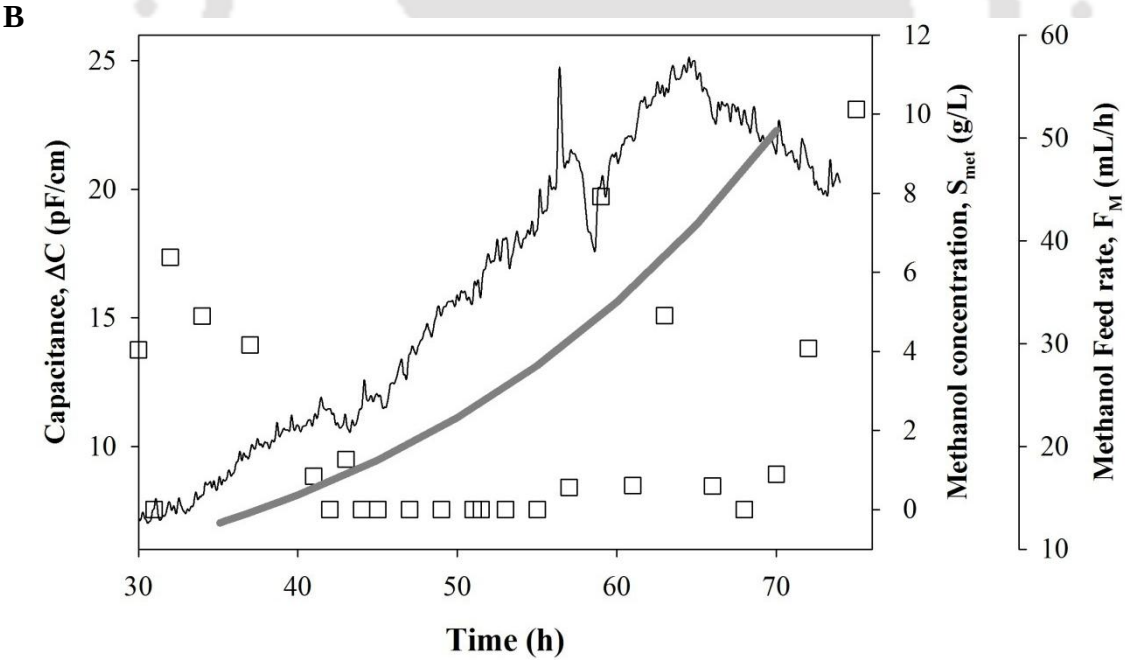

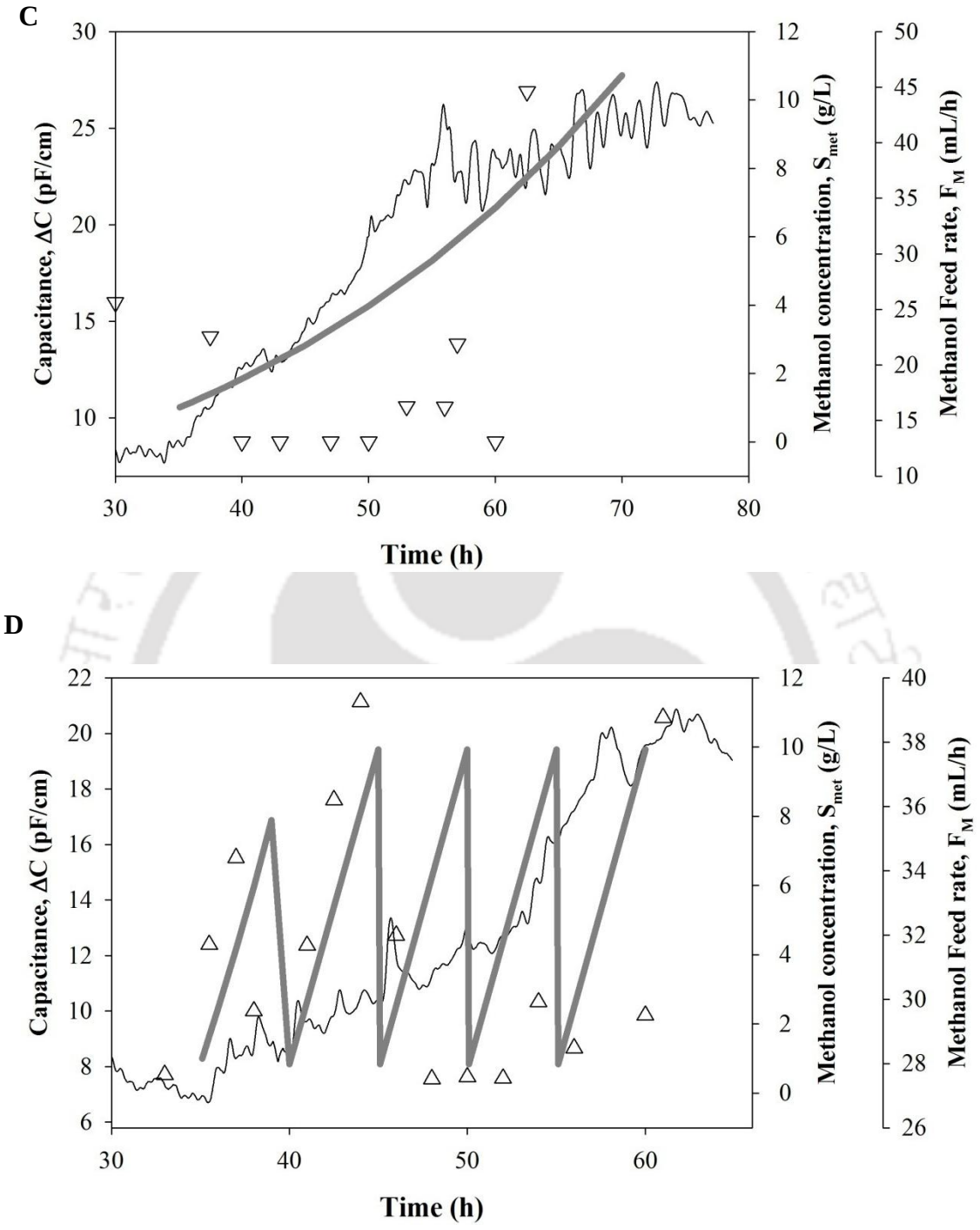

Figure 4.7 Exponential feedback control of methanol (Dark grey line) during induction phase: Capacitance signal, ΔC (Dark Continuous line); Methanol (Dark grey line); Scatter plots representing methanol concentration values during various μ_{sp} runs: A) Open Open Circles ($\mu_{sp} = 0.015\ h^{-1}$), B) Open Squares ($\mu_{sp} = 0.03\ h^{-1}$, C) Open Triangles down ($\mu_{sp} = 0.04\ h^{-1}$), D) Open Triangles up ($\mu_{sp} = 0.06\ h^{-1}$)

Also residual methanol concentration consistently exhibited increasing and decreasing trends at regular intervals (Figure 4.7D). Repeated exponential feed rate showed a passive response for biomass growth during early phases of induction, but later the cells adapted to high methanol load conditions exhibiting the controlled μ_{met} (substantiated by both μ_{est} and $\mu_{offline}$ values).

4.3.4. Control characteristics of capacitance based μ_{est}

Dynamic variation of μ_{sp} to different set values in a single control experiment could be an attractive option from an operational perspective [231], but would in turn exert dynamic pressure on AOX machinery of *P. pastoris*. This would lead to various levels of stress (transient adaptation of cells to different methanol concentrations) and complicate the interpretation of the protein expression level. Independent assessment of huIFNα2b production by controlling μ_{met} at different set point values would be advantageous, as the selective pressure applied on the AOX expression system by methanol feed is uniform throughout the induction phase. The proposed schema of the μ_{met} control as illustrated in Figure 4.3 is highly dependent upon the PID tuning parameters and control characteristics.

In the entire controller tuning experiments, each tuning parameter was set and maintained for atleast 8 h duration for observation. Controller gain (k_C), a ratio between methanol feeding rate (F_M) to the developed μ_{est} is a prominent factor [141] in establishing a stabilized controller output. k_C was maintained in the range between 0.5 – 1.0 and delivered robust controller performance for $\mu_{sp} \leq 0.04\ h^{-1}$. The 'integral' component of the controller was attributed to reduced offset in the controlled variable and to delivering a stable response. Ratio between methanol feeding rate (F_M) to μ_{est} is determined by the controller gain, k_C ; it was set to ≤ 1, in order to avoid accumulation

of methanol to toxic levels. Influence of tuning parameters over μ_{est} signal and their deviation with the proposed μ_{sp} was shown in Table 4.3.

Table 4.3 Assessment of PID controller performance

PID Parameters			μ_{sp}		
Controller gain, k_C	**Integral time, τ_I (min.)**	**Derivative time, τ_D (min.)**	**(h^{-1})**	**$\mu_{est}(h^{-1})$**	**$\mu_{Offline}$ (h^{-1})**
0.5[a]	0.05[a]	0[a]	0.04	0.043±0.0068	0.0389
2[a]	0.1[a]	0[a]		0.0458±0.0081	0.0425
0.5[a]	0.1[a]	0[a]		0.041±0.0056	0.0478
1[a]	0.1[a]	0[a]		0.054±0.0096	0.0391
0.25[a]	0.1[a]	0[a]		0.038±0.0044	0.0412
4.8[b]	0.6[b]	0.15[b]	0.06	0.0578±0.0064	0.0597

a Controller tuning carried out at $\mu_{sp} = 0.04\ h^{-1}$

b Controller tuning carried out at $\mu_{sp} = 0.06\ h^{-1}$

PID controller output was observed to be robust to meet the methanol demand for the biomass growth and huIFNα2b production owing to its effective consumption in the control experiments (Figure 4.7A - 4.7C). Moreover, the methanol accumulation did not exceed the residual concentration (> 2 g/l) for biomass growth and remained consistent for long duration in all the control experiments except for μ_{sp} of 0.06 h^{-1} (Figure 4.7D). μ_{est} values were corroborated well with $\mu_{offline}$ measurements (Figure 4.8A – 4.8D). Continuous feeding of methanol regulated by PID loop proved to be more accurate in maintaining a low μ_{sp} at a narrow range (0.015 – 0.06 h^{-1}) reported elsewhere [141].

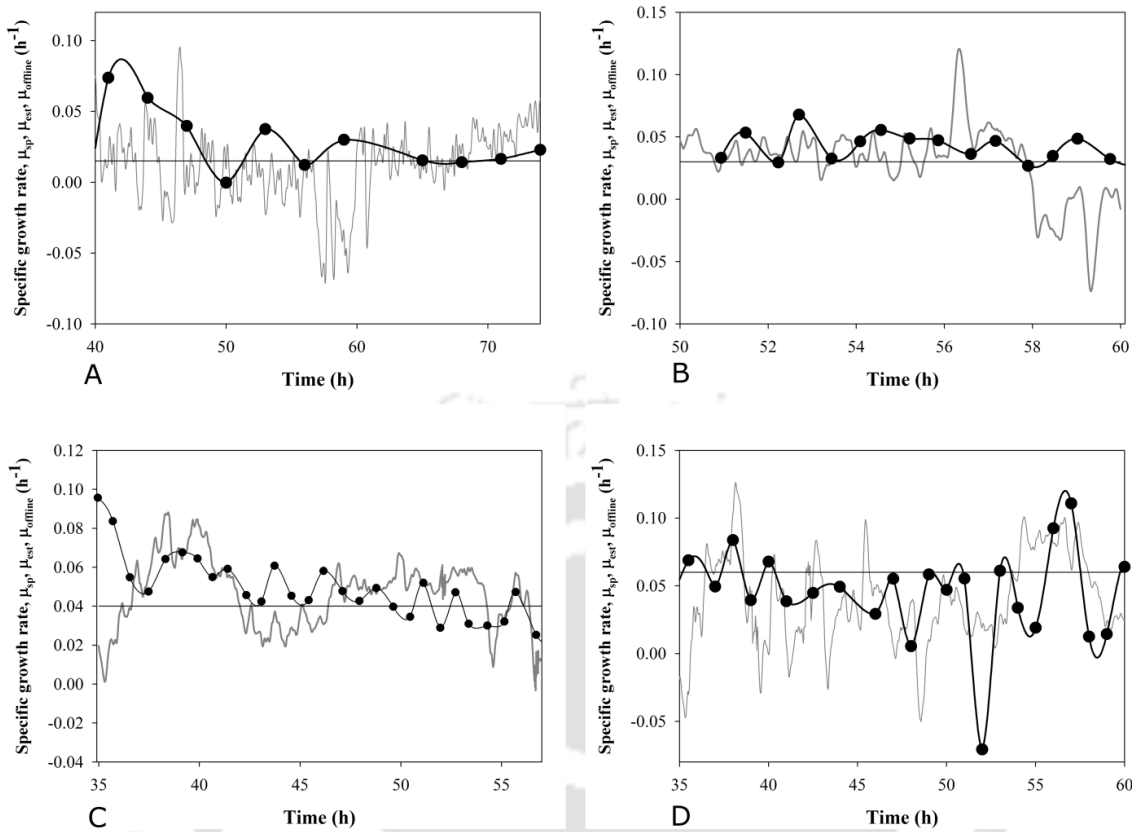

Figure 4.8 PID controller performance based on comparative evaluation of μ_{sp}, μ_{est} and $\mu_{offline}$ values: Dark continuous lines representing μ_{sp}, Dark grey continuous lines representing μ_{est}, Dark circles with continuous lines representing $\mu_{offline}$

Table 4.4 Average tracking error calculated for different μ_{sp} reactor runs and compared with μ_{est} and $\mu_{offline}$

$\mu_{sp}(h^{-1})$	$\mu_{est}(h^{-1})$	$\mu_{Offline}(h^{-1})$	Average tracking error[a] (%)
0.04	0.038±0.0044	0.0412	5
0.06	0.0578±0.0064	0.0597	3.7
0.015	0.0163±0.0011	0.0153	8.7
0.03	0.0342±0.01	0.029	14

a Average tracking error was computed using the relationship $\frac{(\mu_{sp}-\mu_{est})\times 100}{\mu_{sp}}$

4.3.5. Improvement in huIFNα2b productivity

The production of huIFNα2b was found to increase in conformity with DCW in every μ_{sp} run. However, a linear trend in DCW was observed in contrast to the exponential fashion of the huIFNα2b titers (Figure 4.9A and Figure 4.9B). The huIFNα2b production profile exhibited two distinct phases. During 1st phase of induction (30 to 50 h), the specific protein productivities were at lower range, typically of 0.06 – 0.13 $\frac{\text{g.huIFN}\alpha\text{2b}}{\text{g.Biomass}}$.h. At the 2nd phase (> 60 h), the rate of increase in huIFNα2b titers quadrupled (0.26 – 0.47 $\frac{\text{g.huIFN}\alpha\text{2b}}{\text{g.Biomass}}$.h) compared to their former phase in all μ_{sp} runs and a maximum of 1483 mg/L of product was achieved at $\mu_{sp} = 0.04\ h^{-1}$. Glycoengineered *P. pastoris* exhibited an elevated product titers ≥ 500 mg/L in all control runs and the volumetric productivity was found to be higher at $\mu_{sp} = 0.04\ h^{-1}$ (Table 4.2).

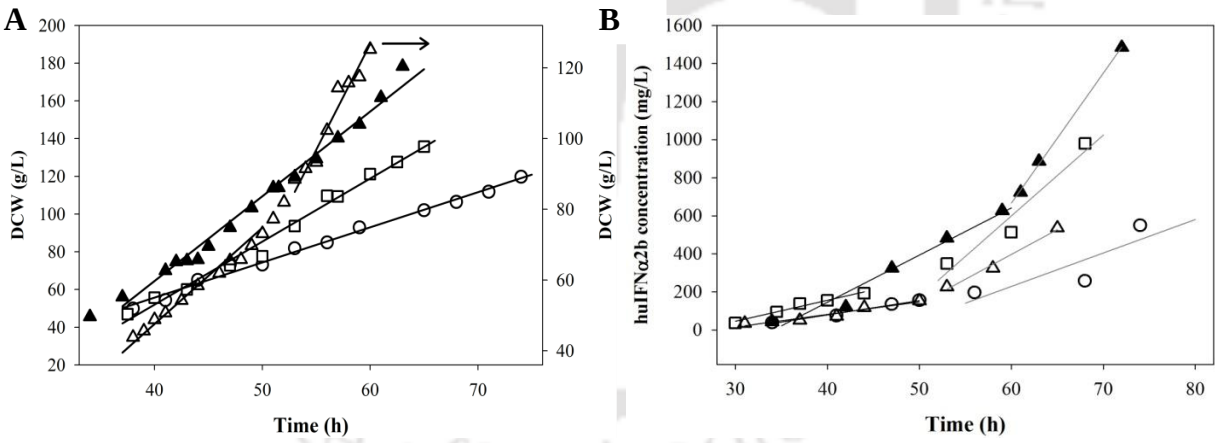

Figure 4.9 Influence of specific growth rate on A) DCW and B) Influence of specific growth rate on huIFNα2b production: Open Circles(μ_{sp}=0.015 h^{-1}), Open Squares (μ_{sp}=0.03 h^{-1}), Filled triangles (μ_{sp}=0.04 h^{-1}), Open Triangles (μ_{sp}=0.06 h^{-1})

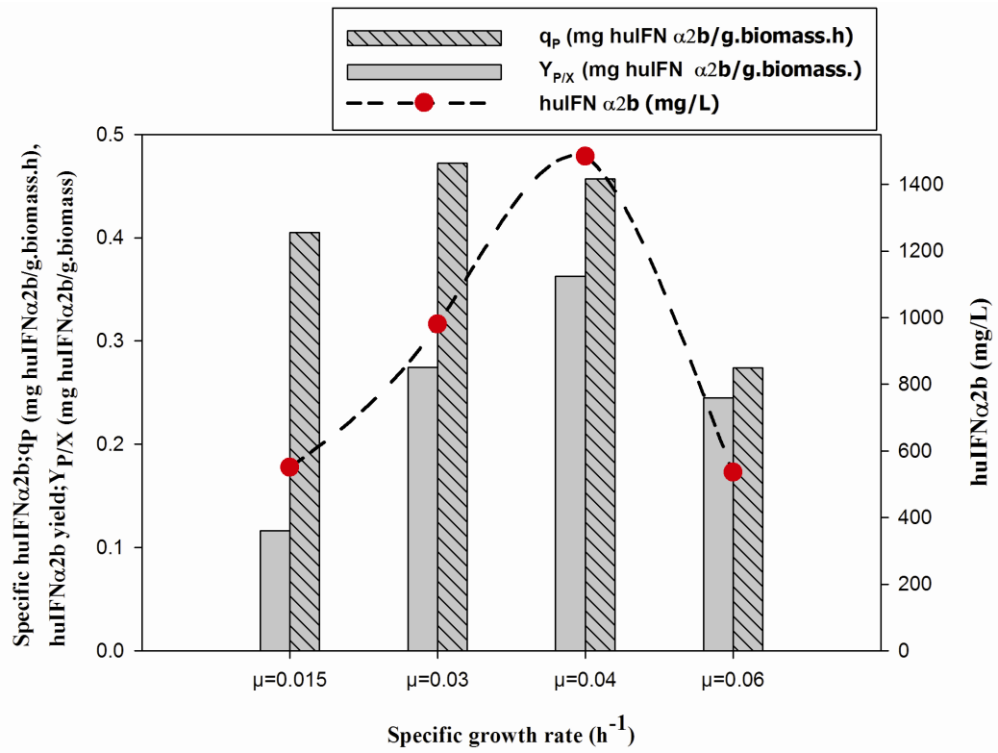

Figure 4.10 Influence of different specific growth rate (μ_{sp}) on huIFNα2b titer, specific productivity (q_P) and protein yield coefficient ($Y_{P/X}$).

The huIFNα2b titer, specific huIFNα2b production ($q_{huIFN\alpha 2b}$) and $Y_{P/X}$ were observed to increase with respect to exponential feeding of methanol till $\mu_{sp} \leq 0.04\ h^{-1}$, and decrease beyond this set point (Figure 4.10). Repetitive feeding leading to methanol accumulation in $\mu_{sp} = 0.06\ h^{-1}$ run resulted in a moderate utilization of substrate when compared to other control runs. Moreover the growth profile exhibited two different linear phases corresponding to $0.0271\ h^{-1}$ and $0.0597\ h^{-1}$ respectively (Figure 4.8A). The product titer (536 mg/L) obtained at the end of the fermentation was substantially reduced than other control runs.

4.3.6. Purification and biological activity of recombinant huIFNα2b

The partial purification of the recombinant huIFNα2b (glycosylated and unglycosylated) from the mixture of other host cell proteins in the clarified supernatant was achieved by

his-tag chromatography (Figure 4.11). The selective recovery of glycosylated huIFNα2b was achieved by Con A chromatography (Figure 4.12).

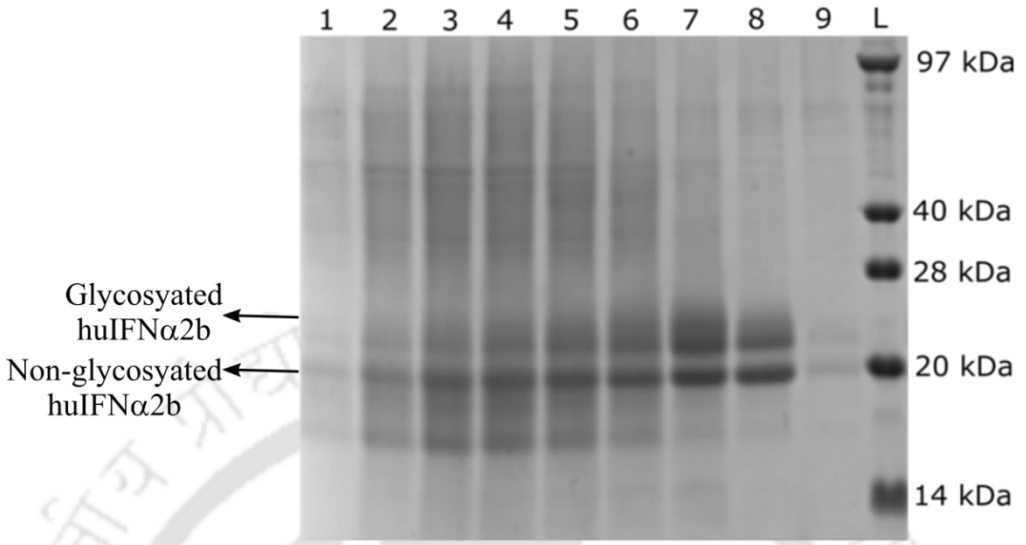

Figure 4.11 Purification of recombinant huIFNα2b by His-Tag affinity chromatography. Lanes 1-9 shows elution fractions and Lane L shows protein ladder. In lane 1-9, 25 µL of sample was loaded and in lane L, 10 µL of protein ladder was loaded.

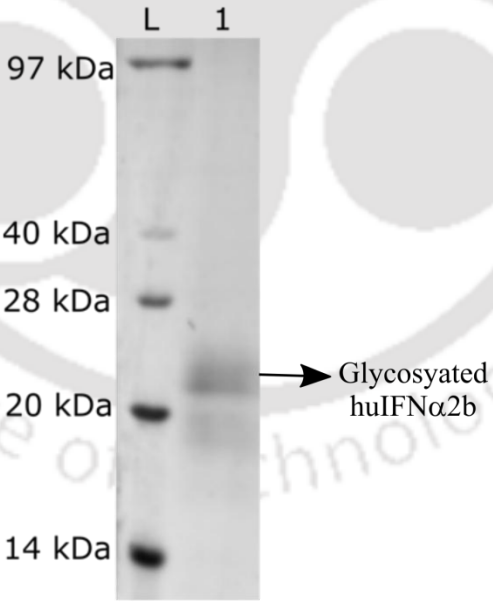

Figure 4.12 Purification of recombinant glycosylated huIFNα2b by Con A chromatography. Lanes 1 shows elution fraction containing purified huIFNα2b and Lane L shows protein ladder. In lane 1, 15 µL of sample was loaded and in lane L, 10 µL of protein ladder was loaded

Antiproliferative activity is one of the key biological attributes exhibited by huIFNα2b [209] and was assessed at varying concentrations of glycosylated huIFNα2b using human breast cancer cell lines (T47D and MCF7). The growth inhibition by huIFNα2b was more pronounced in the MCF7 (~50 %) cell line (Figure 4.13B) compared to T47D (17 %) cell line (Figure 4.13A), and was also dose-dependent. A greater reduction in cell proliferation was observed (~50 %) for MCF7 cell line (Figure 4.13 B) than the T47D cell line (17 %) at the highest concentration, 20nM (Figure 4.13A) and the antiproliferative effect of commercial huIFNα2b drug was slightly higher (10 %) compared to the purified huIFNα2b (of the present study) for both the cell lines.

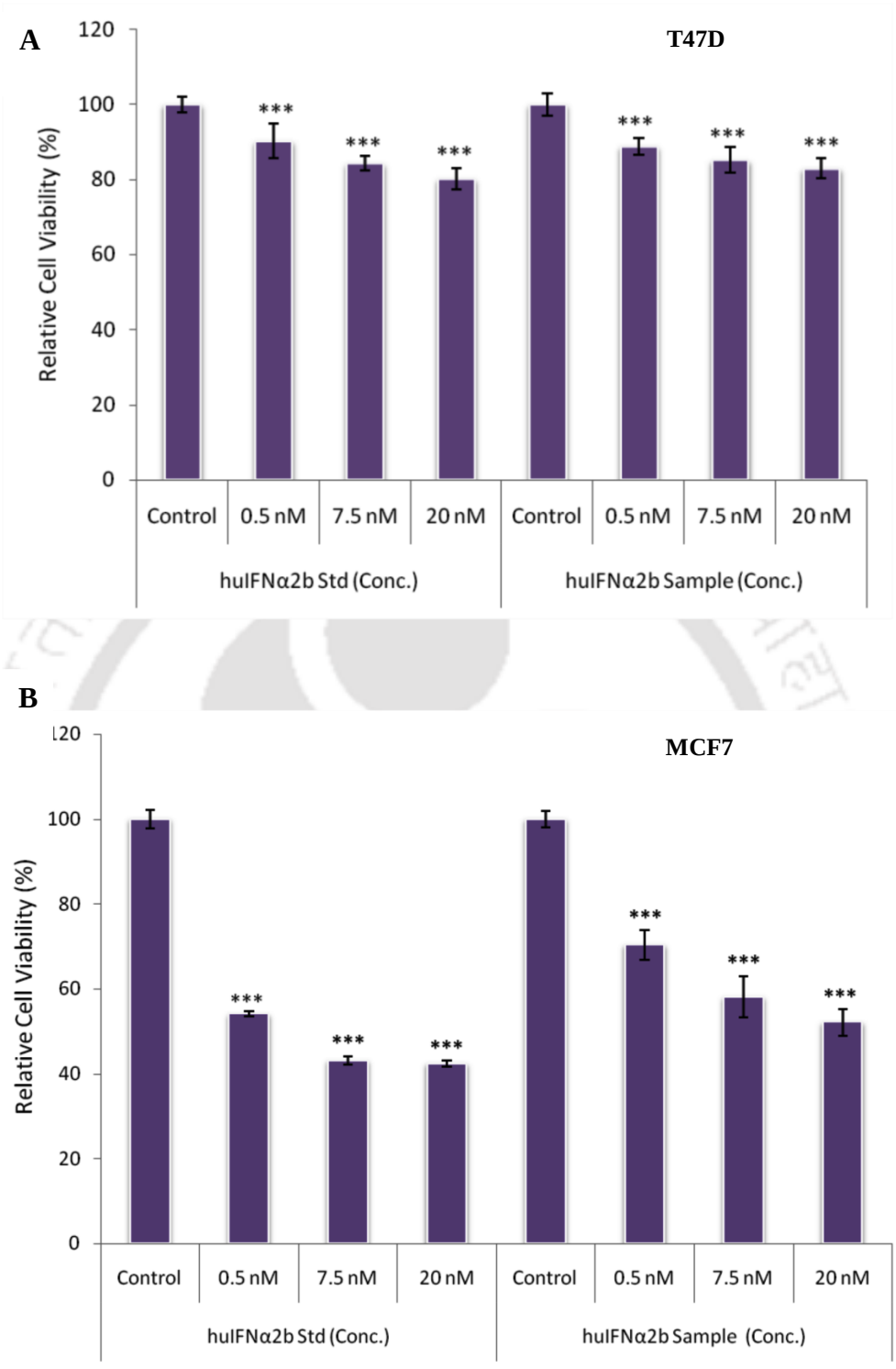

Figure 4.13 Antiproliferative effect of the purified huIFNα2b and standard huIFNα2b against breast cancer cell lines. A) T47D B) MCF7. The assay was performed in five replicates. The values are statistically significant at P<0.001 (***) as analyzed by ANOVA.

4.4 Discussion

4.4.1. Specific growth estimator

Real-time capacitance signal (ΔC) was observed to corroborate well with DCW measurements in exponential batch growth (glycerol limited) and induction phase (methanol limited) of *P. pastoris* (SuperMan5) fermentation. The proposed μ_{est} estimator (Eq. 4.1) deciphered from ΔC signal, was thus deployed to read calculated μ values at different regimes of *P. pastoris* growth. The relationship between the increments in capacitance value to the DCW during the induction (production) phase was estimated to be an average of correlation obtained from different fermentation runs ($Biomass = (6.209) * \Delta C$) (Figure 4.4). The average slope value for biomass and ΔC correltation for induction phase (6.209) was observed to be significantly greater than the exponential growth phase (3.693). This could be attributed due to the fact that 'glycerol' is preferred as 'anabolic' substrate and 'methanol' serves as 'energetic' substrate driving the protein production in *P. pastoris* fermentation [145, 232].

4.4.2 Effect of repeated pulsed feed on specific growth rate

Pulsed feed approaches are of extremely advantageous, if residual inducer concentration in the fermentation is sufficiently maintained at the range between critical methanol concentrations (2 g/L) to its toxic level of 30 g/L (Christian Dietzsch 2011). During the pulsed feed runs of methanol (20 g and 30 g) the specific growth rate of *P. pastoris* was observed to be not consistent and as the methanol depletes, μ drops proportionally towards zero [205]. Methanol dosages of 2 definite pulses, i.e. 20 g and 30 g were fed in 2 separate fed-batch cultivations of *P. pastoris* during induction phase and the average specific growth rate ($\mu_{offline}$) values were found to be 0.02718 h^{-1} and 0.0262 h^{-1}) respectively (Table 4.1). The specific methanol utilization rate ($q_{s,met}$= 0.0921 ± 0.013

g/g.h) in this heterologous expression system was several folds higher than that reported for any of the de-repressed substrates [233] and also was found to be constant throughout the production phase (Figure 4.6A). During the time course of methanol utilization in the pulse feeding strategy, the μ_{met} of *P. pastoris* varies dynamically showing maximum μ_{met} at higher methanol concentrations i.e. immediately after supplementing 20/30 g feed bolus and as the methanol depletes, μ_{met} drops proportionally towards zero [205]. Increase in μ_{met} at the sudden onset of feed could be traced from an increase in ΔC signal (Figure 4.6B). Thus it indicates that the cell metabolism is limited by the methanol feed, leading to its effective assimilation and followed by flattened profile representing methanol depletion. Thus it proves the fidelity of the ΔC signal to indicate/signal the physiological state of the *P. pastoris* during induction phases.

The huIFNα2b titer (627 mg/L) was significantly higher for excess pulse feeding (30 g) as shown in Table 4.1, in spite of μ_{met} value remaining almost unchanged. These findings suggest that pulsed addition of methanol at its temporal excess (30 g) influenced the huIFNα2b production positively at the expense of reduction in biomass yield ($Y_{X/_{met}}$). Possibility of inhibitory effects of methanol on membrane synthesis and DNA replication lead to decrease in the biomass growth and resulted in regulation of energy flux (as a result of methanol utilization) towards huIFNα2b synthesis pathway, which in turn lead to enhancement in the product titer [234]. The constructed recombinant glycoengineered *P. pastoris* in this thesis (Chapter 2) exhibits a better stability in expressing AOX transcription genes amidst higher methanol concentrations in the range of 14 – 16 g/L as shown in Figure 4.6A and 4.6B. This is substantiated by reports suggesting that recombinants with the integration of gene of interest possessed higher methanol tolerance compared with wild type strain [234, 235]

4.4.3. Control of specific growth rates, μ_{est} at various μ_{sp}

Feed-back control of μ_{met} at different levels (0.015, 0.03, 0.04 and 0.06 h^{-1} respectively) was carried out at the end of glycerol phase. Capacitance development over time was proportionate with the increase in DCW and the μ_{est} was found to be accurate (Table 4.4) within the experimental bounds i.e. $\mu_{sp} = 0.015 - 0.06\ h^{-1}$. PID loop based exponential feeding strategy successfully controlled the specific growth rate at desired set point value (μ_{sp}) in all control runs except $\mu_{sp} = 0.06\ h^{-1}$ (Figure 4.8D). The concurrence between the μ_{sp}, μ_{est} and $\mu_{offline}$ values substantiates the successful accomplishment of the PID control (Figure 4.8A-4.8C). Methanol concentration was maintained to trace levels during initial phases of induction (Figure 4.7A – 4.7C). Rapid consumption of methanol in all control runs substantiates that dynamic mass balance was established by the PID controller between methanol availability (feed stream) and its subsequent consumption by *P. pastoris*. During induction phase, methanol serves as the sole carbon source for both the carbon and energy demands of *P. pastoris* growth and huIFNα2b production . Controlled continuous feeding of methanol resulted ineffective utilization of methanol for biomass formation ($Y_{X/met} = 0.262$ g. biomass/g. methanol) at $\mu_{sp} = 0.04\ h^{-1}$. Significant methanol accumulation (4 to 10 g/l) was observed at the early induction phase (35 – 45 h) for the control run at $\mu_{sp} = 0.06\ h^{-1}$ (Figure 4.7D). This methanol accumulation could be attributed to *P. pastoris* reached its maximum substrate uptake capacity (q_S^{max}) while controlled at specific growth rate (μ_{sp} = 0.6 h^{-1}) near to its maximum specific growth rate (μ_{max} = 0.0624 h^{-1}). The imbalance (Figure 4.7D) of the methanol feed rate (physical effect) is the manifestation of metabolic perturbations experienced by organism *P. pastoris* while growing near to its maximum growth rate conditions [236]. The decrease in biomass growth (Figure 4.9A)

confirms the outcome of metabolic stress experienced by the *P. pastoris* growing at high specific growth rate ($\mu_{sp} = 0.06\ h^{-1}$). The control run ($\mu_{sp} = 0.06\ h^{-1}$) was performed by repeated re-initializing the controller (Figure 4.7D) at regular time intervals $F_{FB} =$ 27.98 – 37.77 mL/h) and methanol (S_{met}= 793 g/L) feed rate was maintained at the range 27.98 – 37.77 mL/h. Inspite of the methanol accumulation, the controller maintained the μ_{est} was consistent at 0.0597 h^{-1} (near to μ_{sp}) for 20 h duration OUR/CER signals corroborated with the ΔC signal in all the μ_{sp}control runs (Figure 4.5) and the respiratory quotient (RQ = 0.683 ± 0.128) illustrated the metabolic utilization efficiency of carbon source (glycerol/methanol) during *P. pastoris* fermentation and the RQ value corroborates with the reported literature [237, 238].

4.4.4. Response of μ dependency in the controller function

Noise pretreated μ_{est} values obtained from ΔC signal at a time frame of every 2 h was compared with their corresponding offline values ($\mu_{offline}$) estimated from DCW measurements. The concurrence between μ_{est} and $\mu_{offline}$ values with respect to μ_{sp}, proves the successful accomplishment of the PID control (Figure 4.8A – 4.8D). Lower average tracking error (less than 15 %) obtained for all μ_{met} control runs showing that μ_{est} is in good synchronization with their respective set points (Table 4.4). Moreover, the characteristics of controller especially the long-term stability could be effectively addressed in individual control experiments run at different μ_{sp} values. At different control μ_{sp} runs, a uniform control regime was maintained by feed-back control resulting in consistent biomass and huIFNα2b production. From Table 4.2, huIFNα2b production is strongly influenced by μ_{met} especially when maintained at a narrow range [91, 130]. μ_{est}values were corroborated well with $\mu_{offline}$measurements (Figure 4.8). Exponential feeding of methanol regulated by PID loop proved to be more

accurate/categorical/effective in maintaining a low μ_{sp} at a narrow range (0.015–0.06 h^{-1}) reported elsewhere [141]. The oscillatory behavior observed in μ_{est} in all the control runs (Figure 4.8A – 4.8D) is attributed due to natural metabolic response of the *P. pastoris* but it is unlikely to become the controller effect and non-aligned to actual value of specific growth rate [144]. Similar oscillatory behavior was observed during the exponential batch growth phase (glycerol), where *P. pastoris* was expected to grow at its maximum specific growth rate (μ_{max}). The error value for the optimal $\mu_{sp}(0.04\ h^{-1})$ run was found to be extremely low ($0.0068\ h^{-1}$) and a consistent response (μ_{est}) for a long duration (> 10 h) was observed for different μ_{sp} values (Figure 4.8A – 4.8D). The PID controller performance (long term stability and tracking error) addressed in this study is observed to be better than the DR based feed-back control strategy reported [144]. At higher μ_{sp} say 0.06 h^{-1}, k_C was set to 4.8 to regulate the PID loop. The disproportion in the ratio between feeding rate and μ_{est} signal was key to the excessive supplementation of methanol over a shorter time frame. However a discontinuous phase of controller regulation at $\mu_{sp} = 0.06\ h^{-1}$ attributed to the proposed $\mu_{offline}$ values. During induction phase, *P. pastoris* experiences higher transcriptional load owing to lower huIFNα2b titer coupled with biomass growth and any attempt to cultivate the organism *P. pastoris* at higher μ_{met}, will result in μ_{est} oscillation with larger amplitude (evident from Figure 4.8D).

4.4.5. Relationship between μ_{est} and $q_{huIFN\alpha2b}$

From Figure 4.10 it could be witnessed that both $q_{huIFN\alpha2b}$ and $Y_{P/X}$ were found to be positively influenced by the increase in μ_{sp}. At different μ_{sp} based control runs with the corresponding methanol feeding rates in *P. pastoris* cultivation enabled the protein

translation machinery to be exposed/subject to various levels of metabolic stress [91]. At higher specific growth rates, protein folding errors and heterogeneity was common in other recombinant proteins expressed in *P. pastoris* [239]. Methanol demand as a carbon and induction source competes for biomass growth as well as protein production. In case of *P. pastoris* cultivation at moderate growth rate (μ_{met}= 0.04 h^{-1}) conditions, the methanol concentration in the medium is expected to be utilized for central metabolism (growth and protein production) and relatively a higher carbon flux is diverted for protein (huIFNα2b) expression. Glycoengineered *P. pastoris* strain employed in this investigation is reported to have μ_{max} at 0.0624 h^{-1} during methanol induction phase. Relatively lowest protein titers resulted in the maximum μ_{sp} that could be addressed due to excessive AOX transcription burden. Specific huIFNα2b secretion rate, $q_{huIFN\alpha2b}$ for $\mu_{sp} \leq 0.04\ h^{-1}$ was found to be greater than 0.4 mg/g.h, which emerges as the highest among different recombinant proteins expressed in glycoengineered *P. pastoris* under AOX promoter [91, 162, 240]. The huIFNα2b titer (1483 mg/L) obtained at $\mu_{sp} = 0.04\ h^{-1}$ is the highest reported value for *P. pastoris* and also for any other yeast expression platforms (Table 4.5) reported in literature [52, 55-57, 61, 65]. Hence, this present study delineates that specific growth rate is a paramount factor establishing superior specific protein productivity. Feedback control from a PID output is a relatively a simpler methodology and robustly controlled the inducer feeding in response to the real-time signal (ΔC) than a preset feed-rate.

Table 4.5 Production of huIFNα2b in batch and fed batch cultivation processes

Strain used	Cultivation process	huIFNα2b titer (mg/L)	Reference
S. cerevisiae	Batch	15	[61]
P. pastoris GS115	Fed-batch[a]	298	[65]
P. pastoris GS115	Batch[b]	200	[55]
P. pastoris KM71H	Fed-batch[a]	600	[56]
P. pastoris GS115	Fed-batch[a]	300	[57]
Y. lipolytica	Fed-batch	425	[52]
P. pastoris SuperMan5 (glycoengineered strain)	Batch[b]	1483	(Present study)

a Includes glycerol batch, glycerol fed-batch and methanol induction phase, b Includes glycerol batch and methanol induction phase

4.4.6. Purification and biological activity of recombinant huIFNα2b

The recombinant huIFNα2b secreted extracellularly in the fermentation broth was existed both in glycosylated and unglycosylated form. Glycosylated huIFNα2b was purified from the unglycosylated huIFNα2b using Con A lectin chromatography, where Con A binds to the terminal mannose of the glycan moiety attached to the glycosylated huIFNα2b. The purification yield of recombinant huIFNα2b was found to be 40 % and was in good agreement with reported literature [56]. The biological activities of huIFNα2b are driven by binding to the receptor complex (IFNAR1 and IFNAR2) and inducing JAK-STAT signaling pathway [207], resulting in the activation of interferon-stimulated genes (ISG's). In this present study, the efficacy of purified huIFNα2b on MCF7 cell line (50 % growth inhibition at concentration of 20 nM or 0.4 μg/mL) was significant based on dosage value. This effect of purified huIFNα2b against T47D breast cancer cell line corroborated with the previously published reports [207-209] and also

the human huIFNα2b produced from *E.coli* and *P. pastoris* X33 resulted in a 50 % growth inhibition at a high concentrations at 5 μg/mL [208, 209]. It could be concluded that the observed antiproliferative effect is a result of both apoptosis and cell cycle arrest [210, 211]. Antiproliferative activity of huIFNα2b was more pronounced in MCF7 than the T47D cell line due to the higher expression levels of interferon receptors (IFNAR1 AND IFNAR2) in MCF7 cell lines [207].

4.5. Conclusion

PAT guided approach for stringent control of CPP (μ) determining the higher huIFNα2b yield was successfully achieved using estimator based on real-time capacitance signal. This study also underscores the necessity of maintaining induction phase specific growth rate at a narrow range (μ = 0.015 to 0.04 h^{-1}) that would strongly influence the expression of huIFNα2b in glycoengineered *P. pastoris*. Design of a simple PID control strategy and setting optimal controller tuning parameter values, efficiently modulated the balance between the methanol uptake by the cells and subsequent channeling of its key metabolic activities (growth and protein production). A long-term stability of μ_{est} signal (≈ 15 h) was achieved for very low and narrow range μ_{sp}, which can be attributed to the robustness of the controller. The feedback control of μ_{met} = 0.04 h^{-1} resulted in an enhanced huIFNα2b (1483 mg/L) titer and specific productivity (q_P=0.457 mg huIFNα2b /g.biomass.h) reported till date. The purified huIFNα2b was biologically active exhibiting antiproliferative activity in human breast cancer cell lines (T47D and MCF7). In an overall observation, this study demonstrates the potential of interpreting the real-time soft sensor information into CPP. In future this repertoire can be transformed to monitor a much more delicate biological system by applying various constraints and using advanced process control strategy. The simple and robust PAT based feed-back

control strategy proposed in this study forms a reliable process control approach for Quality by Design (QbD) as FDA mandate for industrial applications.

Chapter 5

Biocalorimetric monitoring of glycoengineered *P. pastoris* cultivation for the production of recombinant huIFNα2b: A quantitative study based on mixed feeding strategies

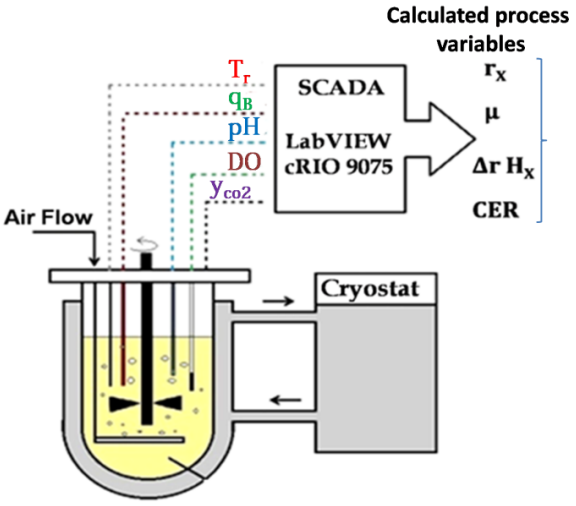

Heat Compensation Biocalorimeter

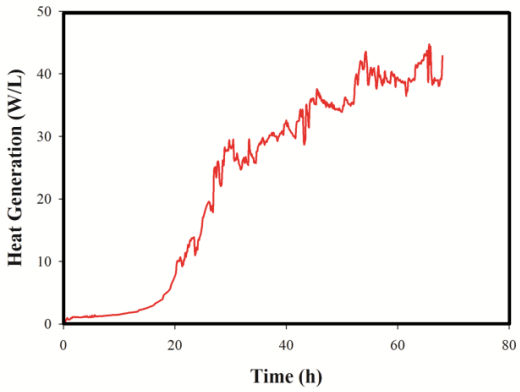

Real-time calorimetric monitoring of glycoenginnered *P. pastoris* cultivation

Chapter 5

Biocalorimetric monitoring of glycoengineered *P. pastoris* cultivation for the production of recombinant huIFN2b: A quantitative study based on mixed feeding strategies

Abstract

Real-time monitoring of glycoengineered *Pichia pastoris* by employing process analytical technology (PAT) tools is vital for gaining deeper insights into the therapeutic protein production process. The present chapter focuses on influence of mixed feed carbon substrates during the induction phase of glycoengineered *P. pastoris* cultivation, for recombinant huIFNα2b (Human Interferon α2b) production, using calorimetric (Biological heat rate, q_B) and respirometric (OUR & CER) measurements. Mixed feeds of carbon substrates (Methanol + Glycerol, Methanol + Sorbitol) at a predetermined 'C-molar ratios' were added during the induction phases. Methanol and sorbitol based mixed feeding approach resulted in an improved huIFNα2b titer of 288 mg/L, predominantly channelling methanol towards an optimal functioning of AOX expression system. A stand-off between biomass yield ($Y_{X/S}$) and biomass heat yield ($Y_{Q/X}$) coefficient, degree of reduction of methanol and its co-substrate (glycerol and sorbitol) determines the fraction of carbon energy channelled towards biomass and protein production, under strict aerobic conditions. Calorespirometric monitoring and assessment of thermal yields enables a reliable prediction of process variables, leading to futuristic efficient PAT based feed rate control.

5.1. Introduction

The protein production process involving *P. pastoris* is carried out in two phases *viz.*, batch growth phase and induction phase. In the batch growth phase sufficient amount of biomass is produced using a carbon source like glycerol. When glycerol is exhausted, the induction phase for protein production is carried out using methanol as a carbon source. However, the use of methanol as a source for inducer is not without its impediments as cells become toxic with high methanol levels and starve when levels are low, making stringent control of methanol supply vital to the success of the process. Again, since methanol is a high degree reductant, it entails heightened heat production during methanol catabolism, which demands robust temperature control; besides methanol also increases cellular oxygen demand. Reports suggests that high levels of protein expression is achieved by reducing the induction temperature to 20°C - 15°C [241, 242] and thus overcoming the problem of high heat generation. But in large scale production, operation at a lower temperatures requires an efficient cooling system which would increase the operating cost of the process.

Mixed feed strategy is an alternative approach for effective heterologous protein expression during the induction phase, as it could enhance both cell growth and protein productivity of interest. Regulated application of alternate carbon sources like glycerol, sorbitol, and mannitol have successfully enhanced protein titers [109, 243]. Glycerol co-feeding at a limited rate, resulted in effective induction for heterologous protein expression [244, 245]. Addition of glycerol should be done with care, as excessive glycerol could repress AOX1 promoter and lead to low specific productivities of recombinant proteins. In contrast to glycerol, sorbitol is a non-repressing carbon source for AOX1 promoter. Hence, sorbitol accumulation during the induction phase will not have any adverse effect on the expression level of protein. Moreover, the use of sorbitol

as co-feed would generate lower amount of biological heat compared with methanol as a sole source due to the of lower enthalpy of combustion for sorbitol (-501.5 kJ/C-mol) in comparison to methanol (-727 kJ/C-mol).

Gaining real-time insights into the cultivation process, leading to the production of a therapeutic protein, is crucial for enhanced comprehension of process parameters. Monitoring and control of the critical process parameters (CPPs) would be useful for achieving process precison and consistent product quality. Moreover, USFDA has made it a prerequisite to employ process analytical technology (PAT) tools for real-time monitoring and control of bioprocesses for the production of therapeutic proteins [112]. Heat energy dissipation during microbial growth is the result of energy released/absorbed due to catabolic and anabolic activities [246]. This heat signal is an vital process variable, enabling real-time insights that reflect changes in metabolism instantaneously. A calorimeter is a time tested, successful and a non-invasive tool, which monitors and quantifies heat signals from bioprocesses. A fermentation calorimeter is a conventional jacketed bioreactor equipped with high sensitive temperature sensors and robust temperature controls [192]. Its versatility as an on-line monitoring tool is evident from its compatibilty in aerobic [247], fermentative [248] and anaerobic [140] systems. Monitoring of heat energy dissipation due to biological activity with key process variables (biomass yield, substrate uptake, oxygen uptake), would enhance the process understanding and serve to increase the efficienct control of bioprocesses. A quantitative relationship between biological heat production rate and oxygen uptake was developed by Cooney and Wang using a calorimeter and exhaust gas analyzer [249], which helped in efficient removal of heat accumulation in large-scale bioreactors. Bench scale calorimeter was successfully employed in fed-batch cultivation of *P. pastoris* for avidin production [250]. Mixed feed substrates were used to study affect of methanol fraction in

mixed feed and heat production rate on different carbon sources viz., methanol, sorbitol, and glycerol [250, 251].

The influence of mixed feed addition of carbon substrates has not been effectively addressed in the few available reports on production of recombinant huIFNα2b in *P. pastoris* [55-57, 65]. This present work provides insights at the metabolic level, on the mixed feeding strategies on huIFNα2b production, by glycoengineered *P. pastoris*, using real-time calorimetric and respirometric (calorespirometry) measurements.

5.2. Materials and Methods

5.2.1. Strain and Media

Recombinant *P. pastoris* SuperMan5 strain expressing huIFNα2b was used in this study [252]. The huIFNα2b expression is under the control of the AOX1 promoter, and it secretes extracellular with the help of the α-factor signal. The construction of this strain has been described earlier in chapter 2 and section 2.2.3 – 2.3.4. The stock culture was maintained at –80˚C, in yeast peptone dextrose (YPD) media containing 20 % (v/v) glycerol. The composition of the various media used in this study are as follow:

- Starter culture medium (YPD), g/L: yeast extract 10; peptone 20; dextrose 20
- Pre-culture medium (YPG), g/L: yeast extract 10; peptone 20; glycerol 20.
- Optimized fermentation medium (BSM) [223]: glycerol 48.84 g/L; K_2SO_4 18.2 g/L; $MgSO_4$ 7.28 g/L; KOH 4.13 g/L; $CaSO_4.2H_2O$ 0.93 g/L; $(NH_4)_2SO_4$ 8.42 g/L; 85 % H_3PO_4 26.7 mL/L; PTM4 salts 4.4 mL/L.
- PTM4 salts composition, g/L: $CuSO_4.5H_2O$ 2; NaI 0.08; $MnSO_4.H_2O$ 3; $Na_2MoO_4.2H_2O$ 0.2; H_3BO_3 0.02; $CaSO_4.2H_2O$ 0.5; $CoCl_2$ 0.5; $ZnCl_2$ 7; $FeSO_4.7H_2O$ 22; biotin 0.2 and 1 mL/L H_2SO_4 98% (v/v).
- Methanol feed solution: methanol 100 % (v/v); PTM4 salts 12 mL/L
- Sorbitol feed solution (for mixed feed): 0.8 C-mol methanol/0.2 C-mol sorbitol
- Glycerol feed solution (for mixed feed): 1.0 C-mol methanol/0.1 C-mol glycerol

5.2.2. Inoculum preparation

The starter culture was prepared by inoculating 5 ml of YPD medium by recombinant *P. pastoris* (SuperMan5 expressing huIFNα2b) from the glycerol stock vial stored at -80˚C. Pre-culture was prepared by inoculating starter culture in 1L baffled Erlenmeyer

flask containing 300 mL of sterile YPG medium. The inoculum was incubated at 30°C and 220 RPM for 24 h to a final OD_{600} of 4 absorbance units.

5.2.3. Real-time monitoring of huIFNα2b production by glycoengineered *P. pastoris* growth using heat PAT tools

5.2.3.1. Biocalorimeter experimental setup and principle

Measurement of heat rate as a result of metabolic activities of *P. pastoris* cultivation was investigated by employing an indigenously developed Heat Compensation Fermentation Calorimeter (Biojenik Engineering, Chennai, India). It comprises a typical jacketed bioreactor (Figure 5.1), enabled with 2 simple modifications; the first being an independent PID controller established to maintain reactor temperature, T_r individually by the power output of 72 ± 0.05 W regulated by the compensation heater. The second is the PID controller installed in the cryostat, to maintain inlet jacket temperature $T_{j,in}$ at its set point, and to insulate the bioprocess system from an external environment. With these modifications the sensitivity of calorimeter was improved to 6.73 mW/L. Biological heat rate measurement range is governed by the power output of the compensation heater and observed to be in the range (6.73 mW/L to 72 ± 0.05 W/L). Estimation of metabolic heat rate is highly susceptible to the process related noises due to various operational/mechanical parameters. For this system, accounting for non-biological heat rate from each source was successfully accomplished by using different calibrations within its operational range. Carefully designed calibration methods for each operating parameter at various ranges were carried out previously to estimate the non-biological heat rates [192], which was later applied to segregate biological heat rate, q_B during high cell density cultivations as shown in Eqn. 5.1. Thus the reliability of the heat rate measurements can be validated by the dynamic energy balance (Eqn. 5.1) developed for

the calorimetric system. Heat rate additions/losses due to different process parameters are enlisted in the following equation (Eqn. 5.1) and the relevant non-biological heat rates can be identified from Table 5.1.

$$q_C - q_J - q_E + q_S - q_A + q_B =, \dot{m}_w C_P \frac{dT_r}{dt} \quad (5.1)$$

'+' or '-' sign correspond to gain or loss. For isothermal operation, $\frac{dT_r}{dt} = 0$.

$$q_{baseline} = q_S - q_J - q_E - q_A \quad (5.2)$$

$$q_B = q_{baseline} - q_C \quad (5.3)$$

Where q_B (biological heat rate, W/L), $q_{baseline}$ (baseline heat rate, W/L), q_C (compensation heat rate, W/L) T_r (reactor temperature), m_w(mass of water, L/s). Heat rate contributions due to nonbiological activities were found to be the environmental heat loss (q_E, W/L), the heat flow from reaction broth to jacket (q_J, W/L), agitation heat rate (q_S, W/L), and aeration heat loss (q_A, W/L).

Table 5.1 Non-biological heat rates due to different reactor operating parameter and their corresponding governing equations

Heat flow terms*	**Measured/Estimated parameters**	**Driving force**	**Governing equation**
$T_r, T_{J,in}, T_{j,out}$	K	NA	NA
q_S	RPM	RPM	$q_S = 2 \times 10^{-8} RPM^{-0.312}$
q_A	LPM	LPM	$q_A = -0.878 * LPM - 0.099$
q_E	$U_E A_E$	$(T_r - T_a)$	$q_E = U_E A_E (T_r - T_a)$
q_J	$U_J A_J$	$(T_r - T_{j,out})$	$q_J = U_j A_j (T_r - T_{j,out})$
q_C	$V_C . I_C$	NA	$q_C = V_C . I_C$

* Heat rate measurement errors are reported elsewhere [192]

All the non biological heat rates were lumped into baseline heat rate (Eqn 5.2), and biological heat rate can be calculated from the difference between power output measured from the compensation heater and baseline heat rate (Eqn 5.3). The schematic representation of the bioclaorimeter experimental setup employed for monitoring the glycoengineered *P. pastoris* cultivation is depicted in Figure 5.1.

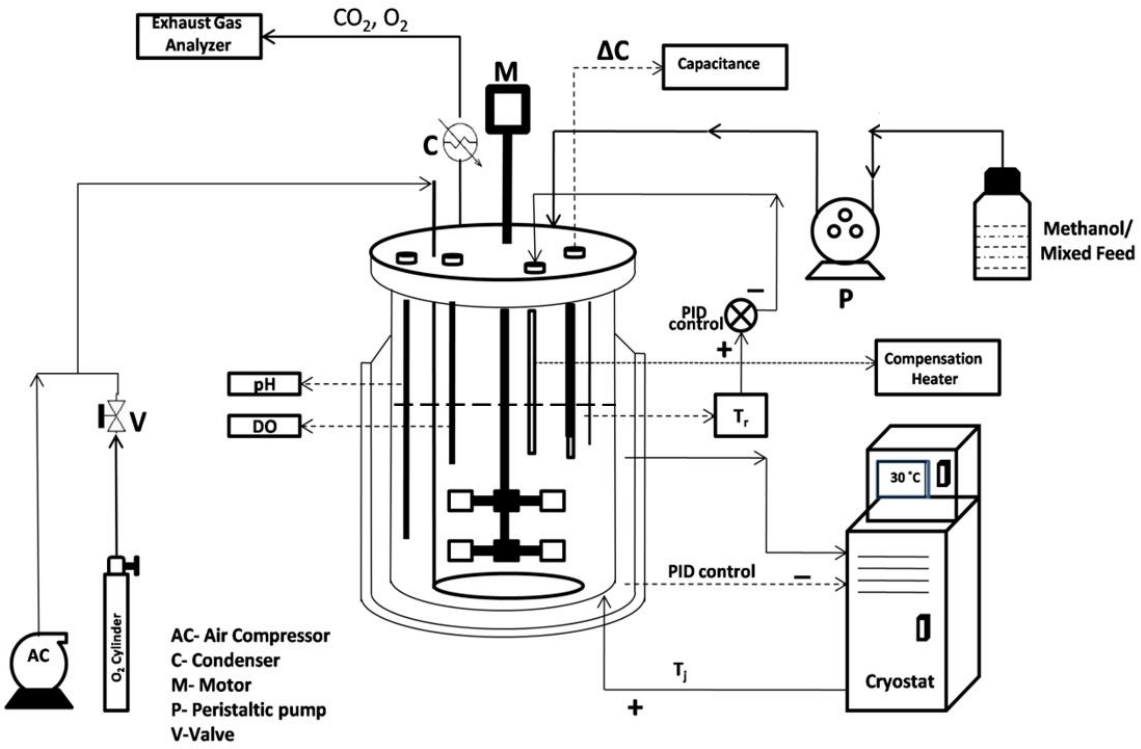

Figure 5.1 Schematic representation of biocalorimetric setup for glyoengineered *P. pastoris* cultivation using methanol as sole carbon source and mixed substrates for huIFNα2b production. ΔC; change in capacitance, T_j; jacket temperature, T_r; temperature of the reaction broth

5.2.3.2. Dielectric Spectroscopy

Dielectric spectroscopy (DS) is a process analytical tool employed to measure Viable cell volume (VCV) on real-time in a fermentation process[144]. The operational principle of DS involves polarization of individual cell membranes by application of electric field where each cell acts as a tiny capacitor [217]. The measured signal (change in capacitance, ΔC or permittivity, ε) is a function of volume fraction of cells with intact

membrane, thereby negating the quantification of dead cells [218]. The instrumentation (Aber Instruments, Aberystwyth, United Kingdom) comprises a capacitance probe with tapering ceramic portion, encircling 2 annular rings. The ceramic portion is easily immersed in the cultivation broth to investigate dielectric properties during the bioprocesses. Futura tool (Aber Instruments, Aberystwyth, United Kingdom), an in-built application records capacitance (0-200 pF/cm), C at dual frequencies (580 kHz and 15.560 MHz). *ΔC* values were obtained by subtracting the measurement frequency (580 kHz) from the signal at the reference frequency (15.580 MHz). DS employed in this study as a complementary PAT tool to measure the VCV of glycoengineered *P. pastoris* and assess the performance of the calorimetry.

5.2.4. Exhaust Gas Analyzer

Gaseous phase O_2 and CO_2 concentration (mole fraction basis) of exit stream air from calorimeter was measured continuously through a laboratory scale exhaust gas analyzer (Ultramat 23, Siemens AG, Berlin andMünich, Germany). Values were logged at 5 s interval in SCADA and mole fraction values obtained from gas analyzer were used to calculate Oxygen uptake rate (OUR) and carbon di-oxide evolution rate (CER) based on Eqn 5.4 and Eqn 5.5 respectively.

$$\text{OUR}, {}^{\text{mg}}/_{\text{L. s}} = \frac{\dot{m}_g}{V_R}\left[y_{O2,in} - y_{O2,out}\left(\frac{y_{inert,in}}{y_{inert,out}}\right)\right] \tag{5.4}$$

$$\text{CER}, {}^{\text{mg}}/_{\text{L. s}} = \frac{\dot{m}_g}{V_R}\left[y_{CO2,out}\left(\frac{y_{inert,in}}{y_{inert,out}}\right) - y_{CO2,in}\right] \tag{5.5}$$

5.2.5. huIFNα2b production

P. pastoris cultivation for the production of huIFNα2b was carried out in a 5 L fermentation calorimeter. *In-situ* sterilization of calorimeter was carried out using distilled water, performed at 121°C and 1 bar pressure for 20 minutes followed by the

aseptic transfer of separately autoclaved optimized BSM medium [223] into the calorimeter. Pre-culture contributing 10 % v/v of V_R was transferred into the calorimeter, such that the total working volume remains 3.0 L. The T_r was set to 29.5°C and pH of the culture was maintained at 5.4 by the addition of ammonia (25 % v/v) solution. Sterile air was supplemented with pure oxygen (total flow maintained at 1 vvm) and the agitation rate was regulated between 400 – 800 RPM in order to ensure 20 % DO level throught the cultivation process. *P. pastoris* cultivation was carried out in three different phases viz, glycerol batch phase, adaptation phase and induction phase. During the batch phase significant amount of biomass was produced using glycerol as carbon source. Upon exhaustion of glycerol which was indicated by spike in DO signal and simultaneous drop in heat signal and off-gas activity, methanol and co-substrates were added in shorter pulses for adaptation of culture (transition phase) to new carbon sources. The transition phase in all the batch runs (methanol, methanol+glycerol and methanol+sorbitol) is characterized by the pulsed feed addition of methanol initially to activate AOX promoter. The adapted cells were further pulsed with methanol/mixed feed to estimate q_s. Single batch run was performed for all these three feed combinations. Samples were collected at regular time intervals during the glycerol growth phase (4 h) and the methanol/mixed feed phase (5 h) for offline analysis.

5.2.6. SCADA application

Data Acquisition (DAQ) hardware (cRIO 9075, National Instruments, Austin, TX, USA) was installed for acquiring real-time process signals such as reactor temperature (T_r), jacket fluid temperatures ($T_{j,in}$ and $T_{j,out}$), power output of a compensation heater (q_B), pH, dissolved oxygen (DO), air flow rate ($\dot{m}_g$), torque (τ), capacitance (ΔC), gaseous phase concentration of O_2, and CO_2 in the exhaust stream at a sampling rate of 5 s. The

SCADA program was developed in-house using graphical programming software (LabVIEW, National Instruments, Austin, TX, USA). The program ensemble included simultaneous data logging, data processing, signal filtering, graphical plots, and control functions

5.2.7. Feed program

A constant feeding strategy has been implemented in the present study, an approach involves simple design and ease of implementation ensuring maintenance of specific growth rate at desired range [253, 254]. Based on the increase in specific substrate uptake rate feed rate was increased in stepwise manner [255, 256]. Feed equation employed in the present study was based on eqn. 5.6.

$$F = \frac{q_s X_O V_O}{S_O} \quad (5.6)$$

Where F is feed rate (mL/h), q_s is specific substrate utilization rate (g.g/h), $X_O$is initial biomass concentration at the start of fed-batch (g/L), $V_o$is initial volume of the reactor broth (L) and $S_O$is initial substrate concentration. Preliminary experiments were carried out by employing different C-molar ratios of mixed feed substrates at shake flask level. The optimal C-mol ratio chosen for reactor study was based on the highest titer value of huIFNα2b obtained from preliminary experiments. The composition of feed solution dealt in this study is as follows:

- Methanol feed solution: methanol 100 % (v/v) and PTM4 salts (12 mL) dissolved in 1 L of methanol
- Sorbitol feed solution (for mixed feed): 0.8 C-mol methanol/0.2 C-mol sorbitol and PTM4 salts (12 mL) dissolved in 1 L of feed solution.
- Glycerol feed solution (for mixed feed): 1.0 C-mol methanol/0.1 C-mol glycerol and PTM4 salts (12 mL) dissolved in 1 L of feed solution.

Mixed feeds of different C-molar ratios were tightly regulated by a variable speed precision pump (Watson Marlow 120U, Falmouth, Cornwall, U.K).The pump was pre-calibrated for different flow rates prior to the reactor operation. Graphical user interface for the feed program was developed in the LabVIEW platform and deployed for the proposed bioprocess strategy.

5.2.8. Offline Analysis

Cell growth was measured for the collected samples by optical density measurements 600 nm (OD_{600}) using UV-visible spectrophotometer (GE Healthcare, UK). Biomass concentration (g/L) was estimated by transferring 1 mL of the cultivation broth into a pre-weighed 1.5 mL tubes and centrifuging them at 8000 *g* for 10 min at 4°C. The supernatant was separated, and stored at –20°C for offline analysis of glycerol, methanol, sorbitol, and huIFNα2b. The pellet was washed twice with distilled water to remove any salts, re-centrifuged and dried at 80°C overnight for DCW estimation. Glycerol, sorbitol, and methanol concentrations in the collected samples (supernatant) were determined using HPLC by ion exchange chromatography (Rezex RHM- monosaccharide H+ Column, Phenomenex Inc, California, USA). In HPLC, 5 mM sulfuric acid was used as mobile phase with an isocratic flow of 0.6 mL/min, and oven temperature was maintained at 50°C. Determination of huIFNα2b concentration in the collected samples was performed by Enzyme linked immunosorbent assay (ELISA) analysis using human IFNα2b ELISA kit (Mabtech AB, Sweden).

Real-time dynamic plots, continuous capacitance (ΔC) and OUR-CER (every 5 s) values, real-time biological heat rate(q_B) and offline values (biomass, substrate concentration, huIFNα2b titer) from collected samples at regular intervals were used in dynamic plots.

Calculation

The growth rate of cells in exponential phase is defined by a mathematical relation as represented in eqn. 5.7. The term $\left(\frac{dX}{dt}\right)$ represents the fractional increase in cell amount over time dt at which the fractional increase was accomplished.

Specific growth rate can be interpreted as function of biomass formed per unit time.

$$\mu = \frac{1}{X}\frac{dX}{dt}\ (h^{-1}) \tag{5.7}$$

Volumetric productivity is defined as yield of product per unit time and is expressed as in eqn. 5.8

$$r_{huIFN\alpha2b} = \frac{d(huIFN\alpha2b)}{dt}\left({}^{mg}/_{L.h}\right) \tag{5.8}$$

Biomass yield coefficient is defined as amount of biomass produced per amount of substrate consumed and yield coefficient during glycerol growth phase and induction phase are represented in eqn. 5.9 and 5.10 respectively [257].

$$Y_{X/gly} = \frac{\Delta X}{\Delta gly}\left(\frac{\text{g.biomass formed}}{\text{g.glycerol utilized}}\right) \tag{5.9}$$

$$Y_{X/IP} = \frac{\Delta X}{\Delta IP}\left(\frac{\text{g.biomass formed}}{\text{g.IP substrate utilized}}\right) \tag{5.10}$$

The heat yield coefficient due to biomass growth could be determined from the slope of linear plot between cumulative metabolic heat production and the biomass concentration [258] as given in eqn. 5.11.

$$Y_{Q/X} = \frac{\Delta Q}{\Delta X}\left(\frac{\text{heat yield (kJ)}}{\text{g.biomass formed}}\right) \tag{5.11}$$

The oxycalorific coefficient can be determined from the slope of linear plot between cumulative metabolic heat production and oxygen uptake as given in eqn. 5.12 [258] .

$$Y_{Q/O_2} = \frac{\Delta Q}{\Delta O_2}\left(\frac{\text{heat yield (kJ)}}{\text{moles of } O_2 \text{ utilized}}\right) \tag{5.12}$$

5.3. Results

5.3.1. Assessment of mixed feeding strategies and their impact on huIFNα2b productivity.

All the reactor runs consistently generated 36 ± 2 g/L of biomass at the end of the glycerol phase, yielding 0.85 g.DCW/g.glycerol and lasted till 26 – 28 h. Substrate consumption was predominantly diverted towards biomass production, as no appreciable amount of byproducts except CO_2, was synthesized owing to the respiratory metabolism of *P. pastoris* [259]. Exhaustion of glycerol was characterized by an immediate spike in DO and a simultaneous slump in the biological heat rate, q_B and respirometric profiles (CER/OUR signals). Before proceeding with the continuous constant feed, few shorter pulses of methanol (5 g), followed by its combination with co-substrates were fed in all the fed-batch runs viz., methanol, methanol+glycerol and methanol+sorbitol. Methanol addition would specifically activate the AOX transcriptional elements of the *P. pastoris* system and the co-substrates (glycerol and sorbitol) would support the cell growth. Under fully adapted condition i.e. significant increase in biomass after providing repeated pulses of methanol and co-substrates, the constant continuous feed was initiated (~30 h). The q_S obtained for different feed combinations (Table 5.2) were employed to determine the constant feeding rates. The initial feed rates were computed (Eqn. 5.6) to be 8 mL/h for methanol, 10 mL/h for methanol + glycerol and 12 mL/h for methanol + sorbitol respectively. The feed rates were gradually increased in a stepwise fashion, as shown in Figure(s) 5.2A, 5.2B and 5.2C to meet nutritional requirements for increasing volumetric biomass concentration. The decisions on the increments were undertaken by pausing the feed rate for a definite time interval to assess the metabolic robustness in assimilating the supplemented carbon in the given time frame. Productivity obtained for each run was computed (Eqn. 5.8) and shown in table 5.2. One of the advantages with

mixed feed is it shortens induction phase duration and enhancement in productivity is observed for mixed feed. Increase in the feed rates was well depicted by the concomitant rise in OUR and CER signals as shown in Figure 5.2. At the end of the 60 h cultivation runs, far lower accumulation of methanol and its co-substrates were detected in comparison to the induction phases.

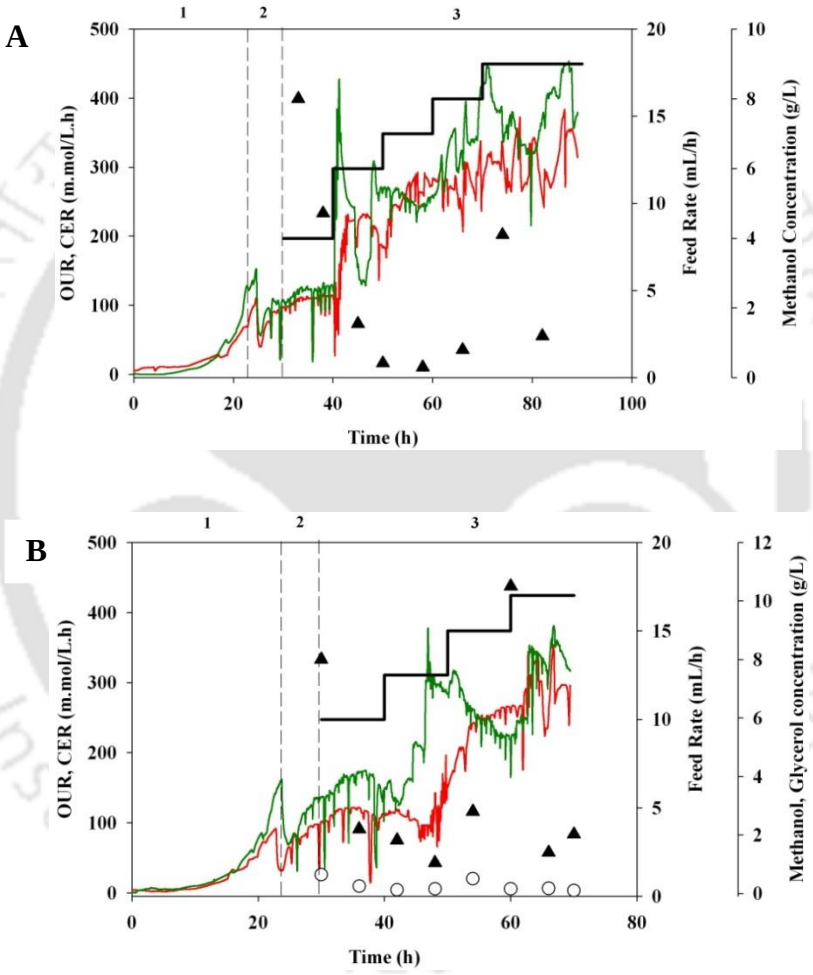

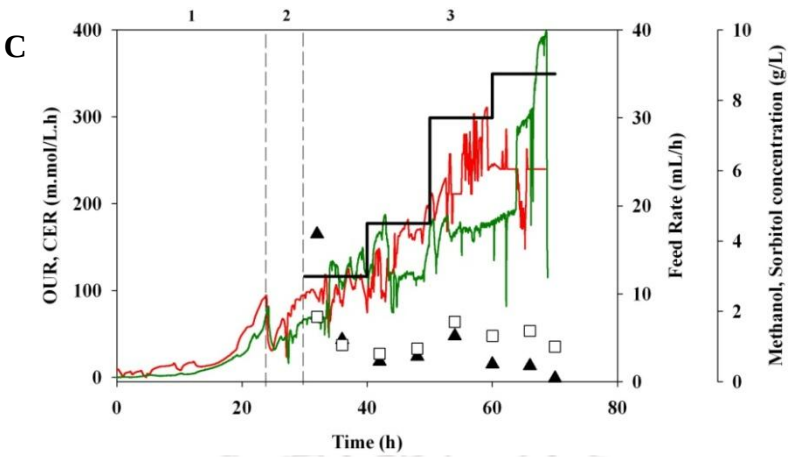

Figure 5.2 Dynamic plots representing OUR, CER and feed rate profileduring different feeding strategies.A. Methanol, B. Methanol + Glycerol, C. Methanol + Sorbitol were continuously fed at their respective flow rates (Black Continuous) and the residual concentrations of substrates were measured and represented: Methanol (Filled upright triangle), Glycerol (Open circles) and Sorbitol (Open squares). Comparison plot representing OUR (Red Continuous) and CER (Green Continuous) signals in concordance with the feed rates. 1: Glycerol growth phase, 2: Pulsed methanol feed during adaptation/transition phase and 3: continuous methanol feed under fully adapted condition (significant increase in biomass)

5.3.2. Calorespirometry and dielectric spectroscopy based monitoring of *P. pastoris* cultivation.

Different phases segregated for the growth (glycerol phase) and huIFNα2b production (methanol induction phase) exhibit characteristic growth kinetic parameters as listed in Table 5.2. The specific growth rate was calculated from dry cell weight measurements and the glycerol phase has achieved a maximum of 0.23 h^{-1}. In the induction phase, the μ_{IP} was observed to be far lesser in the range of 0.024 – 0.066 $h^{-1}$with the average μ_{IP} being 0.024 h^{-1} for methanol as sole carbon source, 0.033 h^{-1} for methanol + glycerol and 0.066 h^{-1} for methanol + sorbitol. Batch growth phase is driven by utilization of glycerol as carbon source, which shows repressing effects on AOX promoter. Hence majority of carbon source is channeled towards biomass formation which was evident from higher biomass yields ($Y_{X/Gly}$). The comparative dynamic plot for biological heat rate, DCW, capacitance signal and huIFNα2b titer, as shown (ure 5.3A, 5.3B and 5.3C) and also

depicts the growth characteristics of *P. pastoris* at glycerol and induction phase. In all the dynamic profiles, both the q_B and ΔC signal concur well with the offline DCW values and could be seen for all the mixed feeding strategies and methanol as sole carbon substrate. The relationship between the capacitance signal and DCW were estimated as an average value for growth phase as Biomass = 3.112 * ΔC and other correlation coefficients measured during the induction phases were found to be 5.548 * ΔC for methanol as sole carbon source, 4.492 * ΔC for methanol + glycerol batch and 6.28 *ΔC for methanol + sorbitol batch. The slope for induction phase is observed to be significantly higher than growth phase in all batches, which could be attributed to glycerol as suitable anabolic substrate for biomass production and methanol as preferred substrate for synthesizing energy intermediates and protein production [260]. During the lag phase of glycerol growth phase, the inoculum adapts to the cultivation medium conditions and requires time for the generation of sufficient biomass and thereby the real-time capacitance signal. Hence, the capacitance values during this phase do not corroborate well with the offline biomass.

The rising profile of the dynamic plots of heat rate and capacitance signals was lowered with the depletion of glycerol (Figure 5.3A, 5.3B and 5.3C).Induction phase was characterized by the continuous feeding of methanol which yielded final biomass titers of 100.16, 102.56 and 143.28 g/L respectively for different feed combinations as mentioned in Table 5.2. Mixed feeding regime (from ~30 h, Figure 5.3A, 5.3B and 5.3C) is characterized by gradual increase in ΔC and q_B signal and is in concurrence with *P. pastoris* growth. The huIFNα2b titers were observed to be 201.04 mg/L (methanol), 166.71 mg/L (methanol+glycerol) and 287.91 mg/L (methanol+sorbitol) corresponding to their feed combinations. For methanol as sole carbon source organism entered

stationary phase after 70 hours of induction and remaining two batches were terminated at 60 hours of induction due to carrying capacity of bioreactor.

Table 5.2 Growth kinetic, huIFNα2b concentration and heat yield parameters obtained for 3 distinct feeding combinations of methanol

Feed	DCW (g/L)	μ_{gly} (h^{-1})[c]	μ_{IP} (h^{-1})[d]	q_s (g/g.h)	$Y_{X/gly}$ (g/g)	$Y_{X/IP}$ (g/g)	$Y_{Q/X}$ (kJ/g)	Y_{Q/O_2} (kJ/mol.)	RQ	huIFNα2b (mg/L)	r_p g/L.h
Methanol	37.6[a] 100.16[b]	0.23	0.0204	0.096	0.806	0.09	-11.67[e] -20.94[f]	-479[e] -830.1[f]	0.97	201.08	2.18
Methanol + Glycerol (1.0 C-mole/0.1 C-mole)	38.58[a] 102.56[b]	0.227	0.033	0.102	0.837	0.14	-12.31[e] -14.11[f]	-471[e] -794.25[f]	1.01	166.17	2.37
Methanol + Sorbitol (0.8 C-mole/0.2 C-mole)	37.12[a] 143.28[b]	0.227	0.066	0.15	0.806	0.12	-12.22[e] -9.04[f]	-488.8[e] -675.9[f]	0.72	287.91	4.23

a. Final dry cell weight achieved during batch phase
b. Final dry cell weight achieved during induction phase
c. Average specific growth rate in growth (glycerol) phase
d. Average specific growth rate in induction phase
e. Heat yield coefficient of biomass formation and oxygen consumption during batch growth phase
f. Heat yield coefficient of biomass formation and oxygen consumption induction phase

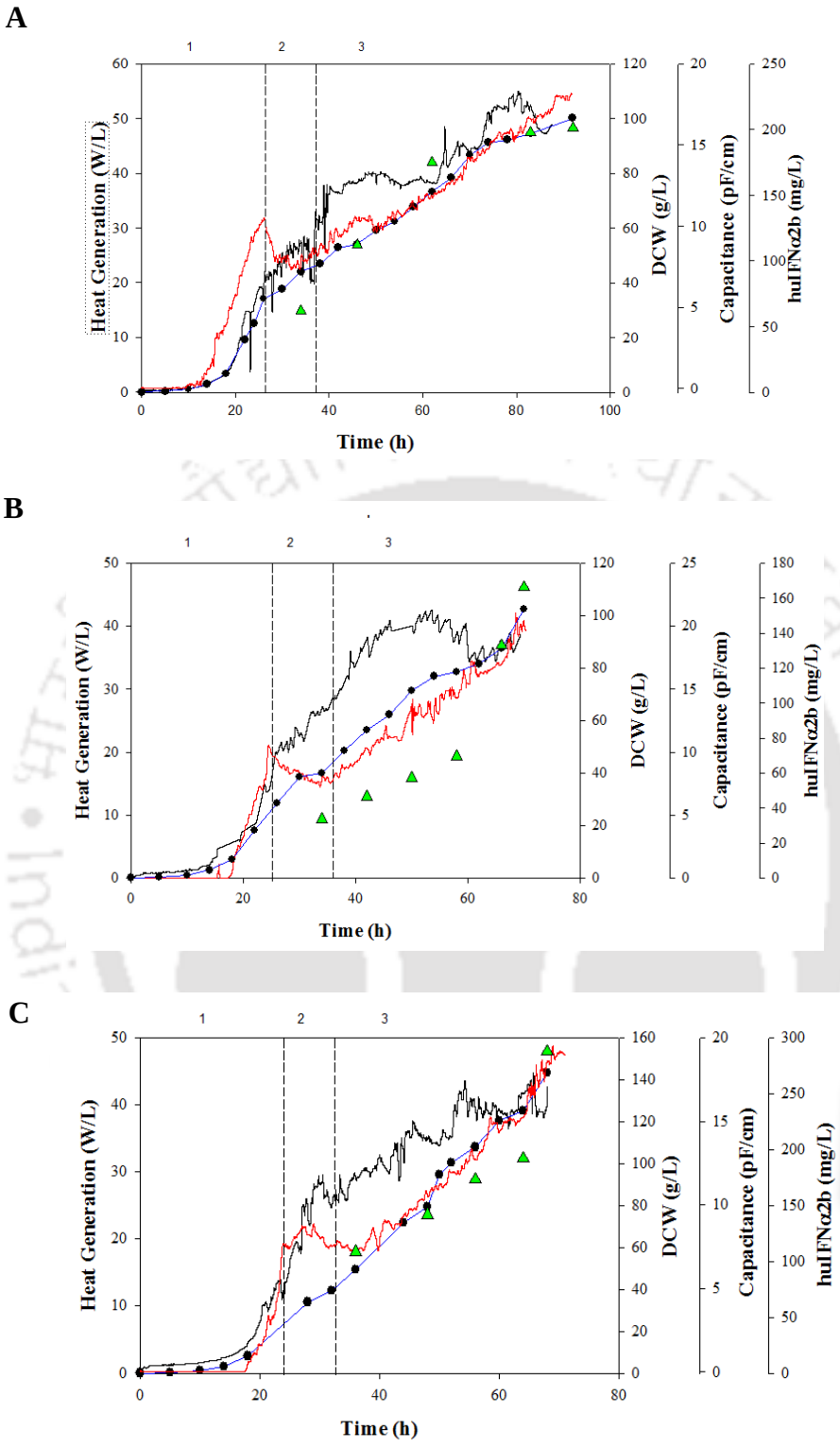

Figure 5.3 Dynamic plot representing the production of huIFNα2b (Green upright triangles) by glycoengineered *P. pastoris* using methanol as sole carbon source and co-feeding sorbitol and glycerol with methanol. A). Methanol, B). Methanol + Glycerol, C. Methanol + Sorbitol. Correlation between heat rate signal (Continuous black), capacitance signal, ΔC (Continuous red) and DCW (Filled circles) were represented in the same plot.

5.3.3. Stoichiometric heat yield coefficient measurement

Heat energy synthesized as a result of the standoff between substrate uptake and its channeling towards various metabolic reactions serves to be an intrinsic characteristic of the organism, representing the coupling between catabolic and anabolic reactions. In all black box microbial stoichiometries, real-time heat rate measurement offered an advantage in addition to alternate process analytical tools for the prediction of different yield coefficients and was dealt with using various calorespirometry based approaches [134]. The ratio of the cumulative biological heat generated (Q) to the amount of biomass production ($Y_{Q/X}$) and the amount of O_2 utilization (Y_{Q/O_2}) established the enthalpic yield of the respective process. Real-time estimation of $Y_{Q/X}$ was made possible by deciphering online biomass signals from dielectric spectroscopy and biological heat rate from calorimetry (Figure 5.4A and 5.4B). The heat yield coefficient, $Y_{Q/X}$ during the glycerol batch phase was found to be 11 kJ/g.biomass and remained consistent in all the runs ($R^2 > 0.92$) and similar values for *P. pastoris* cultivation were reported [134, 192]. The estimated $Y_{Q/X}$ values during induction phases (Figure 5.4) were highly dependent upon the type of inducer and co-substrates fed into the system. Hence, the estimated heat yield values ($Y_{Q/X}$) were found to differ significantly for different type of inducer and co-substrates for instance 20.94 kJ/g.biomass for sole methanol, 9.04 kJ/g.biomass for methanol + sorbitol and 14.11 kJ/g.biomass for methanol + glycerol. The ratio of cumulative biological heat energy generated for the moles of oxygen consumed enumerates the type of metabolism (Aerobic, Anaerobic and Fermentative metabolism) during *P. pastoris* growth. The oxycalorific coefficient value is found to be in the range (460kJ/mol.O_2) for strictly aerobic metabolism. In this present study, experimentally determined oxycalorific coefficient during glycerol batch phases ranged between 471 –

488.9 kJ/mol.O_2, which confirmed the aerobic metabolism of the *P. pastoris* associated with absence of significant byproduct formation. Real-time heat rate signal could be used to decipher successfully the simulated profile of OUR signal [261]. The influence of methanol and its co-substrates resulted in a significant deviation among the experimental group and are dealt with in the discussion section.

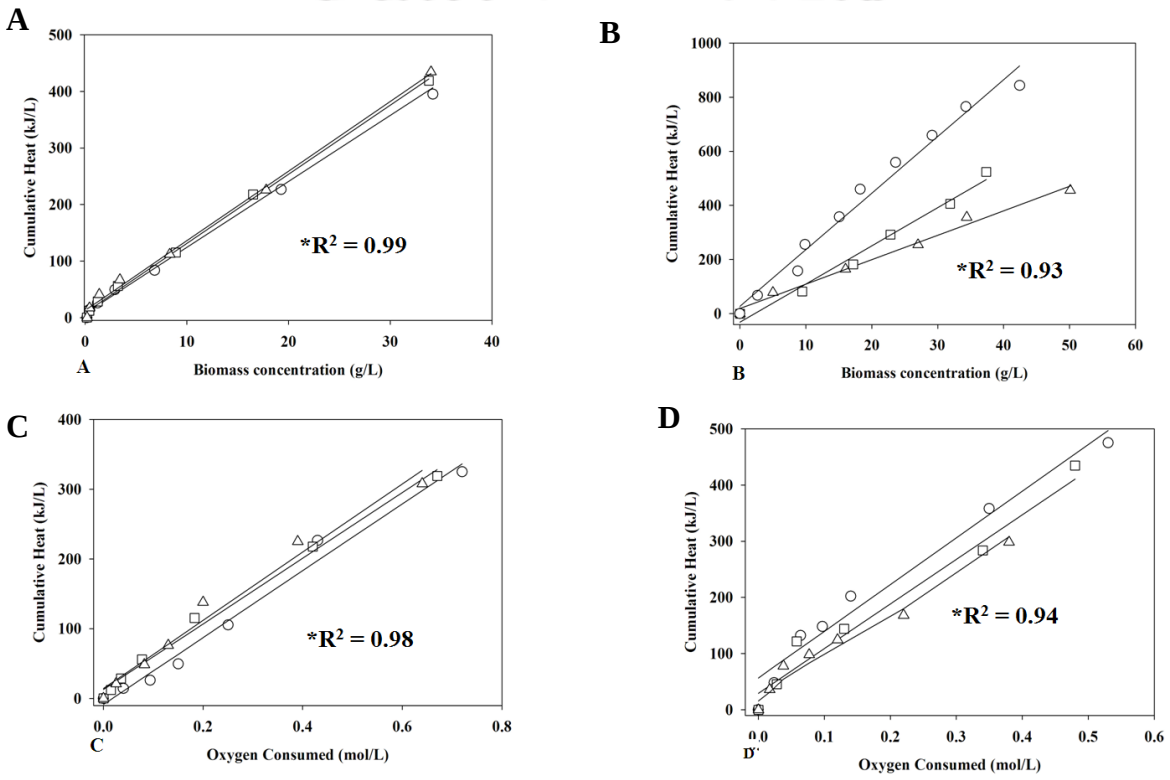

Figure 5.4 Heat yield coefficients of biomass formation and O_2 utilization during glycerol (A and C) and induction (B and D) phases respectively of different co-substrates and methanol as sole carbon source. Methanol (Open circles), Methanol + Glycerol (Open squares) and Methanol + Sorbitol (Open upright triangles).

5.4. Discussion

5.4.1. Influence of constant feed rates exhibiting different proportions of mixed substrates.

Stepwise increment in the feeding of limiting substrates has been attempted in both *E.coli*[262] and *P. pastoris* [255] cultivation for the improved production of recombinant protein. C.Dietzsch *et.al* fed methanol at a constant flow rate, followed by a stepwise increment to replenish the nutritional requirements i.e. maximum methanol utilization rates at different stages of growth by inducing AOX promoter system. Our study successfully elucidated the advantages of methanol feeding with other co-substrates against methanol as the sole inducer. Preliminary investigation on the pulsed feeding strategy at different dosage rates suggested that glycoengineered *P. pastoris* strain is highly unlikely to influence the functional AOX machinery [260]. But continuous feeding of methanol/other limiting substrates has proven to influence the AOX expression system in regulating growth and other metabolic activities. After the glycerol growth phase, *P. pastoris* was initially adapted with methanol, and subsequently the pulsed addition of methanol with co-substrates (glycerol and sorbitol). All the three reactor runs were initiated with the constant feed rate as mentioned earlier, and reached its maximum at 35 mL/h for methanol + sorbitol run, but for other combinations, the feed rate at the end was significantly low (Figure 5.2). Sorbitol addition with methanol turned out to be advantageous for the induced expression of AOX promoter. Sorbitol does not repress the AOX induction and serves as energy supplier for cell growth, co-feeding of sorbitol with methanol could ease the metabolic load of *P.pastoris*. In case of feeding methanol as sole carbon source, central metabolic pathway such as glycolysis and TCA cycle are not essential as the 100 % energy requirement (NADH, ATP) for protein/cell synthesis are generated from formaldehyde dissimilation pathway allied with oxidative

phosphorylation [263, 264]. During mixed feeding (methanol and sorbitol), sorbitol allows optimal carbon flux of methanol channeled towards AOX transcription activities, while it contributes relatively lesser for energy metabolism, but supports protein/cell synthesis [264]. Carbon flux mapping of central metabolic pathway of *P. pastoris* showed no appreciable variation either by mixed feed containing methanol and glycerol or with sole glycerol feeding [200]. This infers that methanol do contribute in the building of biomass, as the significant carbon flux gets assimilated in the central metabolic pathway amidst dissimilated directly to CO_2 evolution. Although methanol plays a crucial role in the AOX transcription, but in the induction phase co-utilization of sorbitol was favored. This is evident from the residual concentrations of individual methanol and sorbitol in the culture broth (Figure 5.2). The final flow rate for methanol + glycerol combination was observed to be 17 mL/h, which is about half compared to methanol + sorbitol mixed feed strategy; the latter being attributed to menthol repression by glycerol. This could also be understood from the fact that residual methanol concentrations at different points were always higher than the glycerol concentration (Figure 5.2B).

It is interesting that the affinity for glycerol by *P. pastoris* found to be high, even after the cells were wholly adapted by methanol induction. Being the terminal electron acceptor, oxygen transfer plays a vital role in the assimilation of the carbon sources. Therefore as the feed rates increased, the mole fraction of pure oxygen (supplementation) in the inlet air was also increased proportionally, by carefully controlling the pure O_2 flow rate in order to maintain the desirable$y_{O_2,in}$. Key process indicators such as growth rate, DO, increase in q_B, ΔC and OUR/CER signals with respect to growth showed a balanced growth under this feeding regime (phase 3 in Figure 5.2) and as residual methanol levels were far below their toxic limits. The sharp increase in the OUR and

CER in methanol (Figure 5.2A) and methanol+glycerol (Figure 5.2B) experimental runs could be attributed to high oxygen consumption due to higher methanol fraction (1 C-mole) in the feed. Conversely inthe methanol+sorbitol feeding, it was observed that increase in OUR/CER signals were not proportionate with the utilized substrate i.e. sorbitol, owing to its lower degree of reduction and its co-feeding could reduce oxidation flux in the peroxisome [265].

Dynamic plot representing concurrence of Biological heat rate q_B, Capacitance, DCW and huIFNα2b plots.

The present investigation discusses the fidelity of the process analyzers such as Calorimetry, Dielectric spectroscopy and exhaust gas analyzer in monitoring *P. pastoris* cultivation for the synthesis of huIFNα2b.Table 5.2 illustrates the final DCW, huIFNα2b titer, specific growth rates and biomass yields calculated during growth and induction phases. Induction phase μ_{IP} , say 0.066 h^{-1} obtained for methanol and sorbitol combination serves to be the highest so far achieved for any glycoengineered strain (287.91 mg/L of final huIFNα2b titer). A flow throughput as high as 35 mL/h was recorded at the end of the induction phase, however only a low fraction of inducer combination was diverted to the growth [$Y_{X/S}$ = 0.12 g.biomass/g. (methanol+sorbitol)]. Sorbitol was redirected towards growth related and major housekeeping activities, thus channeling a higher proportion of methanol for the superior expression of AOX genes [250]. This phenomenon has attributed to the higher productivity of huIFNα2b (4.23 mg/L.h) among other feed combinations (Table 5.2). Also co-feeding with sorbitol reduces oxygen demand without uncompromising the product titers [265] and sorbitol accumulation is harmless to organism and boosts protein titers as it will not interfere with methanol in AOX transcription[266]. The biomass yield, ($Y_{X/S}$) value calculated for other co-substrates were found to be 0.09 g.biomass/g.methanol and 0.137

g.biomass/g.(methanol+glycerol) respectively. Higher yield value obtained for methanol + glycerol proves that the methanol adapted *P. pastoris* reactivates its repressor characteristics if glycerol is included as co-substrate along with methanol as mixed feed. Also, the regulation of feed rates was observed to be lower than the methanol + sorbitol mixed feed, but the co-utilization of both the substrates were evident from the residual substrate concentration (Figure 5.2B). Throughout the reactor run, the affinity of *P. pastoris* towards glycerol was significantly higher than methanol. Therefore, under methanol + glycerol mixed feed strategy, comparatively less methanol was available for the effective functioning of AOX machinery. This eventually resulted in the lowest huIFNα2b titer of 166.17 mg/L for methanol + glycerol mixed feed. Real-time heat rate signal couldn't be perfectly correlated with the product profile or even biomass profile to an extent. Since heat rate fingerprints all the metabolic activities of the process viz, biomass formation, product formation and cell maintenance. As a result cumulative heat profile correlates well with biomass formation, oxygen consumption etc. Subsequent discussions on heat yields will interpret the metabolic bottlenecks with respect to various substrates.

Calorimetric insight of the influence of mixed feed and methanol as sole substrate on huIFNα2b production.

Application of complimentary PAT tools such as exhaust gas analyzer, the calorimetry along with offline measurements allowed the prediction of thermochemical energetic yields i.e. heat yield coefficient due to O_2 utilization, Y_{Q/O_2} and biomass generation, $Y_{Q/X}$.

Heat energy evolution as a result of various metabolic reactions regulates a balanced stoichiometry between substrate uptake and product synthesis. The heat energy released per unit of biomass ($Y_{Q/X}$) under balanced growth condition remains constant. Therefore the heat generated by an individual cell is highly specific and subjective to the type of

metabolism it undergoes [246]. The ratio of the quantum of heat generated and moles of O_2 utilized (Y_{Q/O_2}) were proven consistent for an organism with respect to its metabolism. Cooney *et.al* (2000) and later Cordier *et.al* (1987) developed a relationship between the heat generation and OUR, and suggested a proportionality constant (460 kJ/mol.O_2) under aerobic conditions [249, 267]. While heat evolution is dependent upon the degree of reduction of a substrate involved, but in most cases it remains close to oxycalorific coefficient of 356 to 565 kJ/mol.O_2. In our study, an apparent reproducibility was observed in oxycalorific values, especially in the glycerol phase, which resulted in an average of 475 kJ/mol.O_2, substantiating the aerobic growth profile of *P. pastoris* (Table 5.2). Although in the methanol phase, the variation in oxycalorific coefficients was significant; its representation was based on the complexity of the mixed feeding with different co-substrates. During induction phase, feeding methanol as sole carbon source was estimated to dissipate higher enthalpy of O_2 utilization (830 kJ/mol of O_2). This could be attributed to the highest degree of reduction (8 e^- equivalents) of the substrate (methanol) supplied; subsequently validated from the pre-determined combustion enthalpy of methanol ($Y_{Q/S}$) in the aqueous solution, which was also estimated to be 727 kJ/C.mol [250]. Oxygen regulated thermo-chemical yields for other mixed feed conditions i.e. methanol feeding with co-substrates such as glycerol and sorbitol yielded 794.25 kJ/mol. of O_2 and 675.9 kJ/mol. of O_2 respectively. The relatively lower repression by glycerol and the lower combustion enthalpy value of sorbitol (-501.5 kJ/C.mol.) could be the reasons for the low heat yield values. During the induction phase, a similar trend (Figure 5.3) was observed in the estimated heat yield due to biomass formation ($Y_{Q/X}$).Though heat yield during the glycerol phase was more consistent, it was significantly lower than the heat yield obtained during biomass

formation (Table 5.2). From a thermodynamic perspective, the formation of biomass allows for lower entropy change, but the irreversible nature of highly ordered cell organelle synthesis, allow their cells surfaces to export the excess chemical entropy generated. Thus it can be concluded that any life form synthesizing biomass is always associated with heat energy, which is ubiquitously applicable to all living organisms. It was previously established that an inverse relationship exists between $Y_{Q/X}$ and $Y_{X/S}$ of an organism. Lower thermochemical biomass yields in the later induction phases were always higher than heat yields estimated during growth phases (Table 5.2). Respiratory quotient estimated during the induction phase of both mixed feed and sole methanol induced reactor runs were estimated to be closer to one; thus illustrating the obligate nature of the respiratory metabolism exhibited by *P. pastoris* and it simultaneously proves the availability of required oxygen supply throughout the cultivation. For aerobic cultures, the advantages of calculating heat yields from real-time calorimetry and exhaust gas analyzer offer a robust platform to predict the real-time biomass concentration. $Y_{Q/X}$ was also employed as a reliable parameter in the feed rate expression intended to govern exponential feeding strategy in various biocalorimetric approaches.

5.5. Conclusion

The calorimetric investigation of glycoengineered *P. pastoris* for huIFNα2b production with complimentary PAT tools allowed us to gain metabolic insight on assimilation of substrate and co-substrates under mixed feed conditions. This is the first-of-its-kind report to enumerate the metabolic shifts encountered in *P. pastoris* cultivation with respect to calorimetric perspective supported by the complimentary PAT tool measurements. Metabolic fingerprinting by calorespirometry method corroborates well with the off-line DCW measurements and dielectric spectroscopy (ΔC signal). Reduction in the estimated biomass heat yield coefficients under aerobic conditions are inverse to the biomass yields and highly dependent upon the degree of reduction of the mixed substrate. This study addresses the optimal C-molar ratio of the mixed feed concordant with a fair trade-off between biomass yield coefficient (0.12 g.biomass/(g. of methanol + sorbitol) and specific growth rate (0.066 h^{-1}) of *P. pastoris*. The research outcome of this study is highly crucial for careful selection of substrates and co-substrates for mixed feed during induction phase of *P. pastoris* cultivation at industrial /non -laboratory scale. The complimentary PAT tools approach improvise the scope for checking the inconsistencies in the off-line measurements and implement data reconciliation strategy for reliable monitoring in near future.

Chapter 6

Conclusion and Future Perspective

Chapter 6

Conclusions and Future Perspective

N-glycosylated huIFNα2b was successfully expressed with human type $Man_5GlcNAc_2$ glycan with greater homogeneity by the application of glycoengineering strategy and the glycoengineered SuperMan5 *P. pastoris* strain. The purified glycosylated huIFNα2b was biologically active, inhibiting the viral replication of HCV and HEV at 85 % and 66 %, respectively. Pharmacokinetic studies carried out in Wistar rats revealed 1.3 fold increase in plasma half-life for glycosylated huIFNα2b compared to commercial standard huIFNα2b produced by *E. coli*. DoE (PBD, RSM-BBD) and artificial intelligence based optimization technique (ANN-GA) were employed for optimization studies to maximize the production of huIFNα2b in recombinant glycoengineered *P. pastoris*. ANN-GA model proved to be more reliable compared to RSM-BBD model. Bioreactor study with optimized basal salt medium resulted in an enhanced huIFNα2b titer of 436 mg/L and was found to be the highest reported value in batch cultivation till date. PAT guided approach for the stringent control of CPP (μ_{met}) determining the higher huIFNα2b yield was successfully achieved using μ estimator based on the real-time capacitance (ΔC) signal. A long-term stability of μ_{est} signal (≈ 15 h) was achieved for very low and narrow range μ_{sp}, which attributed to the robustness of the controller. The feedback control of μ_{met}= 0.04 h^{-1} resulted in an enhanced huIFNα2b (1483 mg/L) titer and specific productivity (q_P=0.457 mg huIFNα2b/g.biomass.h) reported for the huIFNα2b production till date. Also real-time monitoring of heat production rate based on measurements recorded from heat compensation calorimeter for the production of huIFNα2b in glycoengineered *P. pastoris* strain was accomplished successfully.

Calorimetric investigation of comparative mixed feed stragey strategies concluded that methanol and sorbitol mixed feeding as more efficient with 57 % reduction in heat yield and 2 fold increase in volumetric productivity of huIFNα2b.

Further N-glycoengineering approach for the development of completely humanized huIFNα2b through the *P. pastoris* platform would help in improving the patient's quality of life by overcoming all the adverse side effects. There is a huge scope for continuous bioprocessing of the production of huIFNα2b that involves the integration of a bioreactor system with a cell recycle and chromatography system for the continuous capture of the produced huIFNα2b. The continuous production system was already successfully in the production of the monoclonal antibody and human recombinant enzyme. The outcome of this thesis suggests that the integration of PAT enabled continuous production of recombinant huIFNα2b is a holistic approach for enhanced process understanding ensuring consistent desired product quality.

Bibliography

Bibliography

[1] A. Isaacs, J. Lindenmann, Virus interference. I. The interferon, Proc. R. Soc. Lond., B, Biol. Sci. 147(927) (1957) 258-267.
[2] Y. Nagano, Inhibition de l'infection vaccinale par un facteur liquide dans le tissu infect'par le virus homologue, CR Soc. Biol. 152 (1958) 1627-1629.
[3] J. Lindenmann, From interference to interferon: a brief historical introduction, Phil. Trans. R. Soc. Lond. B 299(1094) (1982) 3-6.
[4] J. Vilcek, G. Sen, Interferons and other cytokines. In “Fields Virology”(BN Fields, DM Knipe, and PM Howley, Eds.), Lippincott-Raven Publishers, Philadelphia, 1996.
[5] N. Ank, H. West, S.R. Paludan, IFN-λ: novel antiviral cytokines, J. Interferon Cytokine Res. 26(6) (2006) 373-379.
[6] G. Uzé, D. Monneron, IL-28 and IL-29: newcomers to the interferon family, Biochimie 89(6-7) (2007) 729-734.
[7] K. Onoguchi, M. Yoneyama, A. Takemura, S. Akira, T. Taniguchi, H. Namiki, T. Fujita, Viral infections activate types I and III interferon genes through a common mechanism, J. Biol. Chem. 282(10) (2007) 7576-7581.
[8] G.R. Stark, I.M. Kerr, B.R. Williams, R.H. Silverman, R.D. Schreiber, How cells respond to interferons, Annual Reviews 4139 El Camino Way, PO Box 10139, Palo Alto, CA 94303-0139, USA, 1998.
[9] S. Emanuel, S. Pestka, Human interferon-alpha A,-alpha 2, and-alpha 2 (Arg) genes in genomic DNA, J. Biol. Chem. 268(17) (1993) 12565-12569.
[10] G. Allen, M. Diaz, Nomenclature of the human interferon proteinsa, J. Interferon Cytokine Res. 16(2) (1996) 181-184.
[11] R. Bordens, S.E. Grossberg, P.P. Trotta, T.L. Nagabhushan, Molecular and Biologic Characterization of Recombinant Interferon-a2b, Semin. Oncol.-Supplements, [New York] Grune & Stratton., 1997, pp. 41-51.
[12] S. Kaluz, A. Gibadulinová, P. Kontsek, Interferon alpha 2b but not interferon alpha 2a detected in human genomic DNA, Acta Virol. 37(1) (1993) 97-100.
[13] A.T. Nyman, T. Hannele, J. Parkkinen, N. Kalkkinen, Identification of nine interferon-α subtypes produced by Sendai virus-induced human peripheral blood leucocytes, Biochem. J. 329(2) (1998) 295-302.
[14] P. Lengyel, Biochemistry of interferons and their actions, Annu Rev Biochem. 51(1) (1982) 251-282.
[15] S.R. Mohanty, S.S. Kupfer, V. Khiani, Treatment of chronic hepatitis B, Nat Rev Gastroenterol Hepatol 3(8) (2006) 446.
[16] W. Vogel, Treatment of acute hepatitis C virus infection, J. Hepatol. 31 (1999) 189-192.
[17] E. Bajetta, M. Del Vecchio, P. Nova, A. Fusi, A. Daponte, M. Sertoli, P. Queirolo, P. Taveggia, M.G. Bernengo, S. Legha, Multicenter phase III randomized trial of polychemotherapy (CVD regimen) versus the same chemotherapy (CT) plus subcutaneous interleukin-2 and interferon-α2b in metastatic melanoma, Ann. Oncol. 17(4) (2006) 571-577.
[18] P. Terheyden, J. Becker, E. Kämpgen, E.-B. Bröcker, Sequential interferon-α2b, interleukin-2 and fotemustine for patients with metastatic melanoma, Melanoma Res. 10(5) (2000) 475-482.
[19] A.M. Eggermont, S. Suciu, R. MacKie, W. Ruka, A. Testori, W. Kruit, C.J. Punt, M. Delauney, F. Sales, G. Groenewegen, Post-surgery adjuvant therapy with intermediate doses of interferon alfa 2b versus observation in patients with stage IIb/III melanoma (EORTC 18952): randomised controlled trial, The Lancet 366(9492) (2005) 1189-1196.
[20] B.J. Dezube, New therapies for the treatment of AIDS-related Kaposi sarcoma, Curr Opin Oncol 12(5) (2000) 445-449.

[21] G.R. Angstreich, B.D. Smith, R.J. Jones, Treatment options for chronic myeloid leukemia: imatinib versus interferon versus allogeneic transplant, Curr. Opin. Oncol. 16(2) (2004) 95-99.
[22] J.J. Marler, J.B. Rubin, N.S. Trede, S. Connors, H. Grier, J. Upton, J.B. Mulliken, J. Folkman, Successful antiangiogenic therapy of giant cell angioblastoma with interferon alfa 2b: report of 2 cases, Pediatrics 109(2) (2002) E37.
[23] R. Radhakrishnan, L.J. Walter, A. Hruza, P. Reichert, P.P. Trotta, T.L. Nagabhushan, M.R. Walter, Zinc mediated dimer of human interferon-α2b revealed by X-ray crystallography, Structure 4(12) (1996) 1453-1463.
[24] A.J. Sadler, B.R. Williams, Interferon-inducible antiviral effectors, Nat. Rev. Immunol. 8(7) (2008) 559.
[25] J. Bekisz, S. Baron, C. Balinsky, A. Morrow, K.C. Zoon, Antiproliferative properties of type I and type II interferon, Pharmaceuticals 3(4) (2010) 994-1015.
[26] B. Gao, F. Hong, S. Radaeva, Host factors and failure of interferon-α treatment in hepatitis C virus, Hepatology 39(4) (2004) 880-890.
[27] C.E. Samuel, Antiviral actions of interferons, Clin. Microbiol. Rev. 14(4) (2001) 778-809.
[28] C. Weissmann, S. Nagata, W. Boll, M. Fountoulakis, A. Fujisawa, J.-I. Fujisawa, J. Haynes, K. Henco, N. Mantei, H. Ragg, Structure and expression of human IFN-α genes, Philos. Trans. R. Soc. Lond., B, Biol. Sci. 299(1094) (1982) 7-28.
[29] D.V. Goeddel, E. Yelverton, A. Ullrich, H.L. Heyneker, G. Miozzari, W. Holmes, P.H. Seeburg, T. Dull, L. May, N. Stebbing, Human leukocyte interferon produced by *E. coli* is biologically active, Nature 287(5781) (1980) 411.
[30] E. Baron, S. Narula, From cloning to a commercial realization: human alpha interferon, Crit. Rev. Biotechnol. 10(3) (1990) 179-190.
[31] N. Acosta-Rivero, J.C. Sánchez, J. Morales, Improvement of human interferon HUIFNα2 and HCV core protein expression levels in *Escherichia coli* but not of HUIFNα8 by using the tRNAAGA/AGG, Biochem. Biophys. Res. Commun. 296(5) (2002) 1303-1309.
[32] A. Beldarraín, Y. Cruz, O. Cruz, M. Navarro, M. Gil, Purification and conformational properties of a human interferon α2b produced in *Escherichia coli*, Biotechnol. Appl. Biochem. 33(3) (2001) 173-182.
[33] P. Srivastava, P. Bhattacharaya, G. Pandey, K. Mukherjee, Overexpression and purification of recombinant human interferon alpha2b in *Escherichia coli*, Protein expression and purification 41(2) (2005) 313-322.
[34] S. Youngster, Y.-S. Wang, M. Grace, J. Bausch, R. Bordens, D.F. Wyss, Structure, biology, and therapeutic implications of pegylated interferon alpha-2b, Current pharmaceutical design 8(24) (2002) 2139-2157.
[35] D. Pulido, J.A. Vara, A. Jiménez, Cloning and expression in biologically active form of the gene for human interferon α2 in *Streptomyces lividans*, Gene 45(2) (1986) 167-174.
[36] R. Breitling, D. Gerlach, M. Hartmann, D. Behnke, Secretory expression in *Escherichia coli* and *Bacillus subtilis* of human interferon α genes directed by staphylokinase signals, Mol. Gen. Genet. 217(2-3) (1989) 384-391.
[37] A.A. Bianchi, J.T. McGrew, High-level expression of full-length antibodies using trans-complementing expression vectors, Biotechnol. Bioeng. 84(4) (2003) 439-444.
[38] J. Grünberg, K. Knogler, R. Waibel, I. Novak-Hofer, High-yield production of recombinant antibody fragments in HEK-293 cells using sodium butyrate, Biotechniques 34(5) (2003) 968-972.
[39] F.M. Wurm, Production of recombinant protein therapeutics in cultivated mammalian cells, Nat. Biotechnol. 22(11) (2004) 1393.
[40] E.C. Zwarthoff, I.J. Bosveld, W.P. Vonk, J. Trapman, Constitutive expression of a murine interferon alpha gene in hamster cells and characterization of its protein product, J. Gen. Virol. 66(4) (1985) 685-691.

[41] M. Loignon, S. Perret, J. Kelly, D. Boulais, B. Cass, L. Bisson, F. Afkhamizarreh, Y. Durocher, Stable high volumetric production of glycosylated human recombinant IFNalpha2b in HEK293 cells, BMC Biotechnol. 8(1) (2008) 65.
[42] D.C. Andersen, L. Krummen, Recombinant protein expression for therapeutic applications, Curr. Opin. Biotechnol. 13(2) (2002) 117-123.
[43] T. Patel, E. Pequignot, S. Parker, M. Leavitt, H. Greenberg, W. Kraft, Transgenic avian-derived recombinant human interferon-alpha2b (AVI-005) in healthy subjects, Transgenic Res, Springer Van Godewijckstraat 30, 3311 Gz Dordrecht, Netherlands, 2007, pp. 845-845.
[44] J.C. Rapp, A.J. Harvey, G.L. Speksnijder, W. Hu, R. Ivarie, Biologically Active Human Interferon α-2b Produced in the Egg White of Transgenic Hens, Transgenic research 12(5) (2003) 569-575.
[45] K. Sugyiama, H. Ahorn, I. Maurer-fogy, T. Voss, Expression of human interferon-α2 in Sf9 cells: Characterization of O-linked glycosylation and protein heterogeneities, Eur. J. Biochem. 217(3) (1993) 921-927.
[46] C. Rossmann, N. Sharp, G. Allen, D. Gewert, Expression and purification of recombinant, glycosylated human interferon alpha 2b in murine myeloma NSo cells, Protein Expr. Purif. 7(4) (1996) 335-342.
[47] H. Li, Q. Liu, K. Cui, J. Liu, Y. Ren, D. Shi, Expression of biologically active human interferon alpha 2b in the milk of transgenic mice, Transgenic res. 22(1) (2013) 169-178.
[48] Y. Luchakivskaya, O. Kishchenko, I. Gerasymenko, Z. Olevinskaya, Y. Simonenko, M. Spivak, M. Kuchuk, High-level expression of human interferon alpha-2b in transgenic carrot (*Daucus carota L.*) plants, Plant Cell Rep. 30(3) (2011) 407-415.
[49] F.O. Neves, P.L. Ho, I. Raw, C.A. Pereira, C. Moreira, A.L. Nascimento, Overexpression of a synthetic gene encoding human alpha interferon in *Escherichia coli*, Protein expression and purification 35(2) (2004) 353-359.
[50] J.S. Tan, R.N. Ramanan, S.N.A. Azaman, T.C. Ling, M. Shuhaimi, A.B. Ariff, Enhanced Interferon-[alpha] 2 b Production in Periplasmic Space of *Escherichia coli* through Medium Optimization using Response Surface Method, Open Biotechnology Journal 3 (2009) 117-124.
[51] E. Pimienta, R. Fando, J. Sánchez, C. Vallin, Secretion of human interferon alpha 2b by *Streptomyces lividans*, Applied microbiology and biotechnology 58(2) (2002) 189-194.
[52] N. Gasmi, A. Ayed, B.B. Ammar, R. Zrigui, J.-M. Nicaud, H. Kallel, Development of a cultivation process for the enhancement of human interferon alpha 2b production in the oleaginous yeast, *Yarrowia lipolytica*, Microb Cell Fact. 10(1) (2011) 90.
[53] J.N. Garcia, J.A. Aguiar, M. Gill, A. Alvarez, J. Morales, J. Ferrero, B. Gonzalez, G. Padron, A. Menendez, High level expression of human IFN-alpha2b in *Pichia pastoris*, Biotecnologia Aplicada 12(3) (1995) 152-155.
[54] L. Shi, D. Wang, W. Chan, L. Cheng, Efficient expression and purification of human interferon alpha2b in the methylotrophic yeast, *Pichia pastoris*, Protein Expr. Purif. 54(2) (2007) 220-226.
[55] A. Ghosalkar, V. Sahai, A. Srivastava, Secretory expression of interferon-alpha 2b in recombinant *Pichia pastoris* using three different secretion signals, Protein Expr. Purif. 60(2) (2008) 103-109.
[56] A. Ayed, I. Rabhi, K. Dellagi, H. Kallel, High level production and purification of human interferon α2b in high cell density culture of *Pichia pastoris*, Enzyme Microb. Technol. 42(2) (2008) 173-180.
[57] S. Salunkhe, S. Soorapaneni, K.S. Prasad, V.A. Raiker, S. Padmanabhan, Strategies to maximize expression of rightly processed human interferon α2b in *Pichia pastoris*, Protein Expr. Purif. 71(2) (2010) 139-146.
[58] K. Sugyiama, H. Ahorn, I. Maurer-fogy, T. Voss, Expression of human interferon-α2 in Sf9 cells: Characterization of O-linked glycosylation and protein heterogeneities, Eur. J. Biochem. 217(3) (1993) 921-927.

[59] J. Xu, L. Tan, K.J. Goodrum, M.J. Kieliszewski, High-yields and extended serum half-life of human interferon α2b expressed in tobacco cells as arabinogalactan-protein fusions, Biotechnology and bioengineering 97(5) (2007) 997-1008.
[60] D. Mattanovich, P. Branduardi, L. Dato, B. Gasser, M. Sauer, D. Porro, Recombinant protein production in yeasts, Recombinant gene expression, Springer2012, pp. 329-358.
[61] M. Tuite, M. Dobson, N. Roberts, R. King, D. Burke, S. Kingsman, A. Kingsman, Regulated high efficiency expression of human interferon-alpha in *Saccharomyces cerevisiae*, The EMBO journal 1(5) (1982) 603-608.
[62] J.M. Cregg, K. Barringer, A. Hessler, K. Madden, *Pichia pastoris* as a host system for transformations, Mol. Cell. Biol. 5(12) (1985) 3376-3385.
[63] J.M. Cregg, J.L. Cereghino, J. Shi, D.R. Higgins, Recombinant protein expression in *Pichia pastoris*, Mol. Biotechnol 16(1) (2000) 23-52.
[64] G.R. Adolf, I. Kalsner, H. Ahorn, I. Maurer-Fogy, K. Cantell, Natural human interferon-α2 is O-glycosylated, Biochem. J. 276(2) (1991) 511-518.
[65] L. Shi, D. Wang, W. Chan, L. Cheng, Efficient expression and purification of human interferon alpha 2b in the methylotrophic yeast, *Pichia pastoris*, Protein Expr. Purif. 54(2) (2007) 220-226.
[66] H. Hohenblum, B. Gasser, M. Maurer, N. Borth, D. Mattanovich, Effects of gene dosage, promoters, and substrates on unfolded protein stress of recombinant *Pichia pastoris*, Biotechnol. Bioeng. 85(4) (2004) 367-375.
[67] T.R. Gemmill, R.B. Trimble, Overview of N-and O-linked oligosaccharide structures found in various yeast species, Biochim. Biophys. Acta (BBA)-General Subjects 1426(2) (1999) 227-237.
[68] C. Madzak, C. Gaillardin, J.-M. Beckerich, Heterologous protein expression and secretion in the non-conventional yeast *Yarrowia lipolytica*: a review, J. Biotechnol. 109(1-2) (2004) 63-81.
[69] Y. Jigami, T. Odani, Mannosylphosphate transfer to yeast mannan, Biochim. Biophys. Acta (BBA)-General Subjects 1426(2) (1999) 335-345.
[70] S.R. Hamilton, T.U. Gerngross, Glycosylation engineering in yeast: the advent of fully humanized yeast, Curr. Opin. Biotechnol. 18(5) (2007) 387-392.
[71] P. Jacobs, N. Callewaert, N-glycosylation engineering of biopharmaceutical expression systems, Curr. Mol. Med. 9(7) (2009) 774-800.
[72] E. Chatelut, L. Rostaing, N. Grégoire, J.L. Payen, A. Pujol, J. Izopet, G. Houin, P. Canal, A pharmacokinetic model for alpha interferon administered subcutaneously, Br J Clin Pharmacol 47(4) (1999) 365-371.
[73] J.U. Gutterman, Cytokine therapeutics: lessons from interferon alpha, Proc. Natl. Acad. Sci. U.S.A. 91(4) (1994) 1198-1205.
[74] H. Nakamura, N. Oda-Ueda, T. Ueda, T. Ohkuri, A novel engineered interchain disulfide bond in the constant region enhances the thermostability of adalimumab Fab, Biochemical and biophysical research communications 495(1) (2018) 7-11.
[75] H.-S. Chung, J.-S. Kim, S.M. Lee, S.J. Park, Additional N-glycosylation in the N-terminal region of recombinant human alpha-1 antitrypsin enhances the circulatory half-life in Sprague-Dawley rats, Glycoconjugate journal 33(2) (2016) 201-208.
[76] S. Elliott, T. Lorenzini, S. Asher, K. Aoki, D. Brankow, L. Buck, L. Busse, D. Chang, J. Fuller, J. Grant, Enhancement of therapeutic protein in vivo activities through glycoengineering, Nat. Biotechnol. 21(4) (2003) 414.
[77] S. Perlman, B. van den Hazel, J. Christiansen, S. Gram-Nielsen, C.B. Jeppesen, K.V. Andersen, T. Halkier, S. Okkels, H.T. Schambye, Glycosylation of an N-terminal extension prolongs the half-life and increases the in vivo activity of follicle stimulating hormone, The Journal of Clinical Endocrinology & Metabolism 88(7) (2003) 3227-3235.
[78] J.C. Egrie, J.K. Browne, Development and characterization of novel erythropoiesis stimulating protein (NESP), British journal of cancer 84(S1) (2001) 3.

[79] Y.-S. Wang, S. Youngster, M. Grace, J. Bausch, R. Bordens, D.F. Wyss, Structural and biological characterization of pegylated recombinant interferon alpha-2b and its therapeutic implications, Adv. Drug Deliv. Rev. 54(4) (2002) 547-570.
[80] N. Ceaglio, M. Etcheverrigaray, R. Kratje, M. Oggero, Novel long-lasting interferon alpha derivatives designed by glycoengineering, Biochimie 90(3) (2008) 437-449.
[81] K.P. Jayapal, K.F. Wlaschin, W. Hu, M.G. Yap, Recombinant protein therapeutics from CHO cells-20 years and counting, Chem. Eng. Prog. 103(10) (2007) 40.
[82] H. Waegeman, M. De Mey, Increasing recombinant protein production in *E. coli* by an alternative method to reduce acetate, Advances in applied biotechnology, In-Tech2012, pp. 127-144.
[83] J.L. Cereghino, J.M. Cregg, Heterologous protein expression in the methylotrophic yeast *Pichia pastoris*, FEMS Microbiol. Rev. 24(1) (2000) 45-66.
[84] R.B. Kirkpatrick, S. Ganguly, M. Angelichio, S. Griego, A. Shatzman, C. Silverman, M. Rosenberg, Heavy chain dimers as well as complete antibodies are efficiently formed and secreted from *Drosophila* via a BiP-mediated pathway, J. Biol. Chem. 270(34) (1995) 19800-19805.
[85] T.A. Kost, J.P. Condreay, D.L. Jarvis, Baculovirus as versatile vectors for protein expression in insect and mammalian cells, Nat. Biotechnol. 23(5) (2005) 567.
[86] R.G. Soderquist, J.M. Lee, Enhanced production of recombinant proteins from plant cells by the application of osmotic stress and protein stabilization, Plant Cell Rep. 24(2) (2005) 127-132.
[87] Y. Durocher, M. Butler, Expression systems for therapeutic glycoprotein production, Curr Opin Biotechnol. 20(6) (2009) 700-707.
[88] N. Sethuraman, T.A. Stadheim, Challenges in therapeutic glycoprotein production, Curr Opin Biotechnol. 17(4) (2006) 341-346.
[89] Y. Lim, N.S. Wong, Y.Y. Lee, S.C. Ku, D.C. Wong, M.G. Yap, Engineering mammalian cells in bioprocessing–current achievements and future perspectives, Biotechnol. Appl. Biochem. 55(4) (2010) 175-189.
[90] L.-X. Wang, J.V. Lomino, Emerging technologies for making glycan-defined glycoproteins, ACS Chem. Biol. 7(1) (2011) 110-122.
[91] P.P. Jacobs, M. Inan, N. Festjens, J. Haustraete, A. Van Hecke, R. Contreras, M.M. Meagher, N. Callewaert, Fed-batch fermentation of GM-CSF-producing glycoengineered *Pichia pastoris* under controlled specific growth rate, Microb. Cell Fact. 9(1) (2010) 93.
[92] S. Elliott, D. Chang, E. Delorme, T. Eris, T. Lorenzini, Structural requirements for additional N-linked carbohydrate on recombinant human erythropoietin, J. Biol. Chem. 279(16) (2004) 16854-16862.
[93] R. Stork, K.A. Zettlitz, D. Müller, M. Rether, F.-G. Hanisch, R.E. Kontermann, N-glycosylation as novel strategy to improve pharmacokinetic properties of bispecific single-chain diabodies, J. Biol. Chem. 283(12) (2008) 7804-7812.
[94] J.P. Kunkel, D.C. Jan, M. Butler, J.C. Jamieson, Comparisons of the glycosylation of a monoclonal antibody produced under nominally identical cell culture conditions in two different bioreactors, Biotechnol. Prog. 16(3) (2000) 462-470.
[95] M.L. Lipscomb, L.A. Palomares, V. Hernández, O.T. Ramírez, D.S. Kompala, Effect of production method and gene amplification on the glycosylation pattern of a secreted reporter protein in CHO cells, Biotechnol. Prog. 21(1) (2005) 40-49.
[96] M.H. Goldman, D.C. James, M. Rendall, A.P. Ison, M. Hoare, A.T. Bull, Monitoring recombinant human interferon-gamma N-glycosylation during perfused fluidized-bed and stirred-tank batch culture of CHO cells, Biotechnol. Bioeng. 60(5) (1998) 596-607.
[97] S. Nahrgang, E. Kkagten, M. De Jesus, M. Bourgeois, S. Déjardin, U. Von Stockar, I. Marison, The effect of cell line, transfection procedure and reactor conditions on the glycosylation of recombinant human anti-rhesus D IgGl, Animal Cell Technology: Products from Cells, Cells as Products, Springer1999, pp. 259-261.

[98] G. Walsh, R. Jefferis, Post-translational modifications in the context of therapeutic proteins, Nat. Biotechnol. 24(10) (2006) 1241.
[99] J. Zhu, Mammalian cell protein expression for biopharmaceutical production, Biotechnol. Adv. 30(5) (2012) 1158-1170.
[100] P. Hossler, S.F. Khattak, Z.J. Li, Optimal and consistent protein glycosylation in mammalian cell culture, Glycobiology 19(9) (2009) 936-949.
[101] X. Gu, L. Xie, B.J. Harmon, D.I. Wang, Influence of Primatone RL supplementation on sialylation of recombinant human interferon-γ produced by Chinese hamster ovary cell culture using serum-free media, Biotechnol. Bioeng. 56(4) (1997) 353-360.
[102] T.P. Patel, R. Parekh, B. Moellering, C. Prior, Different culture methods lead to differences in glycosylation of a murine IgG monoclonal antibody, Biochem. J. 285(3) (1992) 839-845.
[103] J. Geigert, The challenge of CMC regulatory compliance for biopharmaceuticals and other biologics, Springer2013.
[104] P. Castro, A.P. Ison, P.M. Hayter, A.T. Bull, The macroheterogeneity of recombinant human interferon-gamma produced by Chinese-hamster ovary cells is affected by the protein and lipid content of the culture medium, Biotechnol. Appl. Biochem. 21(1) (1995) 87-100.
[105] N. Kochanowski, F. Blanchard, R. Cacan, F. Chirat, E. Guedon, A. Marc, J.L. Goergen, Influence of intracellular nucleotide and nucleotide sugar contents on recombinant interferon-γ glycosylation during batch and fed-batch cultures of CHO cells, Biotechnol. Bioeng. 100(4) (2008) 721-733.
[106] J. Müthing, S.E. Kemminer, H.S. Conradt, D. Šagi, M. Nimtz, U. Kärst, J. Peter-Katalinić, Effects of buffering conditions and culture pH on production rates and glycosylation of clinical phase I anti-melanoma mouse IgG3 monoclonal antibody R24, Biotechnol. Bioeng. 83(3) (2003) 321-334.
[107] M.C. Borys, D.I. Linzer, E.T. Papoutsakis, Culture pH affects expression rates and glycosylation of recombinant mouse placental lactogen proteins by Chinese hamster ovary (CHO) cells, Bio/technology 11(6) (1993) 720.
[108] R.J. Rothman, L. Warren, J.F. Vliegenthart, K.J. Hard, Clonal analysis of the glycosylation of immunoglobulin G secreted by murine hybridomas, Biochem. 28(3) (1989) 1377-1384.
[109] O. Cos, R. Ramon, J.L. Montesinos, F. Valero, Operational strategies, monitoring and control of heterologous protein production in the methylotrophic yeast *Pichia pastoris* under different promoters: a review, Microb Cell Fact. 5(1) (2006) 17.
[110] W. Zhang, M.A. Bevins, B.A. Plantz, L.A. Smith, M.M. Meagher, Modeling *Pichia pastoris* growth on methanol and optimizing the production of a recombinant protein, the heavy-chain fragment C of botulinum neurotoxin, serotype A, Biotechnol. Bioeng. 70(1) (2000) 1-8.
[111] C. Jungo, J. Urfer, A. Zocchi, I. Marison, U. von Stockar, Optimisation of culture conditions with respect to biotin requirement for the production of recombinant avidin in *Pichia pastoris*, J. Biotechnol. 127(4) (2007) 703-715.
[112] Food, D. Administration, Guidance for industry, PAT-A Framework for Innovative Pharmaceutical Development, Manufacturing and Quality Assurance, http://www. fda. gov/cder/guidance/published. html (2004).
[113] D.C. Hinz, Process analytical technologies in the pharmaceutical industry: the FDA's PAT initiative, Anal. Bioanal. Chem. 384(5) (2006) 1036-1042.
[114] J. Bechmann, F. Rudolph, L. Gebert, J. Schaub, B. Greulich, M. Dieterle, H. Bradl, Process parameters impacting product quality, BMC proceedings, BioMed Central, 2015, p. O7.
[115] F. Clementschitsch, K. Bayer, Improvement of bioprocess monitoring: development of novel concepts, Microb. Cell Fact. 5(1) (2006) 19.
[116] A. Teixeira, R. Oliveira, P. Alves, M. Carrondo, Advances in on-line monitoring and control of mammalian cell cultures: supporting the PAT initiative, Biotechnol. Adv. 27(6) (2009) 726-732.

[117] C. Kaiser, J. Carvell, R. Luttmann, A sensitive, compact, in situ biomass measurement system controlling and monitoring microbial fermentations using radio-frequency impedance, Bioprocess Int 5(1) (2007) 52-56.
[118] T. Maskow, A. Röllich, I. Fetzer, J.-U. Ackermann, H. Harms, On-line monitoring of lipid storage in yeasts using impedance spectroscopy, J. Biotechnol. 135(1) (2008) 64-70.
[119] N.P. Rønnest, S.M. Stocks, A.E. Lantz, K.V. Gernaey, Introducing process analytical technology (PAT) in filamentous cultivation process development: comparison of advanced online sensors for biomass measurement, J. Ind. Microbiol. Biotechnol. 38(10) (2011) 1679-1690.
[120] C. Cannizzaro, R. Gügerli, I. Marison, U. von Stockar, Online biomass monitoring of CHO perfusion culture with scanning dielectric spectroscopy, Biotechnol. Bioeng. 84(5) (2003) 597-610.
[121] T. Noll, M. Biselli, Dielectric spectroscopy in the cultivation of suspended and immobilized hybridoma cells, J. Biotechnol. 63(3) (1998) 187-198.
[122] L. Preziosi-Belloy, B.L. P. Tibayrenc , G. Esteban , G. Moulin, H.B. Ghommid, On-line *Pichia pastoris* physiological state monitoring by dielectric spectroscopy, ECB (2005).
[123] D.C. Andersen, T. Bridges, M. Gawlitzek, C. Hoy, Multiple cell culture factors can affect the glycosylation of Asn184 in CHO produced tissue type plasminogen activator, Biotechnol. Bioeng. 70(1) (2000) 25-31.
[124] F. Meuwly, U. von Stockar, A. Kadouri, Optimization of the medium perfusion rate in a packed-bed bioreactor charged with CHO cells, Cytotechnology 46(1) (2004) 37-47.
[125] C.T. Yuen, P.L. Storring, R.J. Tiplady, M. Izquierdo, R. Wait, C.K. Gee, P. Gerson, P. Lloyd, J.A. Cremata, Relationships between the N-glycan structures and biological activities of recombinant human erythropoietins produced using different culture conditions and purification procedures, Br. J. Haematol. 121(3) (2003) 511-526.
[126] N.K. Khatri, F. Hoffmann, Impact of methanol concentration on secreted protein production in oxygen-limited cultures of recombinant *Pichia pastoris*, Biotechnol. Bioeng. 93(5) (2006) 871-879.
[127] A. Cunha, J. Clemente, R. Gomes, F. Pinto, M. Thomaz, S. Miranda, R. Pinto, D. Moosmayer, P. Donner, M. Carrondo, Methanol induction optimization for scFv antibody fragment production in *Pichia pastoris*, Biotechnol. Bioeng. 86(4) (2004) 458-467.
[128] F. Hong, N.Q. Meinander, L.J. Jönsson, Fermentation strategies for improved heterologous expression of laccase in *Pichia pastoris*, Biotechnol. Bioeng. 79(4) (2002) 438-449.
[129] J.H. Woo, Y.Y. Liu, D.M. Neville Jr, Minimization of aggregation of secreted bivalent anti-human T cell immunotoxin in *Pichia pastoris* bioreactor culture by optimizing culture conditions for protein secretion, J. Biotechnol. 121(1) (2006) 75-85.
[130] J. Schenk, K. Balazs, C. Jungo, J. Urfer, C. Wegmann, A. Zocchi, I.W. Marison, U. von Stockar, Influence of specific growth rate on specific productivity and glycosylation of a recombinant avidin produced by a *Pichia pastoris* Mut+ strain, Biotechnol. Bioeng. 99(2) (2008) 368-377.
[131] J.-M. Puertas, J. Ruiz, M.R. De la Vega, J. Lorenzo, G. Caminal, G. González, Influence of specific growth rate over the secretory expression of recombinant potato carboxypeptidase inhibitor in fed-batch cultures of *Escherichia coli*, Process Biochem. 45(8) (2010) 1334-1341.
[132] R. Nahku, K. Valgepea, P.-J. Lahtvee, S. Erm, K. Abner, K. Adamberg, R. Vilu, Specific growth rate dependent transcriptome profiling of *Escherichia coli* K12 MG1655 in accelerostat cultures, J. Biotechnol. 145(1) (2010) 60-65.
[133] U. Von Stockar, I.W. Marison, The use of calorimetry in biotechnology, Bioprocesses and engineering, Springer1989, pp. 93-136.
[134] S. Sivaprakasam, M.M. Schuler, A. Hama, K.-M. Hughes, I.W. Marison, Biocalorimetry as a process analytical technology process analyser; robust in-line monitoring and control of aerobic fed-batch cultures of crabtree-negative yeast cells, . Therm. Anal. Calorim. 104(1) (2011) 75-85.

[135] T. Schubert, U. Breuer, H. Harms, T. Maskow, Calorimetric bioprocess monitoring by small modifications to a standard bench-scale bioreactor, J. Biotechnol. 130(1) (2007) 24-31.
[136] I. Marison, J.-S. Liu, S. Ampuero, U. Von Stockar, B. Schenker, Biological reaction calorimetry: development of high sensitivity bio-calorimeters, Thermochim. Acta. 309(1-2) (1998) 157-173.
[137] S. Sekar, S. Mahadevan, S.S.D. Kumar, A.B. Mandal, Thermokinetic responses of the metabolic activity of *Staphylococcus lentus* cultivated in a glucose limited mineral salt medium, J. Therm. Anal. Calorim. 104(1) (2011) 149-155.
[138] B. Zentgraf, Bench-scale calorimetry in biotechnology, Thermochim. Acta. 193 (1991) 243-251.
[139] U. Von Stockar, T. Maskow, J. Liu, I.W. Marison, R. Patino, Thermodynamics of microbial growth and metabolism: an analysis of the current situation, J. Biotechnol. 121(4) (2006) 517-533.
[140] J. Liu, I. Marison, U. Von Stockar, Microbial growth by a net heat uptake: a calorimetric and thermodynamic study on acetotrophic methanogenesis by Methanosarcina barkeri, Biotechnol. Bioeng. 75(2) (2001) 170-180.
[141] W. Zhang, L.A. Smith, B.A. Plantz, V.L. Schlegel, M.M. Meagher, Design of methanol feed control in *Pichia pastoris* fermentations based upon a growth model, Biotechnol. Prog. 18(6) (2002) 1392-1399.
[142] I.A. Pla, L.M. Damasceno, T. Vannelli, G. Ritter, C.A. Batt, M.L. Shuler, Evaluation of Mut+ and MutS *Pichia pastoris* phenotypes for high level extracellular scFv expression under feedback control of the methanol concentration, Biotechnol. Prog. 22(3) (2006) 881-888.
[143] R. Ramon, J. Feliu, O. Cos, J. Montesinos, F. Berthet, F. Valero, Improving the monitoring of methanol concentration during high cell density fermentation of *Pichia pastoris*, Biotechnol. Lett. 26(18) (2004) 1447-1452.
[144] M. Dabros, M.M. Schuler, I.W. Marison, Simple control of specific growth rate in biotechnological fed-batch processes based on enhanced online measurements of biomass, Bioprocess Biosyst Eng 33(9) (2010) 1109-1118.
[145] A. Ferreira, F. Ataíde, M. Von Stosch, J. Dias, J. Clemente, A. Cunha, R. Oliveira, Application of adaptive DO-stat feeding control to *Pichia pastoris* X33 cultures expressing a single chain antibody fragment (scFv), Bioprocess Biosyst Eng 35(9) (2012) 1603-1614.
[146] M. Goldfeld, J. Christensen, D. Pollard, E.R. Gibson, J.T. Olesberg, E.J. Koerperick, K. Lanz, G.W. Small, M.A. Arnold, C.E. Evans, Advanced near-infrared monitor for stable real-time measurement and control of *Pichia pastoris* bioprocesses, Biotechnol. Prog. 30(3) (2014) 749-759.
[147] M.M. Schuler, S. Sivaprakasam, B. Freeland, A. Hama, K.-M. Hughes, I.W. Marison, Investigation of the potential of biocalorimetry as a process analytical technology (PAT) tool for monitoring and control of Crabtree-negative yeast cultures, Appl. Microbiol. Biotechnol. 93(2) (2012) 575-584.
[148] R.A. Hitzeman, F.E. Hagie, H.L. Levine, D.V. Goeddel, G. Ammerer, B.D. Hall, Expression of a human gene for interferon in yeast, Nature 293(5835) (1981) 717.
[149] P. Glue, J.W. Fang, R. Rouzier-Panis, C. Raffanel, R. Sabo, S.K. Gupta, M. Salfi, S. Jacobs, Pegylated interferon-α2b: Pharmacokinetics, pharmacodynamics, safety, and preliminary efficacy data, Clin. Pharmacol. Ther. 68(5) (2000) 556-567.
[150] G. Giannelli, G. Antonelli, G. Fera, S. Del Vecchio, E. Riva, C. Broccia, O. Schiraldi, F. Dianzani, Biological and clinical significance of neutralizing and binding antibodies to interferon-alpha (IFN–α) during therapy for chronic hepatitis C, Clin. Exp. Immunol. 97(1) (1994) 4-9.
[151] A.A. van der Eijk, J.M. Vrolijk, B.L. Haagmans, Antibodies neutralizing peginterferon alfa during retreatment of hepatitis C, N. Engl. J. Med. 354(12) (2006) 1323-1324.
[152] A.M. Sinclair, S. Elliott, Glycoengineering: the effect of glycosylation on the properties of therapeutic proteins, Journal of pharmaceutical sciences 94(8) (2005) 1626-1635.

[153] T. BINO, Z. MADAR, A. GERTLER, H. ROSENBERG, The kidney is the main site of interferon degradation, J. Interferon Res. 2(2) (1982) 301-308.
[154] T. Peleg-Shulman, H. Tsubery, M. Mironchik, M. Fridkin, G. Schreiber, Y. Shechter, Reversible PEGylation: a novel technology to release native interferon α2 over a prolonged time period, J. Med. Chem. 47(20) (2004) 4897-4904.
[155] S. Erbayraktar, G. Grasso, A. Sfacteria, Q.-w. Xie, T. Coleman, M. Kreilgaard, L. Torup, T. Sager, Z. Erbayraktar, N. Gokmen, Asialoerythropoietin is a nonerythropoietic cytokine with broad neuroprotective activity in vivo, Proc. Natl. Acad. Sci. U.S.A. 100(11) (2003) 6741-6746.
[156] L. Runkel, W. Meier, R.B. Pepinsky, M. Karpusas, A. Whitty, K. Kimball, M. Brickelmaier, C. Muldowney, W. Jones, S.E. Goelz, Structural and functional differences between glycosylated and non-glycosylated forms of human interferon-β (IFN-β), Pharm. Res 15(4) (1998) 641-649.
[157] T. Sareneva, E. Mørtz, H. Tölö, P. Roepstorff, I. Julkunen, Biosynthesis and N-glycosylation of Human Interferon-γ: Asn25 and Asn97 Differ Markedly in How Efficiently They are Glycosylated and in Their Oligosaccharide Composition, Eur. J. Biochem. 242(2) (1996) 191-200.
[158] G. Gellissen, G. Kunze, C. Gaillardin, J.M. Cregg, E. Berardi, M. Veenhuis, I. van der Klei, New yeast expression platforms based on methylotrophic *Hansenula polymorpha* and *Pichia pastoris* and on dimorphic *Arxula adeninivorans* and *Yarrowia lipolytica*–a comparison, FEMS Yeast Res. 5(11) (2005) 1079-1096.
[159] D. Weinacker, C. Rabert, A.B. Zepeda, C.A. Figueroa, A. Pessoa, J.G. Farías, Applications of recombinant *Pichia pastoris* in the healthcare industry, Braz. J. Microbiol. 44(4) (2013) 1043-1048.
[160] R.K. Bretthauer, Genetic engineering of *Pichia pastoris* to humanize N-glycosylation of proteins, Trends Biotechnol. 21(11) (2003) 459-462.
[161] W. Vervecken, V. Kaigorodov, N. Callewaert, S. Geysens, K. De Vusser, R. Contreras, In vivo synthesis of mammalian-like, hybrid-type N-glycans in *Pichia pastoris*, Appl. Environ. Microbiol. 70(5) (2004) 2639-2646.
[162] E.T. Smith, E.T. Perry, M.B. Sears, D.A. Johnson, Expression of recombinant human mast cell chymase with Asn-linked glycans in glycoengineered *Pichia pastoris*, Protein Expr. Purif. 102 (2014) 69-75.
[163] C. Thomas, I. Moraga, D. Levin, P.O. Krutzik, Y. Podoplelova, A. Trejo, C. Lee, G. Yarden, S.E. Vleck, J.S. Glenn, Structural linkage between ligand discrimination and receptor activation by type I interferons, Cell 146(4) (2011) 621-632.
[164] J. Stratton, V. Chiruvolu, M. Meagher, High Cell-Density Fermentation, in: D.R. Higgins, J.M. Cregg (Eds.), Pichia Protocols, Humana Press, Totowa, NJ, 1998, pp. 107-120.
[165] P. Babu, S.J. North, J. Jang-Lee, S. Chalabi, K. Mackerness, S.R. Stowell, R.D. Cummings, S. Rankin, A. Dell, S.M. Haslam, Structural characterisation of neutrophil glycans by ultra sensitive mass spectrometric glycomics methodology, Glycoconj. J. 26(8) (2009) 975.
[166] B.L. Osborn, H.S. Olsen, B. Nardelli, J.H. Murray, J.X. Zhou, A. Garcia, G. Moody, L.S. Zaritskaya, C. Sung, Pharmacokinetic and pharmacodynamic studies of a human serum albumin-interferon-α fusion protein in cynomolgus monkeys, J. Pharmacol. Exp. Ther. 303(2) (2002) 540-548.
[167] S. Gräslund, P. Nordlund, J. Weigelt, B.M. Hallberg, J. Bray, O. Gileadi, S. Knapp, U. Oppermann, C. Arrowsmith, R. Hui, Protein production and purification, Nat. Methods 5(2) (2008) 135.
[168] M. Shelikoff, A. Sinskey, G. Stephanopoulos, A modeling framework for the study of protein glycosylation, Biotechnol. Bioeng. 50(1) (1996) 73-90.
[169] R. Daly, M.T. Hearn, Expression of heterologous proteins in *Pichia pastoris*: a useful experimental tool in protein engineering and production, J. Mol. Recognit. 18(2) (2005) 119-138.
[170] K.P. Murphy Jr, P. Gagne, C. Pazmany, M.D. Moody, Expression of Human Interleukin-17 in *Pichia pastoris*: Purification and Characterization, Protein Expr. Purif. 12(2) (1998) 208-214.

[171] M. Yamada, K. Inui, D. Hamada, K. Nakahira, K. Yanagihara, N. Sakai, T. Nishigaki, K. Ozono, I. Yanagihara, Analysis of recombinant human saposin A expressed by *Pichia pastoris*, Biochem. Biophys. Res. Commun. 318(2) (2004) 588-593.
[172] D. Todt, C. François, P. Behrendt, M. Engelmann, L. Knegendorf, G. Vieyres, H. Wedemeyer, R. Hartmann, T. Pietschmann, G. Duverlie, Antiviral activity of different interferon (sub-) types against hepatitis E virus replication, Antimicrob. Agents Chemother. (2016) AAC. 02427-15.
[173] K. Song, I.-S. Yoon, N.A. Kim, D.-H. Kim, J. Lee, H.J. Lee, S. Lee, S. Choi, M.-K. Choi, H.H. Kim, Glycoengineering of interferon-β 1a improves its biophysical and pharmacokinetic properties, PloS one 9(5) (2014) e96967.
[174] F. Zhang, M.-r. Liu, H.-t. Wan, Discussion about several potential drawbacks of PEGylated therapeutic proteins, Biol. Pharm. Bull. (2014) b13-00661.
[175] K. Vyas, D.L. Brassard, M.M. DeLorenzo, Y. Sun, M.J. Grace, E.C. Borden, D.W. Leaman, Biologic Activity of Polyethylene Glycol12000–Interferon-α2b Compared with Interferon-α2b: Gene Modulatory and Antigrowth Effects in Tumor Cells, J. Immunother. 26(3) (2003) 202-211.
[176] S. Kalil, F. Maugeri, M. Rodrigues, Response surface analysis and simulation as a tool for bioprocess design and optimization, Process Biochem 35(6) (2000) 539-550.
[177] S.E. Swalley, J.R. Fulghum, S.P. Chambers, Screening factors effecting a response in soluble protein expression: formalized approach using design of experiments, Anal. Biochem. 351(1) (2006) 122-127.
[178] P. Selvakumar, P. Sivashanmugam, Optimization of lipase production from organic solid waste by anaerobic digestion and its application in biodiesel production, FUEL PROCESS TECHNOL. 165 (2017) 1-8.
[179] P. Selvakumar, P. Sivashanmugam, Multi-hydrolytic biocatalyst from organic solid waste and its application in municipal waste activated sludge pre-treatment towards energy recovery, PROCESS SAF ENVIRON 117 (2018) 1-10.
[180] R. Silva, S. Ferreira, M. Bonifacio, J. Dias, J. Queiroz, L. Passarinha, Optimization of fermentation conditions for the production of human soluble catechol-O-methyltransferase by *Escherichia coli* using artificial neural network, J. Biotechnol. 160(3) (2012) 161-168.
[181] P.C. Giordano, H.D. Martínez, A.A. Iglesias, A.J. Beccaria, H.C. Goicoechea, Application of response surface methodology and artificial neural networks for optimization of recombinant Oryza sativa non-symbiotic hemoglobin 1 production by *Escherichia coli* in medium containing byproduct glycerol, Bioresour. Technol. 101(19) (2010) 7537-7544.
[182] A.A. Prabhu, B. Mandal, V.V. Dasu, Medium optimization for high yield production of extracellular human interferon-γ from *Pichia pastoris*: A statistical optimization and neural network-based approach, Korean J Chem Eng 34(4) (2017) 1109-1121.
[183] P. Sagmeister, P. Wechselberger, C. Herwig, Information processing: rate-based investigation of cell physiological changes along design space development, PDA J Pharm Sci Technol 66(6) (2012) 526-541.
[184] T. Broger, R.P. Odermatt, P. Huber, B. Sonnleitner, Real-time on-line flow cytometry for bioprocess monitoring, J. Biotechnol. 154(4) (2011) 240-247.
[185] P. Neubauer, M. Åhman, M. Törnkvist, G. Larsson, S.-O. Enfors, Response of guanosine tetraphosphate to glucose fluctuations in fed-batch cultivations of *Escherichia coli*, J. Biotechnol. 43(3) (1995) 195-204.
[186] M. Dabros, D. Dennewald, D.J. Currie, M.H. Lee, R.W. Todd, I.W. Marison, U. von Stockar, Cole–Cole, linear and multivariate modeling of capacitance data for on-line monitoring of biomass, Bioprocess Biosyst Eng 32(2) (2009) 161.
[187] D. Ehgartner, T. Hartmann, S. Heinzl, M. Frank, L. Veiter, J. Kager, C. Herwig, J. Fricke, Controlling the specific growth rate via biomass trend regulation in filamentous fungi bioprocesses, Chem Eng Sci 172 (2017) 32-41.

[188] H. Niu, M. Daukandt, C. Rodriguez, P. Fickers, P. Bogaerts, Dynamic modeling of methylotrophic *Pichia pastoris* culture with exhaust gas analysis: from cellular metabolism to process simulation, Chem Eng Sci 87 (2013) 381-392.
[189] R.L. Plackett, J.P. Burman, The design of optimum multifactorial experiments, Biometrika 33(4) (1946) 305-325.
[190] G. Sodeifian, S.A. Sajadian, N.S. Ardestani, Evaluation of the response surface and hybrid artificial neural network-genetic algorithm methodologies to determine extraction yield of *Ferulago angulata* through supercritical fluid, J. Taiwan Inst. Chem. Eng. 60 (2016) 165-173.
[191] A. Horta, A. da Silva, C. Sargo, I. Cavalcanti-Montaño, I. Galeano-Suarez, A. Velez, M. Santos, V. Gonçalves, R. Giordano, T. Zangirolami, ON-LINE MONITORING OF BIOMASS CONCENTRATION BASED ON A CAPACITANCE SENSOR: ASSESSING THE METHODOLOGY FOR DIFFERENT BACTERIA AND YEAST HIGH CELL DENSITY FED-BATCH CULTURES, Braz. J. Chem. Eng. 32(4) (2015) 821-829.
[192] N. Mohan, S. Sivaprakasam, Heat Compensation Calorimeter as a Process Analytical Tool To Monitor and Control Bioprocess Systems, Ind. Eng. Chem. Res. 56(30) (2017) 8416-8427.
[193] P. Wechselberger, P. Sagmeister, C. Herwig, Real-time estimation of biomass and specific growth rate in physiologically variable recombinant fed-batch processes, Bioprocess Biosyst Eng 36(9) (2013) 1205-1218.
[194] N. André, N. Cherouati, C. Prual, T. Steffan, G. Zeder-Lutz, T. Magnin, F. Pattus, H. Michel, R. Wagner, C. Reinhart, Enhancing functional production of G protein coupled receptors in *Pichia pastoris* to levels required for structural studies via a single expression screen, Protein Sci. 15(5) (2006) 1115-1126.
[195] Y. Pal, A. Khushoo, K. Mukherjee, Process optimization of constitutive human granulocyte–macrophage colony-stimulating factor (hGM-CSF) expression in *Pichia pastoris* fed-batch culture, Appl. Microbiol. Biotechnol. 69(6) (2006) 650-657.
[196] D. Files, M. Ogawa, C.H. Scaman, S.A. Baldwin, A *Pichia pastoris* fermentation process for producing high-levels of recombinant human cystatin-C, Enzyme Microb. Technol. 29(6) (2001) 335-340.
[197] J. Fricke, K. Pohlmann, F. Tatge, R. Lang, B. Faber, R. Luttmann, A multi-bioreactor system for optimal production of malaria vaccines with *Pichia pastoris*, Biotechnol. J 6(4) (2011) 437-451.
[198] K. Loegering, C. Mueller, J.P. Voss, C. Wagenfuehrer, D. Zahn, H.P. Bertelsen, U. Scheffler, R. Luttmann, An integrated scale down plant for optimal recombinant enzyme production by *Pichia pastoris*, Biotechnol. J 6(4) (2011) 428-436.
[199] A. Pedro, D. Oppolzer, M. Bonifacio, C. Maia, J. Queiroz, L. Passarinha, Evaluation of MutS and Mut+ *Pichia pastoris* strains for membrane-bound catechol-O-methyltransferase biosynthesis, Appl. Biochem. Biotechnol. 175(8) (2015) 3840-3855.
[200] A. Sola, P. Jouhten, H. Maaheimo, F. Sanchez-Ferrando, T. Szyperski, P. Ferrer, Metabolic flux profiling of *Pichia pastoris* grown on glycerol/methanol mixtures in chemostat cultures at low and high dilution rates, Microbiology 153(1) (2007) 281-290.
[201] A. Rumjantsev, O. Bondareva, M. Padkina, E. Sambuk, Effect of nitrogen source and inorganic phosphate concentration on methanol utilization and PEX genes expression in *Pichia pastoris*, Sci. World J 2014 (2014).
[202] C. Zhan, S. Wang, Y. Sun, X. Dai, X. Liu, L. Harvey, B. McNeil, Y. Yang, Z. Bai, The *Pichia pastoris* transmembrane protein GT1 is a glycerol transporter and relieves the repression of glycerol on AOX1 expression, FEMS Yeast Res. 16(4) (2016).
[203] K.M. Desai, S.A. Survase, P.S. Saudagar, S. Lele, R.S. Singhal, Comparison of artificial neural network (ANN) and response surface methodology (RSM) in fermentation media optimization: case study of fermentative production of scleroglucan, Biochem. Eng. J. 41(3) (2008) 266-273.

[204] A. Pekarsky, L. Veiter, V. Rajamanickam, C. Herwig, C. Grünwald-Gruber, F. Altmann, O. Spadiut, Production of a recombinant peroxidase in different glyco-engineered *Pichia pastoris strains*: a morphological and physiological comparison, Microb. Cell Fact. 17(1) (2018) 183.
[205] V. Looser, B. Bruhlmann, F. Bumbak, C. Stenger, M. Costa, A. Camattari, D. Fotiadis, K. Kovar, Cultivation strategies to enhance productivity of *Pichia pastoris*: a review, Biotechnol. Adv. 33(6) (2015) 1177-1193.
[206] P. Chongchittapiban, J. Borg, Y. Waiprib, J. Pimsamarn, A. Tongta, Development of simple kinetic models and parameter estimation for simulation of recombinant human serum albumin production by *Pichia pastoris*, Afr. J. Biotechnol. 15(39) (2016) 2156-2165.
[207] D. Levin, D. Harari, G. Schreiber, Stochastic receptor expression determines cell fate upon interferon treatment, MOL CELL BIOL (2011) MCB. 05251-11.
[208] R.A. Ningrum, D.E. Rahmatika, D.S. Retnoningrum, A.H. Wangsaatmadja, Y.C. Sumirtapura, H. Rachmawati, Development of novel interferon alpha 2b muteins and study the pharmacokinetic and biodistribution profiles in animal model, J. Biomed. Sci. Eng. 5(03) (2012) 104.
[209] R.A. Ningrum, P.H. Wisnuwardhani, A. Santoso, N. Herawati, Antiproliferative activity of recombinant human interferon alpha 2B on estrogen positive human breast cancer MCF-7 cell line, Indonesian Journal of Pharmacy 26(2) (2015) 86.
[210] E. Kalie, D.A. Jaitin, R. Abramovich, G. Schreiber, An interferon α2 mutant optimized by phage display for IFNAR1 binding confers specifically enhanced antitumor activities, J. Biol. Chem. 282(15) (2007) 11602-11611.
[211] G. Roos, T. Leanderson, E. Lundgren, Interferon-induced cell cycle changes in human hematopoietic cell lines and fresh leukemic cells, Cancer Res 44(6) (1984) 2358-2362.
[212] C. Rebnegger, A.B. Graf, M. Valli, M.G. Steiger, B. Gasser, M. Maurer, D. Mattanovich, In *Pichia pastoris*, growth rate regulates protein synthesis and secretion, mating and stress response, Biotechnol. J 9(4) (2014) 511-525.
[213] L.M. Damasceno, C.-J. Huang, C.A. Batt, Protein secretion in *Pichia pastoris* and advances in protein production, Appl. Microbiol. Biotechnol. 93(1) (2012) 31-39.
[214] A. Fazio, M.C. Jewett, P. Daran-Lapujade, R. Mustacchi, R. Usaite, J.T. Pronk, C.T. Workman, J. Nielsen, Transcription factor control of growth rate dependent genes in *Saccharomyces cerevisiae*: a three factor design, BMC Genom. 9(1) (2008) 341.
[215] J. Pinsach, C. de Mas, J. López-Santín, A simple feedback control of *Escherichia coli* growth for recombinant aldolase production in fed-batch mode, Biochem. Eng. J. 29(3) (2006) 235-242.
[216] M.M. Schuler, I.W. Marison, Real-time monitoring and control of microbial bioprocesses with focus on the specific growth rate: current state and perspectives, Appl. Microbiol. Biotechnol. 94(6) (2012) 1469-1482.
[217] H.E. Cole, A. Demont, I.W. Marison, The application of dielectric spectroscopy and biocalorimetry for the monitoring of biomass in immobilized mammalian cell cultures, Processes 3(2) (2015) 384-405.
[218] C.L. Davey, H.M. Davey, D.B. Kell, R.W. Todd, Introduction to the dielectric estimation of cellular biomass in real time, with special emphasis on measurements at high volume fractions, Analytical Biotechnology, Elsevier1993, pp. 155-161.
[219] I.W. Marison, M. Dabros, M.M. Schuler, Beyond Bioprocess Monitoring and Control, Laboratory Journal https://www.laboratory-journal.com (2010).
[220] K.J. Åström, T. Hägglund, The future of PID control, IFAC Proceedings Volumes 33(4) (2000) 19-30.
[221] D. Levisauskas, R. Simutis, D. Borvitz, A. Lübbert, Automatic control of the specific growth rate in fed-batch cultivation processes based on an exhaust gas analysis, Bioproc. Eng. 15(3) (1996) 145-150.
[222] J. Caldwell, W. Wang, P.W. Zandstra, Proportional-integral-derivative (PID) control of secreted factors for blood stem cell culture, PloS one 10(9) (2015) e0137392.

[223] S. Katla, B. Karmakar, S.R.R. Tadi, N. Mohan, B. Anand, U. Pal, S. Sivaprakasam, High level extracellular production of recombinant human interferon alpha 2b in glycoengineered *Pichia pastoris*: culture medium optimization, high cell density cultivation and biological characterization, J Appl Microbiol 126(5) (2019) 1438-1453.
[224] K. Asami, K. Takahashi, K. Shirahige, Progression of cell cycle monitored by dielectric spectroscopy and flow-cytometric analysis of DNA content, Yeast 16(15) (2000) 1359-1363.
[225] A. Horta, A. Silva, C. Sargo, A. Velez, M. Gonzaga, R. Giordano, V. Gonçalves, T. Zangirolami, A supervision and control tool based on artificial intelligence for high cell density cultivations, Braz. J. Chem. Eng. 31(2) (2014) 457-468.
[226] Z. Soons, J. Voogt, G. Van Straten, A. Van Boxtel, Constant specific growth rate in fed-batch cultivation of *Bordetella pertussis* using adaptive control, J. Biotechnol. 125(2) (2006) 252-268.
[227] S. Gnoth, M. Jenzsch, R. Simutis, A. Lübbert, Control of cultivation processes for recombinant protein production: a review, Bioprocess Biosyst Eng 31(1) (2008) 21-39.
[228] S. Valentinotti, Adaptive rejection of unstable disturbances: application to a fed-batch fermentation, These de doctorat, École Polytechnique Fédérale de Lausanne (2001).
[229] R. Howard, D. Cooper, A novel pattern-based approach for diagnostic controller performance monitoring, Control Eng Pract 18(3) (2010) 279-288.
[230] P. Zhang, W. Zhang, X. Zhou, P. Bai, J.M. Cregg, Y. Zhang, Catabolite repression of Aox in *Pichia pastoris* is dependent on hexose transporter PpHxt1 and pexophagy, Appl. Environ. Microbiol. 76(18) (2010) 6108-6118.
[231] V. Looser, D. Lüthy, M. Straumann, K. Hecht, K. Melzoch, K. Kovar, Effects of glycerol supply and specific growth rate on methanol-free production of CALB by *P. pastoris*: functional characterisation of a novel promoter, Appl Microbiol Biotechnol 101(8) (2017) 3163-3176.
[232] M. Jahic, J. Rotticci-Mulder, M. Martinelle, K. Hult, S.-O. Enfors, Modeling of growth and energy metabolism of *Pichia pastoris* producing a fusion protein, Bioprocess Biosyst Eng 24(6) (2002) 385-393.
[233] S. Capone, J. Horvat, C. Herwig, O. Spadiut, Development of a mixed feed strategy for a recombinant *Pichia pastoris* strain producing with a de-repression promoter, Microb. Cell Fact. 14(1) (2015) 101.
[234] Y. Katakura, W. Zhang, G. Zhuang, T. Omasa, M. Kishimoto, Y. Goto, K.-I. Suga, Effect of methanol concentration on the production of human β2-glycoprotein I domain V by a recombinant *Pichia pastoris*: a simple system for the control of methanol concentration using a semiconductor gas sensor, J. Ferment. Bioeng. 86(5) (1998) 482-487.
[235] H.H. Wong, Y.C. Kim, S.Y. Lee, H.N. Chang, Effect of post-induction nutrient feeding strategies on the production of bioadhesive protein in *Escherichia coli*, Biotechnol. Bioeng. 60(3) (1998) 271-276.
[236] L. Trinh, J. Phue, J. Shiloach, Effect of methanol feeding strategies on production and yield of recombinant mouse endostatin from *Pichia pastoris*, Biotechnol. Bioeng. 82(4) (2003) 438-444.
[237] B. Zhang, B. Li, D. Chen, J. Zong, F. Sun, H. Qu, C. Liang, Transcriptional regulation of aerobic metabolism in *Pichia pastoris* fermentation, PloS one 11(8) (2016) e0161502.
[238] J. Xie, R. Yang, Q. Zhou, P. Du, R. Gan, Q. Ye, Efficiencies of Growth and Angiostatin Expression in Cultures of *Pichia pastoris* FedwithMixed Carbon Sources, Chem Biochem Eng Q 27(2) (2013) 235-244.
[239] D. Wu, J. Chu, Y.-Y. Hao, Y.-H. Wang, Y.-P. Zhuang, S.-L. Zhang, High efficient production of recombinant human consensus interferon mutant in high cell density culture of *Pichia pastoris* using two phases methanol control, Process Biochem 46(8) (2011) 1663-1669.
[240] T.I. Potgieter, S.D. Kersey, M.R. Mallem, A.C. Nylen, M. d'Anjou, Antibody expression kinetics in glycoengineered *Pichia pastoris*, Biotechnol. Bioeng. 106(6) (2010) 918-927.

[241] Y. Wang, Z. Wang, Q. Xu, G. Du, Z. Hua, L. Liu, J. Li, J. Chen, Lowering induction temperature for enhanced production of polygalacturonate lyase in recombinant Pichia pastoris, Process Biochem. 44(9) (2009) 949-954.
[242] H. Jin, G. Liu, X. Ye, Z. Duan, Z. Li, Z. Shi, Enhanced porcine interferon-α production by recombinant *Pichia pastoris* with a combinational control strategy of low induction temperature and high dissolved oxygen concentration, Biochem. Eng. J. 52(1) (2010) 91-98.
[243] L. Gu, J. Zhang, B. Liu, G. Du, J. Chen, High-level extracellular production of glucose oxidase by recombinant *Pichia pastoris* using a combined strategy, Appl. Biochem. Biotechnol. 175(3) (2015) 1429-1447.
[244] J.M. Cregg, T.S. Vedvick, W.C. Raschke, Recent advances in the expression of foreign genes in *Pichia pastoris*, Bio/technology 11(8) (1993) 905.
[245] W. Zhang, K.J.H. Potter, B.A. Plantz, V.L. Schlegel, L.A. Smith, M.M. Meagher, *Pichia pastoris* fermentation with mixed-feeds of glycerol and methanol: growth kinetics and production improvement, J. Ind. Microbiol. Biotechnol. 30(4) (2003) 210-215.
[246] T. Maskow, R. Kemp, F. Buchholz, T. Schubert, B. Kiesel, H. Harms, What heat is telling us about microbial conversions in nature and technology: from chip-to megacalorimetry, Microb. Biotechnol. 3(3) (2010) 269-284.
[247] T. Randolph, I. Marison, D. Martens, U. Von Stockar, Calorimetric control of fed-batch fermentations, Biotechnol. Bioeng. 36(7) (1990) 678-684.
[248] D. Voisard, C. Claivaz, L. Menoud, I. Marison, U. Von Stockar, Use of reaction calorimetry to monitor and control microbial cultures producing industrially relevant secondary metabolites, Thermochim. Acta 309(1-2) (1998) 87-96.
[249] C.L. Cooney, D. Wang, R. Mateles, Measurement of heat evolution and correlation with oxygen consumption during microbial growth, Biotechnol. Bioeng. 67(6) (2000) 691-703.
[250] C. Jungo, J. Schenk, M. Pasquier, I.W. Marison, U. von Stockar, A quantitative analysis of the benefits of mixed feeds of sorbitol and methanol for the production of recombinant avidin with *Pichia pastoris*, J. Biotechnol. 131(1) (2007) 57-66.
[251] C. Jungo, I. Marison, U. von Stockar, Mixed feeds of glycerol and methanol can improve the performance of *Pichia pastoris* cultures: A quantitative study based on concentration gradients in transient continuous cultures, J. Biotechnol. 128(4) (2007) 824-837.
[252] S. Katla, K. Yoganand, S. Hingane, C.R. Kumar, B. Anand, S. Sivaprakasam, Novel glycosylated human interferon alpha 2b expressed in glycoengineered *Pichia pastoris* and its biological activity: N-linked glycoengineering approach, Enzyme Microb. Technol. 128 (2019) 49-58.
[253] C. Gurramkonda, A. Adnan, T. Gäbel, H. Lünsdorf, A. Ross, S.K. Nemani, S. Swaminathan, N. Khanna, U. Rinas, Simple high-cell density fed-batch technique for high-level recombinant protein production with *Pichia pastoris*: Application to intracellular production of Hepatitis B surface antigen, Microb. Cell Fact. 8(1) (2009) 13.
[254] C. Gurramkonda, S. Polez, N. Skoko, A. Adnan, T. Gäbel, D. Chugh, S. Swaminathan, N. Khanna, S. Tisminetzky, U. Rinas, Application of simple fed-batch technique to high-level secretory production of insulin precursor using *Pichia pastoris* with subsequent purification and conversion to human insulin, Microb. Cell Fact. 9(1) (2010) 31.
[255] C. Dietzsch, O. Spadiut, C. Herwig, A dynamic method based on the specific substrate uptake rate to set up a feeding strategy for *Pichia pastoris*, Microb. Cell Fact. 10(1) (2011) 14.
[256] C. Dietzsch, O. Spadiut, C. Herwig, A fast approach to determine a fed batch feeding profile for recombinant *Pichia pastoris* strains, Microb. Cell Fact. 10(1) (2011) 85.
[257] P.M. Doran, Bioprocess engineering principles, Elsevier1995.
[258] S. Sivaprakasam, S. Mahadevan, S. Rajakumar, Biocalorimetric studies of the metabolic activity of *Pseudomonas aeruginosa* aerobically grown in a glucose-limited complex growth medium, Biosci. Biotechnol. Biochem. 72(4) (2008) 936-942.

[259] X. Ponte, J.L. Montesinos-Seguí, F. Valero, Bioprocess efficiency in *Rhizopus oryzae* lipase production by *Pichia pastoris* under the control of PAOX1 is oxygen tension dependent, Process Biochem. 51(12) (2016) 1954-1963.
[260] S. Katla, N. Mohan, S.S. Pavan, U. Pal, S. Sivaprakasam, Control of specific growth rate for the enhanced production of human interferon α2b in glycoengineered *Pichia pastoris*: process analytical technology guided approach, J. Chem. Technol. Biotechnol. 94(10) (2019) 3111-3123.
[261] D. Voisard, U. Von Stockar, I. Marison, Quantitative calorimetric investigation of fed-batch cultures of *Bacillus sphaericus* 1593M, Thermochim. Acta. 394(1-2) (2002) 99-111.
[262] E. Faulkner, M. Barrett, S. Okor, P. Kieran, E. Casey, F. Paradisi, P. Engel, B. Glennon, Use of Fed-Batch Cultivation for Achieving High Cell Densities for the Pilot-Scale Production of a Recombinant Protein (Phenylalanine Dehydrogenase) in *Escherichia coli*, Biotechnol. Prog. 22(3) (2006) 889-897.
[263] I.J. van der Klei, H. Yurimoto, Y. Sakai, M. Veenhuis, The significance of peroxisomes in methanol metabolism in methylotrophic yeast, BBA. Molecular cell research 1763(12) (2006) 1453-1462.
[264] G. Minjie, S. Zhongping, Process control and optimization for heterologous protein production by methylotrophic *Pichia pastoris*, Chin. J. Chem. Eng. 21(2) (2013) 216-226.
[265] H. Niu, L. Jost, N. Pirlot, H. Sassi, M. Daukandt, C. Rodriguez, P. Fickers, A quantitative study of methanol/sorbitol co-feeding process of a *Pichia pastoris* Mut+/pAOX1-lacZ strain, Microb. Cell Fact. 12(1) (2013) 33.
[266] L. Chen, A. Mohsin, J. Chu, Y. Zhuang, Y. Liu, M. Guo, Enhanced protein production by sorbitol co-feeding with methanol in recombinant *Pichia pastoris* strains, Biotechnol. Bioprocess Eng. 22(6) (2017) 767-773.
[267] J.-L. Cordier, B.M. Butsch, B. Birou, U. von Stockar, The relationship between elemental composition and heat of combustion of microbial biomass, Appl. Microbiol. Biotechnol. 25(4) (1987) 305-312.

List of Publications

List of Publications

Research outcome of thesis work

Manuscripts accepted/submitted

1. **Srikanth Katla**, K.N.R Yoganand, Smita Hingane, C.T Ranjith Kumar, B. Anand, Senthilkumar Sivaparakasam (2019). Novel glycosylated human interferon alpha 2b expressed in glycoengineered Pichia pastoris and its biological activity: N-linked glycoengineering approach, Enzyme Microb. Technol. 128, 49-58.
2. **Srikanth Katla**, B. Karmakar, S.R.R. Tadi, N. Mohan, B. Anand, U. Pal, Senthilkumar Sivaprakasam (2019). High-level extracellular production of recombinant human interferon alpha 2b in glycoengineered Pichia pastoris: culture medium optimization, high cell density cultivation, and biological characterization, J. Appl. Microbiol, 126(5):1438-1453.
3. **Srikanth Katla**, Naresh Mohan, Satya Sai Pavan, Uttariya Pal, Senthilkumar Sivaprakasam (2019). Control of specific growth rate for the enhanced production of human interferon α2b in glycoengineered Pichia pastoris: process analytical technology guided approach. J. Chem. Technol. Biotechnol, 94(10):3111-3123.
4. **Srikanth Katla**, Satya Sai Pavan, Naresh Mohan, Senthilkumar Sivaprakasam. Biocalorimetric monitoring of glycoengineered P. pastoris cultivation for the production of recombinant huIFNα2b: A quantitative study based on mixed feeding strategies. Biotechnol. Prog. (Revision submitted).

Patent

1. **Srikanth Katla**, Yoganand KNR, Anand B, Senthilkumar S (2018) Production of Glycosylated Human Interferon Alpha 2b in Glycoengineered *Pichia pastoris*. Indian Patent : 201731014991 (Patent published)

Book Chapter

1. **Srikanth Katla**, Senthilkumar Sivaprakasam. Yeasts as Microbial Factories for the Production of Recombinant Human Interferon Alpha 2b of Therapeutic Importance. Next Generation Biomanufacturing Technologies, ACS Publications, 03 December 2019, DOI: 10.1021/bk-2019-1329.ch003.

Manuscripts from collaborative work

1. Indumathi Palanikumar, **Srikanth Katla**, Nariyasu Tahara, MidoriYui, Rui Zhang, Akio Ebihara, Senthilkumar Sivaprakasam. Heterologous expression, purification and functional characterization of recombinant ovine angiotensinogen in the methylotrophic yeast *Pichia pastoris.* Biotechnology Progress, 12 June 2019, DOI: https://doi.org/10.1002/btpr.2866.

2. Satish Cingadi , **Katla Srikanth** , Arun E.V.R , Senthilkumar Sivaprakasam (2015). Statistical optimization of cassava fibrous waste hydrolysis by response surface methodology and use of hydrolysate-based media for the production of optically pure D-Lactic acid. Biochemical Engineering Journal, Volume 102, 15 October 2015, Pages 82-90.

3. Saurav Prasad, **Katla Srikanth**, Anil M. Limaye, Senthilkumar Sivaprakasam (2014). Homo-fermentative production of d-lactic acid by *Lactobacillus sp*. employing casein whey permeate as a raw feed stock. Biotechnology Letters, June 2014, Volume 36, Issue 6, pp 1303-1307

List of Conferences

International

1. **Srikanth Katla**, Naresh Mohan, K. Yoganand, B. Anand, Senthilkumar Sivaprakasam. Recombinant Human Interferon Alpha-2b: Cloning, Expression And Pat-ProcessAnalytical Technology Enabled Production In Glycoengineered *Pichia Pastoris*. European Congress on Biotechnology (ECB 2018), July 1-4, Geneva, Switzerland. (oral)

2. **Srikanth Katla**, Bappa Karmakar, Subbi Rami Reddy Tadi, Naresh Mohan, Anand B, Senthilkumar Sivaprakasam. Media Optimization and Batch Kinetics Studies for Recombinant Human Interferon α2b Production by *Pichia pastoris*. Asian Congress on Biotechnology (ACB 2017), Jul 23-27, Khon Kaen, Thailand.(oral)

National

1. **Srikanth Katla**, Bappa Karmakar, Subbi Rami Reddy Tadi, Naresh Mohan, Satya Sai Pavan, B. Anand, Dr. Senthilkumar Sivaprakasam. Glycosylated Interferon α2b Production by *Pichia pastoris*. Bioprocessing India 2017. Dec 9-11, IIT Guwahati, Guwahati, India. (oral)

2. Satish Cingadi, **Srikanth Katla**, Senthilkumar Sivaprakasam, Anil M Limaye. Statistical optimization of cassava fibrous waste hydrolysis by response surface methodology and use of hydrolysate-based media for the production of optically pure D-Lactic acid. International conference on emerging trends in Biotechnology (ICETB-2014) November 6-9, New Delhi, India. (Best poster award)

3. Vignesh Natarajan, **Srikanth Katla**, Satish Cingadi, Senthilkumar Sivapraksam. Cassava Starch Waste - A Viable Raw Feed Stock for the production of Hyaluronic Acid by *Streptococcus thermophilus* NCIM2904, Asian Congress on Biotechnology (ACB 2013), Dec 15-19, New Delhi, India. (poster)

4. Saurav Prasad, **Srikanth Katla**, Senthilkumar Sivaprakasam, Anil M Limaye. Kinetics Analysis of Growth and D-Lactic acid Production in pH-Controlled Batch Cultures of *Lactobacillus Sp*. Using Synthetic Whey Permeate Medium, International Conference on Advances in Biotechnology and Patenting (ICABP -2013) February 18-21st, 2013, Trichy, Tamilnadu, India. (oral)